Microscale mRNA Amplification, Separation and Detection for

Forensic and Clinical Point-of-Care Applications

Tiffany Renee Layne

Hopewell, Virginia

M.S. Forensic Science, Virginia Commonwealth University, 2016

B.S. Biology, Virginia Commonwealth University, 2016

B.S. Forensic Science, Virginia Commonwealth University, 2016

A Dissertation presented to the Graduate Faculty of the University of Virginia in

Candidacy for the Degree of Doctor of Philosophy

Department of Chemistry

University of Virginia

July 2021

Abstract

Specific, sensitive identification of nucleic targets is an invaluable tool across numerous disciplines, including the forensic and clinical communities. The conventional assays and detection methods for these purposes are laborious, destructive, typically have single target detection, lack specificity and sensitivity, and are time-consuming for the scientist. The development of novel biochemical assays to alleviate these shortcomings can provide faster, multi-target reactions with minimal manual steps and are highly specific and sensitive for identification purposes. Biocompatible technology, such as microfluidics, can enhance an assay by providing rapid, multi-sample, cost-efficient automation for unique bioanalytical techniques. The work outlined in this dissertation discusses development of such centrifugal microdevices for novel amplification and separation methods and subsequent application to differentiation between forensically relevant body fluids, testing tolerance of transplanted organs, and detection of viral targets. Specifically, this dissertation presents two distinct approaches to forensic body fluid identification (bfID) using (1) an isothermal amplification method with colorimetric image analysis and (2) a polymerase chain reaction (PCR)-based primer panel for messenger RNA (mRNA) amplification followed by electrophoretic fluorescent detection. Additionally, this dissertation explores two microfluidic approaches identifying RNA targets in clinical characterization of SARS-CoV-2 infection status and transplanted organ tolerance.

Conventional methods for forensic bfID are ubiquitous, but reply upon time-consuming, laborious microscopic analysis or presumptive (bio)chemical, enzymatic, or immunological assays that are generally limited in specificity and lacking in sensitivity. The work presented in **Chapter**

2 details a novel method for forensic bfID via the optimization of the detection of five mRNA targets using loop-mediated amplification (LAMP) with a colorimetric indicator and image capture and analysis. This method allows for amplification of the mRNA target in <15 min providing single-fluid specificity and sensitivity in the picogram range for venous blood, semen, saliva, vaginal fluid, and menstrual blood. **Chapter 3** describes the construction of a 3D-printed system for isothermal heating and automated image analysis. Along with the optimized amplification method described in Chapter 2, the combined system was evaluated via a single-blind mock study and compared to 'gold standard' conventional approaches. **Chapter 4** details the adaptation of a panel of primers specific to five mRNA targets in various body fluids integral to forensic analysis to a portable, microfluidic platform. The time required for analysis was greatly diminished relative to traditional methods; while the conventional approach requires ≥3 hours of analytical time, the approach described herein is complete in less than 30 minutes, with on-disc reverse transcription and electrophoresis complete in 11 and <15 min, respectively. Finally, **Chapter 5** shows successful detection of an RNA target for SARS-CoV-2 identification in clinical samples using an amplification method 2X faster on-disc than in-tube. This chapter also provides justification for a second clinical application to continue PCR optimization efforts, with the goal of a significantly reduced overall time and reagent cost, that assesses whether a transplanted liver is being tolerated or rejected. The results in this chapter demonstrate the utility of adapting biochemical assays to microfluidic platforms for rapid, point-of-care target for rapid pathogen detection and establishing patient tolerance of a transplanted organ.

Acknowledgements

This journey would not have been possible without the support, motivation, and encouragement from my research advisor, Professor James Landers. I first learned about the research in your lab at AAFS during my master's career at VCU and was very interested and intrigued, as I knew nothing of microfluidic technology. Over the past five years, your mentoring, guidance, and many chocolate sprinkled donuts have shaped me into a hard-working, detail-oriented research scientist. I am incredibly grateful and honored to have had the opportunity to perform research in your laboratory, with access to innovative solutions and state-of-the-art instrumentation. This experience has allowed me to collaborate with scientists across the world, dine and converse with founding members of scientific communities, and attend numerous conferences gaining knowledge on a vast number of topics. Thank you so much for everything you have taught me and making this a memorable journey.

I also had the opportunity to work alongside the incredible scientists and engineers in the Landers lab on various projects while at UVA and throughout collaborations. My sincerest thanks and gratitude to each member, past and present, of the Landers lab for your friendship, Friday group lunches, and late nights in the laboratory. Specifically, a huge thank you to my partner-in-crime and confidant for four years Dr. Anchi Scott, and my coffee-loving, Rams turned Hoos co-alumni Dr. Shane Woolf. For their specific contributions to this research and my mental health over the past five years, Killian O'Connell, Jamila Marshall, Leah Dignan, Dr. Nathan Tanner, Dr. Rachel Fleming, Dion Sheppard, Dr. Joan Bienvenue, Jeff Hickey, Orion Scott, Daniel Mills, Aeren Nauman, Dr. Dan Nelson, Dr. Delphine Le Roux, and various undergraduate students.

Lastly, I would not have completed the past five years without the love, drive, and strength from my friends and family. Thank you to my colleagues and friends from VCU that have listened to my ramblings and lifted my spirits when needed, Samantha Jacobs, April Solomon, Jena Baldaino, Dave and Megan Millard, Dr. Sarah Seashols-Williams, and Dr. Tracy Dawson Green. Thank you to all the friends I have made in Charlottesville who shared margaritas, late nights, sporting events, and concerts; to name a few: Christina Mehrtens, Dr. Reilly Sonstrom, Dr. Spenser Simpson, Taylor Sealy, Dr. Kevin Mayer, Dr. Channing West, and Dr. Philip Hahn. My family has been extremely helpful throughout this journey, from moving into my first apartment in Charlottesville to celebrating new family members to memorable family vacations. My twin pillars, Dad and Mom, there will never be enough words to thank you for all the love and support throughout this time. To my crazy, beautiful family, Jen, Tyler, Grayson, Scott, Aunt Peggy, Aunt Rene and Uncle George, Patti, Franny, and many others, thank you for always supporting my dreams. I have made fun memories, gained scientific knowledge, and accomplished dreams during my time in Charlottesville, and will take the values and lessons from this journey with me into my future endeavors.

Table of Contents

List of Figures

Chapter 1: Emerging Forensic Body Fluid Identification Methods and Rapid Microscale Technology

Chapter 2: Optimization of LAMP & colorimetric image analysis method with mRNA body fluid target

Chapter 3: Integrated device for colorimetric LAMP mock study comparison

Chapter 4: Adaptation of separation & amplification methods for mRNA body fluid panel to a microfluidic platform

Chapter 6: Final Remarks

List of Tables

List of Original Publications

The research described in this thesis resulted in the following publications:

1. **Layne, TR**, Jackson, K, Scott, A, Tanner, N, Piland, A, Haverstick, DM, Landers, JP, Optimization of Novel Loop-mediated Isothermal Amplification with Colorimetric Image Analysis for Forensic Body Fluid Identification. *Journal of Forensic Sciences (*2021)
2. **Layne, TR**, Fleming, R, Blair, H, Landers, JP, Rapid Microchip Electrophoretic Separation of Novel Transcriptomic Body Fluid Markers for Forensic Fluid Profiling. *FSI: Genetics,* Submitted.
3. **Layne, TR**, Scott, A, Tanner, N, Nauman, A, Piland, A, Landers, JP, Mock Study using LAMP Colorimetric Analysis as a Novel Forensic Body Fluid Identification Method. *FSI:Genetics,* In prep.
4. **Layne, TR**, Scott, A, Nauman, A, Maltez, P, Landers, JP, 3D Printed Heating and Imaging system for Isothermal Loop-mediated Amplification assays, *Science Advances,* In prep.
5. **Layne, TR**, Turiello, R, Dignan, L, Hickey, J, Chapman, J, Poulter, M, Landers, JP, Rapid, Microfluidic Amplification of SARS-CoV-2 RNA genes for COVID testing. *Journal of Molecular Diagnostics,* In prep.

Abbreviations

.csv	Comma Separated Values File	MERS-CoV	Middle East Respiratory Syndrome-CoV
.txt	Text File	MG	Malachite Green
µCDs	Microfluidic CDs	miRNA	Micro RNA
µTAS	Micro Total Analysis System	MMP10	Human Matrix Metallopeptidase 10
ABS	Acrylonitrile Butadiene Styrene	MPS	Massive Parallel Sequencing
AC	Alternating Current	mRNA	Messenger RNA
ALS	Alternative Light Source	NASBA	Nucleic Acid Sequence-based Amplification
AP	Acid Phosphatase	NSA	Non-specific Amplification
B	Buffer	NTA	Non-template Amplification
bfID	Body Fluid Identification	NTC	Non-template Control
BIP	Backward Inner Primer	PBMC	Peripheral Blood Mononuclear Cell
bPET	Black PET	PCB	Printed Circuit board
BW	Buffer Waste	PCL	'Print-Cut-Laminate'
CDC	Center for Disease Control and Prevention	PCR	Polymerase Chain Reaction
cDNA	Complementary DNA	PET	Polyethylene Terephthalate
CE	Capillary Electrophoresis	PLA	Polylactic Acid
circRNA	Circular RNA	PMMA	Polymethyl Methacrylate

cLAMP	Combined LAMP and Image Analysis	PR	Phenol Red
CNC	Computer Numerical Control	PSA	Pressure Sensitive Adhesive
COC	Cyclic Olefin Copolymer	PTMB	Phenolphthalein TMB
COVID-19	Coronavirus Disease 2019	qPCR	Quantitative PCR
CYP2B7P	Cytochrome P450 family 2 subfamily A member 7 pseudogene 1	RCA	Rolling Circle Amplification
DEF	Diethyl Formamide	RFU	Relative Fluorescence Units
DNA	Deoxynucleic Acid	RGB	Red, Green, Blue
ESR	Environmental Science and Research Institute, New Zealand	RNA	Ribonucleic Acid
FIP	Forward Inner Primer	ROI	Region of Interest
HAD	Helicase Dependent Amplification	RPA	Recombinase Polymerase Amplification
HBB	Human β-hemoglobin	RPi	Raspberry Pi
HNB	Hydroxynaphthol Blue	RT-LAMP	Reverse Transcription LAMP
HSA	Heat Sensitive Adhesive	RT-PCR	Reverse Transcription PCR
HSB	Hue, Saturation, Brightness	RT-qPCR	Reverse Transcription Quantitative PCR
HTN3	Human Histatin 3	S	Sample
IBV	Infectious Bronchitis Virus	Sa	Saliva

ILS	Internal Lane Standard	SARS-CoV-2	Sudden Acute Respiratory Syndrome-Coronavirus-2
LAMP	Loop-mediated Amplification	SDA	Strand Displacement Amplification
LB	Loop Backward Primer	Se	Semen
LCV	Leucocrystal Violet	SEMG1	Semenogelin 1
LED	Light-emitting Diode	STR	Short Tandem Repeat
LF	Loop Forward Primer	SW	Sample Waste
LFA	Lateral Flow Assay	TMB	Tetramethylbenzidine
LIF	Laser Induced Fluorescence	Vb	Venous Blood
LITMUS	Liver Immune Tolerance Marker Utilization Study	Vf	Vaginal Fluid
LOD	Limit of Detection	VTM	Viral Transport Medium
Mb	Menstrual Blood	μAmpDisc	'Micro-amplification' Disc
ME	Micro-disc electrophoresis	μEDisc	'Micro-electrophoresis' Disc

Chapter 1: Emerging Forensic Body Fluid Identification Methods and Rapid Microscale Technology

1.1 Overview

The development of novel sensitive and specific body fluid identification (bfID) techniques to improve conventional assays is a rapidly growing field of research in forensic science. Newer techniques have many advantages over conventional laborious methods, including single fluid specificity, multi-fluid identification in a single reaction, automated objective analysis, and potential portable or on-site usage. Ribonucleic acids (RNA) have been studied for this application extensively facilitating simple integration into the forensic workflow via co-extraction with deoxyribonucleic acids (DNA) from a single cutting of evidence. This dissertation describes two techniques that address problems arising from current forensic bfID methods detailed below; an isothermal amplification technique identifying five body fluids in less than 60 minutes, and a microfluidic technique that reverse transcribes, amplifies, and size-separates targets for six body fluids in one reaction. The isothermal technique works in tandem with colorimetric image analysis to reduce hardware complexity and provide a simple, objective analysis method. Microfluidic platforms are becoming more accepted due to their advantages of faster analysis, potential automation, and reduced reagent and sample volume. Accordingly, the application of microfluidics to bfID in this dissertation significantly reduced the overall analysis time with minimal loss to specificity and sensitivity. Additionally, the microfluidic device discussed here was adapted for two clinical applications that rapidly identify SARS-CoV-2 and liver transplant

tolerance targets. The development of a technique that is easily adaptable to different nucleic targets while comprehensively reducing the instrumental assay time and footprint is highly advantageous for clinical protocols.

1.2 Forensic Body Fluid Identification

1.2.1 Conventional approaches to bfID

Investigating evidence from crime scenes to determine the sequence of events and ultimately achieve justice for victims is the heart of forensic science. This process starts by collecting evidence from a crime scene (via enhancement techniques) and sending it to a laboratory for analyses that will drive the narrative to solve the mystery (**Fig. 1A**). (1) While DNA analysis is the most well-known and portrayed in court or television shows, the testing for the presence of body fluids is conducted first to determine if the evidence is probative and contains viable genetic material for DNA analysis. In a forensic investigation, evidence is deemed probative if it contributes to or proves a particular aspect of the narrative of the crime.

There are two types of tests used for forensic serology, which is the detection and classification of body fluids for forensic body fluid identification (bfID). The first is presumptive testing which serves as a screening method and may indicate the presence of a particular body fluid. (2) Second, confirmatory tests are those that subsequently substantiate or disprove this assertion and identify a specific biological material (**Fig. 1B**). For example, a presumptive test may indicate that a red stain is blood rather than, e.g., ketchup. A confirmatory test may then verify the presence of blood via hemoglobin detection in the red stain. If a stain result is positive for a

body fluid and is probative to the narrative, another cutting of the evidence will be analyzed for DNA profiling. The sample goes through cell lysis and DNA purification typically using a solid-phase method and then the DNA material is quantified via quantitative polymerase chain reaction (qPCR). The DNA material is amplified for specific short tandem repeats (STRs), which are repeated sequences that vary in number among individuals, and fluorescently detected via electrophoresis to produce a DNA profile. The DNA profile is compared to other profiles on local, state, or federal electronic databases for genetic identification.

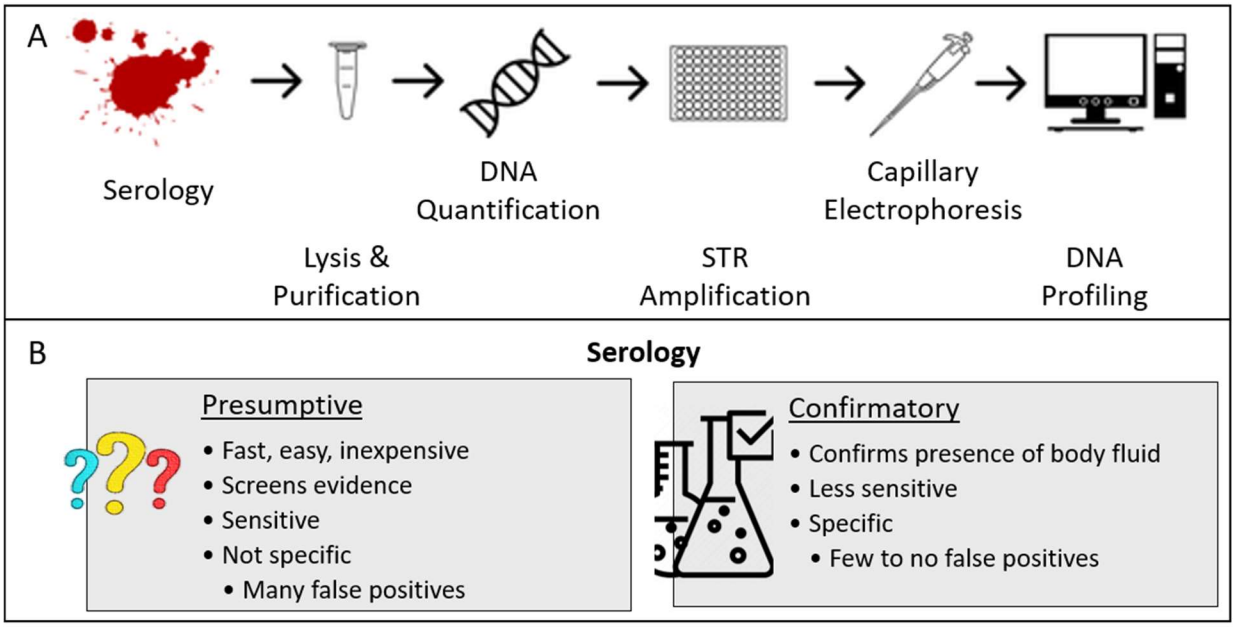

Figure 1: Serology testing of body fluids in forensic laboratories. (A) Illustration of biology workflow in a forensic laboratory. (Adapted from Lynch et al. with permission) (B) Presumptive and confirmatory tests used for identifying body fluids on evidence.

Many of the presumptive tests used in forensic laboratories are ubiquitous and well-established; however, there are several challenges inherent to the use of such analyses. For example, these tests are often destructive, thereby, prohibiting additional downstream analysis. Additionally, most of the tests currently employed are fluid-specific for only one body fluid; that is, these are designed to target a protein in a particular body fluid. As such, the presumptive test

selected must be based on the most probable identity of the fluid. Consequently, tests of this type are often disadvantageous because the tests are laborious, time-consuming, destructive to DNA material, and have limited specificity for a small portion of the fluids secreted from humans. Some of the fluids that do have presumptive tests typically tested for in forensic laboratories are blood, seminal fluid, and saliva. Despite the prevalence of several presumptive and confirmatory tests for bfID, there is no single universal body fluid test to discriminate multiple body fluids for use at a crime scene or in a forensic laboratory.

1.2.1.1 Presumptive and confirmatory tests for blood

Crime scenes are searched for body fluids by various enhancement methods (e.g., alternative light sources (ALS), chemiluminescence, or photoluminescence). A common chemiluminescence method used to visualize blood is Luminol, which produces light with an oxidizing agent (**Fig. 2A**). (3) Common implemented presumptive blood tests include the colorimetric phenolphthalein (or Kastle-Meyer test) and tetramethylbenzidine (TMB) chemical assays that detect hemoglobin, which is found in red blood cells and used to transport oxygen and carbon dioxide, on a piece of evidence. Briefly, the Kastle-Meyer and TMB test is conducted as follows; (4) A drop of phenolphthalein (or Kastle-Meyer reagent) and one drop of hydrogen peroxide are sequentially added to a red-brown stain from evidence. (5) The presence of blood is presumed if the reaction instantly turns pink; this color change occurs due to the oxidation of phenolphthalein (**Fig. 2B**). Critically, the color change must be determined immediately, as the phenolphthalein will naturally oxidize in the air. The nature of this test results in ‘false positives’ from any oxidizing reagent; for example, previous specificity tests have shown false-positive

reactions with vegetable peroxidases (e.g., horseradish, broccoli), copper, and nickel salts. (6) For the TMB test, a drop of TMB reagent is added to a red-brown stain from evidence; if the color instantly turns blue-green, the presence of blood is presumed due to the presence of an oxidizing agent (i.e., hemoglobin) (**Fig. 2C**). (7) The hemoglobin cleaves the oxygen from the hydrogen peroxide and catalyzes the reaction to a reduced form of TMB. (8)

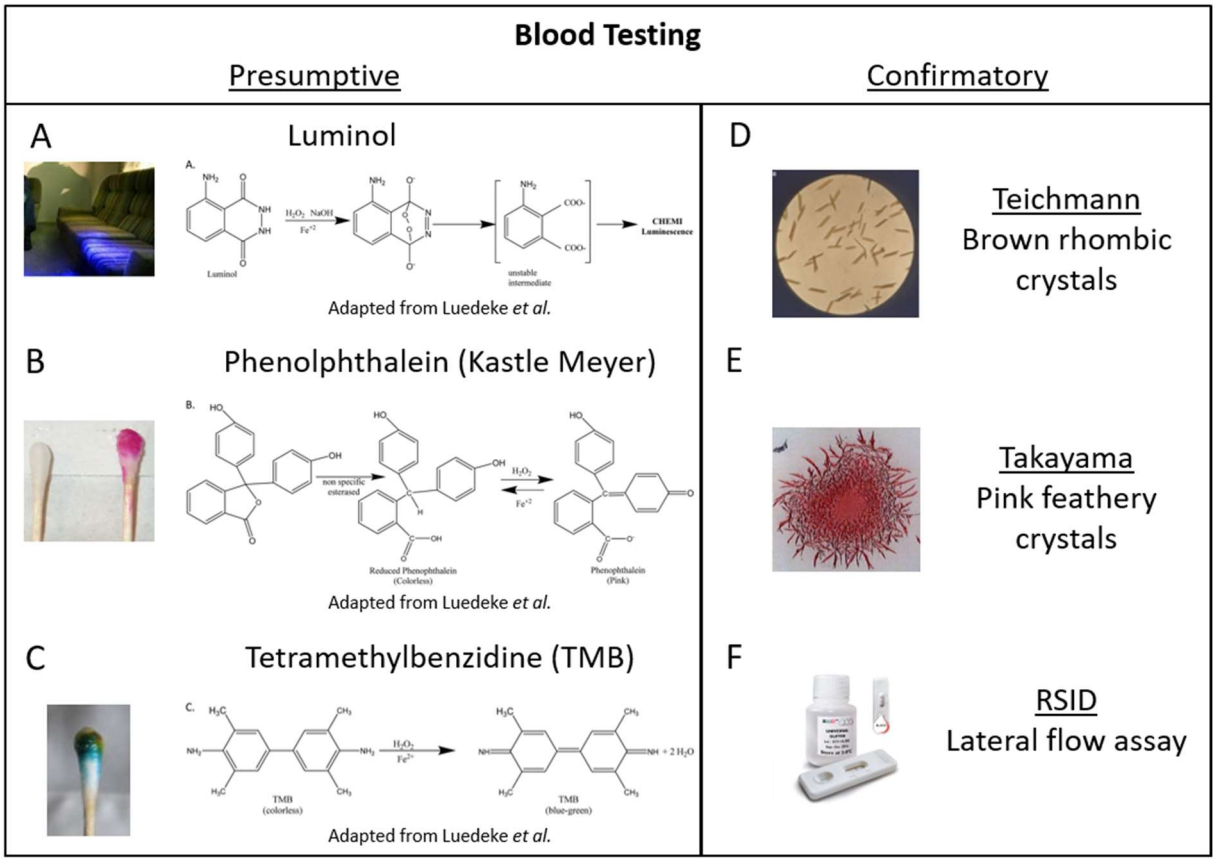

Figure 2: Blood presumptive and confirmatory tests in forensic laboratories. Many of the presumptive tests are colorimetric, while the confirmatory tests are microscopic exams. (Adapted with permission)

The Kastle-Meyer and TMB tests have excellent sensitivities at a 1:1,000,000 dilution (9) and 1:500,000 dilution (7) of neat blood, respectively. While both of these tests are typically used in succession, neither of these colorimetric tests are species-specific to humans. Rarely, one test that was used to identify species in any fluid is the Ouchterlony double immunodiffusion test,

which uses antigen detection to determine if the fluid is human or from another animal (not shown). Nonetheless, neither the presumptive nor this test confirm the fluid as blood.

After a positive presumptive test result, the evidence sample may either be tested to confirm the presence of hemoglobin, or a new portion of the evidence goes directly to DNA analysis via STR profiling. One confirmatory blood test used is a microcrystal assay that forms colored crystals with hemoglobin. (2, 10-12) There are two microcrystal assays, *Teichmann* and *Takayama* tests, used specifically for forensic purposes. In the *Teichmann* test, the NaCl and glacial acetic acid reacts with hemoglobin to form brown, rhombic, hematin chloride crystals (**Fig. 2D**). (2, 10-12) In the *Takayama test*, pyridine reacts with hemoglobin to form pink, feathery, pyridine-hemochromogen crystals (**Fig. 2E**). (2, 12) Although both of these tests confirm the presence of blood through hemoglobin detection, they are laborious and time-consuming for the scientist. The lateral flow assay (LFA) identifying blood shown in **Fig. 2F** is described below in Section 1.2.1.4.

1.2.1.2 Presumptive and confirmatory tests for seminal fluid

Semen, which contains seminal fluid and sperm cells, is visualized at crime scenes by enhancement methods (e.g., ALS) (**Fig. 3A**). Only one test is predominately available for presumptive and confirmatory identification of semen in forensic laboratories. The acid phosphatase (AP) test presumes the presence of seminal fluid but not sperm cells by detecting acid phosphatase, a prostate-specific protein that releases phosphates under acidic conditions. (13, 14) In this test, a drop of Brentamine fast blue is added to a piece of evidence; if the color changes from colorless to deep purple within one-minute, seminal fluid is presumed present (**Fig.**

3B). The color changes due to naphthol being liberated from sodium α-naphthyl phosphate by AP and coupling with the Brentamine salt. (13) The intensity of the color can differ depending on the quantity of AP in the sample. Samples diluted more than 1000X in water or obtained ≤ 24 hours after intercourse have been detected with the AP test. (15) This test is considered presumptive, however, because AP can also be found in other parts of the body (e.g., liver, spleen, bone marrow), in the vaginal cavity after intercourse, and in other animal species. After a piece of evidence is presumed to contain seminal fluid, another cutting is taken to confirm the presence of semen via microscopic examination. 'Christmas Tree' staining uses Picroindigocarmine to color the epithelial cells, sperm tails, and cytoplasm green and Kernechtrot (or Nuclear Fast Red) to color the acrosomal cap of sperm heads pink red (**Fig. 3C**). If any sperm are found, another cutting of the evidence is taken for DNA analysis. This confirmatory test is

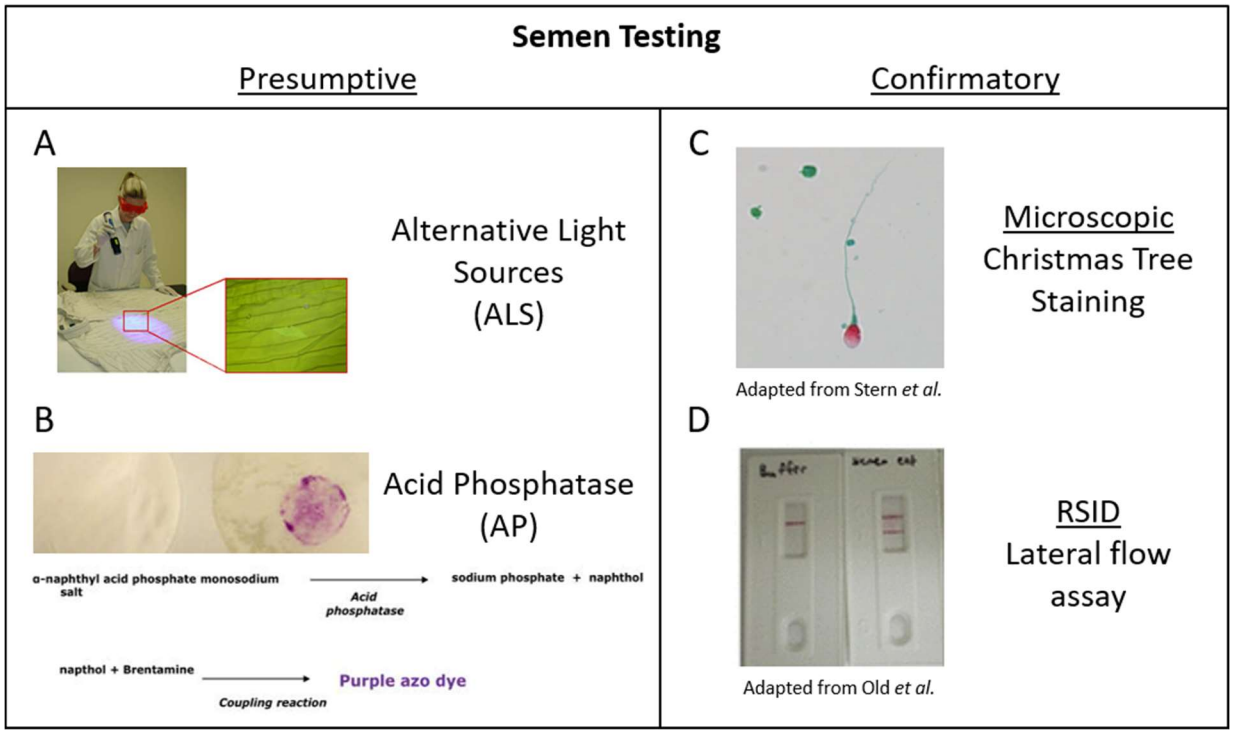

Figure 3: Semen presumptive and confirmatory tests in forensic laboratories. After searching for stains with an ALS, the AP test is used to presume seminal fluid, while a microscopic exam shows if any sperm are present. (Adapted with permissions)

incredibly beneficial for identifying sperm in a sample; however, the process consumes more of the evidence and is laborious and time-consuming for the forensic scientist. The LFA identifying semen in **Fig. 3D** is described below in Section 1.2.1.4.

1.2.1.3 Presumptive test for saliva

At a crime scene saliva can be visualized by enhancement methods (e.g., ALS) (**Fig. 4A**). Alpha-amylase is used in forensic laboratories to detect the presence of saliva presumptively. It is the main form of amylase found in humans and other animals that degrades starch by hydrolyzing alpha-bonds in starch at arbitrary sites. (16) It has been found in the salivary glands and pancreas, as well as in fungi, bacteria, and plants. Typically, this presumptive test is only conducted on unknown evidence samples where saliva is probable, whereas known buccal swabs are sent directly for DNA analysis. The commonly used *Phadebus® test* involves adding a

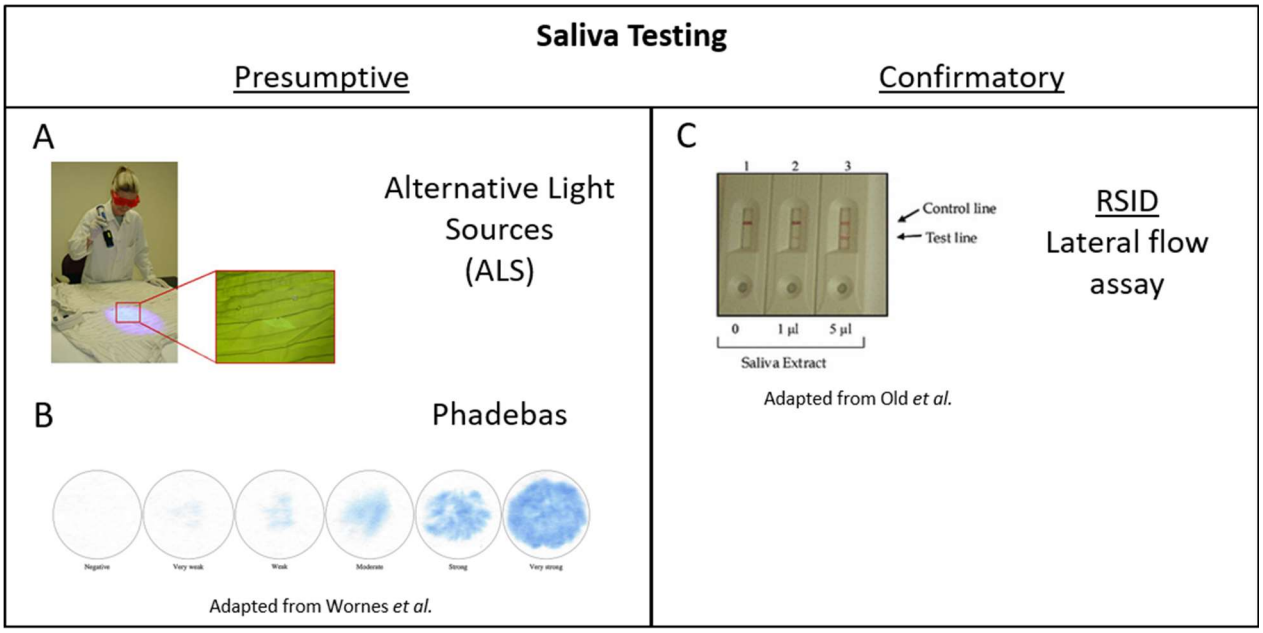

Figure 4: Saliva presumptive and confirmatory tests in forensic laboratories. Not typically tested for, the Phadebas tests would be used to presume α-amylase for saliva or an antigen detection on a lateral flow assay to confirm presence of saliva. (Adapted with permissions)

Phadebus tablet to the supernatant from a cutting of evidence (**Fig. 4B**). Alpha-amylase is presumed if the reaction changes from colorless to blue following heating at 37 °C and centrifugation. Saliva stains diluted up to 200X or stains of 1:3 saliva: blood or saliva: semen were reported to undergo this color change after 5 minutes. (17) While this test is specific to alpha-amylase, the enzyme itself is not only found in saliva, and thus this test can only be considered a presumptive test. The LFA identifying saliva in **Fig. 4C** is described below in Section 1.2.1.4.

1.2.1.4 Antigen tests for body fluid detection

All of the presumptive tests previously mentioned are colorimetric and rely on a chemical reaction to detect an enzyme found in high quantities of the body fluid. An alternative to these presumptive tests is immunochromatographic testing (or LFA) for specific analytes in a body fluid. This analysis requires the deposition of a liquid sample on one end of the chromatographic paper. Capillary action wicks the analyte in the sample into antibodies conjugated to an analyte-specific colloidal gold tag, and the liquid passes to the other end of the paper. A test line comprises antibodies specific to the analyte, and a control line includes antibodies for conjugate antibodies. A positive result is indicated by pink control and test lines; conversely, if only the control line is pink, the test is deemed negative for the specific antigen. Commercialized LFA tests have been produced for body fluids, including blood (**Fig. 2F**), semen (**Fig. 3D**), saliva (**Fig. 4C**), and urine, and are used in forensic laboratories as confirmatory tests. Whether LFA tests should be considered presumptive or confirmatory is controversial in forensics due to false positives.

Despite the prevalence of numerous presumptive and confirmatory tests, there is no universal body fluid test for use at a crime scene. Other body fluids common at crime scenes are

urine, vaginal fluid, feces, and menstrual blood. As such, an assay that definitively identifies all body fluids regardless of type or combination would be indispensable for investigations. These factors, along with limited target specificity and sensitivity, have spurred the forensic community to work keenly to develop alternative analytical methods.

1.2.2 Alternative approaches to bfID

The alternative methods for presumptive and confirmatory bfID are derived from molecular biology and include microbial community profiling, epigenetics, and RNA. Microbial communities vary according to the origin of the body fluid or tissue (**Fig. 5A**). Profiling of these communities have focused on identifying vaginal secretions or distinguishing vaginal secretions from saliva. (18-21) For example, one study was unable to distinguish vaginal secretions from menstrual fluid, demonstrating one of the limitations of this method. (22) However, recent studies investigated microbial signatures from other body fluids as a method for distinguishing one fluid from another fluid. (22, 23) As this area of research grows, the microbial community profile may serve as an alternative method for bfID.

Epigenetic analyses have found that chromosome segments called *tissue-specific differentially methylated regions* show different DNA methylation profiles according to cell or tissue type (**Fig. 5A**). (24) This has been used in recent studies to investigate DNA methylation patterns between different body fluids. (25-31) While DNA methylation analysis is a promising technique, it does have some significant disadvantages: the initial bisulfite conversion and methylation analysis requires a relatively high concentration of DNA, thus limiting the amount of

DNA available for profiling, and DNA methylation sites are susceptible to change in response to environmental factors, aging, and disease. (32)

The most promising approach and the area with the most significant paradigm shift is transcriptomics (or analysis of RNA transcripts) for bfID (**Fig. 5A**). Different types of RNA have been studied, the most common being messenger RNA (mRNA) (33-42) and microRNA (miRNA) (43-51) and recently circular RNAs (circRNA) (52-54). An advantage of RNA profiling is that recovery from stains can be integrated into a typical DNA profiling workflow without compromising the DNA available for profiling via co-elution of DNA and DNA from a single cutting of evidence.

Messenger RNA is stable over long periods and has been purified from DNA extracts. (55, 56) Numerous specific and sensitive mRNA-

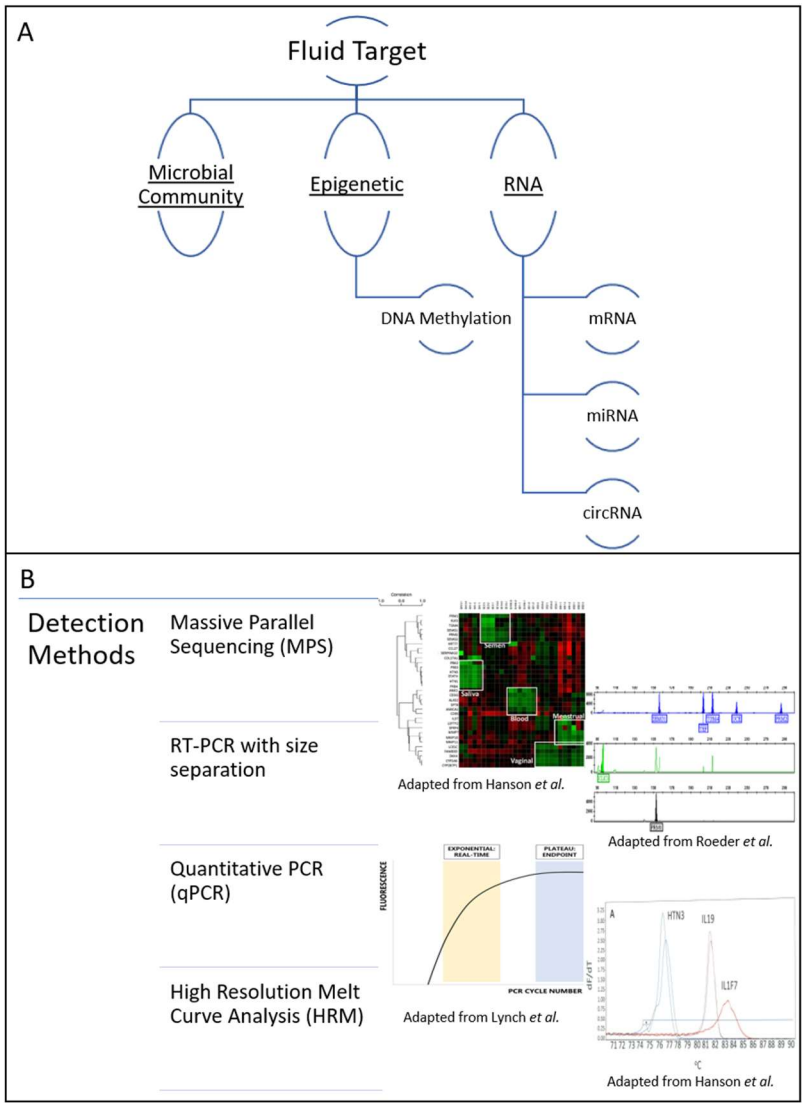

Figure 5: Alternative tests for body fluid identification. (A) Various biological targets have been assessed for body fluid methods. (B) The targets are detected using a variety of methods. (Adapted with permissions)

based bfID methods have been reported but require expensive instrumentation and can produce false negatives or positives. (37, 57) For example, the NanoString® barcoding system has shown the identification of blood and semen with mRNA markers but lacked specificity with other fluids without a statistical algorithm. Additionally, a 12-24-hour hybridization time is required per sample. (58, 59) Conversely, an amplification method for bfID that is easily incorporated into the forensic workflow should use instrumentation currently present in forensic labs. Furthermore, the procedure should be non-destructive to the DNA evidence, sensitive and accurate, and highly specific for each body fluid.

Existing methods for analysing RNA for bfID include massively parallel sequencing (MPS), reverse transcriptase PCR (RT-PCR), and quantitative RT-PCR (RT-qPCR) (**Fig. 5B**). (1) Massively parallel sequencing of RNA for bfID, specifically, have been used in several studies. (46, 60-65) The primary advantage of MPS is the number of RNA markers that can be used to identify each body fluid. However, while MPS is increasingly being used in forensic biology laboratories, it is expensive, time-consuming, and requires extensive training, bioinformatics knowledge, and vast computer storage capabilities. RT-PCR, another commonly used method, is sensitive and capable of detecting low-abundance mRNA obtained from limited samples. (33-38, 40-42) The most widely implemented approach in casework is endpoint RT-PCR coupled with capillary electrophoresis (CE), enabling the detection of several body fluids simultaneously, minimizing sample use and contextual effects (**Fig. 5B**). (33, 36-38) The third method is RT-qPCR typically used to calculate the difference between the nucleic target transcript and a reference or house-keeping gene, or to detect one nucleic target using a DNA intercalating dye. (39, 43-45) A limitation of qRT-PCR is the current restriction on the dyes that can be used, limiting the number

of markers targeted in a single reaction. Improvements such as high-resolution melting analysis have been proposed to overcome this limitation by detecting the melt temperatures of different sized fragments after amplification. (66, 67) Despite the multiple methods mentioned above for bfID, there is no preeminent method that provides an end-to-end solution for reliable, accurate, and fast confirmatory body fluid detection, a critical need by forensic laboratories.

1.2.3 Isothermal amplification methods

While many amplification methods can be used for bfID, an attractive method allowing ultra-rapid amplification of samples with high specificity has recently gained traction. In contrast to PCR, isothermal amplification avoids the need for thermocycling - the primary impediment to mobilizing the molecular assay to the point of need. A variety of new isothermal amplification methods now exists, including Loop-Mediated Isothermal Amplification (LAMP) (68), Recombinase Polymerase Amplification (RPA) (69), Rolling Circle Amplification (RCA) (70), Helicase Dependent Amplification (HAD) (71), Strand Displacement Amplification (SDA) (72), and Nucleic Acid Sequence Amplification (NASBA) (73) (**Fig. 6**). Most of these isothermal methods require simple technology (e.g., hot water bath), produce results in less than 30 minutes, and generate a readout using colorimetric dyes instead of fluorescent detection. In addition, a plethora of new isothermal diagnostic tests aimed at rapidly detecting mRNA targets has been published, with the additional goals of limiting the time and complexity of extraction and detection and improving portability.

Of the available methods, LAMP has emerged as a predominant assay offering equal sensitivity and specificity but significantly simpler and quicker analyses. (74-77) Some examples

of the RT-LAMP assay show in-tube amplification of as little as 2 copies of RNA target in a 25 µL reaction in 30 minutes with a color change detection method (78), 99.5% specificity and 500 copies/mL sensitivity in clinical samples in 30 minutes in-tube with fluorescent detection, (79) or simultaneous 21 sample-to-answer RT-LAMP using microfluidic technology. (80) The experiments described in this dissertation took advantage of the LAMP assay to provide a solution as a method for forensic bfID. In a recent study using isothermal amplification, a reverse-transcription LAMP method was used to analyze a blood target. A limit of detection of 10 femtograms of total RNA was demonstrated after a dilution of 1 ng total RNA from a 50 µl blood lysate. (74)

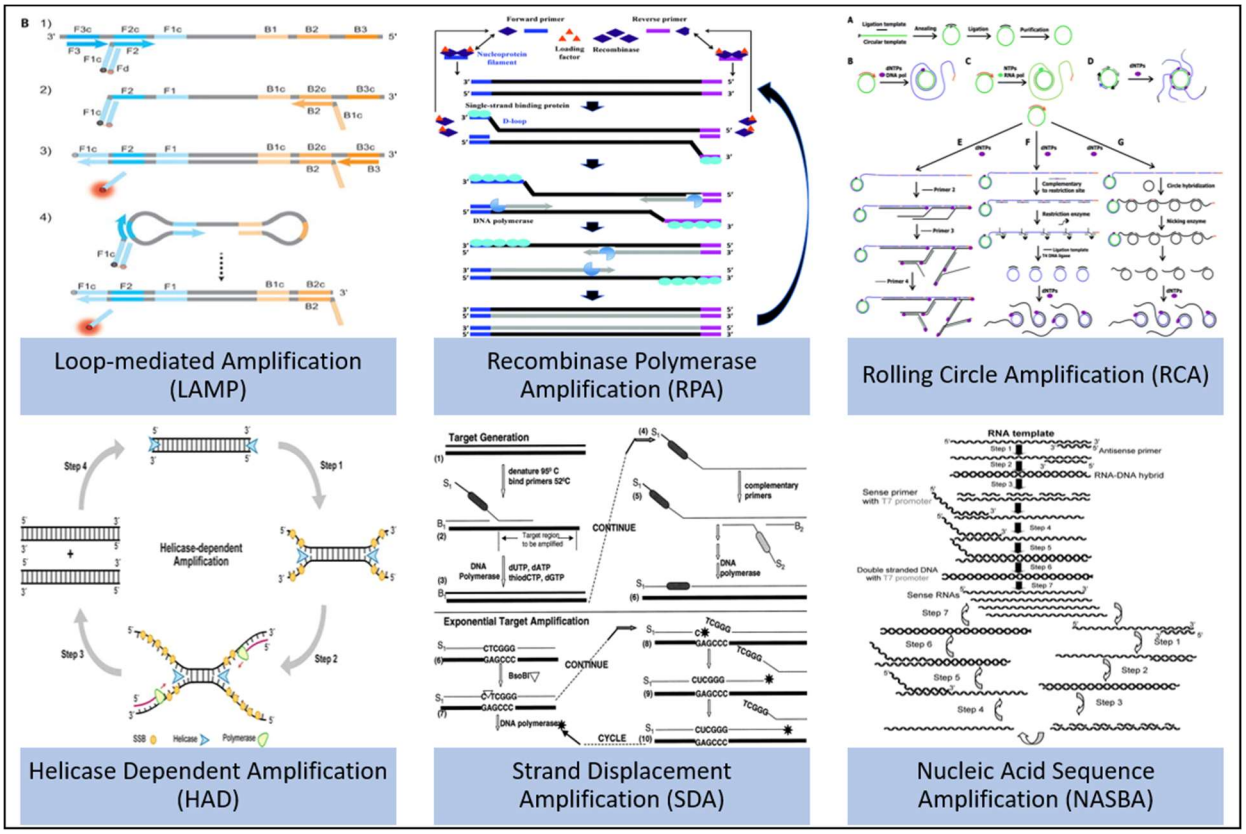

<u>Figure 6</u>: Isothermal amplification methods. Some methods used for forensic or clinical applications are LAMP (Tanner et al.), RPA (Li, Jia et al.), RCA (Ali et al.), HAD (Jeong et al.), SDA (Little et al.), and NASBA (Gill et al.). (Adapted with permissions)

LAMP differs from PCR in four ways; *First*, LAMP is an isothermal method, allowing for simple instrumentation without thermocycling hardware. *Second*, LAMP involves two sets of primers to identify specific target regions, with the option for an additional set of loop primers, whereas PCR uses a single set of primers (**Fig. 7A**). The use of 2-3 sets of primers allows for more annealing sites (6-8 distinct regions) and, thus, faster amplification. (81) One set of primers, the forward inner primer (FIP) and backward inner primer (BIP), are linked in the middle by four thymine nucleotides. One of the primer sites is the complementary sequence to a region upstream and facilitates the formation of a loop. The second set of primers anneals to sites ahead of the FIP or BIP primers (F3 and B3 primers). Upon annealing and elongation of FIP/BIP primers, the F3/B3 primers anneal behind the FIP/BIP primers, followed by strand displacement amplification via the *Bst* 2.0 WarmStart

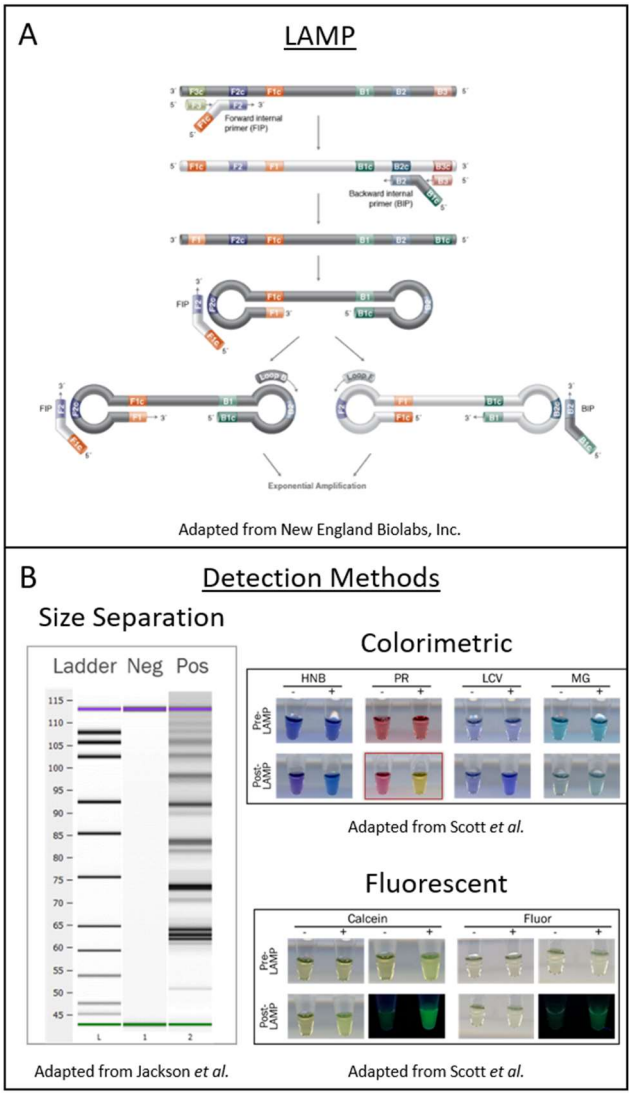

Figure 7: LAMP mechanism. (A) LAMP uses 4-6 primers for one target. The FIP primer anneals first, then the F3 primer anneals directly behind FIP. The polymerase performs SDA. The same reaction occurs with the BIP and B3 primers. A key-like structure is formed, and exponential amplification occurs. Loop primers can be incorporated for more priming sites. (B) Fragments produced from LAMP can be detected by various methods. (Adapted with permissions)

DNA Polymerase (New England Biolabs, Ipswich, MA, USA), thus releasing the product from the FIP/BIP primers creating a 'dumbbell-shaped' structure. (82) The third primer set, or loop primers, anneals to sites on the loop, typically in the area between the FIP/BIP region and its complementary sequence. With the incorporation of the loop primers, faster amplification ensues due to the additional annealing sites. *Third*, the resultant LAMP products include the target sequence but cover a range of fragment sizes, whereas PCR yields a single amplicon of a specific size. The same set of fragments is produced from each primer set, giving a unique profile when size separated. *Fourth*, LAMP is readily used with colorimetric indicators (e.g., hydroxynaphthol blue (HNB), phenol red (PR), leucocrystal violet (LCV), malachite green (MG)) or fluorescent indicators (e.g., Calcein, fluorescence), whereas PCR is coupled primarily with fluorescent labels (**Fig. 7B**). Using a colorimetric indicator enables detection of results using a low-cost analysis method (i.e., capturing an image) rather than an expensive analysis method for fluorescent detection (i.e., light source, filters, etc.). Due to these differences, LAMP is a great alternative to conventional PCR cycling.

Despite the increased complexity of primer design for LAMP, alternative detection methods (e.g., turbidity, color change, fragment pattern) not requiring fluorimeters or lateral flow strips are more readily available, and the necessary reagents may be purchased from multiple vendors. In addition, the LAMP method is capable of performing reverse transcription and target-specific amplification in a single-tube format. The *Bst* polymerase used in LAMP combines reverse transcription and DNA synthesis in a single enzyme. Relative to other isothermal methods demonstrating successful mRNA target amplification, LAMP consistently outperforms other formats in speed, with detection times of 30 min or less, vastly outclasses RT-

PCR in turnaround time and portability due to similar technology, however, in some cases, compromises are made in sensitivity. Nevertheless, this alternative strategy represents an essential front-line response for more rapid and cost-effective screening that can specifically amplify an mRNA target.

1.3 Advantages of Centrifugal Microfluidics for Clinical Diagnostics

1.3.1 Advantages of microfluidic technology

Microfluidic technologies are attractive for lab-based and fieldable applications due to their small footprint, minimal reagent/sample volumes, rapid analysis times, ease of use, automation, and, if needed, portability. (83, 84) When considered holistically, microfluidic technology can potentially address some of the core issues pertaining to protocols currently utilized in clinical and forensic labs and positively impact both communities. Sample preparation steps can be integrated seamlessly - potentially with smaller volumes to enable more efficient heat transfer and thus, expedited thermal cycling, resulting in a standard 120 min PCR reaction to be completed in 15 min. (85) Electrophoresis can be microminiaturized, and the mere fact that separation can be on the order of hundreds of seconds without loss of resolution shifts the paradigm. (86) Specifically, the cost-effective methods using rapid, iterative prototyping of microfluidic CDs (µCDs) with complex, intricate architectures have been developed for chemical and biochemical assays ranging from DNA purification and genome analysis to illicit drug detection and explosives sensing. (83, 87, 88) All functions, including data analysis, can easily be incorporated and operated via a smartphone, 6” touchscreen with Windows 10, or alternating current (AC) or battery power. Fluid movement in these devices is driven by centrifugal force

(rotation). Moreover, the microfluidic platform is ideal for point-of-analysis applications due to minimal external hardware (no bulky external pumps).

Centrifugal microfluidic systems are often referred to as 'lab-on-a-disc' as many assays are usually integrated in parallel. These 'lab-on-a-disc' devices integrate the labor-intensive operations of specific laboratory analytical assays onto a disc with the size of a CD-ROM, often with reduction in reagent volumes, reaction times and human intervention through on-chip automation. (89) Multiple forces influence fluid behavior within the microfluidic discs, including centrifugal (*eq. 1*), Coriolis (*eq. 2*), and Euler (*eq. 3*) forces (**Fig. 8**). The primary force is the centrifugal force (f_ω) that pumps liquids from the center of rotation outwards towards the edge of the disc and is proportional to the square of the angular velocity (ω), distance from center (r), and mass (ρ). The Coriolis force (f_C) facilitates the manipulation of the paths traversed by particles of varying sizes via redirection of flow. The Coriolis force is perpendicular to both the linear velocity and angular velocity, and proportional to twice the mass (ρ), angular velocity (ω), and fluid velocity (v). The third force,

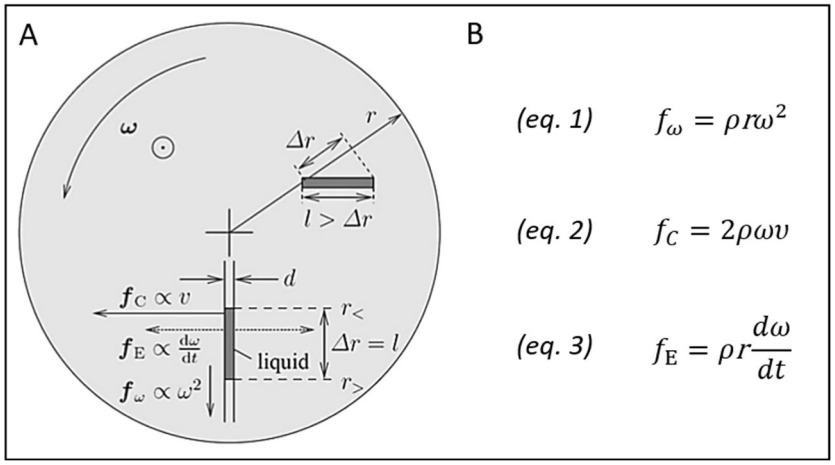

Figure 8: Centrifugal microfluidics. (A) Geometry and forces on a disk spinning at the angular velocity (ω) pointing out of the paper plane toward the reader. The radial coordinate is given by r. The liquid plug of diameter (d) and absolute length (l) extends between its inner and outer radial positions $r_<$ and $r_>$, respectively, with $\Delta r = r_> - r_<$ and $\bar{r} = 0.5(r_< + r_>)$. For a radially oriented plug, $\Delta r = l$, otherwise $\Delta r < l$. The liquid traveling at a speed (v) down the channel is exposed to the centrifugal force density, Euler force density, and Coriolis force density. (B) Equations for centrifugal force (*eq. 1*), Coriolis force (*eq. 2*), and Euler force (*eq. 3*). (Ducrée *et al*. with permission)

termed the Euler force (f_E), is perpendicular to the radial direction and enables mixing by the generation of a lateral motion during acceleration. The Euler force is proportional to the mass (ρ), distance from center (r), and scaling with the rotational acceleration ($\frac{d\omega}{dt}$). (90) Although additional forces may be generated by external hardware, the judicious application of these three forces facilitates control of radial fluid movement within a microfluidic disc using straightforward, motor-generated revolutions.

Along with impressive downsizing of hardware for laboratory assays and moving 'in-lab' detection methods to 'point-of-care' access, the ease of disc fabrication using low-cost materials can reduce the overhead cost for laboratories. The architecture can also be designed to accommodate multiplexing on a single disc (i.e., multiple samples analyzed on a single disc) or adapted for multiple applications (i.e., multiple targets analyzed in tandem). Specifically, using supplies available to the general public to fabricate discs also increases the likelihood that underfunded laboratories could replicate the cost-efficient microfluidic discs. The 'print-cut-laminate' (PCL) method is ideal for this purpose; a simple CO_2 laser cutter (or trophy etcher), office printer, and laminator can be used for fabrication (**Fig. 9**). (87) The materials chosen for fabrication vary according to the intended application. For the projects described herein, the materials used to fabricate microfluidic discs were clear and black transparencies (polyethylene terephthalate; PET, bPET) and heat-sensitive adhesive (HSA). In addition, polymethyl methacrylate (PMMA) and pressure-sensitive adhesive (PSA) were included in the fabrication process if an increase in volume was necessary, and 24-carat gold sheets for electrical conduction for microelectrophoresis.

The first stage in the PCL fabrication process is designing the microfluidic disc in software compatible with the laser cutter where 2D and 3D models can be drafted. Next, these designs are printed onto or cut through materials using an office printer or laser cutter before alignment and cohesion of layers via lamination. The fabrication process and materials are readily available and have been shown to be compatible with various biochemical assays. (91-93)

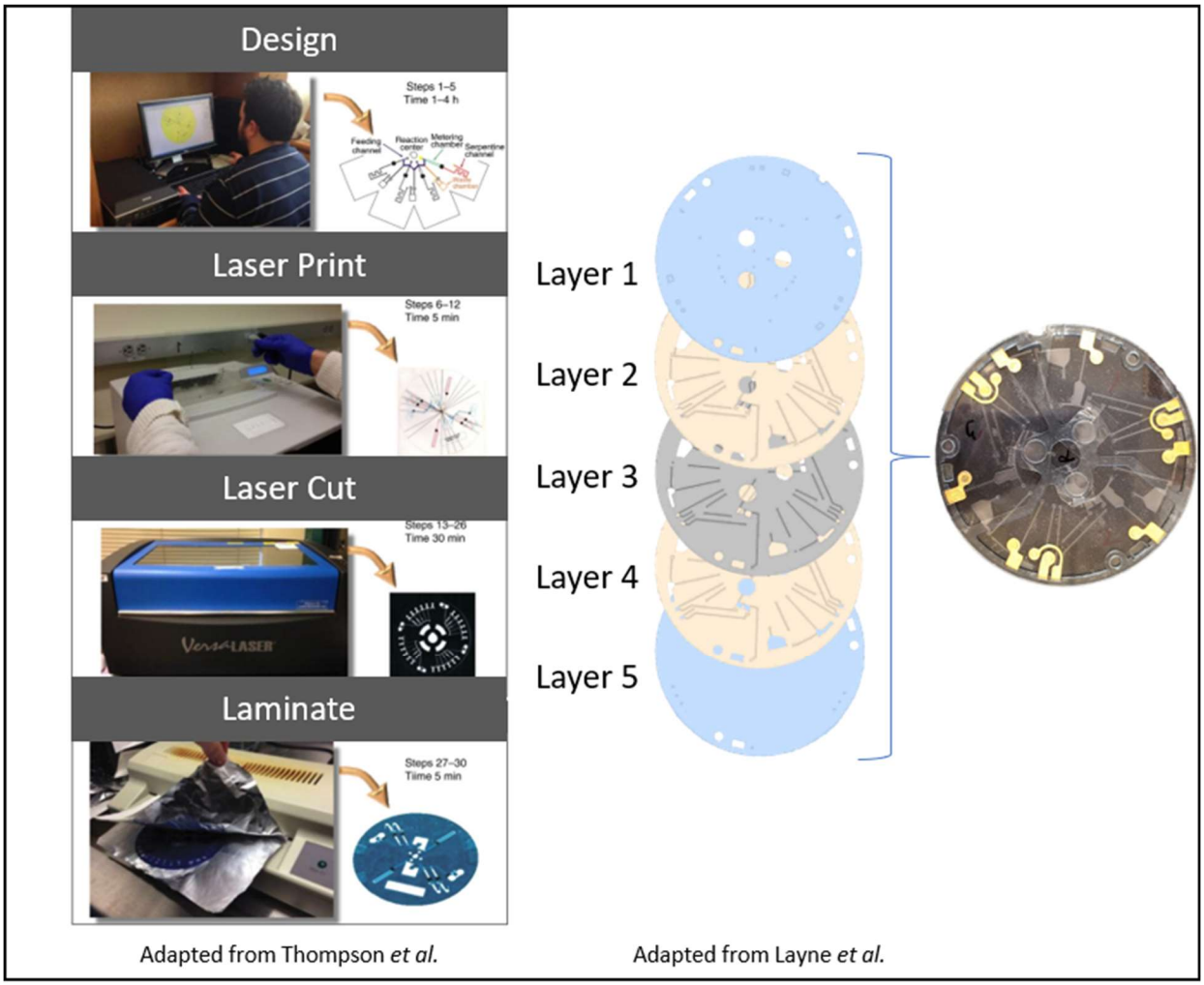

Figure 9: Fabrication method to produce microfluidic devices. Architecture was designed using AutoCAD software and electronically transferred to a CO_2 laser printer. The design was cut through various layers of various plastics and adhesives. All layers were aligned and laminated using a typical office laminator. Any accessory pieces were attached after lamination with adhesives. (Adapted with permissions)

1.3.2 Isolation and detection of SARS-CoV-2

The most recent outbreak of SARS-CoV was in 2020, claiming over 500,000 lives and more than 33 million cases across the world as of June 24, 2021. (94) This worldwide pandemic impelled scientists to build on previous SARS-CoV research to develop rapid diagnostics, therapeutics, and vaccines that would provide details about transmission and preventative measures to stop the spread of the disease. The detection of mRNA targets was adapted to a microfluidic platform to aid recent (and ongoing) efforts to combat the global coronavirus pandemic. Coronaviruses (CoV) are the largest group of viruses in the *Nidovirales* order (**Fig. 10A**). CoV are spherical, enveloped particles with a matrix protein capsid containing single-stranded RNA associated with a nucleoprotein. (95) These viruses have four main structural proteins - the spike, membrane, envelope, and nucleocapsid - in addition to a fifth structural protein

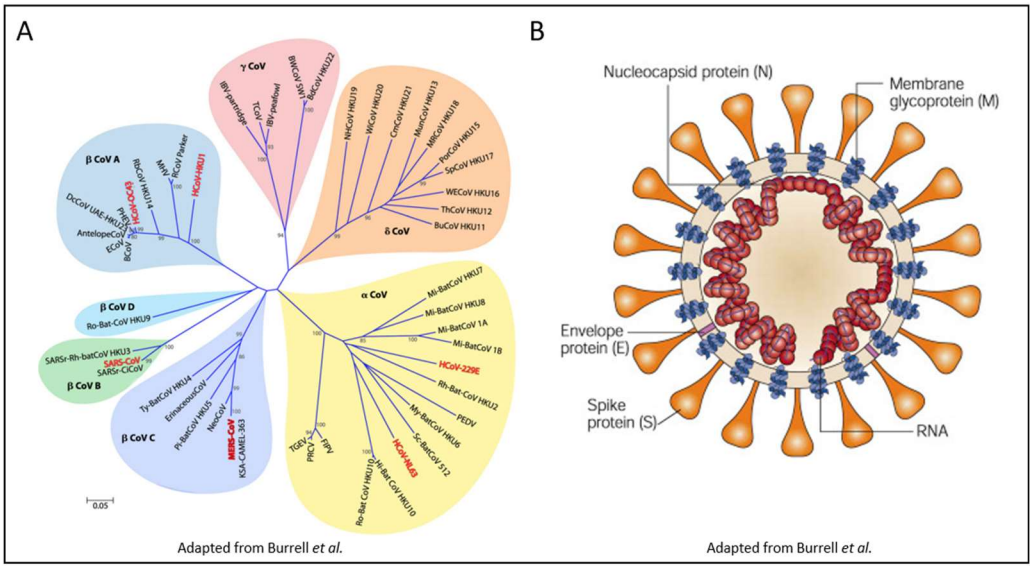

Figure 10: Coronaviruses phylogeny and physical attributes. (A) Phylogenetic tree of 50 coronaviruses from the subfamily *Coronavirinae*, family *Coronaviridae*, order *Nidovirales*. The scale bar indicates the estimated number of substitutions per 20 nucleotides. (B) Model of coronavirus virion structure, showing the supercoiling of the viral nucleocapsid under the envelope. (Adapted with permissions)

(hemagglutinin-esterase) present in a subset of β-coronaviruses (**Fig. 10B**). (96) The viral proteins invade the respiratory tract via the nose and cause symptoms associated with the 'common cold' after 3-day incubation.

This group was first identified as infectious bronchitis virus (IBV) in 1937, following research focusing on a (then) emergent respiratory infection of chickens. (97) The first human CoV were discovered in the 1960s via electron microscopy after the virus was recovered from various students with colds. (97) The next major outbreak in the human population was in China in 2002, when 8,098 cases of illness and 774 deaths (9% mortality rate) were attributed to an unusually lethal form of pneumonia. (96) This sudden acute respiratory syndrome (SARS) seen in patients was found to be due to a group 2b β-coronavirus. (98) Another β-coronavirus outbreak, termed Middle East Respiratory Syndrome-CoV (MERS-CoV), occurred in 2012. In this case, 955 cases and 333 deaths (40 % mortality) were confirmed after a series of highly pathogenic infections in Saudi Arabia and the Middle East. (96)

Diagnostic tests for SARS-CoV-2 must be capable of detecting low viral loads for early detection while avoiding cross-reactivity with other closely related coronaviruses. A third critical feature is the capability to deliver rapid results to best assist in effective containment measures. The current gold standard for molecular diagnoses of SARS-CoV-2 infection is by real-time reverse transcriptase-polymerase chain reaction (RT-PCR). RT-PCR allows for high-throughput of samples, sensitive fluorescent detection, and specific amplification of single targets. Although RT-PCR has been confirmed in multiple comparative studies to provide consistently high diagnostic sensitivity and specificity (typically above 95% in both categories), (99-101) RT-PCR

faces fundamental limitations in its ability to achieve detection times of less than one hour per sample. Doing so has typically required sophisticated instrumentation with unique sample cartridges, which adds to the up-front cost and requires additional technical expertise and training. (102)

To circumvent this, microfluidic technology has shown significant advantages for decreasing the overall time of PCR, the cost of reagents and hardware, and facilitating multiplexing. For example, Ji *et al*. developed a disc for direct RT-qPCR assay for simultaneous 16-target detection in four samples in less than 90 minutes (**Fig. 11**). (103) However, most RT-PCR assays necessitate extensive sample pre-processing, which adds to the total turnaround time

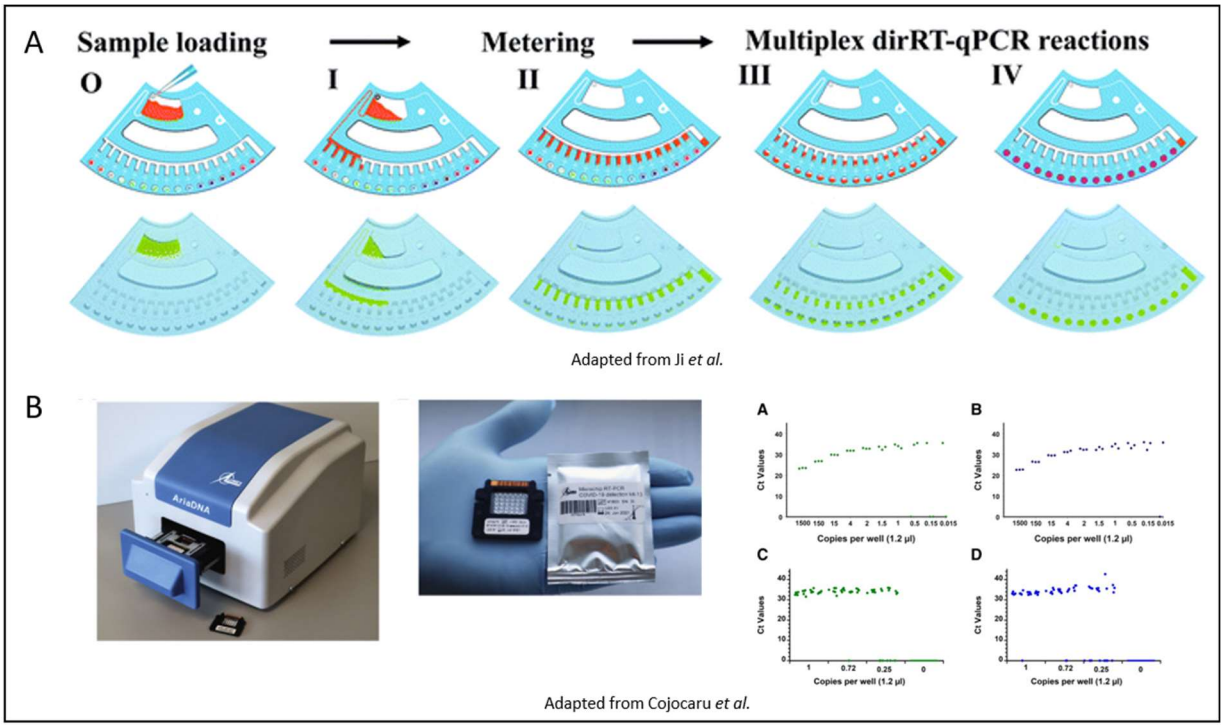

Figure 11: Published microfluidic techniques for detecting SARS-CoV-2 targets. (A) Characterization of the spinning profile via schematic diagram (upper) and photos (lower) showing the sequential steps of the fluid actuation. (B) Microchip for coronavirus disease 2019 detection with lyophilized reagents in the microwells. Limit of detection determination with 10-fold and 2-fold serial dilutions of extracted cultured viral RNA with N1 (green dots) and N2 (blue dots) primers/probes. (Adapted with permissions)

and requires additional costly kits. Critically, the demand for large quantities of high-grade reagents kits has, in some cases, exceeded the supply of available materials. These shortfalls have led to the development of a second class of molecular diagnostic assays meant to diversify the reagents and materials required from manufacturers and lower the total turnaround time and address the particular needs for POC testing.

1.3.3 Gene monitoring for transplanted organ tolerance

Discussion in Chapter 5 is a second clinical application adapted to microfluidic technology for the detection of immunoregulatory genes for monitoring organ tolerance. The goal of organ transplantation is immune tolerance leading to indefinite graft survival and prevention of chronic rejection. (104) Organ transplants are an annual necessity in hospitals worldwide, with nearly 8,000 of those being liver transplant surgeries in the US alone. (105) Specifically, liver transplants are the second most commonly transplanted organ in the US, primarily due to alcohol-related liver or other unknown diseases. (105) Majority of donated livers come from deceased adult male donors who are 50-64 years of age. (106) The liver is unique as it confronts several antigens in blood via the gastrointestinal tract and induces immune responses to pathogens. (107) To monitor the organ's functionality, the patient has to come in for testing weekly in the first months and then monthly in the first year. While these tests are performed out of necessity to prevent organ rejection, the time commitment for each visit to the hospital and cost of testing is a burden on the transplant patient. Currently, the 5-year survival rate of liver transplantation is 75%, and the patients must follow an immunosuppressive drug regimen for the remainder of their lives. (108) While these medications vitally prevent graft rejection by weakening the immune

response, their side effects include increased susceptibility to infections, sepsis, cancer, and renal failure. (109) To reduce susceptibility, patients may be weaned off these drugs, thus bolstering their immune system to fight off pathogens.

Research from the University of Toronto was conducted in this area to facilitate immunological tolerance and enable the cessation of long-term immunosuppression therapy. A panel of immunoregulatory genes was found from his study whose relative expression levels indicate allograft tolerance or rejection. The panel is detected via mRNA target amplification of an RNA sample and size separation via capillary electrophoresis (**Fig. 12**) (110) Following this finding, the Liver Immune Tolerance Marker Utilization Study (LITMUS) clinical trials began, in which patients are weaned off of their antirejection regimen based on his previously studied patterns of immunoregulatory biomarker expression in peripheral blood mononuclear cells (PBMCs). (111) Successful withdrawal from immunosuppressive medications alleviates the drugs' morbid side effects for patients.

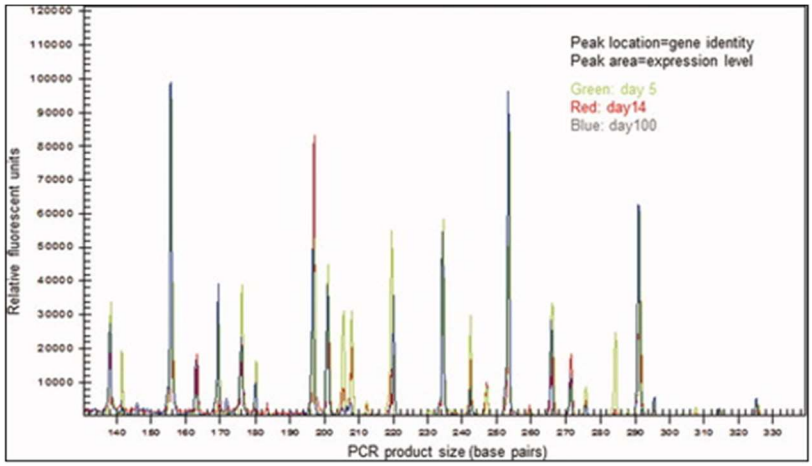

Figure 12: LITMUS panel fluorescently detected. Representative electropherograms corresponding to gene expression profiles generated from hepatic allograft mRNA samples on various postoperative days. (Adapted from Xie *et al*. with permission)

1.4 Description of Research Goals

This thesis focuses on the development of three distinct solutions for forensic body fluid identification and two solutions for clinical applications. Though all of the solutions target a decreased overall time and total volume of the amplification reactions, some also entail adapting biochemical assays for centrifugal microfluidics while maintaining the same high specificity and minute sensitivity as conventional methods. **Chapter 2** details the optimization of an isothermal amplification method for forensic body fluid identification. This method was coupled with a colorimetric dye to provide a simple output that indubitably discerns positive and negative results. As an objective analysis, the reactions were imaged, and the hue of the reaction defined results. Five body fluids commonly found at forensic crime scenes were amplified with primers corresponding to mRNA targets to show single fluid specificity and picogram level specificity.

Building on this optimization, **Chapter 3** details the 3D-printed device built for combined isothermal heating and image analysis of the colorimetric dye in the reactions. This device uses convective heating to heat the reactions and fans to circulate the heat for a relatively consistent temperature across all 96 wells. The device has a raspberry pi to image all 96 reactions with static LED lighting for image capture. The images are analyzed using Image J software for the hue value (or shade of color) of the isothermal reactions to determine each positive or negative result. With this device, both the heating and image analysis are automated to provide a one-step analysis method. Lastly, a mock study was conducted to compare the device with the conventional heating and image analysis method. This device was built for laboratory purposes, but due to its size could also be utilized on-scene.

As an alternative solution for forensic body fluid identification, **Chapter 4** details the adaptation of a 2-step RT-PCR and separation protocols for centrifugal microfluidics as an on-scene analysis method. A published panel of mRNA targets showed single fluid specificity in known single-source and mixture samples with good sensitivity for the same five body fluids. The panel consists of three plex's for buccal, blood (venous and menstrual), and common sexual assault (semen, seminal fluid, vaginal fluid) fluids. First, phase one of this project was the size separation of the mRNA targets, which was optimized using a centrifugal microfluidic disc to demonstrate this method's rapid, sensitive nature. The separation protocol mimicked the conventional capillary electrophoresis instruments used in forensic laboratories for fluorescent size separation. Next, phase two of this project involved optimizing the RT reaction for centrifugal microfluidics. Using the system from phase one, Peltier heaters sandwiched the RT chamber on the microfluidic disc to heat the reaction. The Peltier heaters demonstrated faster ramping rates than conventional thermal cycling for a much faster protocol. Single-source and mixture samples were converted to cDNA with minimal loss on the microfluidic disc.

The same integrated system was adapted for two clinical applications that involved the amplification of mRNA targets. **Chapter 5** details the optimization of two PCR protocols that reduced the overall assay time to detect a SARS-CoV-2 target and panel of genes to determine organ tolerance. For the SARS-CoV-2 target, clinical samples were amplified in a microfluidic disc in <15 minutes with varying target concentrations based on conventional qPCR data. For the panel, initial experiments showed the overall assay time could be reduced by 11 minutes after decreasing the time for one of the steps in the protocol. Additionally, the total volume of the

reaction could be reduced to a quarter reaction and still provide fluorescent data for all the targets in the panel.

In summary, **Chapter 6** details the overall conclusions for each project in this dissertation. A central theme throughout the projects was reducing the overall assay time, reducing the total volume of the reaction, achieving reasonable specificity and sensitivity, and providing a cost-efficient method for various forensic and clinical applications. Some of the projects were designed to provide a solution for either laboratory or point-of-care testing. Overall, the studies detailed in the dissertation demonstrate rapid technology that addresses some of the core issues pertaining to the conventional methods utilized in the clinical and forensic communities.

1.5 References

1. Lynch C, Fleming R. RNA-based approaches for body fluid identification in forensic science. WIREs Forensic Science. [https://doi.org/10.1002/wfs2.1407]. 2020 2020/11/21;n/a(n/a):e1407.

2. Virkler K, Lednev IK. Analysis of body fluids for forensic purposes: from laboratory testing to non-destructive rapid confirmatory identification at a crime scene. Forensic science international. 2009;188(1-3):1-17.

3. White EH, Zafiriou O, Kagi HH, Hill JH. Chemilunimescence of luminol: The chemcial reaction. Journal of the American Chemical Society. 1964;86(5):940-1.

4. Butler JM. Chapter 4 - Sample Collection, Storage, and Characterization. Fundamentals of Forensic DNA Typing. San Diego: Academic Press; 2010;79-97.

5. Sloots J, Lalonde W, Reid B, Millman J. Kastle–Meyer blood test reagents are deleterious to DNA. Forensic Science International. 2017 2017/12/01/;281:141-6.

6. Tobe SS, Watson N, Daeid NN. Evaluation of six presumptive tests for blood, their specificity, sensitivity, and effect on high molecular-weight DNA. Journal of forensic sciences. 2007 2006/12/07;52(1):102-9.

7. Cox M. A study of the sensitivity and specificity of four presumptive tests for blood. Journal of forensic sciences. 1991;36(5):1503-11.

8. Garner DD, Cano KM, Peimer RS, Yeshion TE. An Evaluation of Tetramethylbenzidine as a Presumptive Test for Blood. Journal of Forensic Sciences. 1976;21(4):6.

9. Vennemann M, Scott G, Curran L, Bittner F, Tobe SS. Sensitivity and specificity of presumptive tests for blood, saliva and semen. Forensic science, medicine, and pathology. 2014;10(1):69-75.

10. Greaves AV. THE USE OF TAKAYAMA'S SOLUTION IN THE IDENTIFICATION OF BLOOD STAINS. BMJ. 1932 1932-05-21;1(3724):932-3.

11. Stewart V, Deacon P, Zahra N, Uchimoto ML, Farrugia KJ. The effect of mark enhancement techniques on the presumptive and confirmatory tests for blood. Science & Justice. 2018 2018/11/01/;58(6):386-96.

12. Gaensslen RE. Sourcebook in forensic serology, immunology, and biochemistry: US Department of Justice, National Institute of Justice Washington, DC, 1983.

13. Davidson G, Jalowiecki TB. Acid phosphatase screening — Wetting test paper or wetting fabric and test paper? Science & Justice. 2012 2012/06/01/;52(2):106-11.

14. Lewis J, Baird A, McAlister C, Siemieniuk A, Blackmore L, McCabe B, et al. Improved detection of semen by use of direct acid phosphatase testing. Science & justice : journal of the Forensic Science Society. 2013;53(4):385-94.

15. Gonçalves ABR, de Oliveira CF, Carvalho EF, Silva DA. Comparison of the sensitivity and specificity of colorimetric and immunochromatographic presumptive methods for forensic semen detection. Forensic Science International: Genetics Supplement Series. 2017;6:e481-e3.

16. Ricci U, Carboni I, Torricelli F. False-Positive Results with Amylase Testing of Citrus Fruits. Journal of Forensic Sciences. 2014;59(5):1410-2.

17. Wornes DJ, Speers SJ, Murakami JA. The evaluation and validation of Phadebas® paper as a presumptive screening tool for saliva on forensic exhibits. Forensic Science International. 2018 2018/07/01/;288:81-8.

18. Fleming RI, Harbison S. The use of bacteria for the identification of vaginal secretions. Forensic Science International: Genetics. 2010;4(5):311-5.

19. Giampaoli S, Berti A, Valeriani F, Gianfranceschi G, Piccolella A, Buggiotti L, et al. Molecular identification of vaginal fluid by microbial signature. Forensic Science International: Genetics. 2012;6(5):559-64.

20. Akutsu T, Motani H, Watanabe K, Iwase H, Sakurada K. Detection of bacterial 16S ribosomal RNA genes for forensic identification of vaginal fluid. Legal Medicine. 2012 2012/05/01/;14(3):160-2.

21. Hanssen EN, Avershina E, Rudi K, Gill P, Snipen L. Body fluid prediction from microbial patterns for forensic application. Forensic Science International: Genetics. 2017;30:10-7.

22. Dobay A, Haas C, Fucile G, Downey N, Morrison HG, Kratzer A, et al. Microbiome-based body fluid identification of samples exposed to indoor conditions. Forensic Science International: Genetics. 2019;40:105-13.

23. Hanssen EN, Liland KH, Gill P, Snipen L. Optimizing body fluid recognition from microbial taxonomic profiles. Forensic Science International: Genetics. 2018;37:13-20.

24. Kitamura E, Igarashi J, Morohashi A, Hida N, Oinuma T, Nemoto N, et al. Analysis of tissue-specific differentially methylated regions (TDMs) in humans. Genomics. 2007 2007/03/01/;89(3):326-37.

25. Lee HY, Park MJ, Choi A, An JH, Yang WI, Shin K-J. Potential forensic application of DNA methylation profiling to body fluid identification. International Journal of Legal Medicine. 2012 2012/01/01;126(1):55-62.

26. Choi A, Shin K-J, Yang WI, Lee HY. Body fluid identification by integrated analysis of DNA methylation and body fluid-specific microbial DNA. International Journal of Legal Medicine. 2014 2014/01/01;128(1):33-41.

27. An JH, Choi A, Shin K-J, Yang WI, Lee HY. DNA methylation-specific multiplex assays for body fluid identification. International Journal of Legal Medicine. 2013 2013/01/01;127(1):35-43.

28. Park J-L, Kwon O-H, Kim JH, Yoo H-S, Lee H-C, Woo K-M, et al. Identification of body fluid-specific DNA methylation markers for use in forensic science. Forensic Science International: Genetics. 2014;13:147-53.

29. Antunes J, Balamurugan K, Duncan G, McCord B. Tissue-Specific DNA Methylation Patterns in Forensic Samples Detected by Pyrosequencing®. In: Lehmann U, Tost J, editors. Pyrosequencing: Methods and Protocols. New York, NY: Springer New York; 2015;397-409.

30. Lee HY, An JH, Jung S-E, Oh YN, Lee EY, Choi A, et al. Genome-wide methylation profiling and a multiplex construction for the identification of body fluids using epigenetic markers. Forensic Science International: Genetics. 2015;17:17-24.

31. Silva DSBS, Antunes J, Balamurugan K, Duncan G, Alho CS, McCord B. Developmental validation studies of epigenetic DNA methylation markers for the detection of blood, semen and saliva samples. Forensic Science International: Genetics. 2016;23:55-63.

32. Forat S, Huettel B, Reinhardt R, Fimmers R, Haidl G, Denschlag D, et al. Methylation Markers for the Identification of Body Fluids and Tissues from Forensic Trace Evidence. PLOS ONE. 2016;11(2):e0147973.

33. Fleming RI, Harbison S. The development of a mRNA multiplex RT-PCR assay for the definitive identification of body fluids. Forensic Science International: Genetics. 2010 2010/07/01/;4(4):244-56.

34. Haas C, Hanson E, Morling N, Ballantyne J. Collaborative EDNAP exercises on messenger RNA/DNA co-analysis for body fluid identification (blood, saliva, semen) and STR profiling. Forensic Science International: Genetics Supplement Series. 2011 12/01;3.

35. Hanson E, Haas C, Jucker R, Ballantyne J. Identification of skin in touch/contact forensic samples by messenger RNA profiling. Forensic Science International: Genetics Supplement Series. 2011 12/01;3:e305-e6.

36. Haas C, Hanson E, Ballantyne J. Capillary Electrophoresis of a Multiplex Reverse Transcription-Polymerase Chain Reaction to Target Messenger RNA Markers for Body Fluid Identification. In: Alonso A, editor. DNA Electrophoresis Protocols for Forensic Genetics. Totowa, NJ: Humana Press; 2012;169-83.

37. Richard ML, Harper KF, Craig RF, Onorato AF, Robertson JF, Donfack J. Evaluation of mRNA marker specificity for the identification of five human body fluids by capillary electrophoresis. Forensic Science International: Genetics. 2012 20120522 DCOM- 20120925;6(4):452-60.

38. Roeder AD, Haas C. mRNA profiling using a minimum of five mRNA markers per body fluid and a novel scoring method for body fluid identification. International Journal of Legal Medicine. 2013 2013/07/01;127(4):707-21.

39. Park S-M, Park S-Y, Kim J-H, Kang T-W, Park J-L, Woo K-M, et al. Genome-wide mRNA profiling and multiplex quantitative RT-PCR for forensic body fluid identification. Forensic Science International: Genetics. 2013;7(1):143-50.

40. Haas C, Hanson E, Anjos MJ, Ballantyne KN, Banemann R, Bhoelai B, et al. RNA/DNA co-analysis from human menstrual blood and vaginal secretion stains: results of a fourth and fifth collaborative EDNAP exercise. Forensic science internationalGenetics. 2014;8(1):203-12.

41. Roeder AD, Haas C. Body Fluid Identification Using mRNA Profiling. In: Goodwin W, editor. Forensic DNA Typing Protocols. New York, NY: Springer New York; 2016;13-31.

42. Albani PP, Fleming R. Novel messenger RNAs for body fluid identification. Science & Justice. 2018 2018/03/01/;58(2):145-52.

43. Sauer E, Reinke A-K, Courts C. Validation of forensic body fluid identification based on empirically normalized miRNA expression data. Forensic Science International: Genetics Supplement Series. 2015;5:e462-e4.

44. Li Z, Bai P, Peng D, Long B, Zhang L, Liang W. Influences of different RT-qPCR methods on forensic body fluid identification by microRNA. Forensic Science International: Genetics Supplement Series. 2015;5:e295-e7.

45. Sauer E, Reinke A-K, Courts C. Differentiation of five body fluids from forensic samples by expression analysis of four microRNAs using quantitative PCR. Forensic Science International: Genetics. 2016;22:89-99.

46. Wang Z, Zhou D, Cao Y, Hu Z, Zhang S, Bian Y, et al. Characterization of microRNA expression profiles in blood and saliva using the Ion Personal Genome Machine System (Ion PGM System). Forensic Science International: Genetics. 2016;20:140-6.

47. Dumache R Fau - Ciocan V, Ciocan V Fau - Muresan C, Muresan C Fau - Rogobete AF, Rogobete Af Fau - Enache A, Enache A. Circulating MicroRNAs as Promising Biomarkers in Forensic Body Fluids Identification. (1433-6510 (Print)).

48. Sirker M, Fimmers R, Schneider PM, Gomes I. Evaluating the forensic application of 19 target microRNAs as biomarkers in body fluid and tissue identification. Forensic Science International: Genetics. 2017;27:41-9.

49. Tian H, Lv M, Li Z, Peng D, Tan Y, Wang H, et al. Semen-specific miRNAs: Suitable for the distinction of infertile semen in the body fluid identification? Forensic Science International: Genetics. 2018;33:161-7.

50. O'Leary KRaG, Claire L. Investigating the Isolation and Amplification of microRNAs for Forensic Body Fluid Identification. MicroRNA. 2018;7(3):187-94.

51. Mayes C, Seashols-Williams S, Hughes-Stamm S. A capillary electrophoresis method for identifying forensically relevant body fluids using miRNAs. Legal Medicine. 2018 2018/01/01/;30:1-4.

52. Zhang Y, Liu B, Shao C, Xu H, Xue A, Zhao Z, et al. Evaluation of the inclusion of circular RNAs in mRNA profiling in forensic body fluid identification. International Journal of Legal Medicine. 2018 2018/01/01;132(1):43-52.

53. Song F, Luo H, Xie M, Zhu H, Hou Y. Microarray expression profile of circular RNAs in human body fluids. Forensic Science International: Genetics Supplement Series. 2017 2017/12/01/;6:e55-e6.

54. Liu B, Song F, Yang Q, Zhou Y, Shao C, Shen Y, et al. Characterization of tissue-specific biomarkers with the expression of circRNAs in forensically relevant body fluids. International Journal of Legal Medicine. 2019 2019/09/01;133(5):1321-31.

55. Zubakov D, Hanekamp E, Kokshoorn M, van Ijcken W, Kayser M. Stable RNA markers for identification of blood and saliva stains revealed from whole genome expression analysis of time-wise degraded samples. International journal of legal medicine. 2008;122(2):135-42.

56. Setzer M, Juusola J, Ballantyne J. Recovery and stability of RNA in vaginal swabs and blood, semen, and saliva stains. Journal of Forensic Sciences. 2008 2008/03/19;53(2):296-305.

57. Haas C, Klesser B, Maake C, Bär W, Kratzer A. mRNA profiling for body fluid identification by reverse transcription endpoint PCR and realtime PCR. Forensic Science International: Genetics. 2009 2008/11/14;3(2):80-8.

58. Park J-L, Park S-M, Kim J-H, Lee H-C, Lee S-H, Woo K-M, et al. Forensic Body Fluid Identification by Analysis of Multiple RNA Markers Using NanoString Technology. Genomics & informatics. 2013;11(4):277-81.

59. Danaher P, White RL, Hanson EK, Ballantyne J. Facile semi-automated forensic body fluid identification by multiplex solution hybridization of NanoString® barcode probes to specific mRNA targets. Forensic Science International: Genetics. 2015 2015/01/01/;14(Supplement C):18-30.

60. Lin M-H, Albani PP, Fleming R. Degraded RNA transcript stable regions (StaRs) as targets for enhanced forensic RNA body fluid identification. Forensic Science International: Genetics. 2016;20:61-70.

61. Seashols-Williams S, Lewis C, Calloway C, Peace N, Harrison A, Hayes-Nash C, et al. High-throughput miRNA sequencing and identification of biomarkers for forensically relevant biological fluids. Electrophoresis. 2016;37(21):2780-8.

62. Wang Z, Zhao X, Hou Y. Exploring of microRNA markers for semen stains using massively parallel sequencing. Forensic Science International: Genetics Supplement Series. 2017 2017/12/01/;6:e107-e9.

63. Hanson E, Ingold S, Haas C, Ballantyne J. Messenger RNA biomarker signatures for forensic body fluid identification revealed by targeted RNA sequencing. Forensic Science International: Genetics. 2018 2018/05/01/;34:206-21.

64. Ingold S, Dørum G, Hanson E, Berti A, Branicki W, Brito P, et al. Body fluid identification using a targeted mRNA massively parallel sequencing approach – results of a EUROFORGEN/EDNAP collaborative exercise. Forensic Science International: Genetics. 2018 2018/05/01/;34:105-15.

65. Dørum G, Ingold S, Hanson E, Ballantyne J, Russo G, Aluri S, et al. Predicting the origin of stains from whole miRNome massively parallel sequencing data. Forensic Science International: Genetics. 2019;40:131-9.

66. Hanson EK, Ballantyne J. Multiplex high resolution melt (HRM) messenger RNA profiling assays for body fluid identification. Forensic Science International: Genetics Supplement Series. 2013;4(1):e125-e6.

67. Antunes J, Silva DSBS, Balamurugan K, Duncan G, Alho CS, McCord B. High-resolution melt analysis of DNA methylation to discriminate semen in biological stains. Analytical biochemistry. 2016 2016/02//;494:40-5.

68. Tanner NA, Zhang Y, Evans TC. Simultaneous multiple target detection in real-time loop-mediated isothermal amplification. BioTechniques. 2012 2012/08/01;53(2):81-9.

69. Li J, Macdonald J, Von Stetten F. Review: a comprehensive summary of a decade development of the recombinase polymerase amplification. The Analyst. 2019 2019-01-01;144(1):31-67.

70. Ali MM, Li F, Zhang Z, Zhang K, Kang D-K, Ankrum JA, et al. Rolling circle amplification: a versatile tool for chemical biology, materials science and medicine. Chemical Society Reviews. 2014 2014-01-01;43(10):3324.

71. Jeong Y-J, Park K, Kim D-E. Isothermal DNA amplification in vitro: the helicase-dependent amplification system. Cellular and Molecular Life Sciences. 2009 2009-10-01;66(20):3325-36.

72. Little MC, Andrews J, Moore R, Bustos S, Jones L, Embres C, et al. Strand Displacement Amplification and Homogeneous Real-Time Detection Incorporated in a Second-Generation DNA Probe System, BDProbeTecET. Clinical Chemistry. 1999 1999-06-01;45(6):777-84.

73. Gill P, Ghaemi A. Nucleic Acid Isothermal Amplification Technologies - A Review. Nucleosides, Nucleotides & Nucleic Acids. [Article]. 2008;27(3):224-43.

74. Su C-W, Li C-Y, Lee J, Ji D-D, Li S-Y, Daniel B, et al. A novel application of real-time RT-LAMP for body fluid identification: using HBB detection as the model. Forensic Science, Medicine & Pathology. [Article]. 2015 April 16, 2015;11(2):208-15.

75. Satoh T, Kouroki S, Ogawa K, Tanaka Y, Matsumura K, Iwase S. Development of mRNA-based body fluid identification using reverse transcription loop-mediated isothermal amplification. Analytical and Bioanalytical Chemistry. [journal article]. 2018 July 01;410(18):4371-8.

76. Tsai L-C, Su C-W, Lee JC-I, Lu Y-S, Chen H-C, Lin Y-C, et al. The detection and identification of saliva in forensic samples by RT-LAMP. Forensic Science, Medicine and Pathology. 2018 2018/12/01;14(4):469-77.

77. Jackson KR, Layne T, Dent DA, Tsuei A, Li J, Haverstick DM, et al. A novel loop-mediated isothermal amplification method for identification of four body fluids with smartphone detection. Forensic Science International: Genetics. 2020 2020/03/01/;45:102195.

78. Huang WE, Lim B, Hsu C-C, Xiong D, Wu W, Yu Y, et al. RT-LAMP for rapid diagnosis of coronavirus SARS-CoV-2. Microbial Biotechnology. [https://doi.org/10.1111/1751-7915.13586]. 2020 2020/07/01;13(4):950-61.

79. Jiang M, Pan W, Arastehfar A, Fang W, ling L, Fang H, et al. Development and validation of a rapid single-step reverse transcriptase loop-mediated isothermal amplification (RT-LAMP) system potentially to be used for reliable and high-throughput screening of COVID-19. medRxiv. 2020:2020.03.15.20036376.

80. Tian F, Liu C, Deng J, Han Z, Zhang L, Chen Q, et al. A fully automated centrifugal microfluidic system for sample-to-answer viral nucleic acid testing. Science China Chemistry. 2020 2020/10/01;63(10):1498-506.

81. Notomi T, Okayama H, Masubuchi H, Yonekawa T, Watanabe K, Amino N, et al. Loop-mediated isothermal amplification of DNA. Nucleic Acids Research. 2000 April 15, 2000;28(12).

82. Tanner NA, Zhang Y, Evans TC. Visual detection of isothermal nucleic acid amplification using pH-sensitive dyes. BioTechniques. 2015 2015/02/01;58(2):59-68.

83. Krauss ST, Remcho TP, Lipes SM, Aranda R, Maynard HP, Shukla N, et al. Objective Method for Presumptive Field-Testing of Illicit Drug Possession Using Centrifugal Microdevices and Smartphone Analysis. Analytical Chemistry. 2016 2016/09/06;88(17):8689-97.

84. Whitesides GM. The origins and the future of microfluidics. Nature. 2006 2006/07/01;442(7101):368-73.

85. Li Z, Ju R, Sekine S, Zhang D, Zhuang S, Yamaguchi Y. All-in-one microfluidic device for on-site diagnosis of pathogens based on an integrated continuous flow PCR and electrophoresis biochip. Lab on a Chip. [10.1039/C9LC00305C]. 2019;19(16):2663-8.

86. Yeo JC, Wang Z, Lim CT. Microfluidic size separation of cells and particles using a swinging bucket centrifuge. Biomicrofluidics. 2015;9(5).

87. Thompson BL, Ouyang Y, Duarte GRM, Carrilho E, Krauss ST, Landers JP. Inexpensive, rapid prototyping of microfluidic devices using overhead transparencies and a laser print, cut and laminate fabrication method. Nature Protocols. 2015 2015/06/01;10(6):875-86.

88. Jackson KR, Borba JC, Meija M, Mills DL, Haverstick DM, Olson KE, et al. DNA purification using dynamic solid-phase extraction on a rotationally-driven polyethylene-terephthalate microdevice. Analytica Chimica Acta. 2016 2016/09/21/;937:1-10.

89. Henderson B, Kinahan DJ, Ducrée J. The Centrifugal Microfluidic: Lab-on-a-Disc Platform. Microfluidics for Biologists: Springer International Publishing; 2016;115-44.

90. Ducr é e J, Haeberle S, Lutz S, Pausch S, von Stetten F, Zengerle R. The centrifugal microfluidic Bio-Disk platform. Journal of Micromechanics and Microengineering. 2007;17:S103-S15.

91. Augustine R, Hasan A, Das S, Ahmed R, Mori Y, Notomi T, et al. Loop-Mediated Isothermal Amplification (LAMP): A Rapid, Sensitive, Specific, and Cost-Effective Point-of-Care Test for Coronaviruses in the Context of COVID-19 Pandemic. Biology. 2020;9(8):182.

92. Qin P, Park M, Alfson KJ, Tamhankar M, Carrion R, Patterson JL, et al. Rapid and Fully Microfluidic Ebola Virus Detection with CRISPR-Cas13a. ACS Sensors. 2019 2019/04/26;4(4):1048-54.

93. Xiong H, Ye X, Li Y, Wang L, Zhang J, Fang X, et al. Rapid Differential Diagnosis of Seven Human Respiratory Coronaviruses Based on Centrifugal Microfluidic Nucleic Acid Assay. Analytical Chemistry. 2020 2020-11-03;92(21):14297-302.

94. Allen J, Almukhtar S, Aufrichtig A, Barnard A, Bloch M, Cahalan S, et al. Coronavirus in the U.S.: Latest Map and Case Count. [Web Page] The New York Times; 2021 [updated 2021 May 19, 2021; cited]; Available from: https://www.nytimes.com/interactive/2021/us/covid-cases.html.

95. Tyrrell DA, Myint SH. Coronaviruses. Medical Microbiology 4th edition. 1996.

96. Maier HJ, Bickerton E, Britton P. Coronaviruses. Methods and protocols. 2015.

97. McIntosh K, Peiris JSM. Coronaviruses. Clinical Virology, Third Edition: American Society of Microbiology; 2009.

98. Arena F, Pollini S, Rossolini GM, Margaglione M. Summary of the Available Molecular Methods for Detection of SARS-CoV-2 during the Ongoing Pandemic. International Journal of Molecular Sciences. 2021 2021-01-28;22(3):1298.

99. Corman VM, Landt O, Kaiser M, Molenkamp R, Meijer A, Chu DK, et al. Detection of 2019 novel coronavirus (2019-nCoV) by real-time RT-PCR. Eurosurveillance. 2020 2020-01-23;25(3).

100. Waller JV, Kaur P, Tucker A, Lin KK, Diaz MJ, Henry TS, et al. Diagnostic Tools for Coronavirus Disease (COVID-19): Comparing CT and RT-PCR Viral Nucleic Acid Testing. American Journal of Roentgenology. 2020 2020/10/01;215(4):834-8.

101. van Kasteren PB, van der Veer B, van den Brink S, Wijsman L, de Jonge J, van den Brandt A, et al. Comparison of seven commercial RT-PCR diagnostic kits for COVID-19. Journal of clinical virology : the official publication of the Pan American Society for Clinical Virology. 2020;128:104412-.

102. Pfefferle S, Reucher S, Nörz D, Lütgehetmann M. Evaluation of a quantitative RT-PCR assay for the detection of the emerging coronavirus SARS-CoV-2 using a high throughput system. Eurosurveillance. 2020 2020-03-05;25(9).

103. Ji M, Xia Y, Loo JF-C, Li L, Ho H-P, He J, et al. Automated multiplex nucleic acid tests for rapid detection of SARS-CoV-2, influenza A and B infection with direct reverse-transcription quantitative PCR (dirRT-qPCR) assay in a centrifugal microfluidic platform. RSC Advances. [10.1039/D0RA04507A]. 2020;10(56):34088-98.

104. Madariaga MLL, Kreisel D, Madsen JC. Organ-specific differences in achieving tolerance. Current Opinion in Organ Transplantation. 2015 2015-08-01;20(4):392-9.

105. Fayek SA, Quintini C, Chavin KD, Marsh CL. The Current State of Liver Transplantation in the United States. American Journal of Transplantation. 2016;16(11).

106. Recipients SRoT. OPTN/SRTR 2019 Annual Data Report: Liver Report. U.S. Department of Health & Human Services, Services USDoHH; 2020 Contract No.: Document Number|.

107. Karimi MH, Geramizadeh B, Malek-Hosseini SA. Tolerance Induction in Liver. International journal of organ transplantation medicine. 2015;6(2):45-54.

108. Watt KDS, Pedersen RA, Kremers WK, Heimbach JK, Charlton MR. Evolution of Causes and Risk Factors for Mortality Post-Liver Transplant: Results of the NIDDK Long-Term Follow-Up Study. American Journal of Transplantation. 2010;10(6).

109. Moini M, Schilsky ML, Tichy EM. Review on immunosuppression in liver transplantation. World journal of hepatology. 2015;7(10):1355-68.

110. Xie L, Ichimaru N, Morita M, Chen J, Zhu P, Wang J, et al. Identification of a novel biomarker gene set with sensitivity and specificity for distinguishing between allograft rejection and tolerance. Liver Transplantation. 2011;18(4).

111. Levy GA. Liver Immune Tolerance Marker Utilization Study (LITMUS). ClinicalTrials.gov: NIH; 2015 [updated 2015 April 28, 2021; cited]; The purpose of this study is to validate and test a tolerance gene expression profile for the identification of operationally tolerant liver transplant recipients, allowing for the successful withdrawal of immunosuppression without rejection in these patients.]. Available from: https://www.clinicaltrials.gov/ct2/show/NCT02541916.

Chapter 2: Optimization of LAMP & colorimetric image analysis method with mRNA body fluid targets

2.1 Introduction

Body fluids provide critical contextual biological evidence for forensic investigations; blood, saliva, and semen are three of the most prevalently tested fluids and are presumptively identified using colorimetric serological tests prior to more expensive, downstream genetic analysis. Current best practices for body fluid identification (bfID) involve phenolphthalein or luminol tests for blood, acid phosphatase (AP) screening or prostate specific antigen (PSA) lateral flow assay for seminal fluid, and the alpha-amylase test for saliva. (1) Despite the ubiquitous nature of these enzymatic and immunological tests in the forensic workflow, they generally lack sensitivity and specificity required for a confirmatory fluid identification. (2, 3) For example, a study by Stange et al., showed that the PSA test produced 44% false positives and 20% false negatives among 132 sexual assault samples when compared to the 'gold standard' for DNA amplification, namely the polymerase chain reaction (PCR) with fluorescence detection. (4) Although some alternative confirmatory tests for body fluids exist, they are time-consuming, labor intensive, and require the use of additional sample – which is especially problematic when considering forensic samples, which often contain only trace amounts of genetic material. While microRNA and protein analysis have been explored as bfID approaches, mRNA profiling is especially promising, as total RNA can be purified from conventional forensic DNA extraction methods and has shown stability over long periods of time. (5, 6) To date, the numerous mRNA-

based bfID methods that have been reported are specific and sensitive, but require expensive instrumentation, and can produce erroneous results (e.g., false positives). (7, 8) However, it is important to note that amplification-based methods can be easily incorporated into the forensic workflow by leveraging instruments already commonly in use for downstream analyses.

Among the numerous amplification methods that can be used for bfID, LAMP has gained traction in recent years. This technique exploits up to 3 pairs of primers for rapid, isothermal amplification of nucleic acid targets with high specificity. (9) As an isothermal method, LAMP not only sidesteps thermocycling, but also involves amplification at higher temperatures (60-68°C) permitting less mismatched base pairs, thus allowing for enhanced specificity and amplification efficiency. (10, 11) Recently, reverse-transcription LAMP targeted a locus specific to blood and accomplished a limit of detection of 10 femtograms of total RNA diluted from a blood lysate. (12) LAMP differs from PCR in four keyways; *first*, LAMP is isothermal, which significantly simplifies instrumentation requirements by circumventing need for thermocycling hardware. *Second*, LAMP involves two sets of primers specific to a given target, with the option for an additional set of loop primers, whereas PCR uses a single primer pair (**Fig. 1A**). The use of multiple sets of LAMP primers allows for more annealing sites and, thus, faster amplification. (9) *Third*, the resultant polydisperse LAMP products all include the target sequence but cover a range of fragment sizes, whereas PCR yields a single amplicon of a specific size. The same set of fragments are produced from each primer set giving a unique profile when electrophoretically separated. *Fourth*, LAMP detection is compatible with colorimetric indicators, whereas PCR interpretation relies on inclusion of fluorescent labels. By using a colorimetric indicator, LAMP results can be visually

detected using simple, low-cost analytical methods (i.e., capturing an image) instead of the expensive fluorescent detection systems (i.e., light source, filters, etc.) required for PCR.

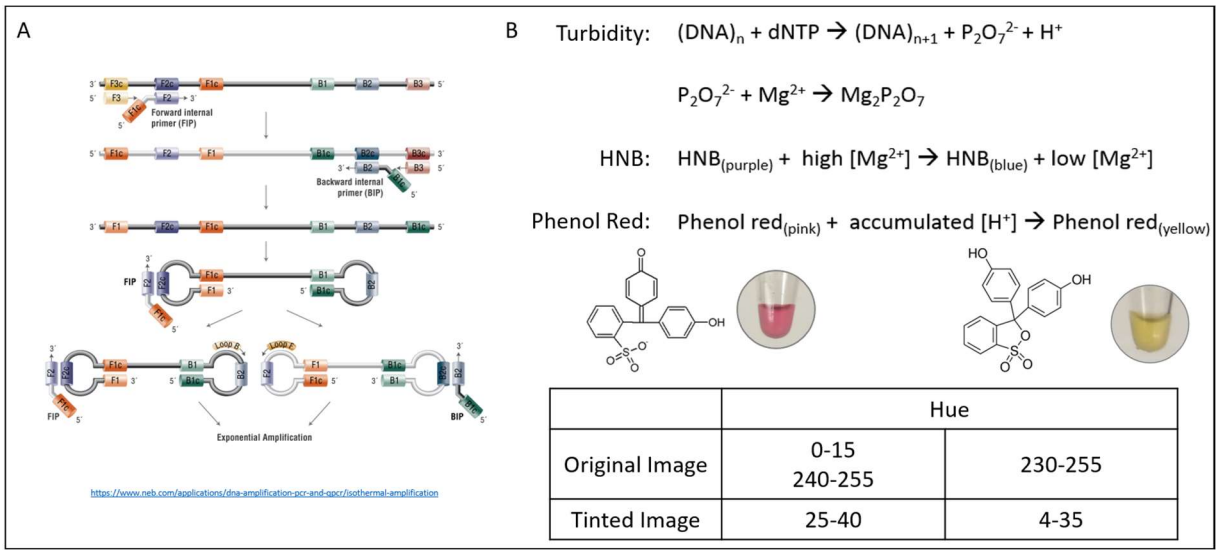

	Hue	
Original Image	0-15 240-255	230-255
Tinted Image	25-40	4-35

Figure 1: LAMP and colorimetric detection. (A) Illustration of key-like structure formation via isothermal LAMP heating. (B) Chemical changes occurring in colorimetric dyes commonly used in LAMP reactions. Phenol Red (pH indicator) was used for this research changing from red (~pH 8) to yellow (~pH 6).

Here, we describe a novel LAMP approach for bfID that pairs colorimetric detection with an empirical image analysis strategy to establish the presence (or absence) of forensically relevant body fluids, including blood (Vb), saliva (Sa), and semen (Se) (**Fig. 1B**). (13, 14) Whereas previous bfID efforts from our laboratory leveraged hydroxynaphthol blue (HNB) dye for colorimetric readout (15), here, we demonstrate the effectiveness of LAMP when combined with phenol red, a colorimetric pH indicator. As the pH of the LAMP reaction changes from ~pH 8 to ~ pH 6, due to hydrogen ions in solution after a nucleotide is added to the growing chain, phenol red has a striking color change, thus enabling simple visual detection; however, naked eye interpretation is subjective, due to inherent variability in how individuals perceive color. (16) To remedy this, we created a user-friendly analytical strategy centered on smart phone analysis (16)

that permits objective, simple, and accurate color detection exploiting components of various color spaces (Red, Green, Blue (RGB), Hue, Saturation, Brightness (HSB)). In this work, we screened for three body fluids, namely Vb, Se, and Sa, by capturing images of the initial and final LAMP reaction mixtures and measuring changes in hue using *FIJI* software. (17) The specificity of the primers designed for the three mRNA assays was assessed by testing five different body fluids, including vaginal fluid (Vf) and menstrual blood (Mb), which are common in sexual assault evidence. Our method (RT-LAMP) is non-destructive to the DNA, preserving it for potential downstream genetic profiling. Furthermore, LAMP-based detection is sensitive, exhibiting high accuracy for even low-concentration RNA samples, with impressive specificity for each intended body fluid target. Notably, completion of the isothermal amplification step is achieved in <30 min with completely unbiased interpretation of colorimetric results.

2.2 Methods & Materials

2.2.1 Sample collection

De-identified body fluid donations, namely Sa, Se, Vf, and Mb, were collected via protocols approved by the University of Virginia's International Review Board (IRB). Vf and Mb samples were collected using sterile cotton swabs and dried overnight. Sa and Se samples were collected in sterile specimen containers, then divided into 50 µL aliquots. All above-described samples were stored at -20 °C until analysis. Venous blood was received de-identified from the University of Virginia Medical Hospital in EDTA vacutainers and stored at 4 °C until extraction.

2.2.2 RNA Isolation

Cellular lysis was achieved using a previously published protocol. (15) Briefly, in a 1.5-mL microcentrifuge tube, a body fluid sample was mixed with 350 µL RLT buffer (Qiagen, Valencia, CA, USA), 90 µL nuclease-free water (Growcells, Irvine, CA, USA), 10 µL Proteinase K (Qiagen), and 4.5 µL of β-mercaptoethanol (Sigma Aldrich, St. Louis, MO, USA). The sample input varied with body fluid identity; RNA was extracted from either 50 µL of Vb, 2 µL of Se, an entire swab of Vf or Mb, or 100 µL of Sa. Each sample was incubated at 56 ^{o}C for 10 minutes before the lysate was recovered via the 'piggy-back' method; the swab sample was placed in a 0.5 mL tube, the bottom of which was punctured with a 21-gauge needle, then nested within a 1.5 mL microcentrifuge tube. Centrifugation for 1-2 seconds at maximum speed eluted the lysate from the sampling substrate and transferred it to the 1.5 mL tube. The lysate was combined with the original lysis sample. These crude lysates were purified using Qiagen's RNeasy Mini kit following manufacturer's protocol. RNA samples were eluted in 50 µL of nuclease-free water and stored at -80°C until amplification.

2.2.3 Primer information

LAMP primer sets (**Table 1**) were designed using PrimerExplorer V5 and purchased from Eurofins Genomics LLC (Louisville, KY, USA). The Vb, Se, and Sa primer sets were designed from the human β-hemoglobin (HBB; NM_000518.5), human semenogelin 1 (SEMG1; NM_003007.4), and human histatin 3 (HTN3; NM_000200.2) mRNA sequences, respectively. The Vf and Mb primer sets were designed from cytochrome P450 family 2 subfamily A member 7 pseudogene 1 (CYP2B7P1; NR_001278.1) and the human matrix metallopeptidase 10 (MMP10; NM_002425.2).

Table 1: Primer sets used for each of the body fluids. The concentrations were 0.2, 0.4, 0.8 uM for F3/B3, LF/LB, and FIP/BIP each, respectively.

Target	Primers	Sequence (5′ -3′)	Target	Primers	Sequence (5′ -3′)
Blood	FIP	CGTTGCCCAGGAGCCTGAAGTTTTACTGAGTGAGCTGCACTGT	Semen	FIP	GTTTCGGTCGTTGTTAAGCTGTTGTTTTTTAATTATAGAGCAGGAAGATGACAG
	BIP	GGTCTGTGTGCTGGCCCATCTTTTCCAGCCACCACTTTCTGAT		BIP	TAAACCTACCATTCGGTAACCATGTTTTCACTGAGGTCAACTGACA
	F3	CCTCAAGGGCACCTTTGC		F3	TCTCATGGGGGATTGGAT
	B3	TTGTGGGCCAGGGCATTA		B3	CATCTCAGAAACATCACAGAA
	LF	AGGATCCACGTGCAGCTTGT		LB	GAAAGGATGGACCAATATCAAG
	LB	CTTTGGCAAAGAATTCACCC			
Vaginal Fluid	FIP	AATGTGGGGCACACCCATGGGCCATACACAGAGGCAGTC	Saliva	FIP	GATGTGAATGATGCTTTTCATGGAATTTTCTGGAGCTGATTCACATGC
	BIP	TTCTGAGGGTACACCATCCCCATCAAAGTAGTGTGGGTCACG		BIP	ATTGATATCTTCAGTAATCACGGGGTTTTAGTCCAAAGCGAATTTGC
	F3	GCTTGATGACCGAGCCAA		F3	TTGGCTCTCATGCTTTCC
	B3	GTCAGGATTGAAGGCGTCTG		B3	GGTATGACAAATGAGAATACACG
	LF	GTCAGCAAATCTCTGAATCTCACGG		LF	TATACCCATGATGTCTCT
	LB	CGGAAGTATTTCTCATCCTGAGCA		LB	CATGATTATGGAGGTTTGAC
Menstrual Blood	FIP	GCTGAGTGAAAGAGCCCCAGAGGCACCAATTTATTCCTCG			
	BIP	CAACACTGAAGCTTTGATGTACCCTTCACATCATCTTGCGAAAG			
	F3	AAAAATGGACAGAAGATGCA			
	B3	CCGTAGAGAGACTGAATGC			
	LF	AGTGGCCAAGTTCATGAGCAG			
	LB	TTCACAGAGCTCGCCCAGTTC			

2.2.4 Colorimetric Loop-mediated Isothermal Amplification

All LAMP reactions contained WarmStart® Colorimetric LAMP 2X Master Mix (DNA & RNA) (New England Biolabs, Ipswich, MA, USA) and were conducted according to manufacturer's instructions. Although the recommended primer concentrations (1X) given by the manufacturer are 0.2 µM for F3 and B3, 0.4 µM for LF and LB, and 1.6 µM for FIP and BIP, LAMP assay was also tested with primer concentrations at 0.5X, 0.75X and 1.5X. The negative controls were nuclease-free water and positive controls were RNA samples from known single-source body fluids. The success of LAMP was assessed by capturing images of colorimetric responses via a 'lightbox' and/or fragment analysis via microchip electrophoresis with Agilent's 2100 Bioanalyzer instrumentation using DNA 1000 series II kit (Agilent Technologies, Santa Clara, CA, USA).

2.2.5 3D-printed lightbox for imaging

The lightbox was 3D printed with white polylactic acid (PLA) in three stackable pieces and a top poly (methyl methacrylate) (PMMA) cover piece. **Fig. 2A** shows all of the pieces required for image acquisition, assembled in this order: the 'Top' black PMMA piece and Huawei phone, 1st PLA component, 2nd PLA component with clear PMMA holders, 3rd layer with three LED strips and diffusive layer connected to a small breadboard. A 96-sample plate is used to keep the tubes aligned when taking an image. Since the samples are flipped 180° to image, the PMMA holders were used to keep all tubes in straight lines for the Image J macro. One holder was designed to fit near the top of the tube, while the second holder fit closer to the end of the tube. The LED

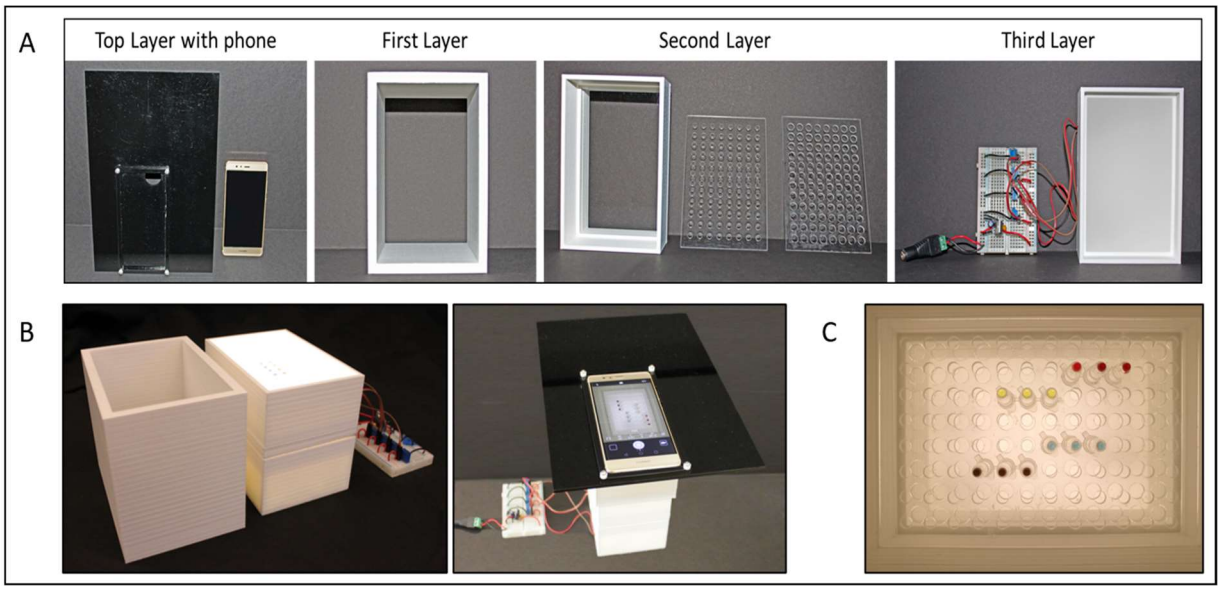

Figure 2: Detailed view of imaging box. (A) The imaging box is made of white polylactic acid. It has three layers to stack for optimal distance and static lighting. The 1st layer is for optimal image distance. The 2nd layer has three PMMA pieces that sit inside to hold the tubes in straight lines. The static lighting comes from a diffusive sheet and three strips of LEDs affixed to the 3rd layer. The top of the imaging box is made of black PMMA, with a circular cutout for the Huawei camera. On the Huawei, the ISO and shutter speed were constant at 50 and 1/160, respectively. (B) The stacked imaging box with samples in place. (C) A single image simultaneously captures 96 wells to be analyzed by ImageJ. (Adapted from Layne et al. with permission)

strips and diffusive layer were for uniform lighting behind the tubes across the 96 wells. **Fig. 2B** illustrates how the pieces stack to achieve optimal distance for imaging. Settings for image acquisition on the Huawei P9 smartphone were ISO 50, shutter speed 1/160, and auto white balance (**Fig. 2C** is an exemplary image).

Using FIJI (17) distribution of ImageJ (18) (2.0.0-rc-69/1.52p), the image was first tinted using the Image > Adjust > Color Balance command path and applying two sequential adjustments: blue channel 0-190 and yellow channel 40-255. The tinting is needed to rotate the hue scale, so all the red values (negative result) congregate at the upper end of the hue scale and the yellow values (positive result) are at the bottom of the hue scale. This is because the hue scale is circular based on Isaac Newton's discoveries, (19) but splits in the red region. An example of hue values before and after tinting is shown in **Fig. 3**. Second, using an in-house Plug-in, the image is analyzed for hue in a circle with radius of 15 pixels and exported to a .csv file. The .csv file contains color analysis for each reaction and various parameters from the Plug-in (e.g.,

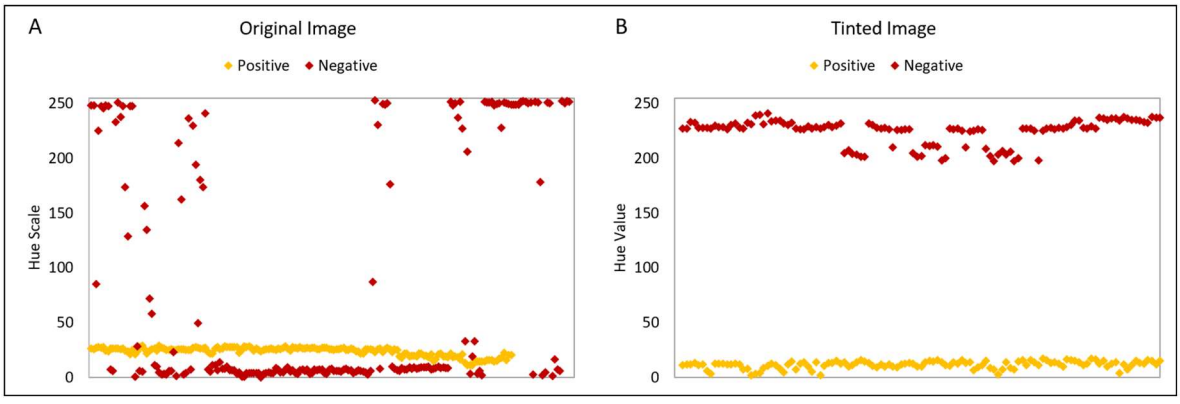

Figure 3: Comparison of hue values. (A) In original images (without tinting), the red color was at either end of the hue scale, while the yellow color was ~35-40 hue value. (B) In tinted images, the hue scale was rotated to allow all the red color hue values at the upper end of the scale with the yellow color hues at the lower end of the scale. (Adapted from Layne et al. with permission)

sample number, area of circle, mean of hue, minimum hue detected, maximum hue value detected).

2.3 Results and Discussion

As an alternative method to current bfID methods, various mRNA targets were assessed for single fluid specificity using a novel amplification method. The isothermal LAMP reactions were detected via an optimized colorimetric dye and image analysis and measured over multiple time points to produce a semi-real time analysis. Components in the LAMP reaction were varied, as well as multiple mRNA targets, to achieve results in less than 30 min. With the additions of a DNase treatment prior to the LAMP reaction, all five body fluids produced high specificity and sensitivity that was compared to conventional methods.

2.3.1 Image capture and analysis

Visual detection of chromogenic reactions may seem trivial, but depending on lighting, color blindness, age, and a number of other parameters, there is inherent subjectivity; it is well-established that no two individuals see color exactly the same way. (20) To alleviate subjectivity in color interpretation, we built a 'lightbox' with static lighting to interface with a smartphone (Huawei P9 vendor) for image acquisition (**Fig. 2**). (21) While we understand the construction of this lightbox is not available to every forensic laboratory, there are other simple approaches that can be employed for image analysis, such as using desktop scanners, provided that strict attention is paid to consistent and homogeneously applied lighting conditions. To receive consistent hue values, the same shade of light, omittance of stray light, camera conditions, etc. should be considered when capturing and analyzing images.

2.3.2 Setting color ranges

Using the lightbox, images of LAMP reactions were captured, then analyzed as both non-tinted and tinted 8-bit RGB images. Specifically, similar to a previous study from our lab, (21) a circular region of interest (ROI) with a 15-pixel radius from each sample was analyzed. To determine the best color attribute for analysis, many images representative of positive and negative samples were analyzed to establish which color parameter exhibited the largest difference in value across conditions. Images with the positive and negative colors were analyzed in different color spaces (i.e., Hue, Saturation, Brightness (HSB), Red, Green, Blue (RGB)). The component that gave the biggest deviation between a positive and negative result using a non-tinted image was the green value, but in a tinted image the hue value showed a much stronger deviation (**Fig. 4**). Due to the larger deviation between a positive and negative color, the hue value was used for image analysis. Hue values were measured across all 96 wells in the lightbox, demonstrating consistent imaging regardless of

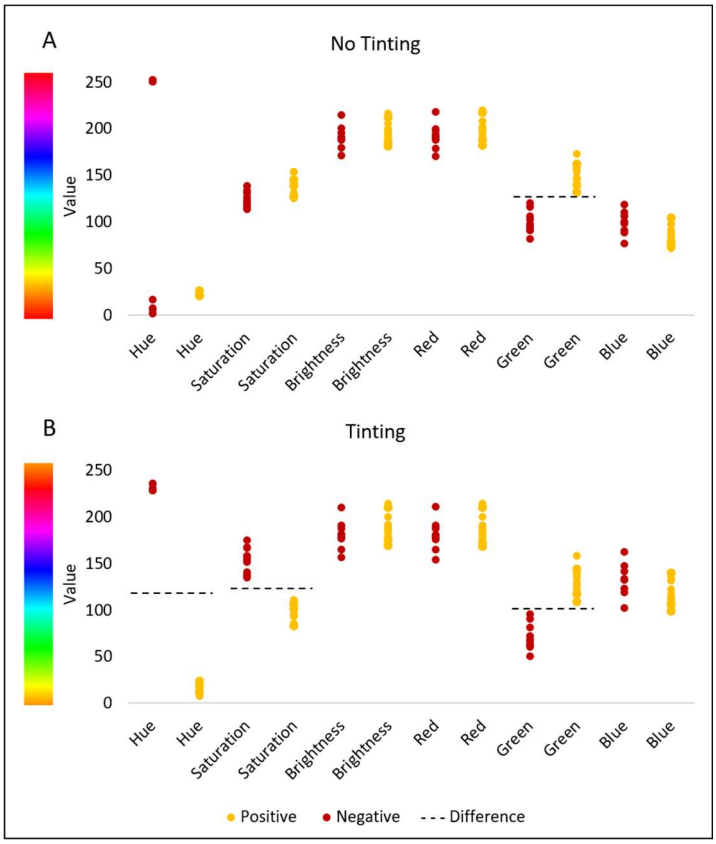

<u>Figure 4</u>: Color attributes from original (A) and tinted (B) images of various negative (red) and positive (yellow) controls for LAMP after 60 minutes. Black dotted line shows if there was a difference between positive and negative values. (Adapted from Layne et al. with permission)

spatial positioning of the reaction within the lightbox. Hue is the shade of a color and once an image is converted to hue greyscale, each pixel is given a value from 0 to 255; thus, the red and yellow colors can be quantitatively distinguished (**Fig. 5**). In a non-tinted image, the red values are split from 0-16 or 240-255 and the yellow values are at 20-35 on the hue scale. When averaging the red color hue values, the standard deviation can be large due to the split in the red region, thus the images were tinted to allow for a single red hue value range (**Fig. 5A**). This change rotated the hue color scale to allow for all red hue values to be between 225-250 and yellow hue values between 2-25. When the tinted images are converted into hue greyscale, the red pixels (225-250) appear white, whereas yellow pixels (2-25) appear black. The greyscale shows a visual difference, and each pixel is assigned a specific hue value. A positive and negative range was empirically determined by measuring and averaging the hue values from more than 100 positive

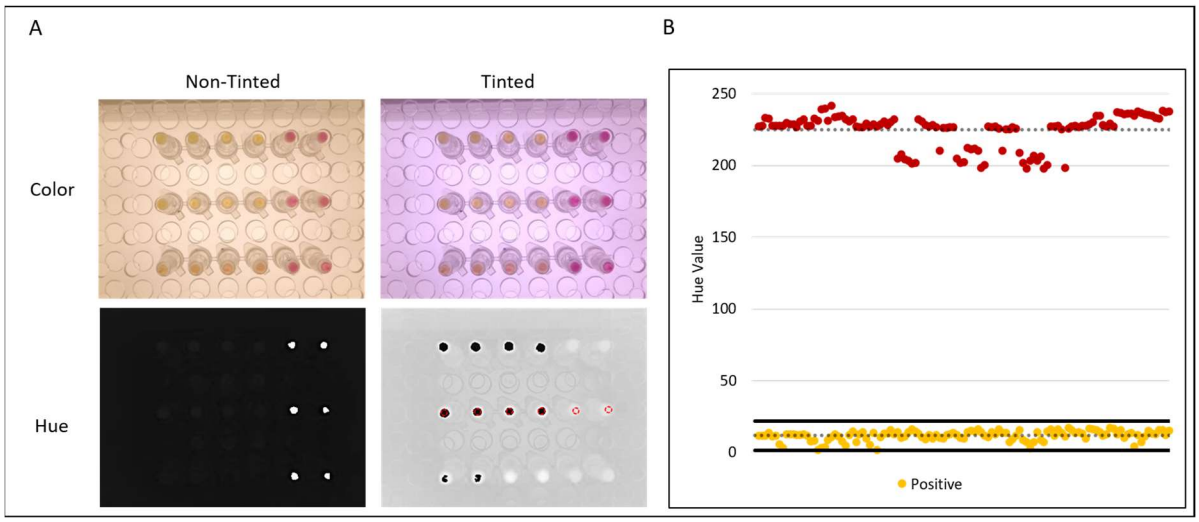

Figure 5: Image Analysis of LAMP reactions and threshold values. (A) After image acquisition, tinting was applied prior to conversion into a hue greyscale image. An in-house Plug-in crops an ROI at the center of the tubes (red dotted circles) and measures the average hue values within the ROI. (B) Dotted lines denote averages for positive or negative hues (n=125 each). The black lines represent 3 standard deviations above or below the averages, showing the ranges for both positive and negative hue values. (Adapted from Layne et al. with permission)

and negative LAMP reactions. A threshold indicating amplification was established three standard deviations above the mean positive hue value found from averaging more than 100 positive LAMP reactions (**Fig. 5B**). Samples were deemed 'positive' if the hue value falls within the empirically discerned positive range, otherwise the samples were deemed 'negative'. Thus, eliminating color subjectivity stemming from error in human-to-human visualization.

2.3.3 Body fluid specificity

The volume of fluids used for extraction were specifically chosen to mimic those typically collected at crime scenes, and similar to volumes used in other literature research methods for bfID. (5, 6, 12) **Fig. 6** shows rapid amplification of the mRNA targets using forensically relevant samples with specificity for the fluids tested here that could potentially benefit forensic laboratories. A number of parameters, including temperature and primer concentration, are critical in optimizing LAMP for specific amplification with a faster 'time to result' (T_r) for all body fluids of interest. Given that effective bfID relies on primer sets that are designed to be tissue-specific (i.e., to a particular body fluid), to mitigate risk for false fluid identification, primers should exhibit minimal opportunity for non-template amplification (NTA) due to self-annealing or amplification of other similar, off-target sequences in the genome. Each primer set was screened against Vb, Se, Sa, Vf, and Mb. However, we recognize that other body fluids exist, and these should be tested against the target mRNA markers to better define specificity.

The Vb primer set was designed to be specific for human β-hemoglobin (HBB), present in the β-chain of one of the subunits comprising adult human hemoglobin in red blood cells. (22) **Fig. 6A** shows that the blood (Vb) primer set amplified the HBB target in a neat Vb sample in 30

minutes with a readily apparent color change from red to yellow. Importantly, the Vb primer set did not amplify Se, Sa or Vf, but showed amplification with Mb in 30 mins. This, however, was not unanticipated as Mb contains human β-hemoglobin mRNA, the target of the Vb primer set. While there are some forensic cases where discrimination of Mb from Vb might be required, this scenario is exceedingly rare. Moreover, our focus was on defining a target for any human blood, thus a mRNA target prevalent in both venous and menstrual blood was specifically chosen.

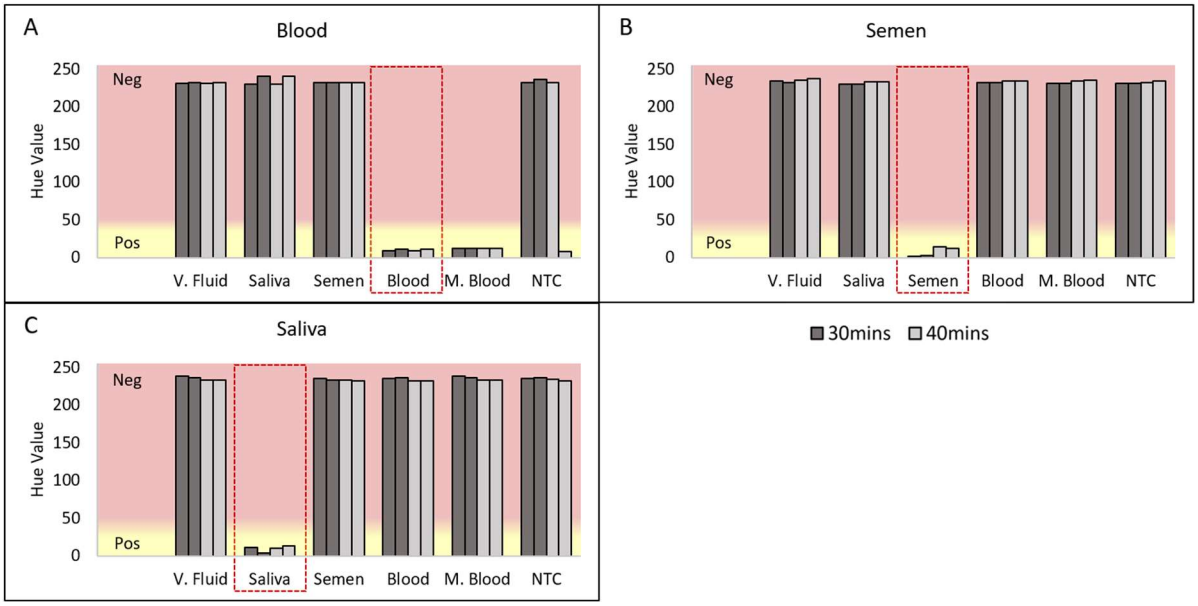

Figure 6: Specificity of Vb, Se, Sa assays at 30/40 min of LAMP with image analysis. Each bar represents one replicate of a sample, and the intended fluid is shown in the dotted red box. The red background represents a negative value, and the yellow background represents a positive value. (A) The Vb assay amplified blood in 30 min. (B) The Se assay amplified semen in 30 min. (C) The Sa assay amplified saliva in 30 min. (Adapted from Layne et al. with permission)

The Se primer set was designed to be specific for SEMG1, a predominant protein in Se involved in the formation of the gel matrix encasing ejaculated spermatozoa. (23) As shown in **Fig. 6B,** the Se primer set amplified the target in the neat Se sample by the 30-minute mark, and nonspecific amplification was not observed with any of the other fluids or no-template controls.

This indicates the capability of the assay to detect SEMG1 mRNA with 2 µL input and discriminate Se from all other fluids tested.

The Sa primer set targets the human histatin 3 (HTN3) gene, which produces small, histidine-rich, cationic proteins in saliva with antibacterial and antifungal activity. (24) **Fig. 6C** shows the Sa primer set amplified targets in neat Sa sample within 30 minutes, with the complete absence of amplification of other fluids. This is significant, because Vf and Sa both possess endogenous bacterial communities, and are rich in mucosal fluid, yet we are able to indicate select amplification in Sa samples only. None of the no-template controls changed color, while all positive controls (target mRNA) exhibited the expected color change, indicating independence from both false positives and false negatives for all three body fluid targets.

2.3.4 Temperature optimization

Although a LAMP incubation temperature of 63 °C was chosen based on previous work, (15) it was imperative to optimize temperature conditions for all targets that permits target amplification while minimizing the opportunity for non-specific amplification (NSA) or NTA. Increasing the amplification temperature drives more stringent base pairing, leading to minimal if any NSA or NTA. Equally important is defining the time allowed for amplification. Lengthy incubation can result in NSA or NTA, and thus a false positive result, whereas a short amplification interval is detrimental to assay sensitivity. With a view towards isothermal amplification and complete detection in 30 minutes, sample amplification was colorimetrically monitored for 40 minutes to assure no NSA or NTA was present. Since LAMP uses more primers than PCR, there is a higher probability for NTA via primer-dimer formation when considering primers with similar

composition (e.g., GC content, length). (25) **Fig. 7** shows resulting hue values generated using Vb, Se, and Sa primer sets at various temperatures (63, 65, 67 °C) with 30- and 40-minute amplification times to determine whether a universal LAMP temperature could be identified. In this study, RNA samples from the target body fluids were used as positive controls, and water used in the NTCs. A red-to-yellow color change, indicated by a shift in hue from the negative ranges (0-1.56 and 225-255) to the positive range (1.57-22.04) (**Fig. 7**; light bars), was observed within 40 minutes using all three primer sets at both 63 and 65 °C, indicating successful amplification.

Although NTA occurred in both NTCs at 40 min when targeting Vb at 63 and 65 °C, when the temperature was elevated to 67 °C, only one of the duplicate NTCs amplified by 40 minutes.

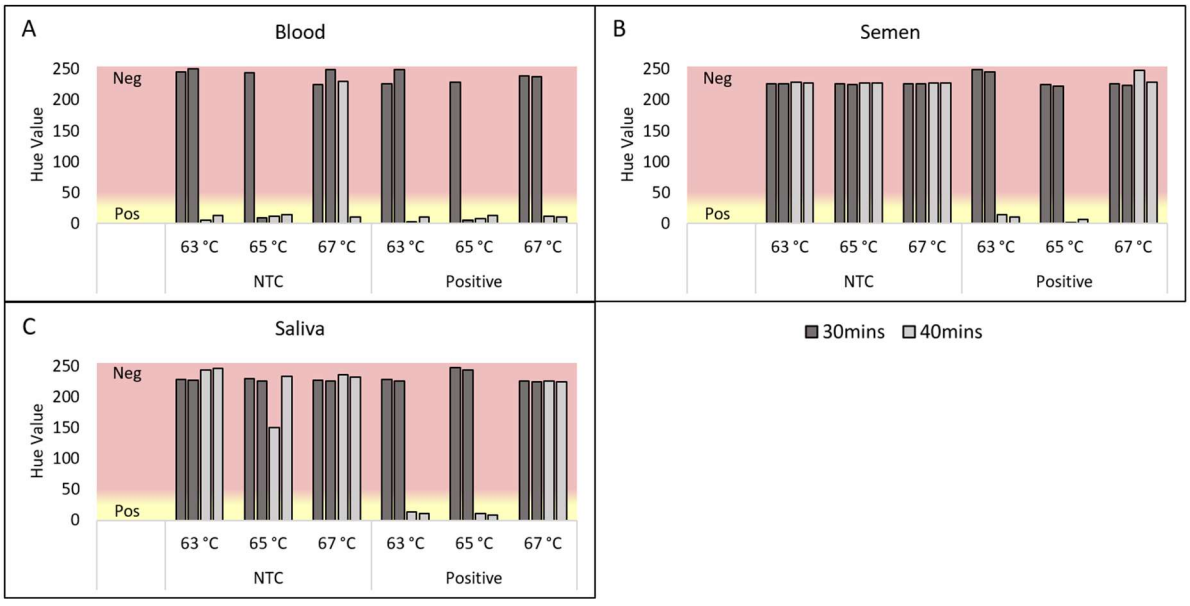

Figure 7: Temperature optimization for the Vb, Se, and Sa LAMP assays at 30 and 40 min. Positive and NTCs were tested at three temperatures in duplicate (each column represents one replicate). Positive and negative reactions are indicated by the pink and yellow zones, respectively. (A) All Vb positive controls amplified, but the NTCs also amplified at all three temperatures. (B-C) At 63 and 65 °C the Se and Sa positive controls amplified at 40 minutes, while the NTCs remained negative. (Adapted from Layne et al. with permission)

This observation suggests that a higher assay temperature minimized NTA. (26, 27) Electrophoretic fragment analysis of the colorimetrically positive Vb NTCs resulted in an amplicon size distribution that strongly suggested primer-dimer formation (data not shown). The Se and Sa assays demonstrated similar results, in that there was no amplification in the NTCs at any temperature, as indicated by the hue values in the negative range (**Fig. 7B & 7C**). The positive controls for both Se and Sa assays changed color at 63 and 65 °C, but not at 67 °C. With the goal of a universal temperature for amplification of all targets, we chose a temperature of 63 °C since all positive controls reproducibly amplified, despite the observation that NTA occurred at 63 °C with the Vb assay. To counter this problem, the primer concentrations can be altered to facilitate a 30-minute assay time with minimal Vb NTA.

2.3.5 Primer concentration optimization

Given that simply adjusting temperature was insufficient to eliminate the NTA observed using the Vb primers, we explored adjusting primer concentration to permit specific, on-target detection in less than 30 minutes. We hypothesized that NTA was promoted, at least in part, due to high primer concentration (25); more dilute primer stocks were tested in parallel with the recommended concentration (1X) tested previously. **Fig. 8** shows that reducing the Vb primer concentrations from 1X to 0.75X did not negatively impact the T_r (time to result), as evidenced by the positive controls changing color at 30 min (**Fig. 8A**). Upon a further decrease to 0.5X primers, however, the T_r became variable and delayed to approximately 40 min; in this dataset, NTA was only observed at the 1X in the Vb assay at 40 min. With 0.75X primer concentration for the Vb primer set, the occurrence of NTA was then found to be reduced dramatically and not

induce a color change. Going forward, the primer concentration for the Vb target was 0.75X for LAMP reactions to avoid false positive results from NTA.

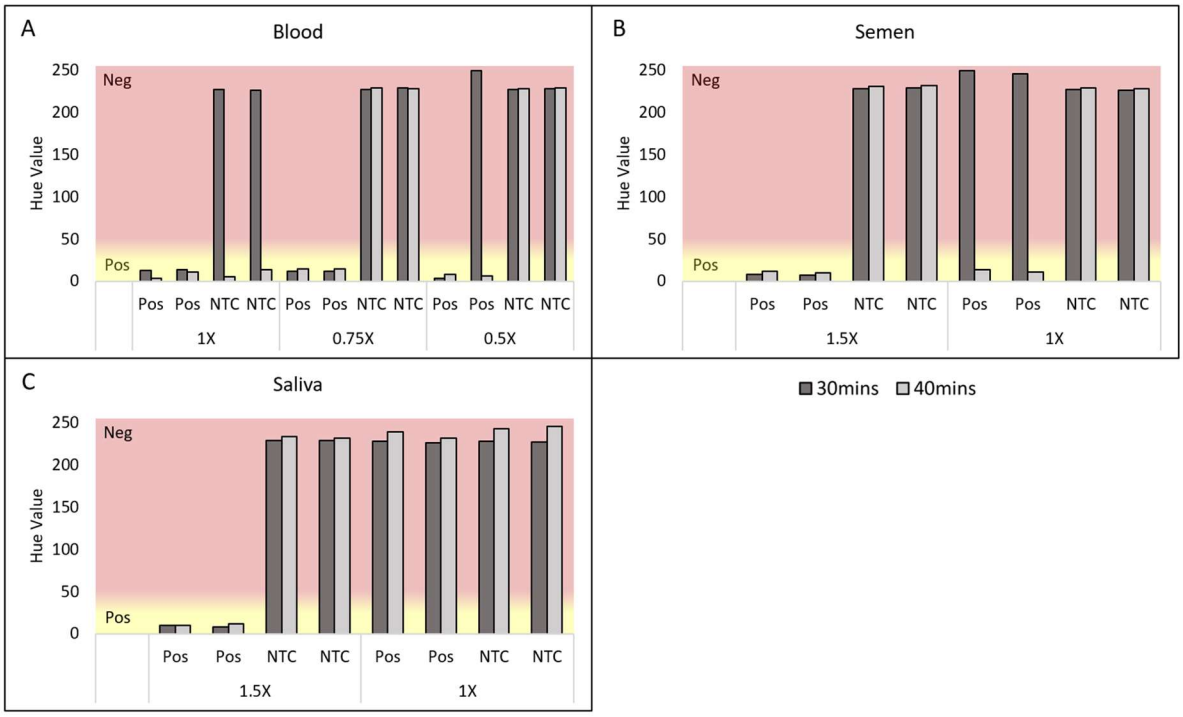

Figure 8: Primer concentration optimization for the Vb, Se, and Sa LAMP assays at 30/40 min. The columns represent hue values from 2 positive controls and 2 NTCs. (A) The Vb assay amplified the positive controls at 30 min with 1X and 0.75X primer concentration, and the NTCs remained negative at 40 min with 0.75X. (B) The Se assay amplified the positive controls at 30 min with 1.5X primer concentration, and the NTCs remained negative at 40 min. (C) The Sa assay amplified the positive controls at 30 min with 1.5X primer concentration, and the NTCs remained negative at 40 min. (Adapted from Layne et al. with permission)

Conversely, we increased the concentrations of Se and Sa primers to evaluate whether a more rapid, consistent T_r can be achieved, which is especially important for low copy number samples. **Fig. 8B** shows that amplification was observed in positive Se samples at 30 min with a 1.5X primer concentration, whereas when a 1X concentration was used, amplification could not be detected until 40 min. Similarly, **Fig. 8C** shows the Sa LAMP assay results at those same concentrations, which indicated that positive samples amplified at 30 min with 1.5X primers, but

no amplification was observed in samples with 1X primer concentration. Importantly, for both targets, no NTA was observed in the NTCs at either primer concentration. This indicates that, for the Se and Sa assays, increasing primer concentration by 50% improves amplification of Sa and Se targets in under 30 min with no observed NTA. This is consistent with our previous work using LAMP for the Se and Sa assays with the Eiken Loopamp LAMP kit, where even with higher primers concentrations, NSA was not observed (15).

2.3.6 Vaginal fluid & menstrual blood testing

LAMP was also explored for vaginal fluid (Vf) and menstrual blood (Mb) targets, although these fluids are known to be more difficult to identify due to 1) a scarcity of known targets specific to those fluids, and 2) similar composition to other fluids, e.g., Mb and Vb. (28) Given these challenges, we explored numerous approaches for designing primer sets specific to Vf and Mb. The literature provided a number of viable mRNA targets for both fluids (5, 29-33) for which multiple primer sets were identified (**Fig. 9**). For vaginal fluid, two mRNA targets (CYP2B7P; HBD1) were amplified by designing two primer sets for each target with multiple loop primer sets. For Mb, three mRNA targets (MMP11, MMP10, LEFTY2) were amplified by designing 2 - 4 primer sets for each target. All primer sets were screened against all fluids at 63, 65, 67 °C with incorporated negative controls. However, NSA provided serious challenges here, since even off-target amplification causes LAMP reactions to turn yellow in color, thus producing false positive results. Many of the primer sets tested showed either amplification with other fluids (i.e., Mb primer set

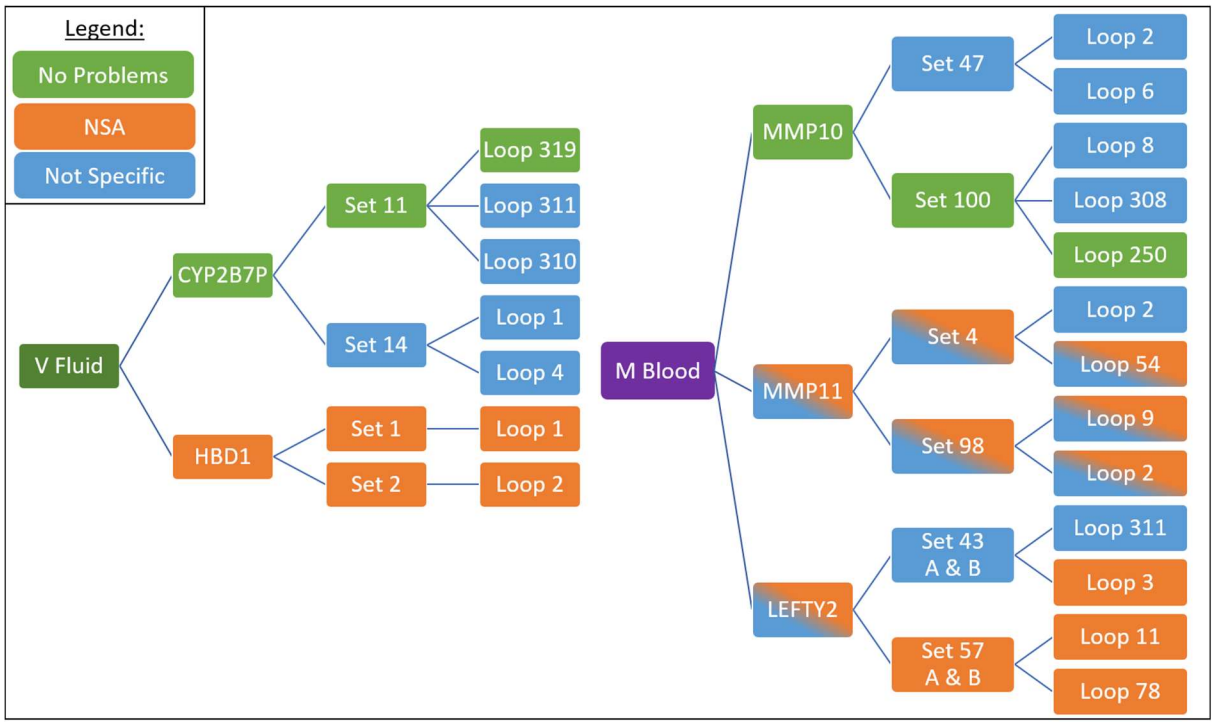

Figure 9: Messenger RNA targets for either Mb or Vf primer sets for amplification in a LAMP reaction. Many of the primer sets were non-specifically amplifying (NSA) an off-target sequence or primer dimers. Some of the primers were not fluid specific. However, one primer set showed amplification in only the target fluid with no NSA.

amplifying Vb) or NSA with NTCs or other fluids. Examples of this are shown in **Fig. 10** where the LAMP banding patterns for true positive Vf or Mb samples were compared with negative controls and colorimetrically positive samples produced from other body fluids that do not contain the intended mRNA target. As discussed previously, the mismatched banding patterns between true positives and samples with suspected NSA indicate that off-target amplification occurred frequently.

The high incidence of NSA led us to explore the inclusion of chemical agents that discourage formation of mismatched base pairs during amplification. One such substance, diethyl formamide (DEF), has been used to increase base-pairing fidelity. (34) While the effects of DEF are less clear, it is thought the organic compound works by binding to the grooves in DNA and

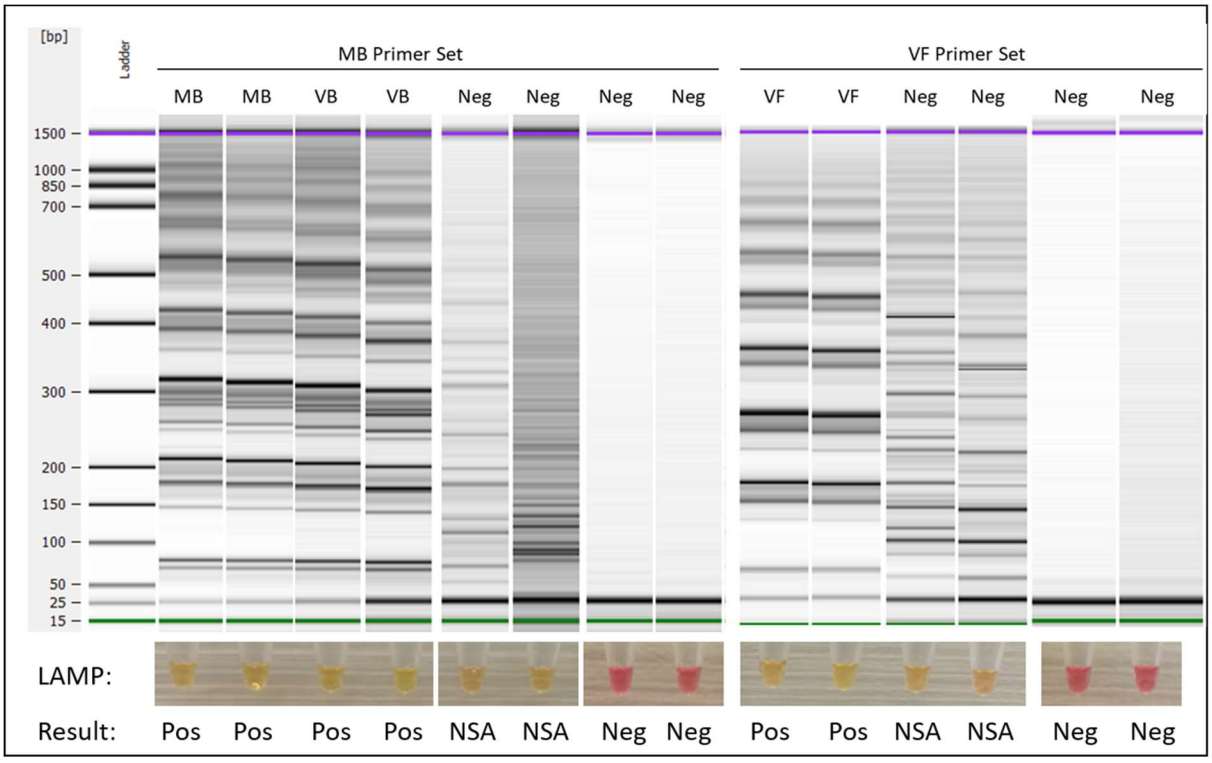

<u>Figure 10</u>: Microchip electrophoretic profiles after LAMP using either MB or VF primer sets. The MB primer set shows fluid non-specificity by on-target amplification in VB and primer non-specificity by off-target amplification in some negative controls. The VF primer set shows primer non-specificity by off-target amplification in some negative controls.

destabilizing the double helix or improving initial melting. (34-36) Here, we explored its effectiveness at minimizing NSA with the Vf and Mb primer sets. Based on the results in **Fig. 11,** addition of the manufacturer recommended DEF concentration (3%) induced an immediate red to yellow color change, which interfered with and prevented colorimetric detection. Since phenol red's color changing behavior is pH-dependent, we attempted to rectify this by titrating Tris into the reaction and increasing the reaction temperature from 63 to 65 °C to increase base-pairing fidelity. As given in **Fig. 11**, inclusion of DEF reduced the incidence of NSA, and thus diminished the rate of colorimetric false positive results. While this presented a viable option for moving forward, it was a superficial solution for NSA, not a comprehensive resolution. Hence, we chose to continue efforts to design and optimize Vf and Mb primer sets that minimized NSA.

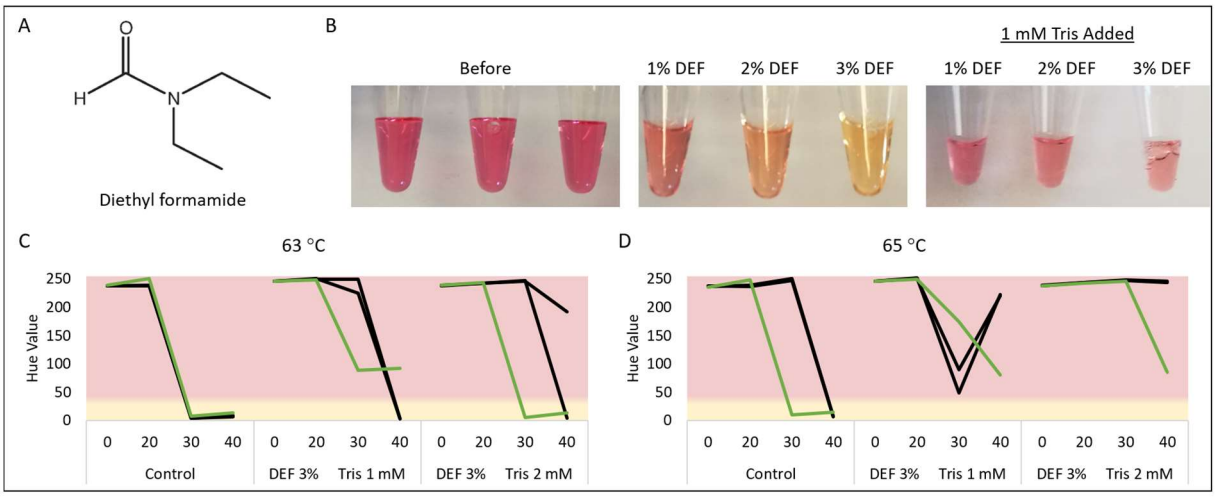

Figure 11: Reduction of non-specific amplification. (A) Diethyl formamide chemical structure. (B) 3% DEF added to LAMP reagents only without sample. (C) Vaginal fluid primer set testing with 3% DEF and 2 mM Tris. The control group did not have DEF or Tris added to the reaction. The green line denotes a known Vf sample and black line denotes a negative control.

2.3.7 Addition of DNase treatment

Numerous primer sets specific for both Vf and Mb target amplification were tested exhaustively with little success, alone or in combination with strategies known to suppress non-specific amplification (previously mentioned). Additionally, as more samples were tested, the results of the LAMP assay with the mRNA targets for Vb, Se, and Sa showed amplification in non-intended fluids (i.e., blood target amplicons in Vf and Sa). This demonstrated that primer sets exhibited off-target annealing with genomic loci in other fluids, and thus were poor candidates for attaining single fluid specificity. However, before redesigning primer sets or selecting new, alternative mRNA targets, we explored how altering other aspects of the protocol, specifically, lysis and purification methods, may affect downstream amplification specificity. We postulated that residual DNA present in the purified RNA sample was contributing to off target annealing and NSA. (37) To eliminate this confounding genetic material, we evaluated the effect of adding an on-column DNase digestion to the RNA purification protocol (**Fig. 12**). (38) DNase I, an

endonuclease that nonspecifically cleaves single-stranded and double-stranded DNA, (39, 40) is typically used in forensic laboratories for RNA processing and requires only 15 minutes additional processing time. (41, 42)

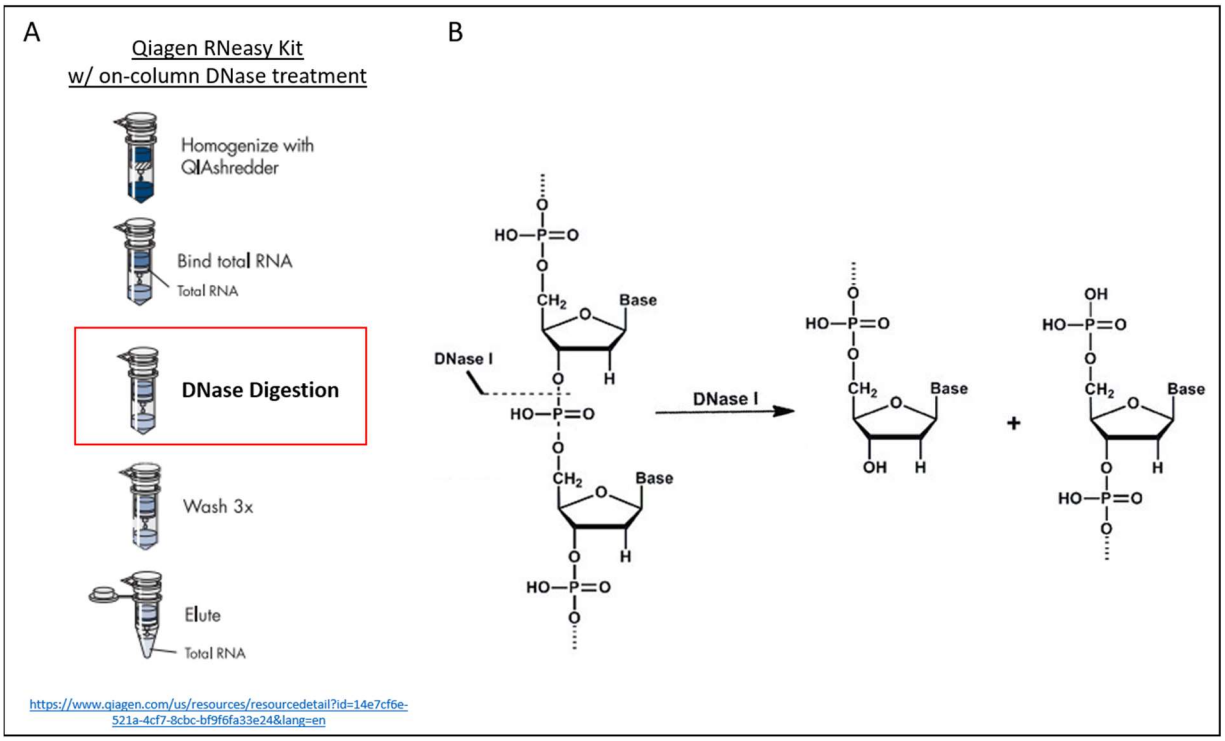

Figure 12: DNase treatment added into lysis and purification. (A) The DNase digestion was added into the on-column RNA purification protocol. (B) Catalytic mechanism of DNase I digest of the DNA backbone. (Adapted from Lauková et al. *Biomolecules* 2020 with permission)

Fig. 13 shows LAMP data for the specific mRNA targets in RNA lysates obtained with and without the on-column DNase I treatment. Notably, implementing the on-column DNase I treatment greatly improved amplification specificity, as seen by comprehensive on-target amplification of the intended body fluids with no NSA observed. Initially, when the primers designed for the blood target were screened against all fluids, amplification was observed not only in Vb and Mb, as expected, but also Vf and Sa. When LAMP was conducted on parallel aliquots from the same samples following lysis and an on-column DNase treatment, amplification was observed in only Vb and Mb samples. The amplification in only the targeted fluids

demonstrates the previous results were false positives, ideally due to similar sequences in the samples. Differentiating Vb from Mb, the difference in amplification of Mb mRNA target MMP10 before and after the addition of a DNase treatment is shown in **Fig. 13E** & **J**. Since the DNase treatment was the only variable that changed throughout the process, we can infer that genomic DNA or some nucleic material with a similar sequence present in the untreated Vb, Se, Sa and Vf samples promotes NSA. Similarly, **Fig. 13D** shows that the Vf primers initially produced NSA in several unexpected body fluids, although this was eliminated following the DNase treatment (**Fig. 13I**). The Mb samples did amplify the Vf target; however, this is to be expected due to the shared anatomical area of origin for both fluids. The result was verified due to concordant peak patterns in Mb and Vf via Bioanalyzer (data not shown). The Se primers only initially exhibited off-target amplification in one other body fluid (Vf), but this was also eliminated with the DNase treatment (**Fig. 13B**). Even though Sa primers did not produce NSA even without the DNase treatment, it

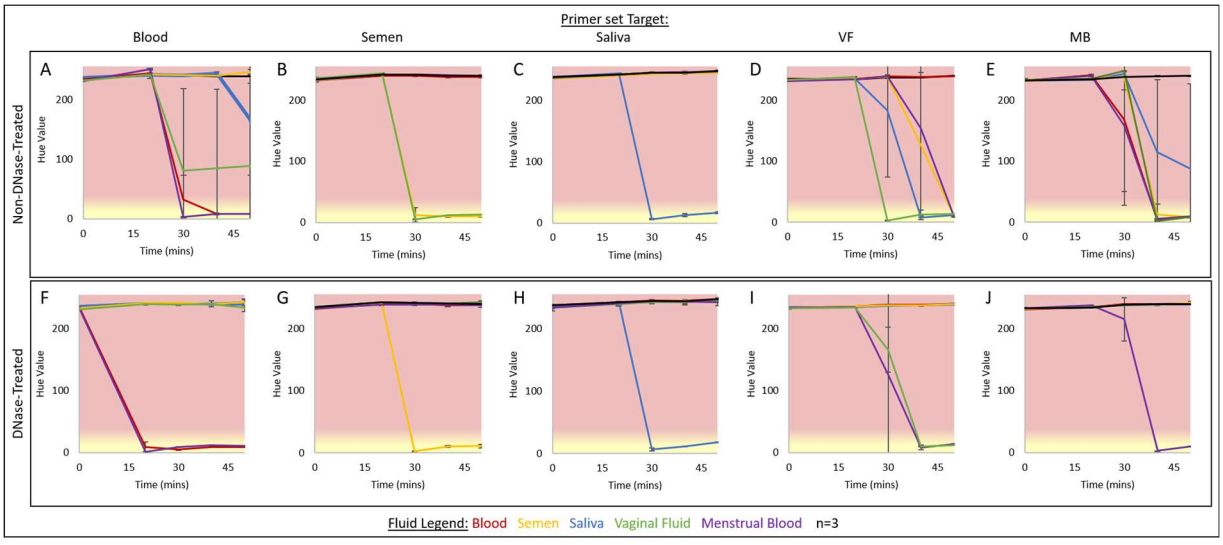

Figure 13: Specific amplification of targets for five fluids. Each of the targets was amplified with non-DNase treated (A-E) and DNase-treated (F-J) samples. The DNase-treated samples show high specificity for each body fluid target. (F) HBB is the blood target and known to amplify with MB. (I) Due to the same anatomical area for MB and VF, both fluids were expected to amplify.

was still included in order to establish a universal preparation method for all sample types (**Fig. 13C** and **H**).

We established an RNA preparation method that (1) largely eliminated erroneous results produced by NSA, (2) allowed the lysis, purification, and LAMP process to be universal for all five body fluid targets, and (3) assured that no residual genomic DNA was present in the lysate after the purification process. The data shows this small adjustment greatly improved the accuracy and specificity of LAMP-based detection of all five body fluids.

2.3.8 Sensitivity of colorimetric LAMP method

Assay sensitivity was assessed by determining the lowest total RNA concentration for successful amplification of individual mRNA targets. Ideally, the limits of detection (LODs) for the body fluid targets should exhibit comparable total RNA concentrations to current, accepted assays. (1) We determined that the body fluids could be successfully amplified with input masses in the picogram or nanogram range, depending on the mRNA target. **Fig. 14A** shows the Vb assay is the most sensitive, consistently amplifying the associated mRNA target (HBB) at 31 picograms of total RNA. Currently, blood is detected via a phenolphthalein tetramethylbenzidine test (PTMB) (i.e., tests for peroxidase-like activity ideally of hemoglobin) or protein lateral flow assay (e.g., human glycophorin A). Both of which have variable sensitivity of approximately 1:1,000,000 dilution of 20 µL whole blood. (43, 44) While it is not a direct comparison (protein to total RNA), our LAMP results are based on total RNA extraction and purification from only 10 µL of whole blood.

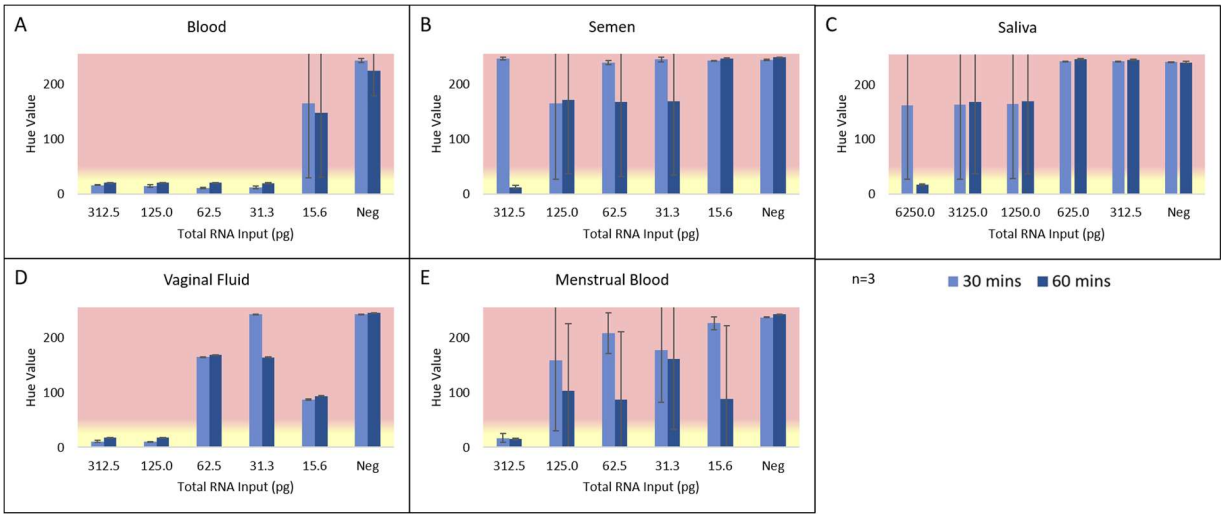

Figure 14: Various concentrations of RNA input for body fluid LAMP at 63 °C. Each bar represents amplification for blood (A), semen (B), saliva (C), vaginal fluid (D), and menstrual blood (E). The dashed lines are 3 standard deviations above or below the averages and show the ranges for both positive and negative hue values.

Seminal fluid and/or Se is presumptively detected using either an enzyme test (e.g., acid phosphate) or protein lateral flow assay (e.g., semenogelin, prostate-specific antigen (PSA)), and confirmatory tested by 'Christmas Tree' cell staining, which uses kernechtrot to visualize epithelial cells in green and picroindigocarmine to visualize the acrosomal cap of the sperm heads in red/pink (45). Using a microscope, if a single sperm cell is found, the evidence is carried forward to DNA profiling. **Fig. 14B** shows LAMP was able to detect approximately 300 pg of total RNA after 40 minutes of heating. For comparison, the sensitivities of the lateral flow assay are approximately 2.5 nL (46) and for the enzyme test a 1:200 dilution of human Se. (47) The Vf and Mb targets also showed sensitivity at approximately 100 pg and 300 pg total RNA after a 30-minute LAMP incubation, respectively (**Fig. 14D and E**). Although there is no presumptive or confirmatory test currently used in forensic science to compare with the LAMP assay, other research endeavors in literature show sensitivity similar to these values. (48-50)

With the addition of a DNase-treatment, no color change or amplification was observed with the Sa target in LAMP reactions. It was hypothesized the lack of amplification could be due to a low expression of the Sa target in the sample and, because of the DNase treatment, no genomic DNA with a similar sequence to amplify. It is known that Sa has lower RNA concentration than other body fluids (51) due to the presence of abundant RNases. Various approaches were examined to improve amplification performance, including increasing the volume of lysate added to the LAMP reaction and/or increasing input volume of neat Sa to the lysis and purification process. Even when RNA sample volume was increased to 25% of the total LAMP reaction (3.12 of 12.5 µL), there was no detectable amplification (**Fig. 15A**) over a total RNA mass range of 2.5 to 9.4 ng from two different donors. However, consistent amplification of the Sa target in 30 minutes was achieved by increasing the input sample volume from 30 µL to 200 µL to the lysis and purification process (**Fig. 15B**). Successful amplification was also observed for whole dry or wet buccal swabs. Data collected from samples from three different donors correlated well, indicating low variability of the RNA target across samples at these volumes. Using 200

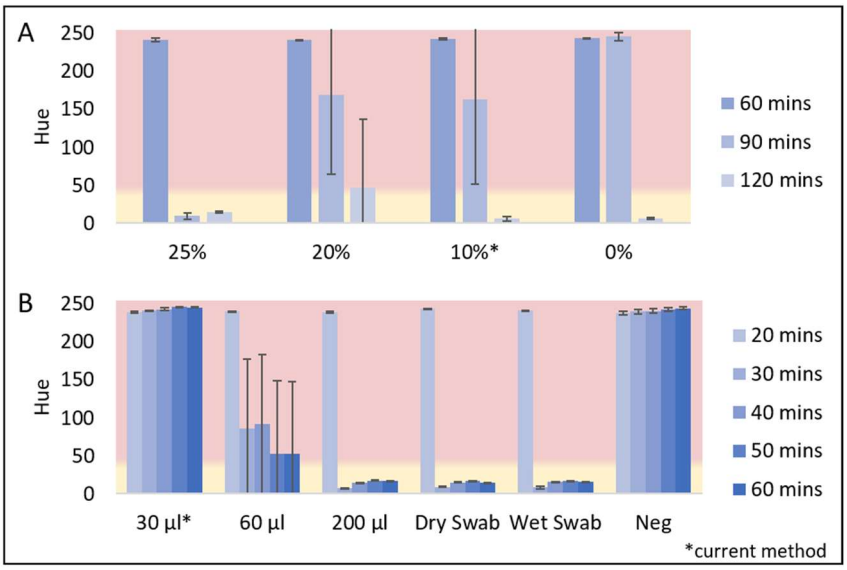

Figure 15: Various approaches to increase amplification of Sa RNA target. (A) By increasing the volume of purified sample to the LAMP reaction, amplification was achieved, but at a slower rate. (B) After a DNase treatment, 200 µl of neat Sa or a buccal swab showed consistent amplification of the Sa RNA target. Each bar represents an n=9 across three donors.

µL of neat Sa, the lower limit of detection of the LAMP assay was greater than 6.25 ng of total RNA (**Fig. 14C**). While amplification of this target is not as sensitive as we would like, the sensitivity is, however, relatively comparable to other research methods. (41, 52, 53) The common presumptive Sa methods (α-Amylase or Lateral Flow Assay) used in forensics have sensitivities at dilutions of approximately 1:100 (54), but these methods do not target genetic material and instead detect enzymes or proteins that are also present in other body fluids. Thus, continued efforts towards a Sa LAMP assay exhibit promise for a more specific saliva identification test.

2.4 Summary

The current presumptive and confirmatory tests for body fluids have served the forensic community well over many years, but have defined limitations, including high incidences of false positives and cross-reactivity. The work described here aimed to develop an innovative, sensitive, and specific colorimetric mRNA amplification-based confirmatory method for identification and differentiation of body fluids. The LAMP method is easily incorporated into existing workflow by using a common thermal cycler and a simple lightbox with a smartphone or easily accessible scanner. The amplification targets tissue-specific mRNA loci in body fluids (venous blood, semen, saliva, vaginal fluid, menstrual blood) with 'objective' results owing to empirical colorimetric analysis, which circumvents the analyst bias inherent in simple visual detection. There was a significant increase in specificity for all five mRNA targets after a DNase treatment was implemented in the lysis and purification method. The data also shows that picogram levels of total RNA can be consistently detected via LAMP by targeting mRNA regions specific to each body

fluid. The isothermal amplification of the Vb mRNA target was the most sensitive, while amplification of the Sa mRNA target was the least sensitive. This data shows the first step towards developing a novel approach for forensic body fluid identification.

2.5 References

1. Butler JM. Chapter 4 - Sample Collection, Storage, and Characterization. Fundamentals of Forensic DNA Typing. San Diego: Academic Press; 2010;79-97.

2. Tobe SS, Watson N, Daeid NN. Evaluation of six presumptive tests for blood, their specificity, sensitivity, and effect on high molecular-weight DNA. Journal of forensic sciences. 2007 2006/12/07;52(1):102-9.

3. Romero-Montoya L, Martínez-Rodríguez H Fau - Pérez MA, Pérez Ma Fau - Argüello-García R, Argüello-García R. Relationship of spermatoscopy, prostatic acid phosphatase activity and prostate-specific antigen (p30) assays with further DNA typing in forensic samples from rape cases. Forensic Science International. 2011 March 20, 2011;206(1-3):7.

4. Stange V, Pelição F, Mendonça J, Pissinate J, Barbirato C, Gonçalves F, et al. Increased Male Evidence Detection Rates by Utilization of DNA Markers in Forensic Rape Cases of Espírito Santo, Brazil. Annals of Forensic Research and Analysis. 2014 Sept. 30, 2014;1(2).

5. Zubakov D, Hanekamp E, Kokshoorn M, van Ijcken W, Kayser M. Stable RNA markers for identification of blood and saliva stains revealed from whole genome expression analysis of time-wise degraded samples. International journal of legal medicine. 2008;122(2):135-42.

6. Setzer M, Juusola J, Ballantyne J. Recovery and stability of RNA in vaginal swabs and blood, semen, and saliva stains. Journal of Forensic Sciences. 2008 2008/03/19;53(2):296-305.

7. Richard ML, Harper KF, Craig RF, Onorato AF, Robertson JF, Donfack J. Evaluation of mRNA marker specificity for the identification of five human body fluids by capillary electrophoresis. Forensic Science International: Genetics. 2012 2012/05/22;6(4):452-60.

8. Haas C, Klesser B, Maake C, Bär W, Kratzer A. mRNA profiling for body fluid identification by reverse transcription endpoint PCR and realtime PCR. Forensic Science International: Genetics. 2009 2008/11/14;3(2):80-8.

9. Notomi T, Okayama H, Masubuchi H, Yonekawa T, Watanabe K, Amino N, et al. Loop-mediated isothermal amplification of DNA. Nucleic Acids Research. 2000 April 15, 2000;28(12).

10. Mueller JD, Pütz B, Höfler H. Self-sustained sequence replication (3SR): an alternative to PCR. Histochemistry and Cell Biology. 1997 1997/10/01;108(4):431-7.

11. Compton J. Nucleic acid sequence-based amplification. Nature. 1991 1991/03/01;350(6313):91-2.

12. Su C-W, Li C-Y, Lee J, Ji D-D, Li S-Y, Daniel B, et al. A novel application of real-time RT-LAMP for body fluid identification: using HBB detection as the model. Forensic Science, Medicine & Pathology. [Article]. 2015 April 16, 2015;11(2):208-15.

13. Goto M, Honda E, Ogura A, Nomoto A, Hanaki K-I. Colorimetric detection of loop-mediated isothermal amplification reaction by using hydroxy naphthol blue. Biotechniques. 2009;46(3):167-72.

14. Tanner NA, Zhang Y, Evans TC. Visual detection of isothermal nucleic acid amplification using pH-sensitive dyes. BioTechniques. 2015 2015/02/01;58(2):59-68.

15. Jackson KR, Layne T, Dent DA, Tsuei A, Li J, Haverstick DM, et al. A novel loop-mediated isothermal amplification method for identification of four body fluids with smartphone detection. Forensic Science International: Genetics. 2020 2020/03/01;45:102195.

16. Krauss ST, Remcho TP, Lipes SM, Aranda R, Maynard HP, Shukla N, et al. Objective Method for Presumptive Field-Testing of Illicit Drug Possession Using Centrifugal Microdevices and Smartphone Analysis. Analytical Chemistry. 2016 2016/09/06;88(17):8689-97.

17. Schindelin J, Arganda-Carreras I, Frise E, Kaynig V, Longair M, Pietzsch T, et al. Fiji: an open-source platform for biological-image analysis. Nature Methods. 2012 2012/07/01;9(7):676-82.

18. Rueden CT, Schindelin J, Hiner MC, DeZonia BE, Walter AE, Arena ET, et al. ImageJ2: ImageJ for the next generation of scientific image data. BMC Bioinformatics. 2017 2017/11/29;18(1):529.

19. Rhyne T-M. Applying Color Theory to Digital Media and Visualization. 2016.

20. Woolf MS, Dignan LM, Scott AT, Landers JP. Digital postprocessing and image segmentation for objective analysis of colorimetric reactions. Nature Protocols. 2020 2020/12/09.

21. Scott AT, Layne TR, O'Connell KC, Tanner NA, Landers JP. Comparative Evaluation and Quantitative Analysis of Loop-Mediated Isothermal Amplification Indicators. Analytical Chemistry. 2020 2020/10/06;92(19):13343-53.

22. Levings PP, Bungert J. The human β-globin locus control region. European Journal of Biochemistry. 2002 2002-03-15;269(6):1589-99.

23. Lilja H, Abrahamsson PA, Lundwall Å. Semenogelin, the Predominant Protein in Human Semen. Journal of Biological Chemistry. 1989 1989-01-01;264(3):1894-900.

24. Oppenheim FG, Xu T, Mcmillian FM, Levitz SM, Diamond RD, Offner GD, et al. Histatins, a novel family of histidine-rich proteins in human parotid secretion. Isolation, characterization, primary structure, and fungistatic effects on Candida albicans. Journal of Biological Chemistry. 1988 1988-06-01;263(16):7472-7.

25. Tanner NA, Zhang Y, Evans TC. Simultaneous multiple target detection in real-time loop-mediated isothermal amplification. BioTechniques. 2012 2012/08/01;53(2):81-9.

26. Malhotra K. Interaction and effect of annealing temperature on primers used in differential display RT-PCR. Nucleic Acids Research. 1998 1998-02-01;26(3):854-6.

27. Yang F, Yang N, Huo X, Xu S. Thermal sensing in fluid at the micro-nano-scales. Biomicrofluidics. 2018 2018-07-01;12(4):041501.

28. Haas C, Hanson E, Anjos MJ, Ballantyne KN, Banemann R, Bhoelai B, et al. RNA/DNA co-analysis from human menstrual blood and vaginal secretion stains: results of a fourth and fifth collaborative EDNAP exercise. Forensic science internationalGenetics. 2014;8(1):203-12.

29. Albani PP, Fleming R. Novel messenger RNAs for body fluid identification. Science & Justice. 2018 2018/03/01/;58(2):145-52.

30. Fleming RI, Harbison S. The development of a mRNA multiplex RT-PCR assay for the definitive identification of body fluids. Forensic Science International: Genetics. 2010 2010/07/01/;4(4):244-56.

31. Satoh T, Kouroki S, Ogawa K, Tanaka Y, Matsumura K, Iwase S. Development of mRNA-based body fluid identification using reverse transcription loop-mediated isothermal amplification. Analytical and Bioanalytical Chemistry. [journal article]. 2018 July 01;410(18):4371-8.

32. Nussbaumer C, Gharehbaghi-Schnell E, Korschineck I. Messenger RNA profiling: A novel method for body fluid identification by Real-Time PCR. Forensic science international. 2006;157(2–3):181-6.

33. Lindenbergh A, de Pagter M, Ramdayal G, Visser M, Zubakov D, Kayser M, et al. A multiplex (m)RNA-profiling system for the forensic identification of body fluids and contact traces. Forensic Science International: Genetics. 2012;6(5):565-77.

34. Farell EM, Alexandre G. Bovine serum albumin further enhances the effects of organic solvents on increased yield of polymerase chain reaction of GC-rich templates. BMC Research Notes. 2012 2012-01-01;5(1):257.

35. Chakrabarti R. The enhancement of PCR amplification by low molecular weight amides. Nucleic Acids Research. 2001 2001-06-01;29(11):2377-81.

36. Poole CB, Ettwiller L, Tanner NA, Evans TC, Wanji S, Carlow CKS. Genome Filtering for New DNA Biomarkers of Loa loa Infection Suitable for Loop-Mediated Isothermal Amplification. PLoS ONE. 2015 09/28

05/29/received

09/09/accepted;10(9):e0139286.

37. Heinrich M, Matt K, Lutz-Bonengel S, Schmidt U. Successful RNA extraction from various human postmortem tissues. International Journal of Legal Medicine. 2007 2007-02-07;121(2):136-42.

38. Lauková L, Konečná B, Janovičová Ľ, Vlková B, Celec P. Deoxyribonucleases and Their Applications in Biomedicine. Biomolecules. 2020;10(7):1036.

39. Kunitz M. CRYSTALLINE DESOXYRIBONUCLEASE : I. ISOLATION AND GENERAL PROPERTIES SPECTROPHOTOMETRIC METHOD FOR THE MEASUREMENT OF DESOXYRIBONUCLEASE ACTIVITY. Journal of General Physiology. 1950;33(4):349-62.

40. Vanecko SF, Laskowski M, Sr., Laskowski M, Sr. Studies of the specificity of deoxyribonuclease I. III. Hydrolysis of chains carrying a monoesterified phosphate on carbon 5'. Journal of Biological Chemistry. 1961;236(12):3312-6.

41. Juusola J, Ballantyne J. mRNA Profiling for Body Fluid Identification by Multiplex Quantitative RT-PCR*. Journal of forensic sciences. 2007;52(6):1252-62.

42. Bauer M, Patzelt D. Identification of menstrual blood by real time RT-PCR: Technical improvements and the practical value of negative test results. Forensic Science International. 2008 2008/01/15/;174(1):55-9.

43. Garner DD, Cano KM, Peimer RS, Yeshion TE. An Evaluation of Tetramethylbenzidine as a Presumptive Test for Blood. Journal of Forensic Sciences. 1976;21(4):6.

44. Horjan I, Barbaric L, Mrsic G. Applicability of three commercially available kits for forensic identification of blood stains. Journal of Forensic and Legal Medicine. 2016 2016/02/01/;38:101-5.

45. Arend A, Kolts I. Carmine-picroindigocarmine: An alternative multiple staining method. Annals of Anatomy - Anatomischer Anzeiger. 2002 2002/03/01/;184(2):149-52.

46. Old J, Schweers BA, Boonlayangoor PW, Fischer B, Miller KWP, Reich K. Developmental Validation of RSID™-Semen: A Lateral Flow Immunochromatographic Strip Test for the Forensic Detection of Human Semen*. Journal of Forensic Sciences. 2012 2012/03/01;57(2):489-99.

47. Gonçalves ABR, de Oliveira CF, Carvalho EF, Silva DA. Comparison of the sensitivity and specificity of colorimetric and immunochromatographic presumptive methods for forensic semen detection. Forensic Science International: Genetics Supplement Series. 2017;6:e481-e3.

48. Blackman S, Stafford-Allen B, Hanson EK, Panasiuk M, Brooker A-L, Rendell P, et al. Developmental validation of the ParaDNA® Body Fluid ID System—A rapid multiplex mRNA-profiling system for the forensic identification of body fluids. Forensic Science International: Genetics. 2018 2018/11/01/;37:151-61.

49. Xu Y, Xie J, Cao Y, Zhou H, Ping Y, Chen L, et al. Development of Highly Sensitive and Specific mRNA Multiplex System (XCYR1) for Forensic Human Body Fluids and Tissues Identification. PLOS ONE. 2014;9(7):e100123.

50. Silva DSBS, Antunes J, Balamurugan K, Duncan G, Alho CS, McCord B. Developmental validation studies of epigenetic DNA methylation markers for the detection of blood, semen and saliva samples. Forensic Science International: Genetics. 2016;23:55-63.

51. Park NJ, Li Y, Yu T, Brinkman BMN, Wong DT. Characterization of RNA in Saliva. Clinical Chemistry. 2006;52(6):988.

52. Hanson E, Ingold S, Haas C, Ballantyne J. Messenger RNA biomarker signatures for forensic body fluid identification revealed by targeted RNA sequencing. Forensic Science International: Genetics. 2018 2018/05/01/;34:206-21.

53. Dawnay N, Stafford-Allen B, Moore D, Blackman S, Rendell P, Hanson EK, et al. Developmental Validation of the ParaDNA(R) Screening System - A presumptive test for the detection of DNA on forensic evidence items. 20140602 DCOM- 20150105(1878-0326 (Electronic)).

54. Old JB, Schweers BA, Boonlayangoor PW, Reich KA. Developmental Validation of RSID™-Saliva: A Lateral Flow Immunochromatographic Strip Test for the Forensic Detection of Saliva. Journal of Forensic Sciences. 2009 2009/07/01;54(4):866-73.

Chapter 3: Integrated device for colorimetric LAMP mock study comparison

3.1 Introduction

Loop-mediated amplification (LAMP) was first reported in 2000 using a viral DNA target for Hepatitis B with detection being accomplished via gel electrophoresis.(1) Since then, LAMP has been utilized for various clinical and forensic applications.(2-5) Much of this research has detailed methods for increasing the specificity and speed of the reaction by including more primers that anneal on the loop ends of the main structure. This has facilitated the production of target amplicons in less than 10 minutes of isothermal heating while using an elementary heating apparatus (i.e., hot water bath, heat block). In addition to describing reaction speed, various detection methods have been described in the literature.(4, 6, 7) Visual detection is common and may include observation of a color change using colorimetric dyes or visual assessment of the turbidity of the reaction. Additionally, quantitative analysis using a fluorescence detection instrument and intercalating dyes is often employed.(8-11) However, a real-time fluorescence detection device can be costly for a laboratory. Although there are also sensitivity and specificity concerns that must be considered when selecting a detection method, a more cost-effective and straightforward detection method for analyzing LAMP reactions could prove advantageous.

Colorimetric dyes are most often used for detection in LAMP reactions. Colorimetric dyes give a visual color change which discerns a positive from a negative result. The dyes used to detect amplicons in LAMP reactions include hydroxynaphthol blue, phenol red, and malachite

green, among others(12), which characteristically change color in response to chemical changes. For example, hydroxynaphthol blue, a colorimetric dye that functions as a metal-based indicator, changes from violet to sky blue as the Mg^{2+} binds with pyrophosphates and precipitates out of solution.(13) While colorimetric dyes have been used in various research applications, these endpoint assays are highly subjective due to variations in individual perception of color.(12) Although endpoint analysis has been used for many years, recent research has been trending towards employing real-time analysis to obtain a more rapid response and to facilitate quantification of results based on signal intensity. Colorimetric detection is inherently less sensitive than detection via fluorescence measurements; however, the shift from endpoint to real-time analysis could potentially provide significant enhancements that minimize the impact of this limitation.

Real-time colorimetric analysis can be most simply achieved by capturing images of the reactions at various time points. Additionally, image analysis can be as elementary as using a smartphone or small camera to capture an image of the reactions and using software to analyze the color of the reaction.(14, 15) It is imperative that the camera, camera settings, and lighting remain static for every capture to ensure consistency of experimental conditions. Lighting, in particular, must remain consistent as the color of the image can be affected by the type of light - white, sunlight, incandescent, among others - as well as “stray” light from the environment. Concordant conditions can be maintained by capturing smartphone images in “manual” mode rather than the default “auto” settings. Once established, the software parameters used to assess color attributes should also be kept consistent. An example of software routinely used in literature to analyze images is Image J. (16, 17) This program features a suite of tools that can be

used to analyze an image via adaptation of colorimetric parameters. For example, a specific area of an image can be isolated and assessed for evaluation. An image can also be "tinted" to enhance subtle color variations, thereby allowing for improved detection of minute differences in color and increased sensitivity.(18, 19) This type of analysis allows for programmed, objective, and consistent measurement of color at specific time points across lengthy reaction times by analyzing images captured as the reaction progresses. This technology can thus help to address the inherent deficiencies in the sensitivity of colorimetric analysis as compared to fluorescence methods.

The research described herein capitalizes on innovative technology while advancing an emergent amplification method that can be adapted for various applications. Optimization of a LAMP assay for five messenger RNA targets for identifying body fluids from forensic samples has been previously described by the Landers Lab.(20, 21) This method was coupled with image analysis of colorimetric dyes within the LAMP reactions. Accordingly, this manuscript details the development of a 3D-printed, automated, convective heated image analysis device to streamline the optimized process as the next phase of this research. Briefly, the hardware of the device has three stackable 3D-printed pieces and uses a thermocouple to maintain the temperature inside the heating chamber, while the complementary software was developed in-house in LabVIEW software. The reactions were monitored by image capture via Raspberry Pi camera at multiple time points to assess the color change in the LAMP reactions over time. Various mock forensic samples were analyzed and compared to a conventional method (thermal cycler and light box) to validate the device. Summarily, the successful development of a one-step, isothermal heating,

and automated colorimetric image analysis device that can be used as an alternative, cost-effective method for real-time monitoring of colorimetric LAMP assays was achieved.

3.2 Methods & Materials

3.2.1 Sample collection

Venous blood (denoted Vb hereafter) samples were provided by the University of Virginia Medical School. These samples were collected via a standard venipuncture technique as a part of routine care and treated with 5.4 mg of K_2EDTA to prevent coagulation. The samples were stored at 4 °C until used. All other donated deidentified semen (Se), saliva (Sa), vaginal swabs (Vf), and menstrual blood (Mb) swabs were collected using procedures approved by the University Institutional Review Board. Freshly donated, deidentified Se and Sa samples were collected in sterile specimen containers, and 50 µL aliquots were prepared and stored at -20 °C until needed. Fresh, deidentified Vf and Mb were collected on sterile cotton swabs, dried overnight, and stored at 4 °C. Mock samples were prepared on either cotton swabs, cotton cloth, jeans, or filter paper and dried for 24-hours before testing. The deidentified post-coital swabs were collected at various intervals and stored at room temperature. The 4-year-old samples were prepared in 2015 by aliquoting 100 µL of neat blood or Se on filter paper, dried for 24-hours, then stored in a dark at room temperature.

3.2.2 RNA isolation with DNase treatment

For lysis of Vb, Vf, or Mb swabs, Sa, or Se samples, 350 µL of RLT buffer was combined with 90 µL RNA-free water, 10 µL Proteinase K (Qiagen, Valencia, CA), and 4.5 µL of β-

mercaptoethanol (Sigma Aldrich, St. Louis, MO). 10 µL of Vb, 2 µL of Se, whole swab of Vf or Mb, or 200 µL of Sa was added as appropriate to each known single-source RNA isolation. For mock samples, either ¼ swab, a similarly sized cutting, or 2 mm biopsy punch was added to the RNA isolation. The samples were incubated at 56 °C for 10 minutes, and then swab and cloth samples (post-lysis) were put through a second centrifugation step to retrieve all lysis liquid. The swab and cloth samples were placed in 0.5 mL tubes which had been punctured in the bottom with a 21-gauge needle. The punctured tubes were then placed in a 1.5 mL microcentrifuge tube and centrifuged at a short spin cycle in a tabletop centrifuge for 1-2 seconds at maximum speed.(22, 23) The remaining fluid from the swab and cloth samples was spun through to the 1.5 mL tube and combined with the original lysed sample. The RNeasy Mini kit (Qiagen, USA) with the on-column DNase treatment was used for all purifications of samples according to manufacturer instructions. The DNase mix contained 5 µL DNase I (1 unit/µL; New England Biolabs, USA) and 75 µL DNase I Reaction buffer (New England Biolabs, USA) for each sample. After completing the purification protocol, all samples were eluted in 50 µL nuclease-free water and stored at -80 °C until needed.

3.2.3 Primer information for messenger RNA targets

Human B-globin (HBB; accession no. NM000518.5) was targeted for Vb identification, cytochrome P450 family 2 subfamily B member 7 (CYP2B7P; accession no. NR_001278.1) for Vf, human semenogelin-1-precursor (SEMG1; accession no. NM003007.4) as a Se marker, histatin-3 precursor (HTN3; accession no. NM000200.2) for Sa, and matrix metallopeptidase 10 (MMP10;

accession no. NM_002425.2) for Mb detection. The LAMP primer sets were designed using PrimerExplorer V5 and purchased from Eurofins Genomics LLC (Louisville, KY, USA).

3.2.4 Colorimetric LAMP analysis

The WarmStart® Colorimetric LAMP 2X Master Mix (DNA & RNA) (M1800) (New England Biolabs, Ipswich, MA, USA) was used at half reaction volume with a 10% input sample volume for all the experiments according to the manufacturer's instructions. LAMP reactions were amplified at 63 °C for up to a 60-minute amplification with primer concentrations of 0.2 µM for F3 and B3, 0.8 µM for LF and LB, and 1.6 µM for FIP and BIP. Once the amplification was finished, the reactions were placed inside of an in-house 3D-printed 'lightbox' made of white polylactic acid (PLA) in three stackable pieces and a top poly (methyl methacrylate) (PMMA) cover piece.(24) Image acquisition of all samples were taken with a HUAWEI P9 (HUAWEI Technologies Co., Shenzhen, China) with settings ISO 50, shutter speed 1/160, and auto white balance. Using FIJI(17) distribution of ImageJ(16) (2.0.0-rc-69/1.52p), the images were tinted using Image > Adjust > Color Balance command path and applying two sequential adjustments: blue channel 0-190 and yellow channel 40-255. With a custom PlugIn, the images were analyzed for hue in a cropped circle with radius of 15 pixels and exported to a .csv file. The .csv file contains sample number, area of circle, mean of hue, minimum hue detected, and maximum hue value detected. A positive and negative range was empirically determined to assign a LAMP reaction as positive or negative. The Vb mock LAMP reactions were analyzed on Agilent 2100 instrumentation using DNA 1000 series II kits (Agilent Technologies, Santa Clara, CA) for confirmation of target

amplification. A set of Se mock LAMP reactions were further analyzed using an ABAcard® p30 test (Abacus Diagnostics, USA) following manufacturer's protocol.

3.2.5 cLAMP system

The combined LAMP and Image Analysis (cLAMP) system was 3D-printed using white acrylonitrile butadiene styrene (ABS) or black polylactic acid (PLA). When using white ABS, the heating chamber is 6.75 x 7.5 x 7.5 in, with the top attached by a hinge that is 6.75 x 5.25 x 2.5 in. Using black PLA, the electronics are held at the bottom of the system, which has dimensions of 8.5 x 8.5 x 2.5. The total height of the system is 12.5 in and 8.5 x 8.5 in. Three strips of white light-emitting diodes (LED) are located inside the top of the device and are covered by a diffusive layer. A Raspberry Pi (RPi) camera v2.1 and Raspberry Pi 2 Model B+ v1.2 controller were used for image capture. The 120C AC Single Phase Heater was attached to the back of the heating chamber in a white ABS holder. Inside the heating chamber are four 25x25x10 mm 12V DC fans and two LED strips on either side of the RPi camera.

3.3 Results and Discussion

One goal of this project was to build an automated system to isothermally heat the LAMP reactions, while simultaneously capturing and analyzing the color of the reactions. Using convective heating and cost-effective materials, a 3D printed system was designed to heat, image capture, hue analyze, and compare each time point to an averaged threshold for a 'positive' or 'negative' result. Furthermore, the system was compared to a conventional method via a mock study with prepared forensically similar samples.

3.3.1 Colorimetric analysis

In Chapter 2, the LAMP assay was optimized for various forensic body fluid messenger RNA (mRNA) targets which were validated by analyzing mock samples in a single-blind study.(20) In these studies, the samples were heated in a conventional thermal cycler, and images were captured using a stand-alone 3D-printed imaging box and smartphone (**Chapter 2- Fig. 2**). The LAMP reactions were analyzed using two colorimetric dyes, Hydroxynaphthol blue (HNB) and Phenol red (PR), to determine the presence or absence of an mRNA target (**Fig. 1**). HNB changes color from purple (negative) to blue (positive) as the Mg^{2+} reacts with pyrophosphates and precipitates out of solution, leading to decreased concentration. PR changes color from red/pink (negative) to yellow (positive) as the pH of the solution changes from ~8.4 to ~6.4, becoming more acidic. Within the HSB (hue, saturation, and brightness) color space, hue value was determined to be the most discriminatory for the colorimetric analysis of both dyes, as each hue

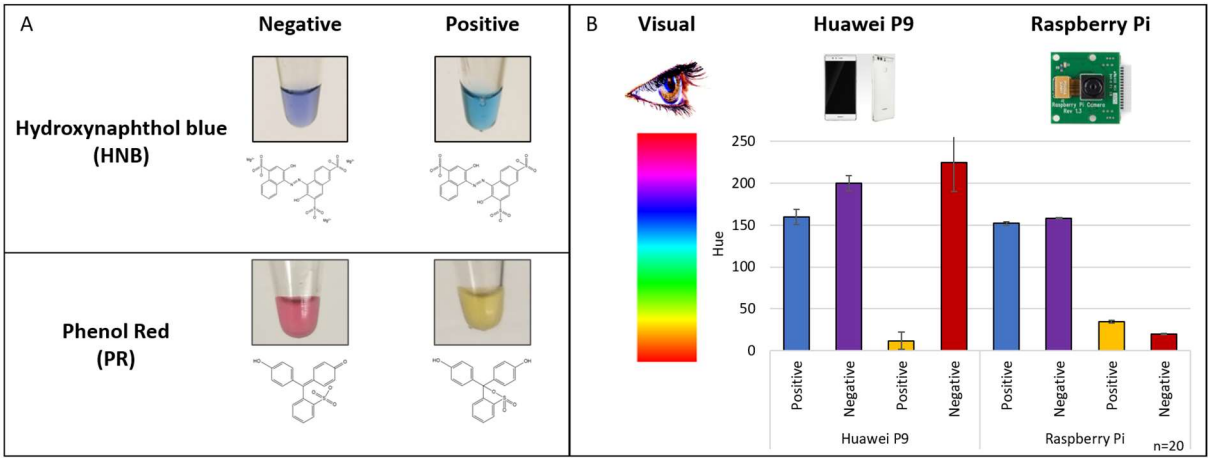

<u>Figure 1</u>: Colorimetric dyes used for analysis of LAMP reactions. (A) HNB changes from purple to blue as Mg^{2+} concentration decreases in the reaction. PR changes from red/pink to yellow as the pH changes from ~8.4 to ~6.4 in the reaction. (B) Color is analyzed differently between the human eye, Huawei smartphone, and Raspberry Pi camera. Previously, the Huawei smartphone was used for color analysis, but the integrated system was built with a cost-effective Raspberry Pi camera. The Raspberry Pi camera has provided more strict bounds for positive and negative colors than the Huawei smartphone.

value reflects a ‘shade’ of a color. The color change was quantitated using hue for analysis, and a threshold was set to show positive and negative regions.

The lightbox described in Chapter 2 allowed for static lighting and image conditions which gave consistent colorimetric detection (**Chapter 2- Fig. 2**). However, there were a few faults with this system. For example, the reactions had to be taken out of the thermal cycler and placed in the imaging box for every instance of image capture. This requirement led to the reduction of the reaction temperature and potential non-specific amplification (NSA). If there is enough NSA, a consequent color change in the reaction could erroneously be detected as positive. Another fault of the imaging box was the reaction tubes needed to be rotated 180° for the image to be taken. If the reactions were flipped or placed in the imaging box with too much force, the liquid would move to the top of the tube, thereby prohibiting image analysis. In this case, the reactions would require centrifugation to relocate the liquid to the bottom of the tube for proper image analysis. Furthermore, the extra time taken to perform this centrifugation resulted in a decrease in the reaction temperature and increased the likelihood of NSA. The cLAMP system (**Fig. 2**) was built for one-step isothermal heating for LAMP reactions and automatic real-time colorimetric image analysis to alleviate these shortcomings.

3.3.2 cLAMP system hardware

The cLAMP system consists of a 3D-printed ABS enclosure, a forced convection heating system, an imaging system, direct front lighting, diffused backlighting, integrated electronics, and a user interface with an automated image analysis program. The accompanying software will be discussed in a later section. **Fig. 2A** shows the cLAMP system connected to a laptop with the

software via an ethernet cord. Once connected to a wall outlet, the cLAMP system can be turned on to preheat using the red in-line switch.

The cLAMP system is programmed to preheat to 80 °C, giving an in-tube temperature of ~68 °C. This preheat temperature is achieved (starting from room temperature) after ~45 minutes. **Fig. 2B-D** show the inside of the cLAMP system. In the heating chamber (**Fig. 2B**), the RPi camera is set in the center at the bottom of the chamber with polyethylene terephthalate (PET) covering the electronics. LED strips are located on either side of the camera for lighting. Four fans were mounted in the corners of the heating chamber to circulate the heat, producing consistent temperatures in all 96 wells. The heating element is fixed to the outside of the heating chamber, which has an opening to its backside. The temperature is recorded by a thermocouple fixed directly below the metal plate nearest to the reaction tubes.

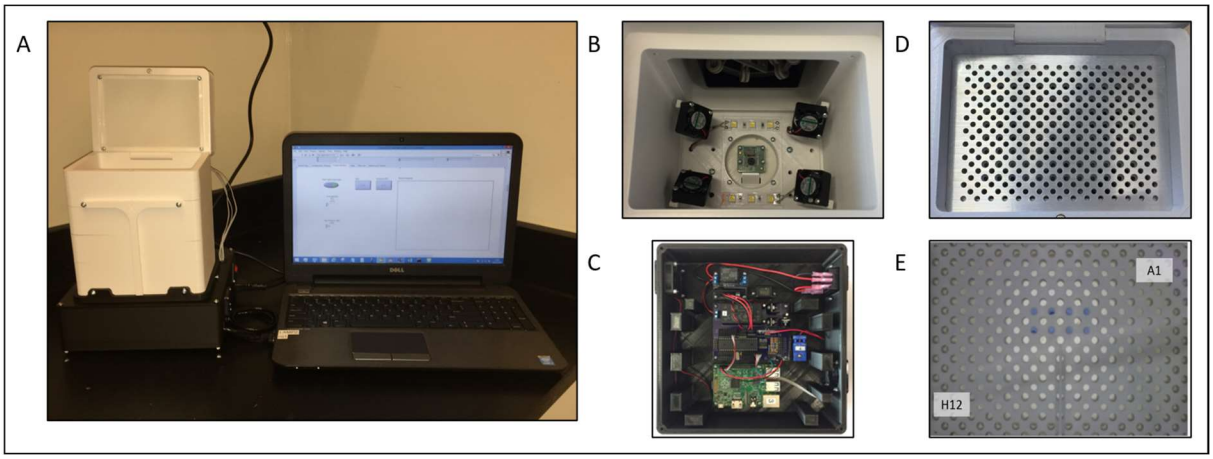

Figure 2: Simple integrated cLAMP system for real-time amplification and image analysis. (A) The 3D-printed cLAMP system is connected to a laptop with LabVIEW software via ethernet cord. (B) Inside the cLAMP system, the heating chamber contains a heating element, 4 fans, direct front lighting on either side of a Raspberry Pi camera. (C) Below the heating chamber is the electronics necessary for heating and image capture. (D) LAMP reactions in 0.1 mL microcentrifuge tubes are seated in a CNC machined metal plate, which sits on top of the heating chamber. (E) Exemplary Image captured inside the cLAMP system.

The electronics were placed underneath the heating chamber (**Fig. 2C**). This area contains the RPi 2 Model B+ v1.2 and printed circuit board (PCB). Sitting inside the heating chamber is a computer numerical control (CNC) machined metal plate with conical-shaped holes for 96 0.1 mL microcentrifuge tubes and cylindrical holes as air vents for heat flow above and below the tubes (**Fig. 2D**). The bottom of the metal plate was painted matte white to alleviate reflection on the metal surface from the LED lights beside the RPi camera in the images captured. The metal plate has etchings to denote row letters and column numbers for correct placement. The two metal plates were machined to a conical shape that fits a 0.1 ml microcentrifuge tube at ~6.5 mm and ~9.75 mm in height (**Fig. 3**). Initially, the contact between the 6.5 mm metal plate and tube ended farther from the bottom of the tube, giving a larger area for image analysis. However, it was determined that the heat transfer using this configuration was insufficient due to the minimized contact area between the metal plate and tube. Therefore, a portion of this area was sacrificed for imaging, and the 9.75 mm metal plate was used to enhance the contact area and heat transfer to the reaction liquid while maintaining

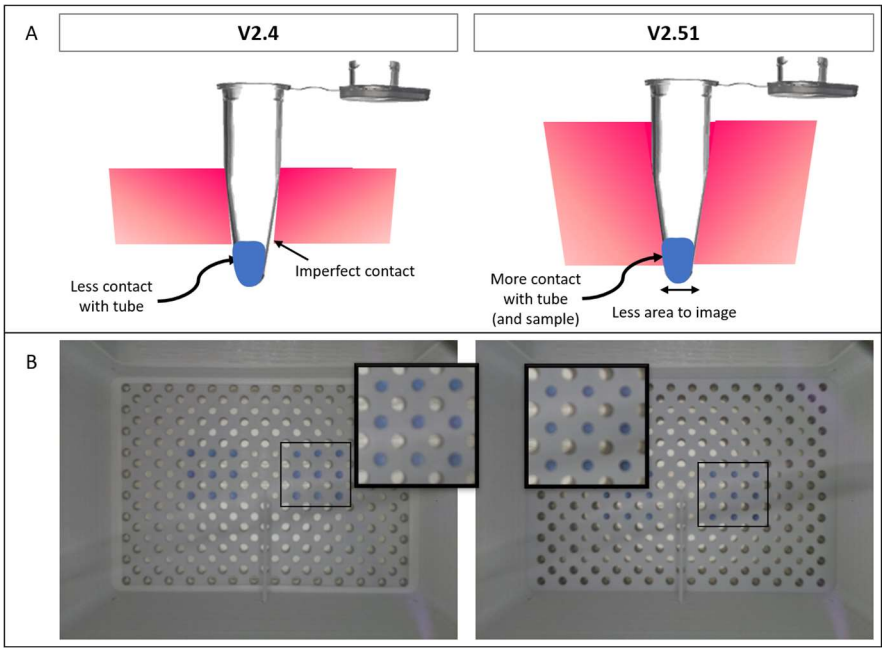

Figure 3: Comparison of different structured metal plates. (A) The 6.5 mm metal plate was initially tested with contact ending at a higher part of the tube and then compared to a 9.75 mm metal plate with more contact, but less area to image. (B) Exemplary images acquired from the camera during heating.

consistent image analysis conditions. In the top of the cLAMP system is a diffusive layer and four LED strips, which complete the static lighting for imaging. An exemplary image of the LAMP reactions inside the cLAMP system is shown in **Fig. 2E**. The cLAMP system is simple to operate: the user loads samples into the sample plate, opens the cLAMP protocol in the laptop-driven LabVIEW software, specifies a name for the test, defines an image capture interval, enters an end time for the test, and presses the start button. The cLAMP system will heat and analyze images until the assay is complete and then saves all data in a single folder with the user-specified name.

3.3.3 cLAMP system software

The heating and image capture for the cLAMP software are controlled by custom written code via Propellor and LabVIEW software. Prior to using the cLAMP system, the RPi controller is programmed with the Propellor code, which starts the heater and monitors the temperature in the heating chamber via a Type-T thermocouple. This will happen once the in-line switch on the cLAMP system is flipped to 'on'. The heating chamber temperature is set to 80 °C, which will preheat to ~68 °C (in-tube temperature) in 45 minutes. To start a run on the cLAMP system, the user will open the LabVIEW file to the 'Splash Page' (not shown). The 'Control' tab allows the user to define the parameters for each run on the cLAMP system (**Fig. 4**). The parameters to be defined are total assay time, image acquisition frequency, assay temperature, number of reactions, and type of colorimetric dye. In case of user or system errors, the 'Control' tab also has options to stop the camera or stop the run, and any errors detected during the run will be displayed in the error menu. Once the parameters are filled in, the user can start the run, and data will be shown on the 'Data' tab. The 'Data' tab will populate various tables and graphs with hue data from real-

time image analysis of the reaction tubes. The user will be able to see the current minute's image along with the hue values in table and graphical format. A threshold is calculated by averaging the hue values from minutes 0-2 for each reaction and adding 5 standard deviations (**Fig. 5**). Once a sample has passed the threshold, the tube location will light up bright green in the sample array (**Fig. 4B**). The user is visually alerted when samples in the 96 well array are considered to have a positive hue value.

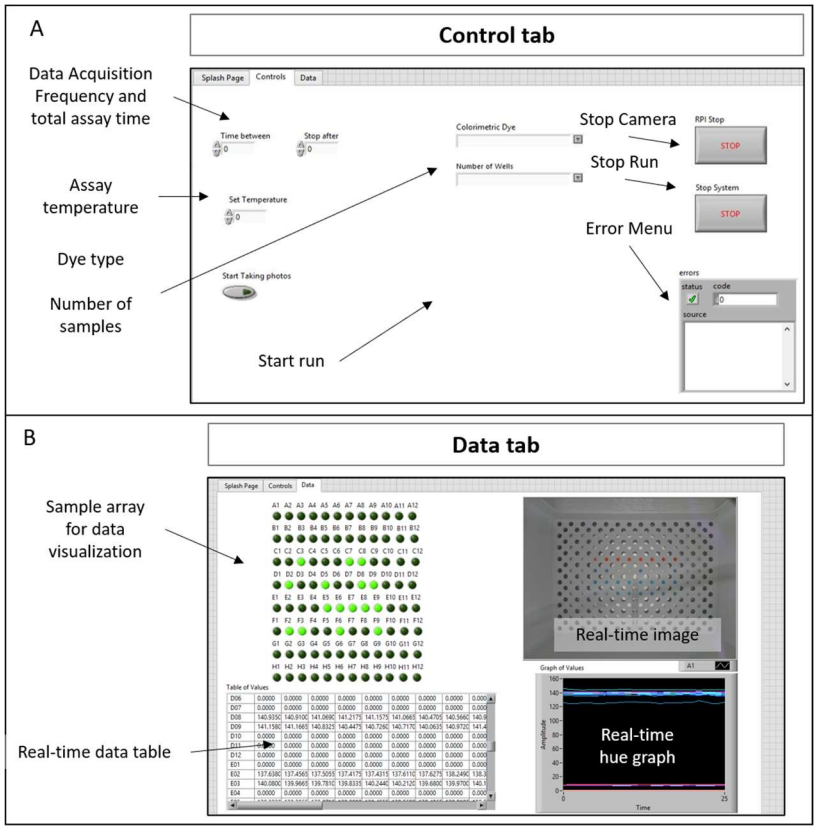

Figure 4: LabVIEW software for image capture and analysis in the cLAMP system. (A) In the Control tab, experimental variables pertaining to overall time, image acquisition time, heat temperature, number of reactions, and colorimetric dye are entered and saved before starting the experiment. (B) In the Data tab, the color analysis of all 96 wells is shown in real-time. The image will change after a new capture and ~45 secs after the values are shown in table and graphical format. A threshold is calculated from averaging the hue from minutes 0-2 for each reaction and adding 5 standard deviations. Once a sample has passed the threshold, the location will light up in the sample array.

The LabVIEW software creates files that contain data from the run on the cLAMP system. After the run is started, a text file (.txt) is created containing all of the parameters defined on the 'Control' tab. After each image is produced, it is saved as 'Image_X.jpg' for each interval in the previously described image acquisition frequency. The raw hue values for each image are saved

in a comma-separated values (.csv) file, and the averaged hue values for each image are saved in a separate .csv file. Both of these files contain hue values for all 96-wells over the defined total assay time. The LabVIEW software for the cLAMP system produces relevant data from a run in one folder titled by the user and allows the user to manipulate the raw or averaged data as needed.

A

$$Phenol\ Red\ Threshold = \left(Average\ Hue(Min\ 0,1,2)\right) + (5 * Standard\ Deviation\ (Min\ 0,1,2))$$

$$HNB\ Threshold = \left(Average\ Hue(Min\ 0,1,2)\right) - (3 * Standard\ Deviation\ (Min\ 0,1,2))$$

B

Table of Values

	0	1	2	3	4	5	6
A01	35.755	35.518	35.676	35.884	35.838	35.656	34.967
A02	35.621	35.317	35.572	35.779	35.704	35.597	36.253
A03	34.390	35.341	35.548	34.967	35.418	35.149	35.558
A04	34.625	33.846	34.606	34.086	34.832	34.593	34.462
A05	34.025	34.231	34.243	34.032	34.038	34.026	34.586
A06	34.661	34.324	34.516	34.402	34.858	34.624	34.386
A07	0	0	0	0	0	0	0
A08	0	0	0	0	0	0	0
A09	0	0	0	0	0	0	0
A10	0	0	0	0	0	0	0

Table of Values Averaged

	0.000000	1.000000	2.000000	3.000000	4.000000	5.000000	6.000000	7.000000	8.00000
A01	35.7550	35.5180	35.6760	35.6927	35.7993	35.7927	35.4870	35.0530	35.0853
A02	35.6210	35.3170	35.5720	35.5560	35.6850	35.6933	35.8513	35.5230	35.6860
A03	34.3900	35.3410	35.5480	35.2853	35.3110	35.1780	35.3750	35.0893	35.0803
A04	34.6250	33.8460	34.6060	34.1793	34.5080	34.5037	34.6290	34.6183	34.7337
A05	34.0250	34.2310	34.2430	34.1687	34.1043	34.0320	34.2167	34.1500	34.3297
A06	34.6610	34.3240	34.5160	34.4140	34.5920	34.6280	34.6227	34.4250	34.4810
A07	0.0000	0.0000	0.0000	0.0000	0.0000	0.0000	0.0000	0.0000	0.0000
A08	0.0000	0.0000	0.0000	0.0000	0.0000	0.0000	0.0000	0.0000	0.0000
A09	0.0000	0.0000	0.0000	0.0000	0.0000	0.0000	0.0000	0.0000	0.0000
A10	0.0000	0.0000	0.0000	0.0000	0.0000	0.0000	0.0000	0.0000	0.0000

Figure 5: Threshold calculation and exported data from the integrated system. (A) The software can calculate and use the threshold for two colorimetric dyes. Previous testing showed that a moving average of three points is sufficient for thresholding. (B) All of the hue data is exported into two csv files (Raw, Averaged) and can be seen on screen if desired.

3.3.4 Heating chamber optimization

After constructing the cLAMP hardware and software, heat testing was performed to determine the necessary heating chamber temperature, optimize the rapid temperature increase required for the LAMP reactions, and evaluate the temperature stability over 60 minutes. The air temperature in the heating chamber is monitored by a thermocouple placed directly below the metal plate of the cLAMP system during preheating and amplification. **Fig. 6A** illustrates the curves obtained from multiple wells following preheating runs (from room temperature to ~ 67 – 68 °C) within 45 minutes.

Initially, the heating chamber was set to match the desired temperature of the LAMP reactions (65 °C), and after 45 minutes, these reactions were placed into the cLAMP system. However, the reactions did not subsequently reach ≥ 65 °C until ~10 minutes. This delay was attributed to the loss of chamber heat that resulted when the lid was opened for sample insertion. The preheat temperature was set ~ 2 - 3 °C above the desired amplification temperature to account for this loss. Consequently, the reactions reached the desired amplification temperature within 30 seconds after preheating the cLAMP system (**Fig. 6B**). Many wells were tested to verify that the temperature ramp across the 96 wells is consistent. The reactions remained at the desired amplification temperature for the duration of the run (60 minutes). A minimal temperature difference observed in some cases (~1.5 °C) was correlated to the well location in the heating chamber. Overall, the cLAMP system was shown to be capable of quickly heating the LAMP reactions to the desired amplification temperature and subsequently maintaining that temperature for the entire testing period.

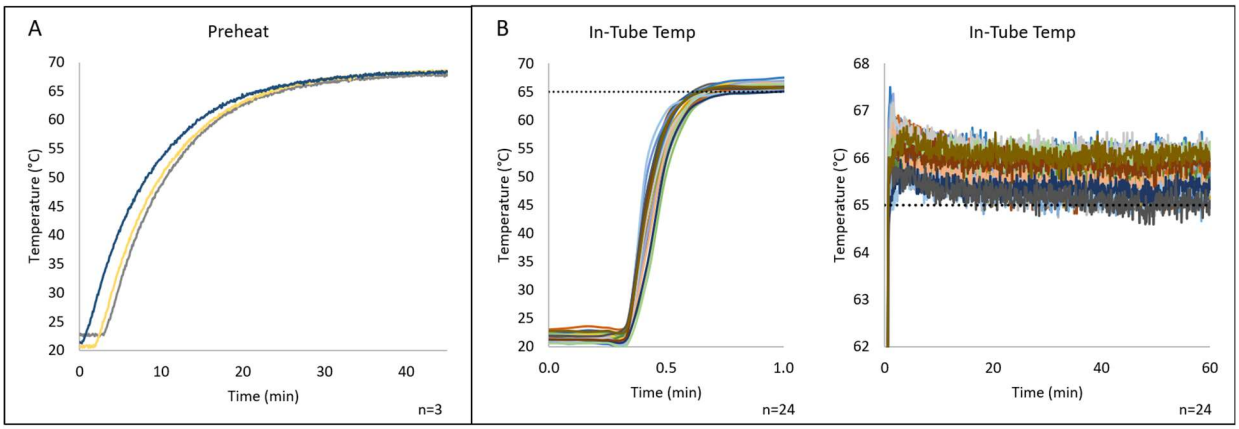

Figure 6: Temperature stability inside the heating chamber of the cLAMP system. (A) Metal block temperature during the 45 min preheat step which achieves desired temperature. (B) The in-tube temperature after being placed in the cLAMP system. All samples ramp to 65 °C within 30 sec and are stable at 65 °C over time. Various wells were monitored to assess correct temperature.

The temperatures in multiple wells were then compared to those obtained from a conventional thermal cycler to determine if the heat generated in the cLAMP system was sufficient. Multiple 0.1 mL tubes were filled with 12.5 µL colored water, and a thermocouple was placed through the top of the tubes. The tubes were then heated in either a conventional thermal cycler or the cLAMP system to 65 °C for 45 minutes. These experiments were conducted over four days to account for any slight changes in the ambient temperature, and the temperature data sets from the cLAMP system vs. the conventional thermal cycler were averaged and compared. **Fig. 7A** shows the ramping profiles for various wells from room temperature after the preheat time. It was determined from calculations that the ramp rates from the cLAMP system were higher than those from the conventional thermal cycler. This is pertinent as the ramp time is critical for any amplification reaction as it can determine if non-specific binding is inhibited in the initial steps. Still, both systems were able to reach the desired amplification temperature within 30 seconds. Once ramp rates were established, temperatures from various wells were then averaged to evaluate consistency over time. A temperature of ~65 – 66.5 °C was set as a baseline target for the cLAMP system. This temperature was chosen as it was consistently maintained by the conventional thermal cycler in most wells for over 45 minutes (**Fig. 7B**). The temperature in the heating chamber was adjusted correspondingly to approximate temperatures in the conventional thermal cycler. An air temperature of 77 °C in the cLAMP heating chamber was found to be optimal for consistent detection of an in-tube temperature of ~ 65 – 66.2 °C across wells.

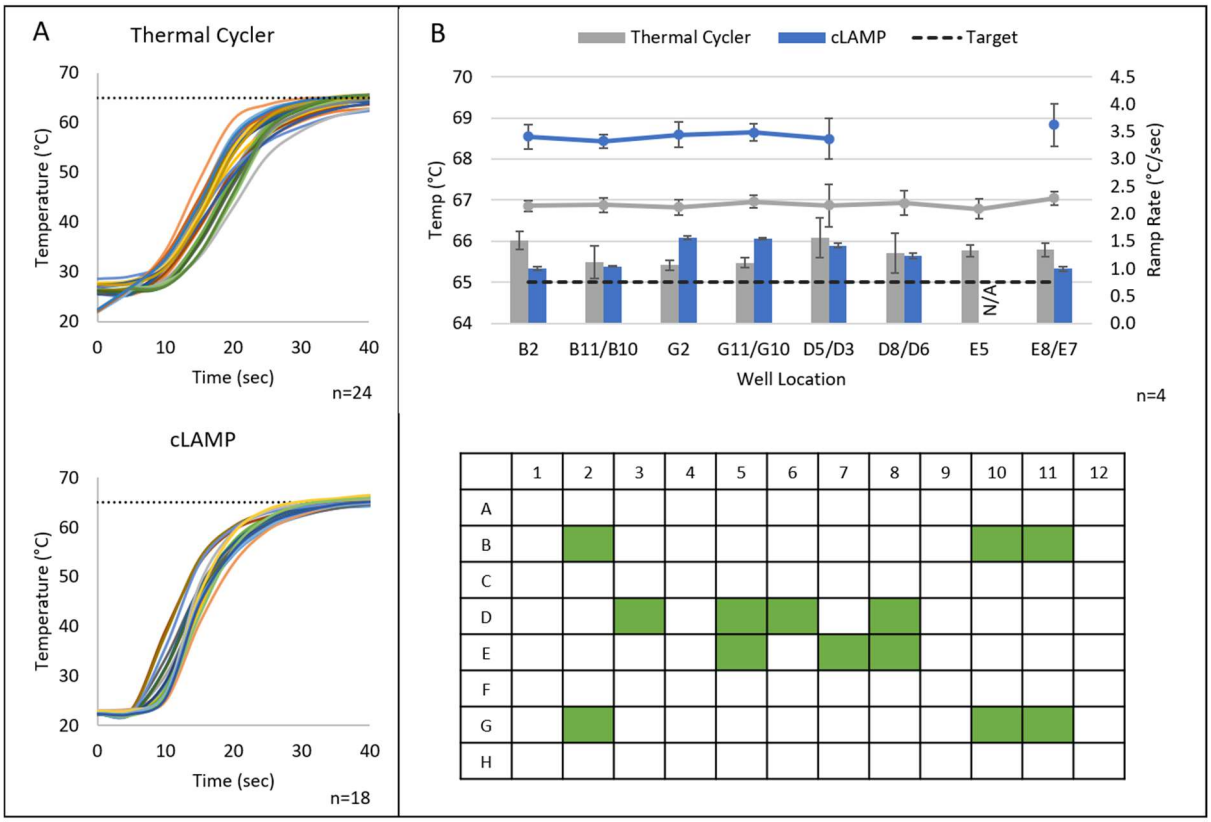

Figure 7: Comparison of integrated cLAMP system temperatures and ramp rates with a conventional thermal cycler. (A) All wells achieved the desired temperature within 30 sec on both systems. (B) Various wells were analyzed to compare temperature across the 96 well plate in a conventional thermal cycler and cLAMP system. Each bar is an average of the temperature across 45 minutes for four days. The ramp rate was higher for the cLAMP system than the thermal cycler.

Additionally, the potential correlation between fluctuations in temperature with a change in the number of reactions was investigated. Although the holes drilled into the metal plate of the cLAMP system were intended to facilitate airflow, it stood to reason that the in-tube temperature might change with an increase in the number of tubes. Accordingly, it was found that minor adjustments to the heating chamber temperature were required to accommodate a full plate but not for ≤ 72 wells (**Fig. 8**). These experiments demonstrated that the cLAMP system operates as reliably as a conventional thermal cycler concerning ramping times and reliable and consistent maintenance of target temperatures.

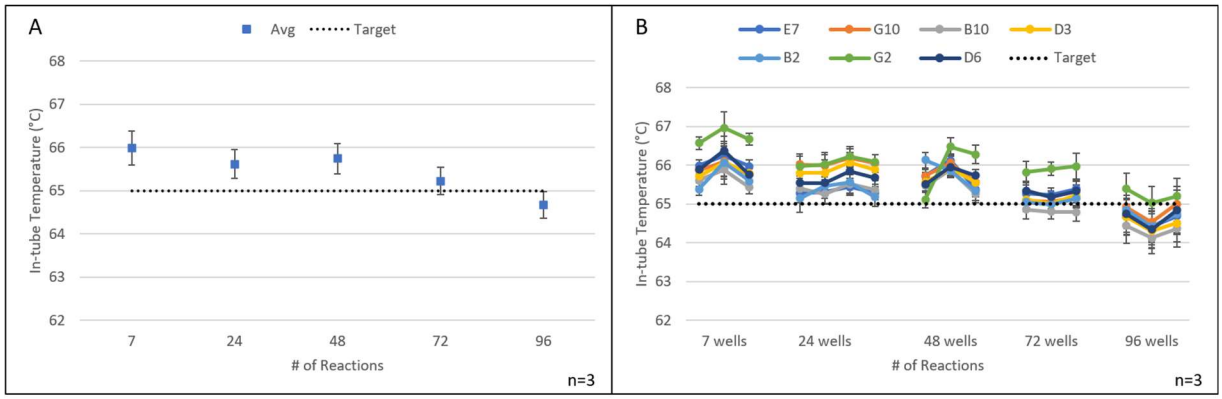

Figure 8: Assessing number of reactions in the cLAMP system. (A) The heating chamber temperature was held constant, while the number of reactions (tubes) inside the cLAMP system increased. The in-tube temperature did not fall below 65 °C until 96 reactions were placed inside the cLAMP system. To achieve 65 °C when 96 wells are occupied, the heating chamber temperature is increased by one degree. (B) Each well was assessed for temperature, showing G2 has the highest in-tube temperature and B10 has the lowest in-tube temperature.

3.3.5 Initial analysis of mRNA targets

The second major component of the cLAMP system is automated colorimetric image analysis. As shown in **Fig. 1**, the hue value for the color of a captured image may vary slightly between camera models but remains consistent for repeated captures taken with the same camera. The image analysis of the cLAMP system produces similar results to those obtained from our previous studies using this method with LAMP reactions (Chapter 2).(20, 25) However, our recent studies show the RPi camera has more minor variations in blue, purple, yellow, and red than the Huawei P9 smartphone used previously. Table 1 compares the camera specifications of the Huawei P9 and RPi camera, which affect how the hue value is determined in each captured image.

The hue values from the cLAMP system are graphed in the 'Data' tab in real-time as a moving average. Initially, the raw hue values are saved as a .csv file for the user. However, due to deviation from minute to minute, the raw hue values are processed as a moving average of

three in Microsoft Excel. The measurement at each minute becomes an average of the two previous hue values and the current hue value. This function allows for a 'smoothing' of the data, as shown in **Fig. 9**. The figure shows various samples (n=54) amplified using the cLAMP system. After minute 4, the threshold is determined, and a sample is classified as 'positive' or 'negative'. The threshold calculation is described in **Fig. 5**. Both the raw and averaged hue values are saved in separate .csv files for the user, with the averaged hue values and threshold shown on the 'Data' tab of the software.

Table 1: Comparison of camera between the Huawei P9 previously used in a 3D-printed static light box and Raspberry Pi camera v2.1 in the cLAMP system.

	Huawei P9 Camera	Raspberry Pi Camera v2.1
Sensor	Dual Sony IMX 286 12MP 12MP RGB main sensor 12MP monochrome chip	Sony IMX219 8MP
Pixel Size	1.25 µm	1.12 µm
Resolution	3968x2976 pixels	3280x2464 pixels
Focal Length	27 mm	3.04 mm
F-stop	f/2.2	f/2.0
Optical Size	1/2.9"	1/4"
Focus	Laser-assisted autofocus	Manual focus
Price	$429 USD	$25 USD

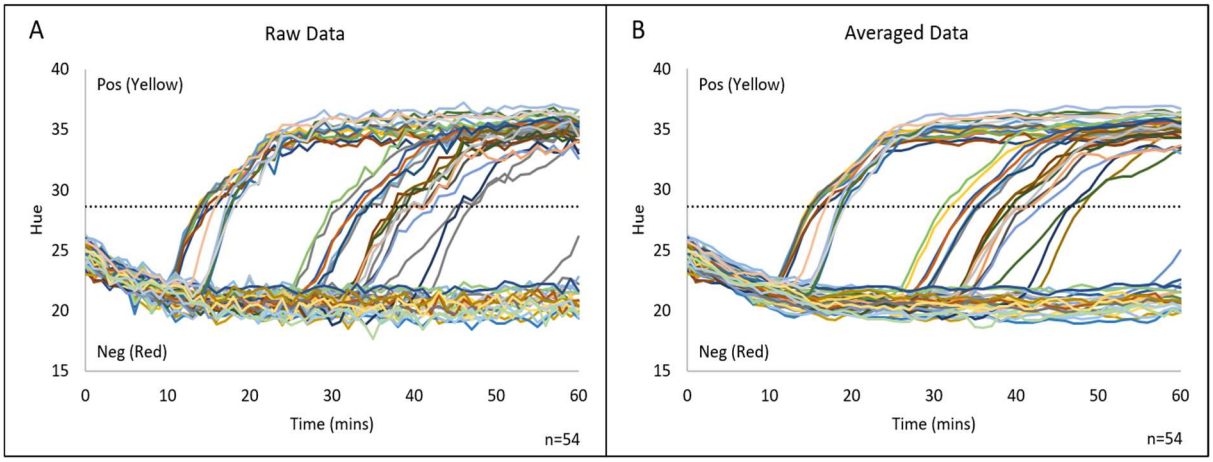

Figure 9: Hue smoothing via moving average calculation in Microsoft Excel software. (A) The raw image analysis shows how the hue can vary from minute to minute. (B)The averaged image analysis data smooths the transition between time points by averaging the previous two data points and the current data point. Each line represents image analysis from one sample.

The developed image analysis method can be applied to any colorimetric dye used in any LAMP reaction. **Fig. 10** shows the data obtained for LAMP reactions conducted using the cLAMP system with PR and HNB dyes. A threshold was calculated either above or below the starting hue value for both dyes. These dyes were used due to their opposing direction in color change (low to high value vs. high to low value). Consequently, any colorimetric dye change in a LAMP reaction can be analyzed using the cLAMP system. The user selects the desired colorimetric dye before starting the LAMP assay. This input then directs the program to either add or subtract the threshold from the average starting values, as appropriate. Unlike previous iterations of this device, the cLAMP system uses a RPi camera rather than a Huawei P9 smartphone(20) for image analysis. A previous iteration of the device was described in Chapter 2. Comparison of previous and current image analysis systems indicates that the change in PR hue value from negative to positive is more prominent when using the P9 device (**Fig. 10C**). However, the hue color changes from red to yellow, which encompasses the highest and lowest hue values (see **Fig. 1B**), and was accounted for by tinting the image to rotate the hue scale.(12) Additionally, although the change in hue value is more significant for both dyes using the P9 smartphone, the cLAMP system was

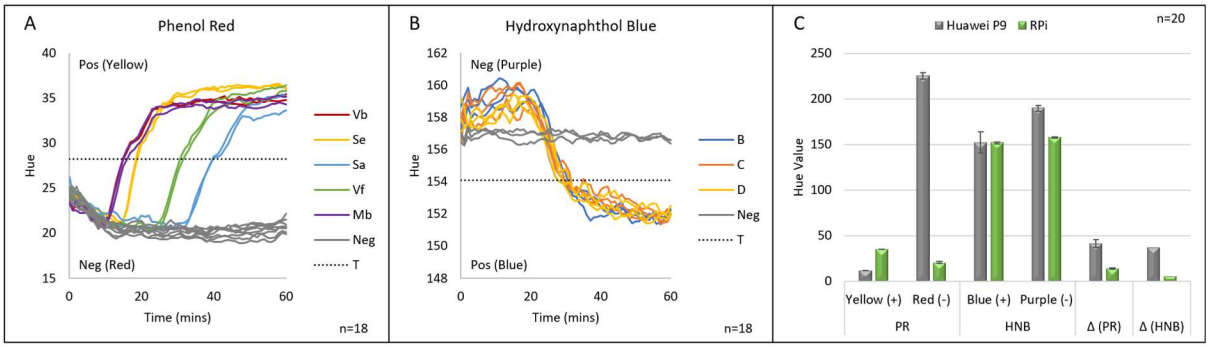

Figure 10: Integrated LAMP runs. (A) LAMP with phenol red where the hue values increase if samples become positive. (B) LAMP with HNB where hue values decrease if samples become positive. (C) The averaged hue values for positive and negative reactions for both indicators and the differential in hue values for each setup.

still able to show the color change numerically for both dyes with much smaller standard deviations. This feature indicates that the cLAMP system performs comparably, or potentially better, than the image analysis method described in Chapter 2 for these dyes.

3.3.6 Analysis of mock forensic samples

The goal of this mock study was to assess specificity of our final protocol using twenty mock samples that best imitate crime scene samples. The samples were prepared by depositing a range of body fluids at various concentrations, as single source or mixtures, onto cotton swabs, cloth, or denim (**Fig. 11**). The deposited fluids were not limited to the body fluid panel described thus far, but also included breast milk and nasal mucus. The samples were dried overnight or aged up to 5 years at room temperature (RT) without light. Approximately ¼ of the swab (or similar-sized cutting for samples on fabric) was cut, sealed in a tube, and assigned a sample ID

A

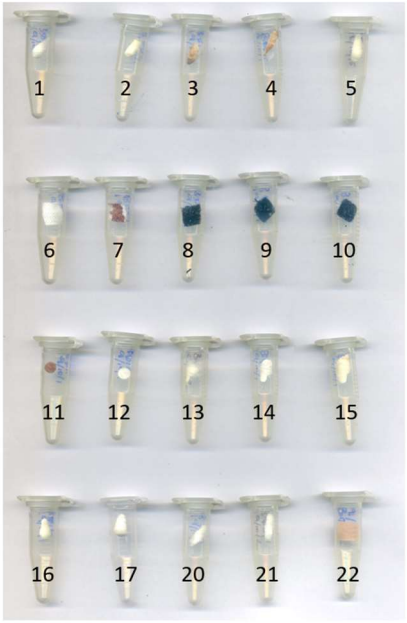

B

Sample Contents	Sample Number
VF swab spiked with semen	B001
VF swab spiked with semen	B002
MB swab spike with semen	B003
MB swab	B004
Female nasal swab spiked with male saliva	B005
VF smear on cloth, spiked with male saliva	B006
Female blood smear on cloth	B007
Male blood smear on outside jeans	B008
VF smear on inside jeans, spiked with semen	B009
VF smear on outside jeans, spiked with male saliva	B010
4 yr old blood on filter paper	B011
4 yr old semen on filter paper	B012
Female nasal swab	B013
PCI 24h	B014
PCI 48h	B015
PCI 120h	B016
PCI 48h	B017
Breast milk	B020
Breast milk on swab, spiked with male saliva	B021
PCI 48h from underwear cutting	B022

Figure 11: Mock sample composition for the single blind study. The samples contained various mixtures of body fluids, fluids that are known to cross contaminate conventional methods, post-coital swabs, and aged body fluid samples. All the samples were on sterile cotton swabs, jean material, or cotton material.

before transferring it to a scientist for processing and analysis; the scientist was blind to the identity of the sample. The mock samples were amplified for detection of each body fluid target using the optimized assay conditions and, when necessary, a confirmatory test was performed. The confirmatory test was either a microchip electrophoresis or a PSA lateral flow assay for Se. The LAMP assay was performed in a Veriti thermal cycler with the optimized conditions for lysis and purification, amplification, and colorimetric analysis.

Table 2: Comparison of research and conventional analysis methods to determine the correct composition of the mock samples.

Sample Number	Blood		Semen		Saliva	V Fluid	M Blood	Overall Conclusion (Veriti Results)
	Veriti	Bioanalyzer	Veriti	PSA Test	Veriti	Veriti	Veriti	
B001	Neg		Neg	Pos	Neg	Pos	Pos	Incorrect
B002	Pos	TRUE	Neg	Pos	Neg	Pos	Pos	Incorrect
B003	Pos		Pos		Neg	Pos	Pos	Correct
B004	Pos		Neg		Neg	Pos	Pos	Correct
B005	Pos	TRUE	Neg		Pos	Pos	Pos	Incorrect
B006	Neg		Neg		Pos	Pos	Pos	Incorrect
B007	Pos		Neg		Neg	Neg	Neg	Correct
B008	Pos		Neg		Neg	Neg	Neg	Correct
B009	Neg	TRUE	Neg	Pos	Neg	Pos	Pos	Incorrect
B010	Pos	TRUE	Neg		Pos	Pos	Pos	Incorrect
B011	Pos		Neg		Neg	Neg	Neg	Correct
B012	Neg	NS	Neg	Pos	Neg	Neg	Neg	Incorrect
B013	Neg	NS	Neg		Neg	Neg	Pos	Incorrect
B014	Neg	NS	Pos	Neg	Neg	Pos	Neg	Correct
B015	Neg	NS	Neg	Neg	Neg	Pos	Pos	Incorrect
B016	Neg	NS	Neg	Neg	Neg	Pos	Pos	Incorrect
B017	Pos	TRUE	Neg	Neg	Neg	Pos	Pos	Incorrect
B020	Neg		Neg	Neg	Neg	Neg	Neg	Correct
B021	Neg		Neg		Pos	Pos	Pos	Incorrect
B022	Neg	TRUE	Pos		Neg	Pos	Pos	Incorrect
Correct Identification	80%		65%		100%	90%	40%	35%

The results from the five body fluid targets ranged from perfect amplification of a mRNA target in all mock samples to only eight of the mock samples amplifying a mRNA target correctly (**Table 2**). To our disappointment, this study correctly identified only seven of the 20 mock samples; we have a few postulates as to why the outcome was poor. Assays targeting Sa and Vf performed the best when tested with all of the mock samples in the Veriti thermal cycler (**Fig. 12**). The Sa assay amplified all of the mock samples correctly, and the Vf target amplified 90% (18/20) of the mock samples correctly in the Veriti thermal cycler. The two samples misidentified in the Vf assay consisted of female nasal swab with male saliva, and breast milk with male saliva. It has been

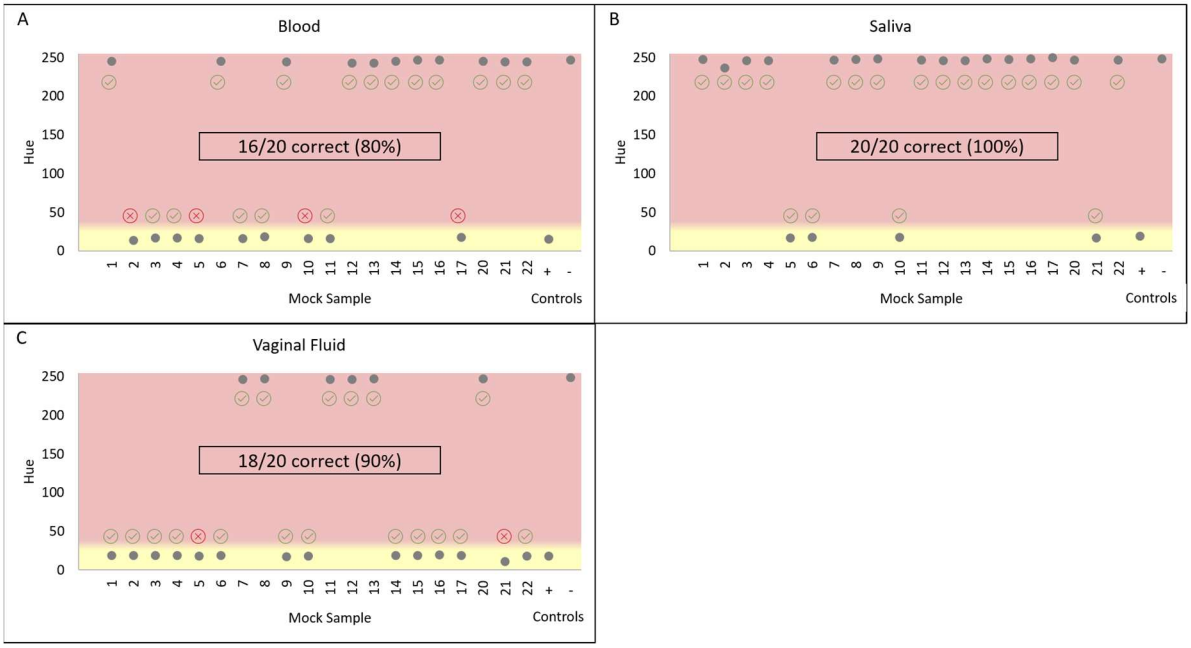

Figure 12: Analysis of mock samples with and without mixture analysis. (A) The Vb mRNA target correctly amplified 16 of the 20 mock samples. (B) The Sa mRNA target correctly amplified all the mock samples. (C) The Vf mRNA target correctly amplified 18 of the 20 mock samples.

shown that low concentrations of the Vf mRNA target (CYP2B7P) can be found in Sa, providing a potential reason for the false positive identification.(26, 27) The LAMP assay with the Vb target performed fairly in the Veriti thermal cycler showing 'positive' results with samples devoid of blood. To identify what was amplifying in the sample, amplicons were separated via microchip electrophoresis to determine if the amplified fragments were specific for the Vb mRNA target (HBB) or the result of NSA (**Fig. 13**). This confirmed that the Vb primer set is amplifying an mRNA target in a sample where Vb is not present. To troubleshoot, various tests were conducted to determine the root cause of the misidentifications (e.g., reagent contamination, incorrect temp, etc.). The results indicate that there could have been some contamination with the old purification kit, or the water used in the LAMP assay (**Fig. 14**). Even though there are misidentifications, the results show promise for future use in a forensic assay.

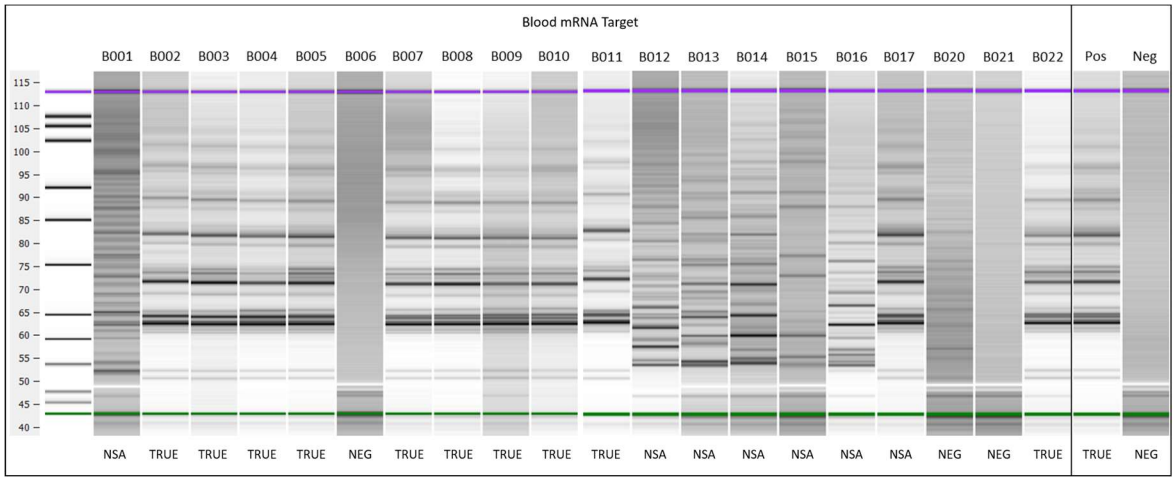

Figure 13*: Further analysis of the Blood mRNA target with the mock samples.* All the mock samples were size separated using microchip electrophoresis on the Agilent Bioanalyzer. If the profile matches the positive control profile, the sample is considered have amplified the correct target (TRUE). If a profile is present but different than the positive control profile, the sample is considered to have non-specifically amplified (NSA). If there is no profile as shown in the negative control, the sample is considered to have no amplified fragments (Neg).

Not all of the mRNA targets amplified via the LAMP method produced results with as much success. For the Se assay, seven mock samples did not amplify in the Veriti thermal cycler (**Fig. 15**). After the sample identities were revealed, it became clear that inclusion of samples that have been aged over years (B012), on denim (B009), or have PCI >24 hours, could play into the

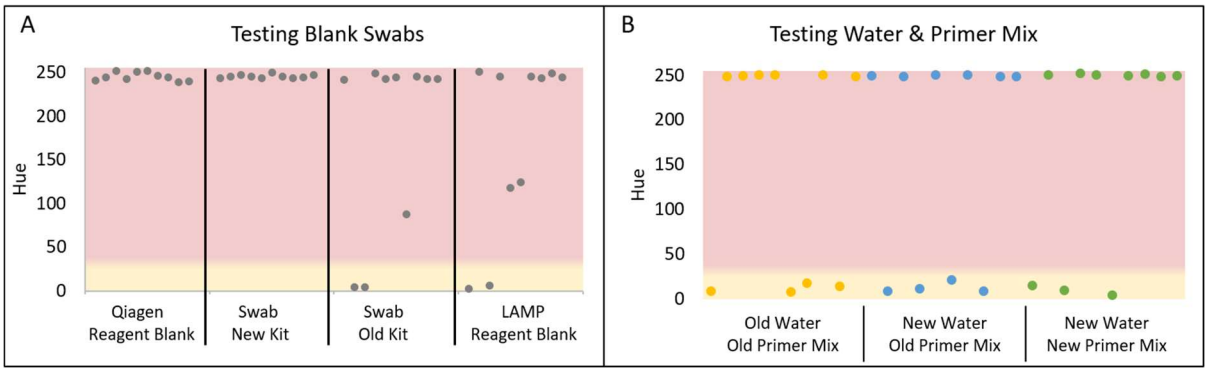

Figure 14: Troubleshoot testing of the venous blood mRNA target. (A) Sterilized cotton swabs were extracted using a new and old RNeasy Mini kit, along with a reagent blank (water) and LAMP reaction reagent blanks. Each sample was amplified 10x to determine if the cotton swabs, extraction kit reagents, or LAMP reagents were contaminated. (B) The Vb primer set and sterilized water were tested to determine if contamination was present. Multiple reactions amplified; thus, the primer set is thought to have high NSA from primer dimer formation.

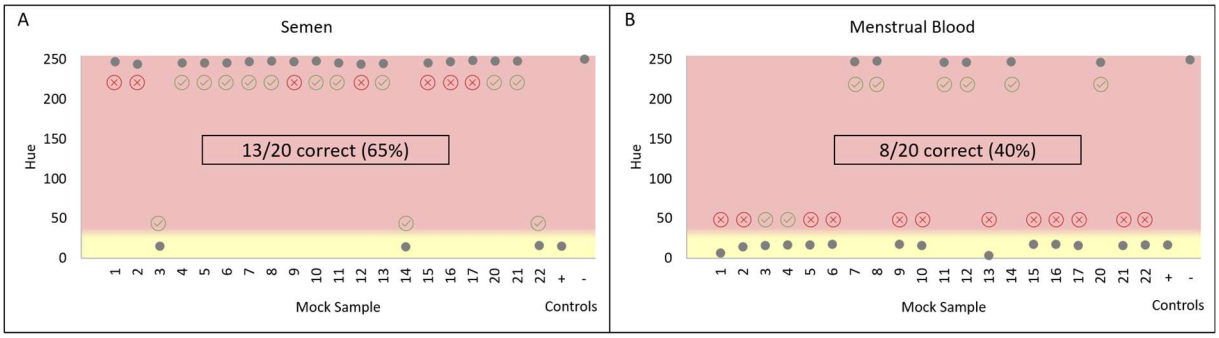

Figure 15: Analysis of difficult samples with and without mixture analysis. (A) The Se mRNA target was amplified with all mock samples. (B) The Mb mRNA target was amplified with all mock samples. Both mRNA targets provided less than optimal results.

false negative results. The false negative samples were analyzed with a commercial lateral flow assay for the presence of PSA (**Fig. 16A**); the test confirmed the presence of PSA in all samples, except the PCI samples and breast milk. However, the LAMP Se assay was able to detect the target in the PCI 24hr sample, where the PSA test did not. The assay that performed the worst was the Mb mRNA target (MMP10). This mRNA target correctly amplified only eight mock samples, thus an overall correctness rate of 40% (**Fig. 15**). The majority of the incorrectly identified samples contained Vf, and the remaining incorrect samples contained male saliva. Focusing on the Vf samples, one theory is that the Mb target is present in the Vf samples without the visual color. Historically, birth control pills were the popular choice of contraception for women, which allowed for one menstrual cycle per month. Newer contraceptive approaches allow for cycles every few months or no cycle at all. This presents the possibility that the Mb target is secreted without the visual color of the fluid because the body may discard any extracellular matrix to prevent the menstrual cycle from initiating.(28) To provide evidence for this, freshly donated Vf samples were extracted with on-column DNase treatment. The swabs did not show any evidence of red discoloration indicative of blood. Following extraction, the samples were LAMP amplified with the Mb target (**Fig. 16B**). All Vf samples amplified with the Mb target

in 30 minutes, indicating the presence of MMP10 in the samples. This indicates there is a problem with the mRNA target amplifying in an unintended body fluid. This indicates that the target is not specific for Mb and a new mRNA target will need to be optimized.

A

SEMEN			60 mins 63 C
Sample	Key	PSA Test	LAMP
1	Pos	Pos	Neg
2	Pos	Pos	Neg
9	Pos	Pos	Neg
12	Pos	Pos	Neg
14	Pos	Neg	Pos
15	Pos	Neg	Neg
16	Pos	Neg	Neg
17	Pos	Neg	Neg
20	Neg	Neg	Neg
Neg	Neg	Neg	Neg
Pos	Pos	Semen	Pos

B

Sample Contents	Sample Number	M Blood Veriti
VF swab spiked with semen	B001	Pos
VF swab spiked with semen	B002	Pos
Female nasal swab spiked with male saliva	B005	Pos
VF smear on cloth, spiked with male saliva	B006	Pos
VF smear on inside jeans, spiked with semen	B009	Pos
VF smear on outside jeans, spiked with male saliva	B010	Pos
Female nasal swab	B013	Pos
PCI 48h	B015	Pos
PCI 120h	B016	Pos
PCI 48h	B017	Pos
Breast milk on swab, spiked with male saliva	B021	Pos
PCI 48h from underwear cutting	B022	Pos

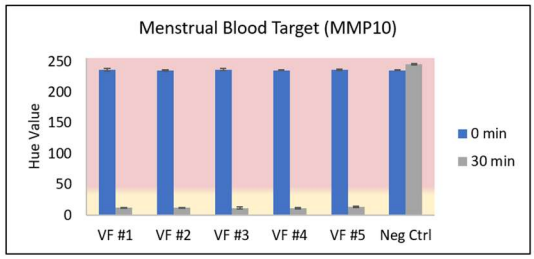

Figure 16: Results from troubleshooting the mock study samples with the Se and Mb mRNA targets. (A) The samples were tested with a conventional method targeting the prostate specific antigen. Comparatively, the conventional method falsely identified less samples. (B) Most of the mock samples incorrectly identified contained Vf. To further test the Mb target, known Vf samples were amplified with the Mb target.

3.3.7 Comparison of conventional methods vs cLAMP device

This study aimed to compare the amplification of fifteen mock samples achieved using the cLAMP system to results obtained using a conventional thermal cycler and imaging method. **Table 3** shows the overall comparison of results obtained from the thermal cycler and cLAMP system, outlining which samples were incorrectly identified. Except for the mRNA Vf target, the cLAMP correctly identified fewer samples than the conventional thermal cycler. The LAMP reactions targeting the mRNA Vf gene performed the best on the cLAMP system, outperforming the thermal cycler by correctly identifying 14 of the 15 samples. Sample 21, which contained

breast milk and saliva, was incorrectly identified by both systems. It has been shown that low concentrations of VF target can be found in saliva, providing a potential reason for the false-positive identification. (26, 27) The reactions targeting the mRNA Sa gene amplified 12 of the mock samples correctly, and the mRNA Vb target amplified 11 of the mock samples correctly in the cLAMP system. Three samples misidentified Se as the mRNA Sa target, likely because the HTN3 target has been detected in low concentrations in seminal fluid. (29) The four samples misidentified as the mRNA Vb target were not further analyzed, but mixtures of various fluids and materials which were incorporated may have contributed to the misidentification. Additionally, previously observed NSA for this target could have played a role in the misidentifications. Lastly, the reactions targeting the mRNA Se gene misidentified seven of the fifteen samples. After the sample identities were revealed, it became clear that the inclusion of samples that have been aged over multiple years (Sample 12), on denim (Sample 9), or have PCI

Table 3: Comparison of mock samples after thermal cycler heating with smartphone image analysis and the cLAMP system with RPi image analysis. The red boxes denote inconsistent identifications between the two testing platforms.

	Blood		Semen		Saliva		V Fluid	
Sample Number	Thermal Cycler + Smartphone	cLAMP + RPi	Thermal Cycler + Smartphone	cLAMP + RPi	Thermal Cycler + Smartphone	cLAMP + RPi	Thermal Cycler + Smartphone	cLAMP + RPi
1	-	-	Neg	Neg	-	Pos	+	+
3	+	+	+	Neg	-	Pos	+	+
4	+	+	-	-	-	-	+	+
5	Pos	Pos	-	-	+	+	Pos	-
6	-	-	-	-	+	+	+	+
8	+	+	-	-	-	-	-	-
9	-	Pos	Neg	Neg	-	-	+	+
11	+	+	-	-	-	-	-	-
12	-	-	Neg	Neg	-	Pos	-	-
13	-	-	-	-	-	-	-	-
14	-	Pos	+	Neg	-	-	+	+
16	-	-	Neg	Neg	-	-	+	+
20	-	-	-	-	-	-	-	-
21	-	-	-	-	+	+	Pos	Pos
22	-	Pos	+	Neg	-	-	+	+
# of Correct IDs:	**14 / 15**	**11 / 15**	**11 / 15**	**8 / 15**	**15 / 15**	**12 / 15**	**13 / 15**	**14 / 15**

>24 hours could be linked to the false-negative results. All of these samples would theoretically have low concentrations of semen or seminal fluid, so the sensitivity of the mRNA target could be a contributing factor to the larger than expected misidentifications. Overall, the mock sample study shows the cLAMP system is not as efficient at identifying these body fluid targets as a conventional thermal cycler paired with image analysis. However, it has been demonstrated that the cLAMP system can reliably achieve and maintain constant temperatures with a more favorable ramp rate than observed for the conventional thermal cycler.

3.4 Summary

Overall, the data provided demonstrate the functionality of a simple, 3D-printed combined system for LAMP reactions with image analysis (cLAMP). This system provides objective results based on hue color change, similar to quantitative fluorescence detection systems typically used for polymerase chain reactions (PCR). The hardware and software are user-friendly and compatible with multiple colorimetric dyes. A threshold is calculated with every LAMP run on the cLAMP system and displayed on the 'Data' tab in the software. The cLAMP system can rapidly heat LAMP reactions from room temperature to the desired amplification temperature and steadily maintain this for more than 60 minutes. Compared to a conventional thermal cycler, the cLAMP system demonstrated similar temperature outputs and ramp times across multiple well locations. The mock study showed which mRNA targets performed well and which need further optimization. The saliva and vaginal fluid targets worked effectively in both systems (>80%), the venous blood target performed moderately (>70%), and the semen and menstrual blood targets performed the worst (>50%). The Se target underwent further analysis

that showed the LAMP assay was not as sensitive as the PSA test but could amplify the target in PCI samples and the Mb target was deemed not specific. The cLAMP system was also able to amplify single source known samples and mock forensic samples for four mRNA targets for blood, semen, saliva, and vaginal fluid with moderate success.

3.5 References

1. Notomi T, Okayama H, Masubuchi H, Yonekawa T, Watanabe K, Amino N, et al. Loop-mediated isothermal amplification of DNA. Nucleic Acids Research. 2000 April 15, 2000;28(12).

2. Huang WE, Lim B, Hsu C-C, Xiong D, Wu W, Yu Y, et al. RT-LAMP for rapid diagnosis of coronavirus SARS-CoV-2. Microbial Biotechnology. [https://doi.org/10.1111/1751-7915.13586]. 2020 2020/07/01;13(4):950-61.

3. Bartosik M, Jirakova L, Anton M, Vojtesek B, Hrstka R. Genomagnetic LAMP-based electrochemical test for determination of high-risk HPV16 and HPV18 in clinical samples. Analytica Chimica Acta. 2018 2018/12/26/;1042:37-43.

4. Tsai L-C, Su C-W, Lee JC-I, Lu Y-S, Chen H-C, Lin Y-C, et al. The detection and identification of saliva in forensic samples by RT-LAMP. Forensic Science, Medicine and Pathology. 2018 2018/12/01;14(4):469-77.

5. Satoh T, Kouroki S, Ogawa K, Tanaka Y, Matsumura K, Iwase S. Development of mRNA-based body fluid identification using reverse transcription loop-mediated isothermal amplification. Analytical and Bioanalytical Chemistry. [journal article]. 2018 July 01;410(18):4371-8.

6. Parida M, Horioke K, Ishida H, Dash PK, Saxena P, Jana AM, et al. Rapid Detection and Differentiation of Dengue Virus Serotypes by a Real-Time Reverse Transcription-Loop-Mediated Isothermal Amplification Assay. Journal of Clinical Microbiology. 2005;43(6):2895.

7. Shirato K, Semba S, El-Kafrawy SA, Hassan AM, Tolah AM, Takayama I, et al. Development of fluorescent reverse transcription loop-mediated isothermal amplification (RT-LAMP) using quenching probes for the detection of the Middle East respiratory syndrome coronavirus. Journal of Virological Methods. 2018 2018/08/01/;258:41-8.

8. Wang Y, Li H, Wang Y, Zhang L, Xu J, Ye C. Loop-Mediated Isothermal Amplification Label-Based Gold Nanoparticles Lateral Flow Biosensor for Detection of Enterococcus faecalis and Staphylococcus aureus. Frontiers in Microbiology. [10.3389/fmicb.2017.00192]. 2017;8:192.

9. Goto M, Honda E, Ogura A, Nomoto A, Hanaki K-I. Colorimetric detection of loop-mediated isothermal amplification reaction by using hydroxy naphthol blue. BioTechniques. 2009 2009/03/01;46(3):167-72.

10. Miyamoto S, Sano S, Takahashi K, Jikihara T. Method for colorimetric detection of double-stranded nucleic acid using leuco triphenylmethane dyes. Analytical Biochemistry. 2015 2015/03/15/;473:28-33.

11. Nogami H, Tsutsumi H, Komuro T, Mukoyama R. Rapid and simple sex determination method from dental pulp by loop-mediated isothermal amplification. Forensic Science International: Genetics.2(4):349-53.

12. Scott AT, Layne TR, O'Connell KC, Tanner NA, Landers JP. Comparative Evaluation and Quantitative Analysis of Loop-Mediated Isothermal Amplification Indicators. Analytical Chemistry. 2020 2020/10/06;92(19):13343-53.

13. Fischbach J, Xander NC, Frohme M, Glökler JF. Shining a light on LAMP assays' A comparison of LAMP visualization methods including the novel use of berberine. BioTechniques. 2015 2015/04/01;58(4):189-94.

14. Woolf MS, Dignan LM, Scott AT, Landers JP. Digital postprocessing and image segmentation for objective analysis of colorimetric reactions. Nature Protocols. 2020 2020/12/09.

15. Priye A, Ball CS, Meagher RJ. Colorimetric-Luminance Readout for Quantitative Analysis of Fluorescence Signals with a Smartphone CMOS Sensor. Analytical Chemistry. 2018 2018/11/06;90(21):12385-9.

16. Rueden CT, Schindelin J, Hiner MC, DeZonia BE, Walter AE, Arena ET, et al. ImageJ2: ImageJ for the next generation of scientific image data. BMC Bioinformatics. 2017 2017/11/29;18(1):529.

17. Schindelin J, Arganda-Carreras I, Frise E, Kaynig V, Longair M, Pietzsch T, et al. Fiji: an open-source platform for biological-image analysis. Nature Methods. 2012 2012/07/01;9(7):676-82.

18. Shin J, Choi S, Yang J-S, Song J, Choi J-S, Jung H-I. Smart Forensic Phone: Colorimetric analysis of a bloodstain for age estimation using a smartphone. Sensors and Actuators B: Chemical. 2017 2017/05/01/;243:221-5.

19. Krauss ST, Nauman AQ, Garner GT, Landers JP. Color manipulation through microchip tinting for colorimetric detection using hue image analysis. Lab on a Chip. [10.1039/C7LC00796E]. 2017;17(23):4089-96.

20. Layne T, Jackson K, Scott A, Tanner NA, Piland A, Haverstick DM, et al. Optimization of novel loop-mediated isothermal amplification with colorimetric image analysis for forensic body fluid identification. Journal of Forensic Sciences. 2021.

21. Scott A, Birch C, Mills D, Panesar S, Li J, Le Roux D, et al. An Portable UltraRapid DNA System for Human Identification. Science Advances. 2020;Submitted.

22. Norris JV. Advances in forensic science: improving sexual assault evidence analysis. 2008.

23. Kimes D, Tamir M. An extraction procedure for seminal/vaginal stains to eliminate streaking in the electrophoresis phosphoglucomutase. Crime Laboratory Digest. 1985;12:32-3.

24. Layne T, Jackson K, Scott A, Tanner NA, Piland A, Haverstick DM, et al. Optimization of novel loop-mediated isothermal amplification with colorimetric image analysis for forensic body fluid identification. Journal of Forensic Sciences. 2021.

25. Scott A, Jackson K, Carter M, Comeau R, Layne T, Landers J. Rapid sperm lysis and novel screening approach for human male DNA via colorimetric loop-mediated isothermal amplification. Forensic science international Genetics. 2019 2019/11//;43:102139.

26. Sakurada K, Akutsu T, Watanabe K, Fujinami Y, Yoshino M. Expression of statherin mRNA and protein in nasal and vaginal secretions. Legal Medicine. 2011 2011/11/01/;13(6):309-13.

27. Xu Y, Xie J, Cao Y, Zhou H, Ping Y, Chen L, et al. Development of Highly Sensitive and Specific mRNA Multiplex System (XCYR1) for Forensic Human Body Fluids and Tissues Identification. PLOS ONE. 2014;9(7):e100123.

28. Hatcher RA. Contraceptive technology. 21 ed: Managing Contraception LLC, 2018.

29. Richard ML, Harper KF, Craig RF, Onorato AF, Robertson JF, Donfack J. Evaluation of mRNA marker specificity for the identification of five human body fluids by capillary electrophoresis. Forensic Science International: Genetics. 2012 2012/05/22;6(4):452-60.

Chapter 4: Adaptation of separation & amplification methods for mRNA body fluid panel to a microfluidic platform

4.1 Introduction

The identification of select body fluids from forensic evidence provides context in a criminal investigation, informs downstream genetic analysis, and can corroborate witness testimony in court. However, body fluid identification (bfID) is often not straightforward as they may be difficult to visually locate, present in small quantities, or discovered in mixtures. The majority of ubiquitous bfID techniques reply upon time-consuming, laborious microscopic analysis or presumptive (bio)chemical, enzymatic, or immunological assays that are generally limited in specificity and lacking in sensitivity. (2)

Presumptive and confirmatory tests are used to either presume or confirm a particular body fluid is present on an item of evidence, respectively. In addition, these tests help to determine which evidence may be probative for deoxyribonucleic acid (DNA) analysis. Many conventional presumptive tests for bfID are unable to differentiate between closely related samples, and a misidentification of fluids could significantly shift the narrative of a crime. One example of this is with a commonly used presumptive test for blood, referred to as the phenolphthalein tetramethylbenzidine (PTMB), which cannot differentiate between venous and menstrual blood. For differentiation, protein-based methods for bfID testing have emerged, such as the presumptive Clearview® rapid D-dimer test for the indication of menstrual fluid, and several confirmatory mass-spectrometry techniques.(3) However, these methods are either

presumptive, thus, not confirming the presence of a fluid, or limited by the requirement for expensive instrumentation, highly-trained personnel, and the need for a library of peptide/protein sequences.(4) Additional methodological approaches for fluid discrimination via proteins include machine learning methods based on the relative abundance of both marker and non-marker proteins(5), and spectroscopic-based tests, such as raman(6) or Fourier transform infra-red spectroscopy.(7)

Recent advances in molecular biological approaches for confirmatory bfID include microbial community profiling, epigenetics, and ribonucleic acid (RNA) profiling. Microbial community profiling is based on the premise that different body fluids exhibit dissimilar microfauna; to date, this type of identification has been used to discriminate body fluids including vaginal secretions and saliva.(8) Similar to the phenolphthalein approach, the Microbial community profiling method has also been unable to differentiate between fluids like vaginal secretions and menstrual blood.(9, 10) Epigenetic methods for identification analyze DNA methylation patterns based on cell or tissue type(11, 12); however, this method requires high amounts of input DNA and is associated with variability originating from changes to the methylation signature in response to environmental factors (e.g., aging and disease).(13) Finally, RNA analysis via transcriptomics is arguably the most promising approach to bfID with several different types of RNA under investigation, including messenger RNA,(14, 15) microRNA,(16, 17) and circular RNAs.(18, 19) A critical advantage of RNA profiling is that recovery of RNA from biological stains can be integrated into a typical forensic workflow without compromising or consuming the DNA essential for downstream genetic profiling for human identification.

Methods involving reverse transcription (RT) are used for accurate, reliable confirmatory bfID; the majority of methods leverage RT-PCR (polymerase chain reaction), a sensitive method capable of detecting low-abundance mRNA obtained from small volume samples.(14, 20) Although the most widely implemented approach utilizes end-point RT-PCR coupled with capillary electrophoresis (CE),(21, 22) quantitative RT-PCR (qRT-PCR) can be employed for either relative quantitation from a reference or house-keeping gene, or to detect a single amplicon using a DNA chelating dye or fluorescent probe.(23, 24) Limitations of this technique, such as non-specific annealing, have been mitigated by high-resolution melting analysis(25, 26) and involve a restricted number of markers that can be targeted in a single reaction. More recently, a method coupling reverse transcription with real-time loop-mediated isothermal amplification (LAMP) has demonstrated comparable sensitivity and specificity through simplified, rapid analyses; however this technique is still limited to a single target per reaction.(27, 28) Lastly, massively paralleled sequencing (MPS) of RNA for high-throughput bfID has been used in a number of academic studies, but the technique is expensive, time-consuming, requires extensive training and bioinformatics knowledge, and vast computer storage capabilities, limiting implementation in forensic labs.(26, 29, 30) Although a number of methods for bfID have been proposed, none are independently capable of providing a sample-to-result solution for reliable, accurate, and fast confirmatory bfID.

Many sample-to-result analyses can be accomplished with microtechnology. Microfluidic technologies are attractive for both lab-based and fieldable applications, due to a small footprint, minimal reagent and sample volume requirements, rapid analysis times, ease of use, and the potential for automation and portability.(31, 32) Academic advancements in microfluidic

technologies have focused on both clinical (e.g., virus detection,(33) biomolecule cleaning,(34) etc.) and forensic (e.g., short tandem repeat (STR) profiling,(35) epithelial and sperm separation,(36) etc.) applications. However, limitations in adopting microfluidics systems in laboratories often stem from failing to address the cost of materials and fabrication of the microfluidic consumable or training associated with the technology.(37) Our lab has defined a cost-effective method for rapid, iterative prototyping of microfluidic CDs (print-cut-laminate technique; PCL(32)) with complex, intricate architectures for chemical and biochemical assays ranging from DNA purification and genome analysis(38) to illicit drug detection and explosives sensing.(38, 39)

By leveraging the PCL technique, rapid prototype microdevices were developed for rapid amplification of mRNA targets and electrophoretic separation coupled with laser-induced fluorescence (LIF) detection of mRNA amplicons associated with individual body fluids. This system incorporates the microdevices, an associated mechatronic platform, and microfluidic chemistries for integrated bfID. Two microdevices, the 'micro-electrophoresis' disc (μEDisc) and the 'micro-amplification' disc (μAmpDisc), were fabricated for electrophoretic analysis of PCR-amplified fragments and amplification of targets, respectively, with the final goal of integration on one device. Using this platform, the electrophoretic analysis and amplification times can be decreased 4-fold (15 mins) over conventional CE (45 min) and cycling systems (2+ hr.), with significant reduction in the cost per sample by decreasing the total volume of the reactions. Here, we demonstrate electrophoresis of amplicons produced from in-tube extracted RNA with the first generation μEDisc exhibit concordance with profiles generated from mock forensic samples via conventional, benchtop (CE) at University of Virginia (UVA) and the Environmental Science

and Research Institute (ESR) in New Zealand. Subsequently, on-disc RT-PCR from extracted RNA was completed with the μAmpDisc using both single-source and mixture samples. An advantage of adapting biochemical assays to microfluidic technology is the reduction in overall time, which was the main focus for the RT-PCR protocol. This research demonstrates proof-of-concept microelectrophoresis with on-disc fluorescence detection and RT-PCR of a transcriptome-based method for forensic body fluid identification.

4.2 Methods & Materials

4.2.1 Sample collection

Body fluid samples were collected from volunteers with fully informed consent (IRB # 19947). Blood was collected via fingerprick, where 50 µL was placed on sterile Cultiplast® rayon swabs (LP Italiana SPA, Milano, Italy) and left to dry overnight. Buccal, vaginal fluid, and menstrual fluid (day 2 and 3 of the menstrual cycle) samples were self-collected by volunteer participants using sterile Cultiplast® rayon swabs that were left to dry overnight. Freshly ejaculated semen samples were collected from the volunteers themselves in sterile plastic containers. From those, 50 µL aliquots were placed on sterile Cultiplast® rayon swabs and left to dry overnight.

4.2.2 RNA isolation

The RNA was isolated as previously described.(40) Total RNA for all samples were extracted using the Promega® ReliaPrep™ RNA Cell Miniprep System (Promega Corporation, Madison, WI, USA) following the manufacturer's instructions. DNA was removed from extracted

RNA using on-column DNase I treatment during the RNA extraction process. RNA was eluted in 70 µL of elution buffer. Purified RNA samples were immediately treated with DNase from the TURBO DNA*free*™ Kit (Thermo Fisher Scientific, Waltham, MA, USA). The manufacturer's instructions were followed, adding 7.0 µL 10x TURBO DNase Buffer and 2 µL TURBO™ DNase to each sample. Complete removal of human DNA was verified using the Quantifiler® Human DNA quantification kit (Life Technologies Corp., Carlsbad, CA, USA) using 1 µL of sample in a 12.5 µL reaction. The RNA was stored at -80°C until required.

4.2.3 Primer information

In previous work, Albani et al. optimized three bfID panels consisting of eleven mRNA genes for identifying five forensically-relevant body fluids.(1) These targets are divided into three multiplex panels, identifying six body fluids. A single primer for each target is tagged with either FAM or HEX and all targets generate a fragment less than 200 bp in length. The Duplex Panel consists of FDCSP (170 bp; HEX) and HTN3 (138 bp; HEX) to identify buccal mucosa or saliva. The Quadruplex Panel consists of HBD (176 bp; FAM) and SLC4A1 (102 bp; HEX) to identify venous blood, and MMP10 (108 bp; HEX) and STC1 (105 bp; FAM) to identify menstrual blood. The Pentaplex Panel consists of PRM1 (150 bp; HEX), TNP1 (102 bp; FAM) to identify spermatozoa, KLK2 (135 bp; HEX), MSMB (142 bp; FAM) to identify seminal fluid, and CYP2B7P (113 bp; HEX) to identify vaginal fluid. For each panel, resultant amplicons can be electrophoretically-separated and detected using fluorescently labeled primers (FAM and HEX). All PCR amplicons were less than 200 base pairs (bp) in length, and widely published in the forensic literature (**Table 1**), with analysis typically performed using conventional CE instrumentation.(22, 41) Conversely, we

describe adaption of such assays onto a μEDisc capable of electrophoretically separating and differentiating mRNA amplicons, and adaptation of the amplification method to a μAmpDisc, both with similar peak heights as the conventional method.

Table 1: Three multiplexes were designed for body fluid identification from Albani *et al*. (with permission). (1) Each multiplex is comprised of messenger RNA markers that are specific for each fluid and create fragments that are less than 200 bp.

Multiplex	Target Body Fluid	mRNA	Primer Sequence	Final Concentration in PCR assay (µM)
Duplex	Saliva / Buccal	FDSCP	F- HEX-CTCTCAAGACCAGGAACGAGAA	0.05
			R - GGGCAGATTCAGGTATTGGAATAG	
		HTN3	F - HEX/AAGCATCATTCACATCGAGGCTAT	0.03
			R - ATGCGGTATGACAAATGAGAATACAC	
Quadruplex	Circulatory Blood	HBD	F - ACTGCTGTCAATGCCCTGTG	0.05
			R - FAM/ACCTTCTTGCCATGAGCCTT	
		SLC4A1	F - HEX/AACTGGACACTCAGGACCAC	0.04
			R - GGATGTCTGGGTCTTCATATTCCT	
	Menstrual Fluid	MMP10	F - HEX/CCCACTCTACAACTCATTCACAGAG	0.04
			R - GGTTCCTCAGTAGAGGCAGG	
		STC1	F - FAM/CTGCCCAATCACTTCTCCAACA	0.02
			R - TTTCTCCATCAGGCTGTCTCT	
Pentaplex	Spermatozoa	PRM1	F - HEX/GCCAGGTACAGATGCTGTCGCAG	0.03
			R - GTGTCTTCTACATCTCGGTCTG	
		TNP1	F - GATGACGCCAATCGCAATTACC	0.04
			R - FAM/CCTTCTGCTGTTCTTGTTGCTG	
	Seminal Fluid	KLK2	F - TTCTCTCCATCGCCTTGTCTG	0.14
			R - HEX/AGTGTGCCCATCCATGACTG	
		MSMB	F - CTTTGCCACCTTCGTGACTTTATG	0.03
			R - FAM/ACAGTTGTCAGTCTGCCACT	
	Vaginal Material	CYP2B7P	F - CCGTGAGATTCAGAGATTTGCTGAC	0.02
			R - HEX/TGAGAAATACTTCCGTGTCCTTGG	

4.2.4 RT-PCR method

RNA samples (5 µL) were reverse transcribed using the High-Capacity cDNA Reverse Transcription Kit (Applied Biosystems®, Foster City, CA, USA) according to the manufacturer's instructions. Each reaction comprised a total volume of 20 µL. To perform RT optimizations, the total volume was reduced to 10 µL on the μAmpDisc and the time for each step was decreased. Whole blood samples were lysed, purified for RNA using the RNeasy Mini Kit (Qiagen), and combined into one tube. This sample was used for the time optimization of each step in the RT

protocol. Total RNA in all of the time reduction reactions was assessed via qPCR of a 18S rRNA target on a QuantStudio 5 (Applied Biosystems) instrument. All data is shown as the difference between the no-template control (NTC) and sample for in-tube and on-disc reactions (dC_T). Statistical calculations were performed in R Project for Statistical Computing software v4.0.0 (R Core Team). For mixed body fluid samples, vaginal and buccal complementary DNA (cDNA) samples were diluted by 1/10 using nuclease-free water. The semen cDNA was diluted by ½ using nuclease-free water. For the vaginal/buccal mixed samples, diluted vaginal cDNA (2 µL) was added to 1 µL of the buccal diluted cDNA. The vaginal/semen mixed sample contained diluted vaginal cDNA (2 µL) and 1 µL of the semen diluted cDNA.

For separation optimization, PCR was performed on a GeneAmp PCR System 9700 (Thermo Fisher Scientific) in 25 µL reactions using 12.5 µL Qiagen® Multiplex PCR buffer (Qiagen, Hilden, Germany), 2.5 µL primer mix, and 3 µL cDNA. The total reaction volume of 25 µL was achieved by the addition of 7 µL nuclease-free water. The PCR conditions included initial denaturation at 95 °C for 15 min, followed by 35 cycles of 94 °C for 30 s, 60 °C for 3 min and 72 °C for 1 min, final elongation at 72 °C for 10 min, and cooling down to 4 °C. For RT optimization, PCR was performed on a 7500 Fast Real-Time PCR system (Applied Biosystems®) in 20 µL reactions using 10 µL TaqMan Fast Advanced Master Mix (2X), 1 µL TaqMan Assay with FAM (20X), and 2 µL ul cDNA. The total reaction volume of 20 µL was achieved by the addition of 7 µL nuclease-free water. The PCR conditions were initial denaturation at 95 °C for 2 min, followed by 40 cycles of 95 °C for 3 s and 60 °C for 30 s, and cooling down to 4 °C. The reactions were stored in -20 °C.

4.2.5 Capillary electrophoresis

The amplified samples were separated on either a 3500xl or 3130xl Genetic Analyzer (Applied Biosystems®). The samples separated on the 3500xl Genetic Analyzer used 2 µL amplified sample, 10 µL Internal Lane Standard, and Hi-Di formamide (9.6 µL Hi-Di™ was mixed with 0.4 µL GeneScan™ 600 LIZ® dye Size Standard v2.0 (Applied Biosystems®)). The samples were injected for 24 seconds at 1.2 kV and analyzed using GeneMapper® ID-X v.1.5 (Applied Biosystems®). The samples separated on the 3130xl instrument contained 1 µL amplified sample, 10 µL Internal Lane Standard (1500 kb), and Hi-Di formamide (9.5 µL Hi-Di™ was mixed with 0.5 µL WEN ILS 500 dye v2.0 (Applied Biosystems®, Promega)). The samples were injected for 5 seconds at 3 kV and analyzed using GeneMarker HID v.2.8.2 (SoftGenetics, LLC, State College, PA, USA).

4.2.6 Microchip and fabrication

The centrifugal microfluidic chip for performing DNA separation and detection was developed using the PCL method described by Thompson *et al.*(32) Architecture of the separation and amplification domains, described previously, was minimally changed and replicated on a single μEDisc or μAmpDisc.(42) Briefly, both the μEDisc and μAmpDisc were assembled using five polymeric layers (clear polyethylene terephthalate (PET); TRANS-NS, Filmsource Inc., Maryland Heights, MO, USA and black PeT) with applied adhesives (HSA: heat-sensitive adhesive; Adhesives Research, Inc., Glen Rock, PA, USA) (**Fig. 1**). All layers were laser ablated using a CO_2 laser system (VLS3.50, Universal® Laser Systems, Scottsdale, AZ, USA) to transmit microfluidic architecture. The layers were washed using two 10-minute cycles of

deionized water for and dried in a chemical hood overnight. The layers were aligned and heat-bonded by passing the aligned disc through an office laminator heated to ~180 °C.

Each μEDisc domain contained an injection molded cyclic olefin copolymer (COC) microfluidic chip bonded to the underside of the μEDisc via pressure sensitive adhesive (PSA; Adhesives Research, Inc., Glen Rock, PA, USA) in which electrophoretic separation of complementary DNA (cDNA) fragments transpired (**Fig. 1**). The separation channel is 6 cm in length at 80 µm x 80 µm and a cross section for sample injection. To complete the electrophoretic circuit for separation, gold electrodes were fabricated from 24K gold sheets (L.A. Gold Leaf Wholesalers, Covina, CA, USA) bonded to PSA and PeT that were laser-ablated to achieve the correct architecture and bonded on the top of the μEDisc. The μEDisc measured ~133 mm in diameter and ~0.6–3.5 mm in height depending on the features.

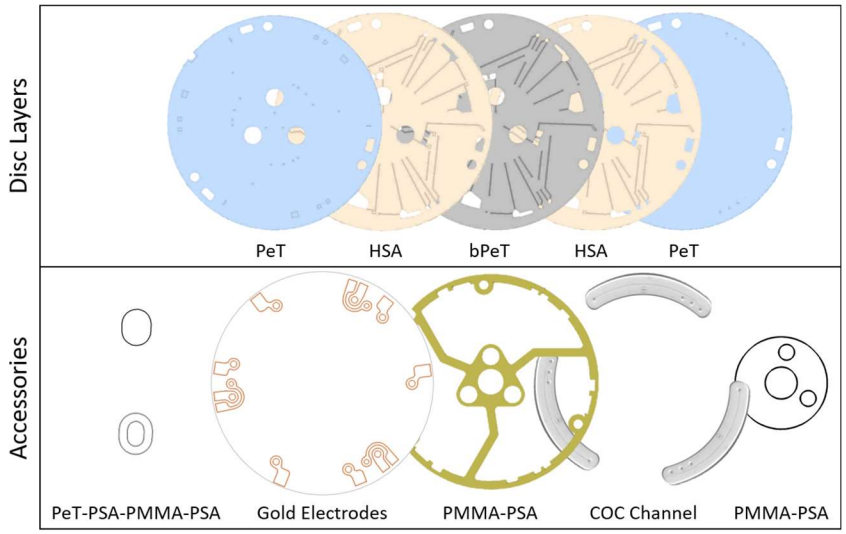

Figure 1: Fabrication of the discs. The disc consists of five layers of polyethylene terephthalate (PeT), heat sensitive adhesive (HSA), and black PeT. The top and bottom layers are affixed with pressure sensitive adhesive (PSA) on polymethyl-methacrylate (PMMA), gold electrodes, and cyclic-olefin copolymer (COC) separation channel, respectively. Each layer was cut using a CO_2 laser cutter and laminated together.

Each μAmpDisc was assembled similarly to the μEDisc with the same polymeric layers with adhesives, ablating with a CO_2 laser system, and washing protocol. After the layers were

aligned and laminated, small polymethyl methacrylate (PMMA) pieces capped with PeT were bonded to the topside of the μAmpDisc via PSA for larger volumes. Both discs had a final PMMA piece bonded to the underside with PSA that fits an adapter piece. The 3D-printed adapter piece for interfacing the μEDisc and μAmpDisc with the centrifugal platform was made of black EverydayPLA (polylactic acid; Type A Machines, CA, USA) filament using a Series 1 PRO (Type A Machines, San Leandro, CA, USA). The completed adapter measured ~46 mm in diameter with an inner hole of ~13 mm diameter and ~1.4-2.8 mm in height.

4.2.7 Micro-disc electrophoresis

The automated system was connected to a laptop with Atmel Studio software v7.0 (Atmel Corporation, San Jose, CA, USA) to control all the necessary movements of the μEDisc and μAmpDisc to collect and adapt the data for analysis in GeneMarker HID software. For heating studies, there is a heated stage under the separation channel held at 37 °C either not at all, prior to, during separation, or right before the separation. Once fluidic movement was complete, the μEDisc separation channel was located rotationally *via* the photo-interrupter and clamped by the clamping motor to establish electrical contact between the gold pogo pins in the mechatronic device with the gold electrode pads on the μEDisc.(43)

The μEDisc is comprised of three replicate separation domains, each having independent electrodes and separate separation channels. With this architecture, one post-PCR sample can be electrophoresed in ~15 minutes. Each domain allows for an amplified sample to be input and 'heat-snap-cooled' before micro-disc electrophoresis (ME), the separation polymer pipetted into

the polymer chamber and centrifugally driven into the separation chamber, and alignment of the gold electrodes to the POGO pins for ME to occur.

After the sample (3 µL amplified products (cDNA), 3 µL WEN Internal Lane Standard (ILS) 500 (Promega, Madison, WI, USA) and 6.5 µL nuclease-free water (Molecular Biologicals International, Inc., Irvine, CA, USA)) was loaded into the μEDisc, it was heated 'heat-snap-cooled' at 95 °C for 3 min, and then snap cooled on ice for 3 min. Before a separation, a novel hydrophobically-modified polyacrylamide polymer (44) was loaded via device rotation at 3000 RPM for 5 min, followed by the actuation of two laser valves (45) (described in Woolf *et al*.) to establish electrical connectivity with the polymer in the sample waste (SW) and buffer (B) electrodes. A third laser valve was actuated and the μEDisc was spun at 3000 rpm for 10 sec to allow the sample to interface with the sample (S) electrode. Electrophoretic injection was performed at 600 V for 120 sec from S to SW electrodes, and separation at 1500 V from B to buffer waste (BW) with a pullback voltage applied at 200 V at S and SW for 500 sec.

At completion of the separation, integrated data analysis was performed in the software through a data analysis pipeline, which involves trimming of primer peaks, baseline subtraction, pullup correction, and 10X signal amplification using a digital filter. The processed data was then re-formatted and saved as a ".txt" file for compatibility with Microsoft Excel, as well as a ".fsa" file for forensic analysis in GeneMarker HID software (V2.8.2). The μEDisc and automated system were used to separate all of the single- and multiple-body fluid samples amplified with one of the three body fluid panels. A threshold was set at 100 RFU beneath which any peaks detected would be designated as background noise and not automatically detected by the software.

The fluorescent data from the μEDisc was compared to an ABI 3130xl and an ABI 3500. Due to the differences in instrument sensitivity, the data was minimum-maximum-normalized for each detection system to compare it more easily from the three separation platforms. The equation used for comparison, which shows the relative fluorescence intensity (RFU) for each peak was subtracted from the lowest RFU value and then divided by the highest RFU value subtracted from the lowest RFU that was detected across all samples and genes from that system. (46) This min-max normalization was performed on the fluorescent data from all three systems to allow direct comparison between detection systems across body fluids.

4.2.8 On-disc reverse transcription and amplification

The previously published amplification architecture was adapted to create the μAmpDisc, which contains 6 domains (for 6 samples) that allow for RT and PCR to amplify RNA targets on-disc.(35) The μAmpDisc and automated system were used to reverse transcribe and amplify the mRNA targets on the three panels, developed by ESR. For heating, there were two Peltier heaters on the automated system used for amplification purposes on the μAmpDisc. The total volume of the RT reaction is 10 µL and the PCR reaction is 20 µL, with 5 µl RNA sample and 5 µl cDNA sample, respectively. The RT reaction is pipetted into the RT chamber, and the μAmpDisc is spun to align the Peltier heaters above and below the chamber, then clamped to sandwich the μAmpDisc. After reverse transcribing the RNA into cDNA, the μAmpDisc is unclamped, a laser valve is irradiated, and spun to move the cDNA into the RT Excess and PCR chamber. The cDNA in the RT Excess chamber can be pipetted out to perform PCR in-tube, if preferred. The volume of cDNA spun into the PCR chamber becomes the aliquot for the PCR reaction. After the PCR master mix is pipetted

on the μAmpDisc, a laser valve is opened, and the liquid is spun into the PCR chamber. The Peltier heaters are clamped to sandwich the μAmpDisc and heated to conditions for PCR. The amplified fragments can be pipetted off the μAmpDisc to be size separated by electrophoresis, whether that be by integrating the μEDisc architecture with the μAmpDisc architecture or in a conventional capillary.

4.3 Results & Discussion

As a portable version of the conventional methodology, the protocols optimized by ESR scientists for body fluid profiling were adapted for microfluidic technology. Starting at the end of the workflow process, the body fluid panels were optimized for ME using a previously developed integrated system and a microfluidic disc specifically designed for size separation of fragments. The ME protocol was assessed using single-source and mixture samples for rapid ME (<15 min) and fluorescent detection of low concentrated samples. The next phase of the project was to adapt the RT and PCR 2-step protocol for microfluidic technology. After optimizing the RT protocol on-disc, the production of cDNA was assessed as well as the overall assay time.

4.3.1 Integrated system

An instrument capable of electrophoresis in a polyethylene disc with the corresponding software was developed to allow for automated microfluidic steps on a centrifugal disc.(35, 42) The same instrument and software were repurposed to enable fluidic control and LIF detection for amplification and separation on the μEDisc and μAmpDisc (**Fig. 2A**). Briefly, the discs are mounted onto a rotational platform, much like a CD-ROM, and an optical sensor placed near the outer perimeter of the disc, which allows for accurate positioning of the μEDisc and μAmpDisc

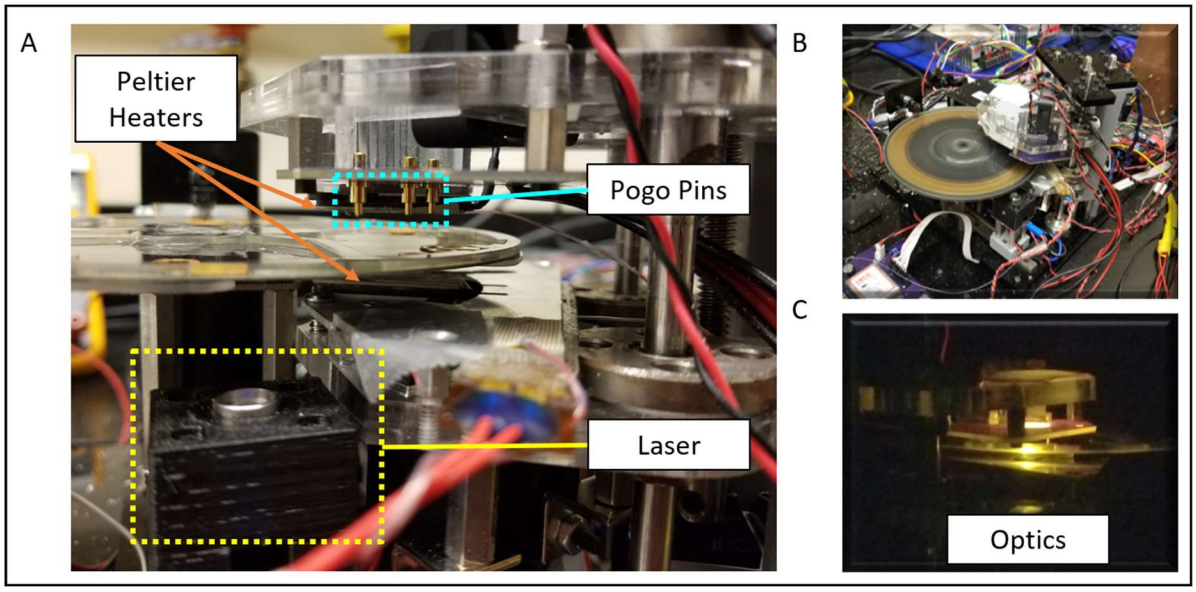

Figure 2: Automated system for microchip electrophoresis and amplification. (A) The integrated system has a laser for opening valves, peltier panels for heating, and pogo pins to attach to the gold electrodes to complete the connection for electrophoresis. (B) Top view of the integrated spin system. (C) Housed below the disc is the optical detector and blue laser for excitation.

(**Fig. 2B**). The motor driving the rotational platform is controlled by software (Atmel Studio v7.0) where the spin speed is defined by user input. The system associates architectural features with coordinates that are defined by: 1) the distance from the center of the disc (radius), and 2) the number of degrees from 'home,' defined as 0° radially; these are input to the software for accurate positioning (e.g., align the red laser diode with valves that are opened by ablation). Similarly, defined by coordinates relative to 'home', the system can rotate the disc to the accurate position needed to align the POGO pins for contact with the gold electrodes for application of voltage to the separation microchannel or Peltier heaters for heating. Specific voltage/times are used to define consistent injection at the cross-t followed by size-based separation of the fragments. The detection system is equipped with a blue laser (488 nm) for excitation, and emitted light is funneled by the optics to a four-color optical detector (photomultiplier tube) as fragments pass through the detection window (**Fig. 2C**).

Due to the multi-function nature of this automated system, one of the main advantages is the ability to adapt the system to other microfluidic discs. However, the layout of the system requires certain architectural features are integrated onto microfluidic devices in a prescribed manner. For example, the separation channel should be placed towards the outside of the μEDisc for three primary reasons, including: 1) to permit necessary pressure from centrifugal forces for rapid polymer filling, 2) to align the separation channel with the optics for fluorescent detection, and 3) to align the static POGO pins with the gold electrodes featured on either end of the separation channel. Designing the architecture of a microfluidic disc to fit this system can be challenging due to limitations in alignment of hardware for specific actions to areas on a microfluidic disc.

Previously, the integrated system was built to accommodate microfluidic discs that produced DNA profiles in a 'sample-to-result' format.(35, 42) Since the 'sample-to-result' microfluidic disc previously used contained functional domains for DNA extraction, amplification, and electrophoresis, this architecture presented a launch point for creating the μEDisc and μAmpDisc given that the sample preparation domains are not required at this point. The μEDisc was comprised of three replicate separation domains, each having independent electrodes and separate separation channels. With this architecture, one post-PCR sample can be electrophoresed in ~15 minutes (**Fig. 3**). The μAmpDisc shown below contains 6 domains (for 6 samples), allows for RT and/or PCR on-disc to amplify nucleic acid targets, and then pipette out the amplified sample (**Fig. 12**).

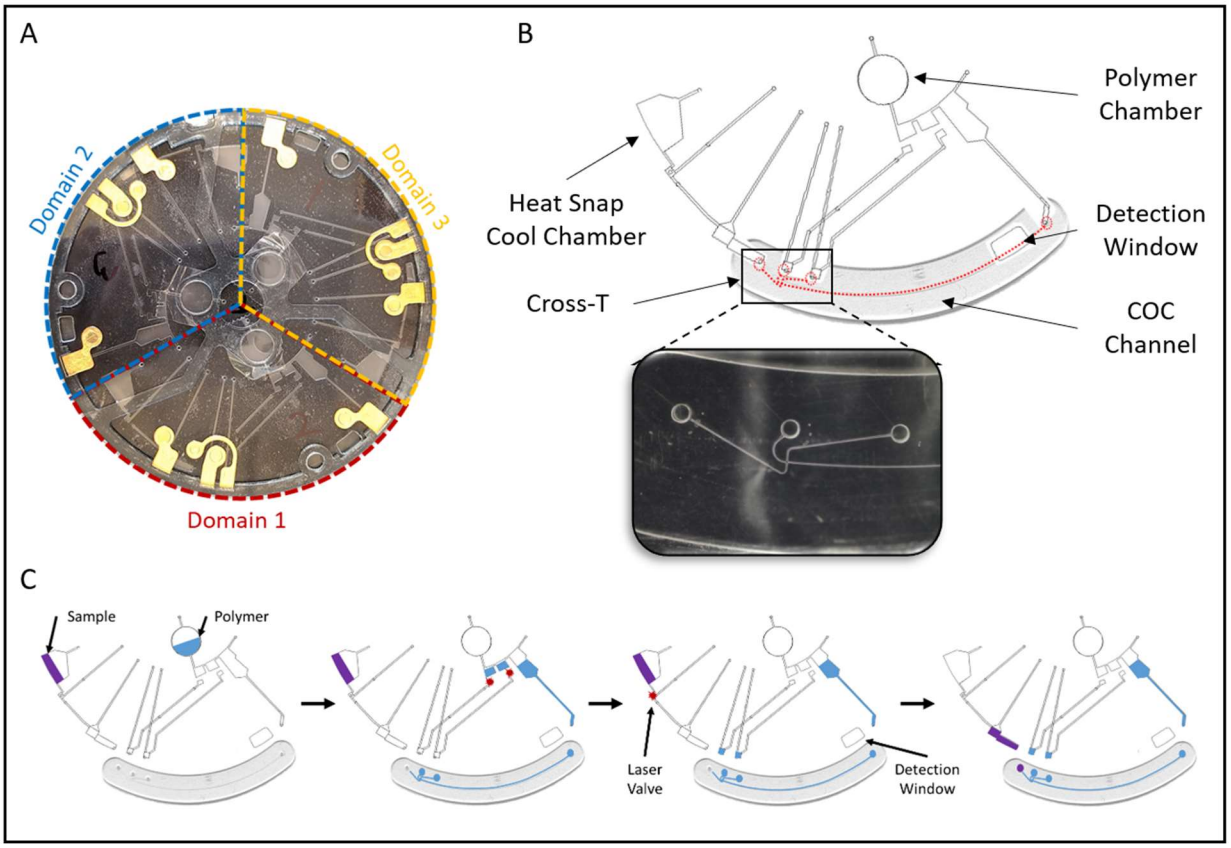

Figure 3: Design and architecture of μEDisc for size separation of amplified fragments. (A) Triplicate domains can be analyzed per disc. (B) Architecture of an individual domain, with an exploded view of the cross-t section. (C) Fluidic movement within the separation disc.

4.3.2 Optimizing on-disc separation parameters

Similar to commercial CE systems exploited for forensic analysis (e.g., ABI 3130xl, ABI 3500xl) where extensive optimization of commercial systems is performed by the manufacturer, CE on novel systems such as this inherently requires that a number of parameters be optimized for effective functioning of the system as a whole. (47) Previous work has shown sufficient separation of 10 STR loci ranging from 80 to 500 bp using this on-chip platform with 1 base pair resolution (35); thus, in this study we focused on optimizing sample injection time, sample input, and thorough heating of the separation channel during electrophoresis to adequately separate the amplicons in three body fluid panels.

When compared to the gold standard instrumentation, in which the electrokinetically-injected sample contains amplified fragments, ILS, and formamide, the sample injected on the μEDisc system contains amplified fragments, internal lane standard (ILS), and water. While this difference (water versus formamide) may cause concern for denaturation of amplicons or evaporation, previous work has shown this has no adverse effects on the size separation on-disc. (42) The ratio of sample volume to injection total volume is doubled on this system: 1 µL of amplified sample goes into 9 µL of Hi-Di formamide and ILS on a conventional CE system, whereas 3 µL amplified sample goes into 10 µL of water and ILS on this system. Due to differences between conventional CE and this system, the parameters for electrophoresis should be optimized to show sufficient size separation of the amplified fragments.

To assure optimal separation of the fragments, the volume of qRT-PCR product electrokinetically injected and the optimal channel temperature for electrophoretic separation was determined by assessing height, size, and shape of the fluorescent signal. Previously, a total volume of 13 µL (3 µL of amplicons, 10 µL of water and ILS) was previously demonstrated(42) to sufficiently separate amplified STR fragments by size. Here, we analyzed a smaller input of an amplified sample in the same total volume (**Fig. 4A**) to determine if a similar input volume as the conventional CE system could be used on-chip. As expected, peak heights decreased with the lower sample volumes. Higher input volumes were considered, but we wanted to balance using the least volume of sample while obtaining peak heights that are high without saturating the detector. Therefore, injected sample was composed of a total sample volume of 13 µL, with 3 µL sample, 4 µL ILS, and 6 µL water as this yielding the most robust detection of both ILS peaks and sample amplicons peaks.

A

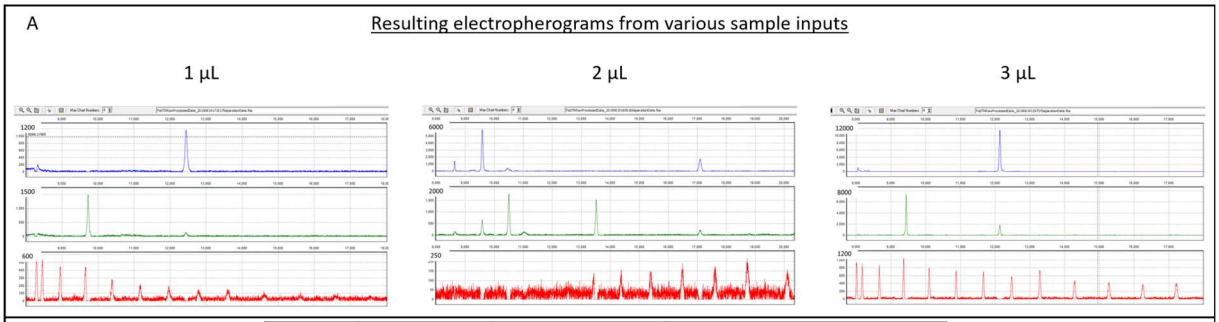

B

	No Heating	Heating During Separation	5 min Preheat with Heating During Separation
FAM	4846	878	3950
JOE	1340	360	448
WEN	4000	3000	4000

Figure 4: Optimization of microchip electrophoresis. (A) Electropherograms of various sample inputs for microchip electrophoresis. (B) Microchip electrophoresis highest peak height (RFU) via fluorescence detection with and without heat.

The optimal channel temperature was assessed by heating before, during, and omitting heating on the μEDisc. Since the capillaries on conventional systems are heated by an oven during separation, it was hypothesized that heating of the COC channel on the μEDisc would be advantageous to create uniform heating across the channel. A metal plate is housed within the automated system that was previously heated underneath the COC channel to 37 °C. It was found that with heating before or during a separation the peak heights in the blue and green channel decreased, while the red channel was virtually unchanged (**Fig. 4B**). It was theorized that there was a heat gradient vertically through the channel that could impede the separation due to a change in viscosity of the polymer. Alternatively, the heat produced from the voltage through the capillary combined with extra heating from the metal plate could cause joule heating affecting the resolution of the peaks and peak broadening, leading to smaller peak heights. Due to these possibilities and the experimental data, the metal plate was not heated during all the separations in this project.

Finally, optimization of sample injection time was important in balancing maximum peak height with minimal peak broadening. The electrokinetic injection was tested with a voltage (600 mV) similar to conventional CE systems for various amounts of time to the sample waste electrode (30-180 sec). If the injection time is not long enough, the sample will not reach the cross-t for sufficient fluorescent detection (**Fig. 3B**). On the other hand, if the injection time is too long, the bulk of the sample may bypass the cross-t leading to decreased fluorescent signal. **Fig. 5** shows the electropherogram with each fluorescent channel after a separation on-chip. Using a 30-second injection with 600 mV, the amplicon peaks associated with mRNA targets and ILS peaks were not present. However, using a 60- or 90-second injection with 600 mV the peaks associated with amplicons of mRNA targets were present and ILS peaks were detected with lower peak heights over time. Detection of the ILS peaks, especially in the 80 – 200 base pair range, are important for accurate sizing of the amplicon peaks as all of the mRNA targets in the panel range from 100 to 200 bp in size. Of all the injection times, the 120- and 180-second injections with 600

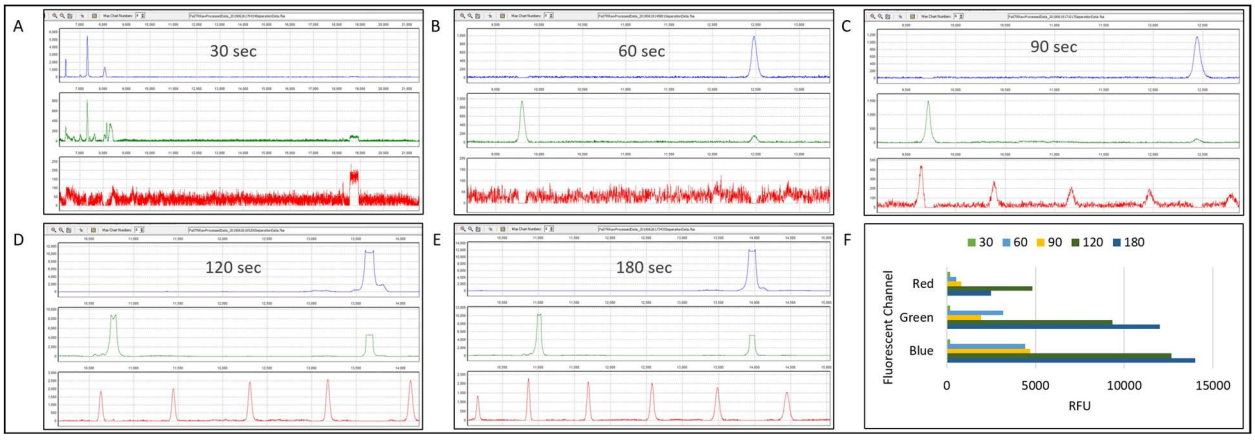

Figure 5: Various injection times were evaluated to allow sufficient sample across the T-junction. The sample, ILS, and voltage (600 mV) were kept constant. (A-E) Fluid profiles of separations show highest fluorescent peak heights at both 120 and 180 sec injections. (F) When comparing the profiles, the 120 and 180 sec injections allowed for high sample and ILS peaks. The lower injection times did not separate the ILS sufficiently (shown by low peak heights in A-C).

mV were the only two that detected the ILS peaks and all of the sample peaks associated with mRNA targets saturated the detector. While either injection time could be used to detect all the necessary ILS peaks with the on-chip electrophoresis, we selected 120-second injection, ultimately decreasing overall separation time by one minute.

Continuing forward, a separation on the μEDisc was performed with 3 µL of amplified product, without extra heating from the metal plate on the automated system, and at an injection of 120 sec with a separation of 300 sec.

4.3.3 Single source fluid comparison

Received from ESR, single source body fluid amplified samples were separated on the μEDisc with the optimized conditions, described above. To compare the μEDisc and integrated system to conventional methods, the fluorescent data was normalized using a minimum-maximum calculation (**Fig. 6**). The normalized peak heights for replicate separations were averaged across multiple donors. The 11 peaks associated with the target body fluids were consistently detected when separated on the μEDisc and demonstrate comparable results to gold-standard instruments. This is significant because not only did the μEDisc detect all of the gene peaks associated with amplicons of the mRNA targets, but in some of the body fluids the μEDisc detected the peaks as well or better than the 3130xl or 3500. For example, peaks associated with amplicons of both mRNA targets specific to venous blood (HBD and SLC4A1), were detected in both samples with comparable intensity relative to the commercial instruments (**Fig. 7**). These samples consistently showed peak heights from the μEDisc that were higher than or similar to the 3130 and 3500 systems. The Quadruplex panel associated with amplicons of

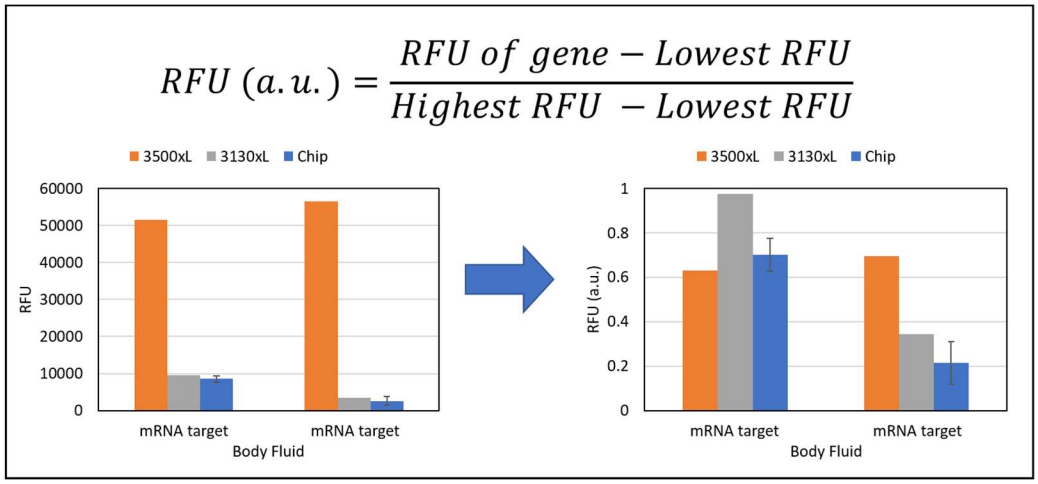

Figure 6: Normalization calculation. The fluorescent data from three electrophoresis instruments were analyzed, but the three instruments produce fluorescent signal on different scales. By normalizing the signal, the signal from the instruments can be more easily compared.

mRNA targets specific to Vb (HBD, SLC4A1) and Mb (STC1, MMP10). Similar trends were observed when considering the two peaks associated with menstrual blood targets (STC1, MMP10). The two peaks associated with venous blood targets (HBD, SLC4A1) were also detected in both menstrual blood samples, but in much lower peak heights using the μEDisc. This shows the integrated system can detect multiple amplicons with high and low fluorescent signal on the μEDisc.

The duplex peaks associated with amplicons of mRNA targets specific to buccal contributions (HTN3, FDCSP) were consistently detected in all three systems in amplified samples from different swabs. **Fig. 7** shows the HTN3 peak to be consistently higher than the FDCSP peak using the μEDisc system; this phenomenon was also exhibited by separation and detection with the 3130xl instrument. On the 3500 instrument, however, these two peaks had relatively balanced peak heights. This imbalance with the 3500 system could be attributed to the effect of environmental on the samples prior to detection with the three platforms (i.e., shipping,

environment, etc.). After the samples were extracted, reverse transcribed, amplified, and separated using the 3500 system in one laboratory (ESR, NZ), the samples were shipped to the UVA laboratory and detected using the 3130 instrument and μEDisc system. During this process, the sample composition may have degraded or slightly changed causing the differences. Regardless of minor differences in peak balance, both mRNA amplicons in the Duplex panel were consistently detected using all three systems.

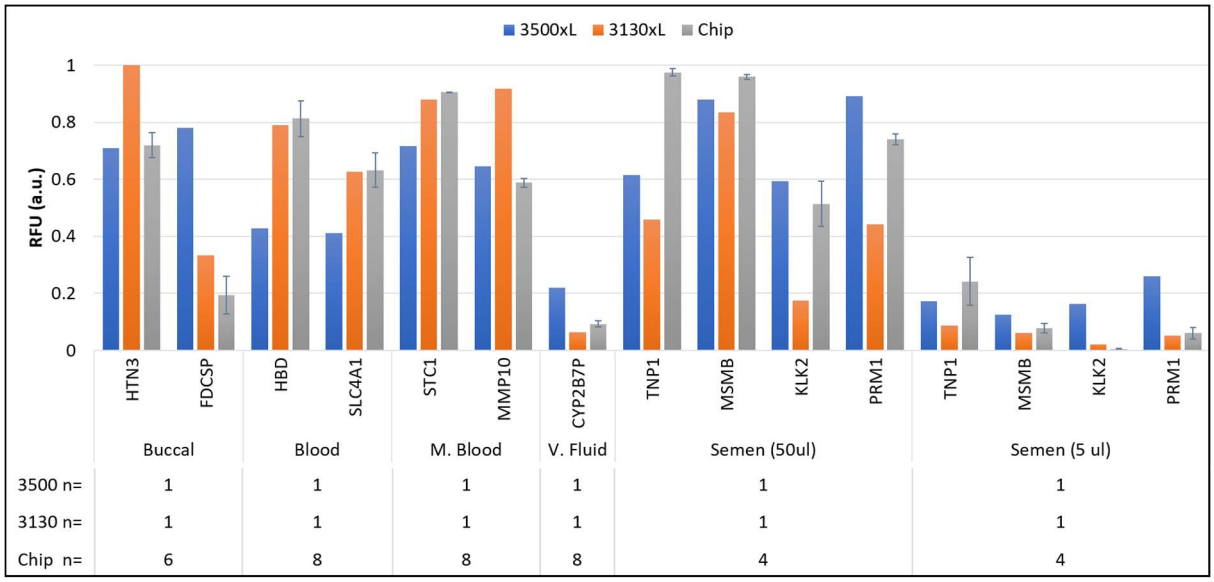

Figure 7: Single source fluid comparison of peak heights from gold-standard CE systems and the chip microfluidic system. The sample was separated on the chip microfluidic system in either duplicate, triplicate, or quadruplicate, respectively, then averaged for the graph.

Finally, the Pentaplex panel, containing the vaginal fluid and semen mRNA targets, was used to identify samples from two vaginal fluid donors and two semen donors (50 µL and 5 µL) using the three separation platforms using. While the vaginal fluid marker (CYP2B7P) was one of the lowest normalized peak heights detected across all three platforms, the peak height was consistently detected above the lower threshold using the μEDisc system (**Fig. 8**). This peak had higher peak heights on the μEDisc system than the 3130 instrument, but lower than the 3500 instrument, showing the μEDisc system is comparable with both gold standard systems. Similarly,

all four peaks associated with amplicons of semen mRNA targets (TNP1, MSMB, KLK2, PRM1) were detected using the μEDisc system at higher or comparable peak heights than in the 3130 or 3500 instruments with the 50 µL semen sample, again showing a strong comparison between the μEDisc system and the gold standard systems. This trend continued with the 5 µL semen sample, with the exception of the KLK2 gene. The KLK2 gene peak height was much lower than the three other genes and the allele was not automatically called by the software in one of the four replicates. However, the KLK2 peak was able to be manually called with the lowest value of 47

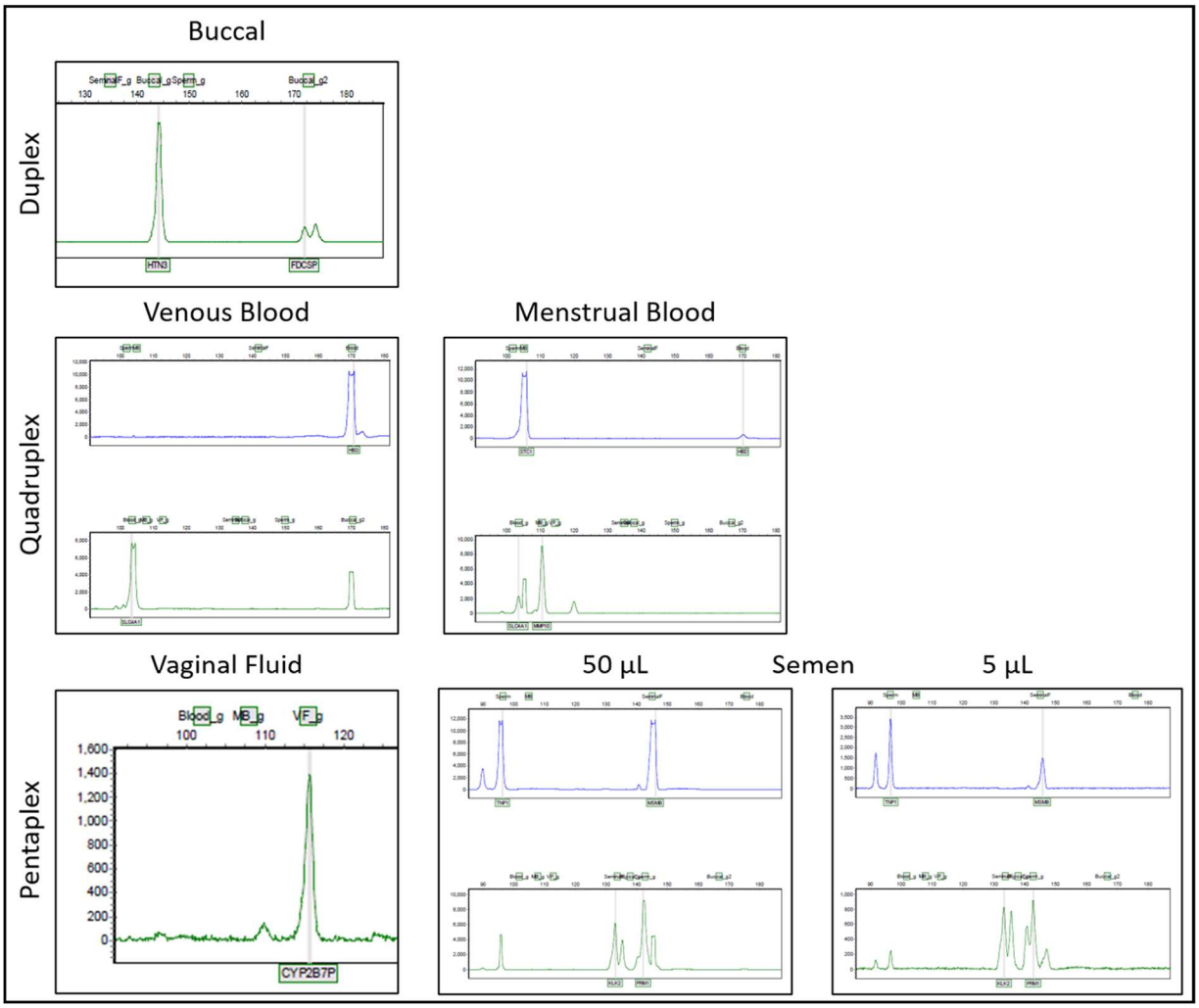

Figure 8: Representative electropherograms from single-source body fluid samples after microchip electrophoresis.

RFU (under threshold) and highest of 845 RFU using the μEDisc system. This data shows that even though the sample was small in volume, the μEDisc system was still able to detect all of the semen genes in the Pentaplex panel, similarly to the conventional instruments. Additionally, the data shows that all of the vaginal fluid and semen samples were detected in the μEDisc system comparably to the gold standard systems.

4.3.4 Multiple source fluid comparison

While detection of single-source fluids is important, many forensic samples are not single source and often contain anywhere from one fluid to all five fluids, in addition to others not tested here. The amplified products from two mixed samples (e.g., samples containing multiple body fluids) were separated on each of the three platforms for comparison. To simulate the type of sample that would be present in one of ~45,000 forensic samples received and backlogged(48) from sexual assault evidence kits, a mock sample was constructed to contain both vaginal fluid and semen. All associated mRNA markers for these targets can be probed using a single primer panel (Pentaplex). The data in **Fig. 9** shows simultaneous detection of all five targets consistently across replicates. The semen target (TNP1) and seminal fluid target (MSMB) amplicons were detected using the μEDisc system at peak heights higher than both the 3130XL and 3500 instruments after normalization, while the other three genes in the panel for vaginal fluid (CYP2B7P), seminal fluid (KLK2) and semen (PRM1) had comparable peak heights to the 3130 and 3500 instruments. The overall lower peak height of the vaginal fluid (CYP2B7P) in this sample could be due to the sample itself or imbalanced amplification of all five targets during the RT-PCR

heating. However, the entire Pentaplex was successfully detected using the μEDisc system better or comparable to the two conventional instruments (**Fig. 9**).

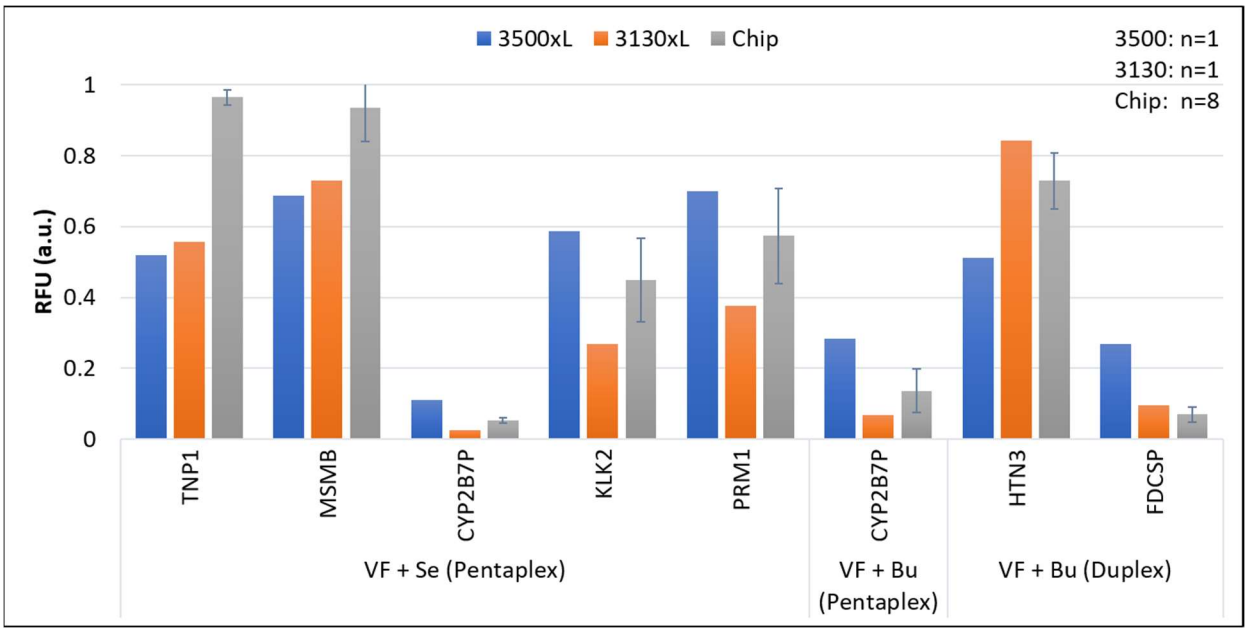

Figure 9: Multi-source fluid comparison of peak heights from gold-standard CE systems and the chip microfluidic system. The samples were separated on the chip microfluidic system in either quadruplicate, respectively, then averaged for the graph.

The second mixture sample was comprised of vaginal fluid and buccal fluid that was amplified with the Duplex and Pentaplex panels. The buccal amplicon (HTN3) was detected on the μEDisc with higher peak heights more similar to the 3130 system, while the vaginal fluid (CYP2B7P) and buccal (FDCSP) genes were much lower in peak height across all three platforms. The vaginal fluid gene (CYP2B7P) had higher peak heights using the μEDisc system than the 3130 system, but lower peak heights than the 3500 system. The buccal gene (FDCSP) was detected similarly in the μEDisc and 3130 systems, but much higher in the 3500 system. The imbalance with the 3500 system could be attributed to environmental effects on the samples prior to detection with the 3130 and μEDisc platforms (i.e., shipping, environment, etc.). However, the

three genes required to accurately determine the composition of this mixture sample were consistently present on all three platforms. The electropherograms are compared for both mixture samples in **Fig. 10**. This data shows the μEDisc system can perform just as well as or better than the gold standard systems with single- and multiple-body fluid samples. It also shows replicate consistency in the μEDisc system among both types of samples.

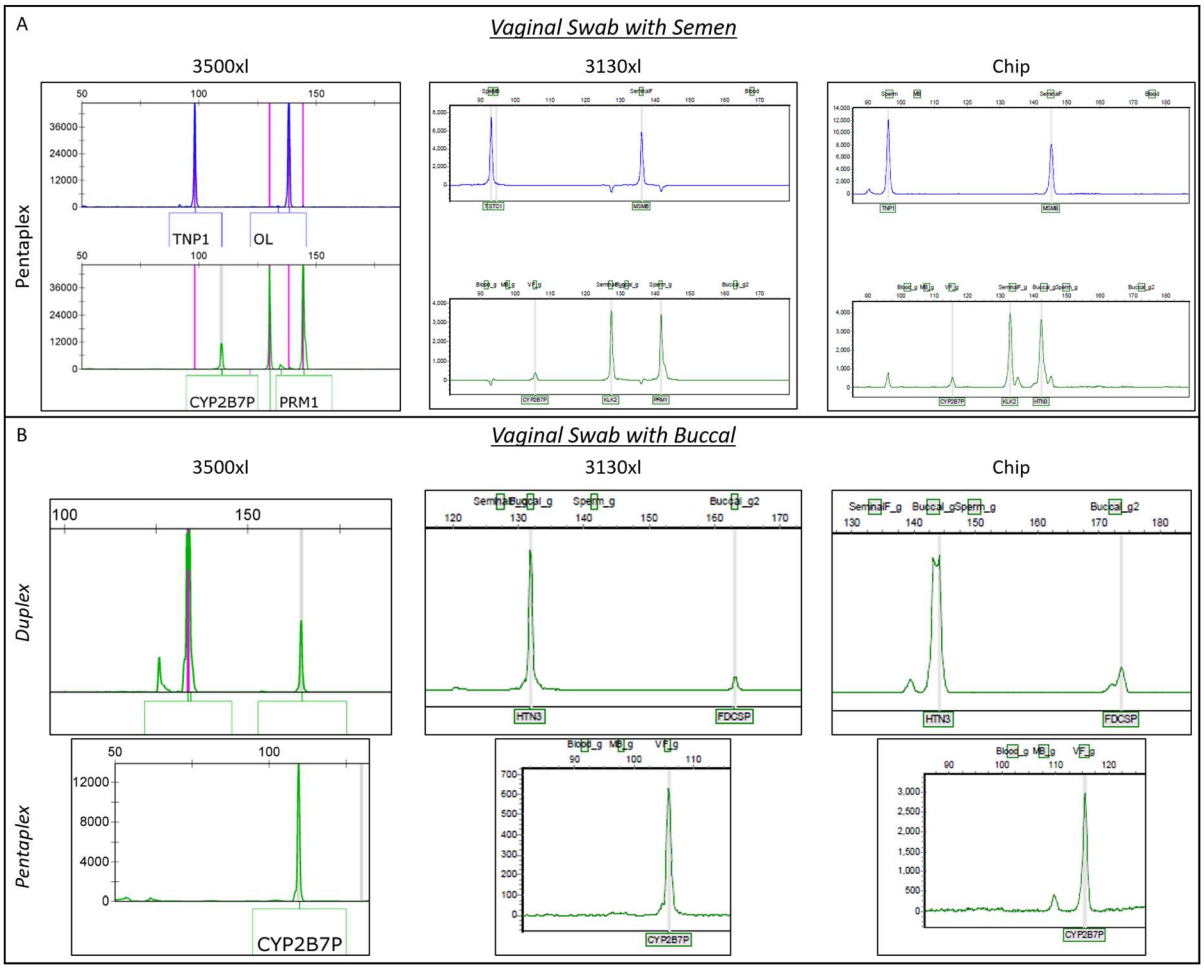

Figure 10: Electropherograms from mixture samples after microchip electrophoresis. (A) All mRNA targets were detected from a vaginal fluid swab with 50 µL of semen sample. (B) All mRNA targets were detected from a vaginal fluid swab with buccal sample. Both samples were extracted and amplified at ESR, and microchip electrophoresed at UVA.

4.3.5 On-chip separation sensitivity

We sought to interrogate the sensitivity of our μEDisc system by empirically determining an analytical limit of detection for each body fluid panel. Each PCR product was serially diluted from the initial sample (neat) to a 1:32 factor, representative of low-concentration samples frequently encountered in forensic casework. **Fig. 11** shows the non-normalized fluorescence signal detected on the μEDisc system using the diluted samples. Any analytical system has thresholds that determine what is called as an actual peak versus what is considered background noise. For the μEDisc system, we set a threshold beneath which any peaks detected would be designated as background noise and not automatically detected by the software, which was at 100 RFU. However, some of the peaks were visually seen and manually given a peak height. Unsurprisingly, after a 1:2 dilution, the fluorescence signal considerably decreased for all amplicons in the three panels. Even with the decrease in signal, 10 of the 11 genes were automatically detected by the GeneMarker software at the 1:8 dilution and all of the Quadruplex was detected at the 1:8 dilution.

The Quadruplex panel contains primers to interrogate the four genes specific to venous blood and menstrual blood. The data in **Fig. 11** demonstrates that dilutions greater than 1:2 exhibit a sharp decline in fluorescent signal; yet, even at the 1:32 dilution, both genes for venous blood and menstrual blood were detected above the threshold using the μEDisc system. Additionally, both genes for venous blood and menstrual blood were detected in both donor's samples using the μEDisc system. Using the same two standards stated before, the μEDisc system

for venous blood and menstrual blood is 1:32 dilution of liquid or whole swab sample, respectively.

Similarly, the Duplex panel, which contains the two genes for buccal fluid (HTN3, FDCSP), was detected in both donors on the μEDisc system (**Fig. 11**). The peak associated with the amplicon of mRNA target HTN3 was detected above the threshold at the 1:32 dilution, but the peak associated with the amplicon of mRNA target FDCSP was only detected above the threshold from the neat to the 1:8 dilution. For the Duplex panel, the sensitivity of the μEDisc system for buccal fluid is 1:8 dilution of a whole swab sample.

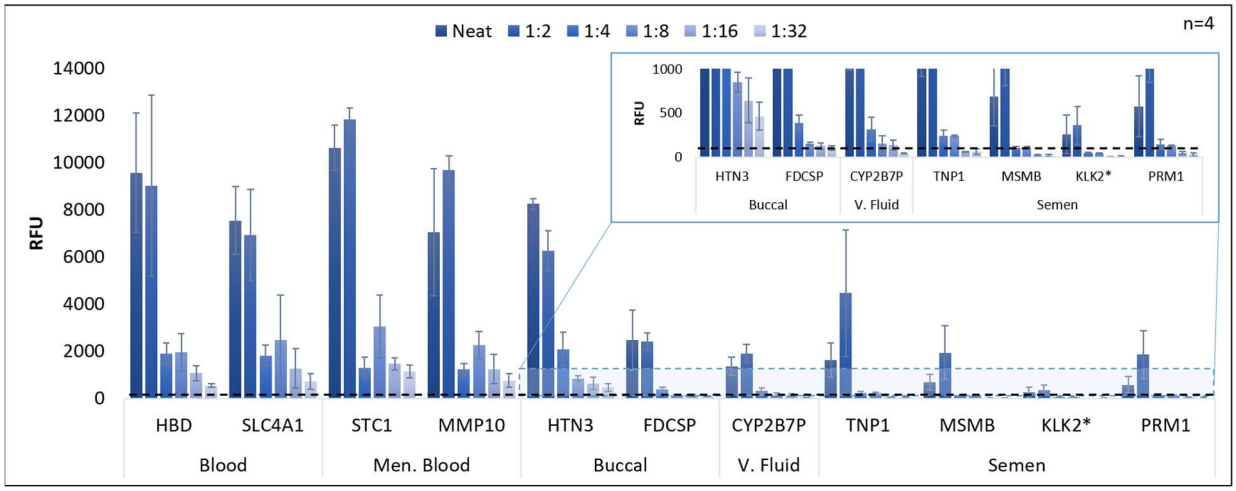

Figure 11: Sensitivity of on-chip fluorescent detection. Two donor amplified samples were serially diluted before microelectrophoresis via the μEDisc and integrated system and averaged for this graph. Each sample was separated in quadruplicate. Inset shows fluorescent signal of three fluid's targets near the calculated threshold. * = all dilutions were manually called.

Lastly, the Pentaplex panel contains the genes specific to semen, seminal fluid, and vaginal fluid. After dilutions, the vaginal fluid gene (CYP2B7P), was detected at the dilution of 1:16 using the μEDisc system. The KLK2 gene for semen was the only gene that completely dropped out (was not visibly present) after a 1:8 dilution of the 5 µL semen sample and not automatically after a 1:2 dilution, while the other three semen genes were visibly present at all

dilutions of a 5 µL semen sample. Nonetheless, to reliably determine semen is present in the sample, all four genes should be detected by the μEDisc system. By this standard, the μEDisc system could consistently detect all four genes from the Pentaplex panel in the neat sample (50 ul dried on swab) isolated, purified, amplified, and diluted down to a 1:2 dilution. Using both our guidelines (threshold and detection of all body fluid amplicons), the sensitivity of the μEDisc system for semen is 1:2 dilution of a 5 µL sample and for vaginal fluid is 1:16 dilution of a whole swab sample.

4.3.6 Optimization of sample volume and on-disc heating

To develop an integrated device capable of performing sequential assays, the next phase of this project worked to integrate the on-disc RT and PCR prior to separation. The architecture of the μAmpDisc permits the RT reaction to flow into the PCR chamber as the sample input (**Fig. 12**). The size of the chambers was approximated in AutoCAD and the experimental volume moving into the PCR chamber was tested to verify the correct sample volume for the PCR reaction. The architecture of the μAmpDisc included a laser valve and RT Excess chamber upstream of the PCR chamber to aliquot the necessary sample volume in the PCR reaction. Additionally, extra cDNA in the RT Excess chamber can be pipetted off disc and amplified in-tube, if necessary. Previous studies by ESR scientists used either 2 or 10 µL of sample in the in-tube PCR reactions, thus the architecture for the μAmpDisc was fabricated to produce a sample input that averaged the two volumes. The size of the RT Excess chamber was designed to hold the remaining 4 µL of cDNA after spinning the sample (6 µL) into the PCR chamber. To determine fluid volumes, known volumes of red dye (0.5 to 10 µL), which encompassed the volumes used in the previous

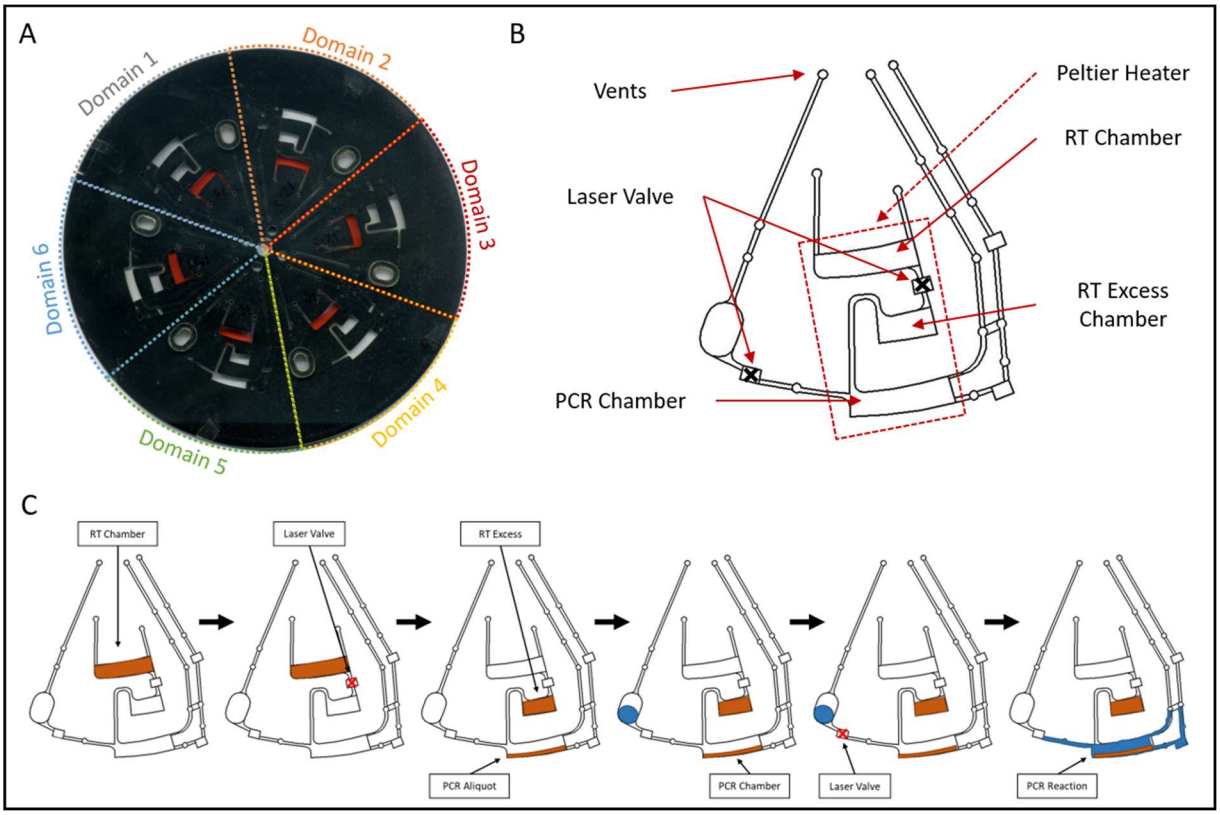

Figure 12: μAmpDisc with six identical RT & PCR domains. (A) The disc consists of five layers of polyethylene terephthalate (PeT), heat sensitive adhesive (HSA), and black PeT. (B) Each domain has individual chambers for RT, excess cDNA, and PCR. (C) Fluidic movement within the layers of the disc.

in-tube studies(1), were pipetted into the PCR chamber and imaged for pixel count. The number of red pixels were counted using FIJI and a standard curve was constructed to approximate the volume flowing into the PCR chamber (**Fig. 13A**; R^2=0.9945).(49) Multiple μAmpDiscs were fabricated with different RT Excess chamber heights (y-axis) to vary the volume of sample input to the PCR chamber. To simulate the correct volumes, 10 µL of red dye was pipetted into the RT chamber, the laser valve was opened, and the μAmpDisc was centrifugally spun into the RT excess and subsequently the PCR chamber. The number of red pixels were measured, and the volumes were determined based on the standard curve (**Fig. 13B**). It was determined that the optimal

height for the RT Excess chamber chosen was ~1.43 mm (y-axis), permitting a sample input of ~6 µL for the PCR reaction.

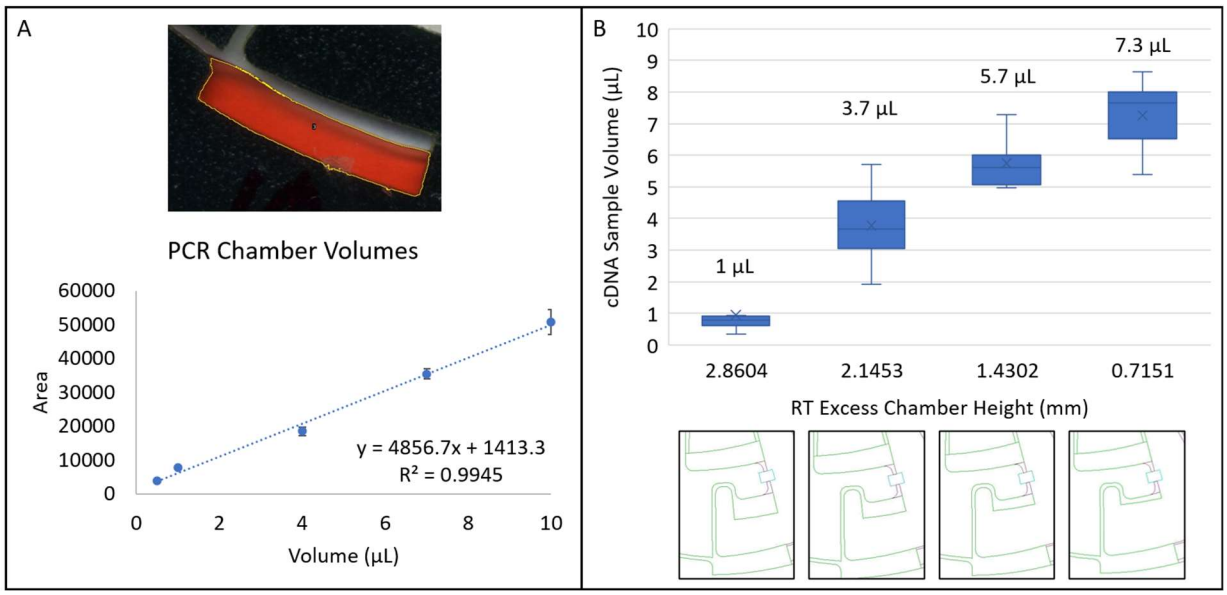

Figure 13: Analyzing the volume of cDNA in the PCR reaction after RT assay. (A) Using FIJI software, the pixels colored red were located and counted for each volume of liquid inside the PCR chamber. A standard curve was generated to determine the volume of cDNA overflowing into the PCR chamber. (B) The RT Excess chamber was changed in size to change the volume flowing into the PCR reaction. The liquid flowed into the PCR chamber was averaged to determine the sample volume in the PCR reaction.

Using the μAmpDisc, the Peltier heaters were optimized to produce the desired in-chamber temperatures for the RT protocol. The temperature was tested by inserting a thermocouple into the RT chamber with or without 10 µL of water and recording the measured temperature with a Versalog. Both Peltier heaters sandwiched the μAmpDisc, while the software inputs were toggled. **Fig. 14A** shows minimal difference between the temperature when testing air or water and demonstrates a very stable temperature across replicates. The 25 °C step was the most difficult to optimize due to the proximity to room temperature (22-23 °C). Initially, it was thought the reaction could sit in-chamber for the 25 °C step time without the use of Peltier heaters, but the temperature did not average at 25 °C (**Fig. 14B**). In testing of the Peltier heaters,

it was determined that a software input of 26 – 28 would illicit an average response temperature of 25 °C in the requisite chamber and the software inputs for 25, 37, 85 °C were 26, 41, 97, respectively. Once the software input temperatures were determined, the RT protocol was tested multiple times (n=5) to show stability of the temperature from run to run (**Fig. 14C**).

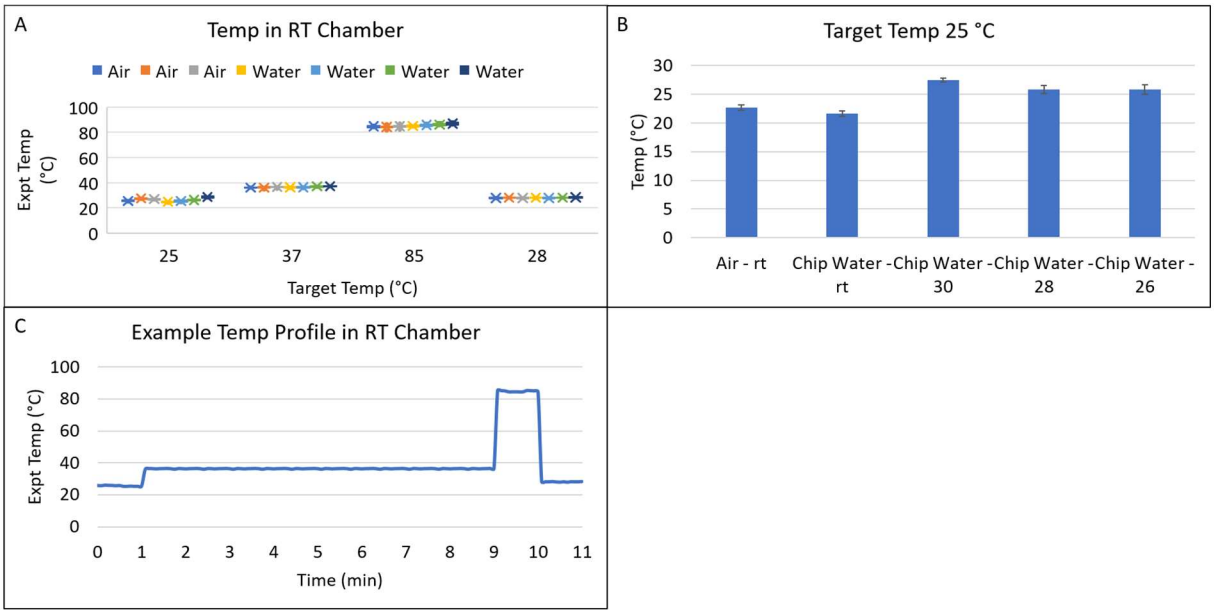

Figure 14: Temperature optimization inside RT and PCR chambers. (A) Air and water temperature measurements averaged over 60 sec inside the RT chamber. (B) Exemplary temperature profile with the optimized RT protocol. (C) Optimization for the 25 °C temperature.

4.3.7 Decreasing overall time of RT reaction on-disc relative to in-tube

After the in-chamber temperature was optimized, each step of the RT protocol was decreased and assessed for cDNA quantity via qPCR. Initially, the RNA from a blood sample was converted to cDNA in-tube with and without the RT enzyme (**Fig. 15A**). The conversion without the RT enzyme was performed to determine if any residual DNA in the RNA lysate would amplify the 18S target, while the conversion with the RT enzyme served as a 'baseline' for total RNA in the blood sample. The results indicate that the neat sample with RT enzyme converted RNA to cDNA and amplified around cycle 25. **Fig. 15B-D** shows how each step of the RT protocol can be

reduced significantly to decrease the overall assay time. The 25 °C primer annealing step was reduced from 10 min to 1 min. However, there was a statistical difference between the in-tube and on-disc cDNA production at all three intervals. The 37 °C step was the most reduced from 120 min to 8 min with a slight difference in cDNA production, as was evidenced by the shifting Ct value. While this step is critical step to this assay, the data shows it can be drastically reduced with similar results as in-tube reactions.(50, 51) Comparing in-tube vs. on-disc cDNA production, a statistical difference from a t-test was found at 60, 45, 30 min, but not at 15 and 8 min. When the 85 °C step was reduced from 5 min to 1 min, the production of cDNA changed based on dC_T value for both in-tube and on-disc but decrease the time any further and the quantity of cDNA diminishes. There was a significant difference in cDNA production between the in-tube and on-disc with 30 and 15 sec, but not at 1 min. However, **Fig. 15D** does show we can reduce this step by 4 minutes and still produce cDNA. Finally, the concentration of the RT enzyme was increased to determine if more cDNA could be produced. **Fig. 15E** shows that an increase in enzyme can

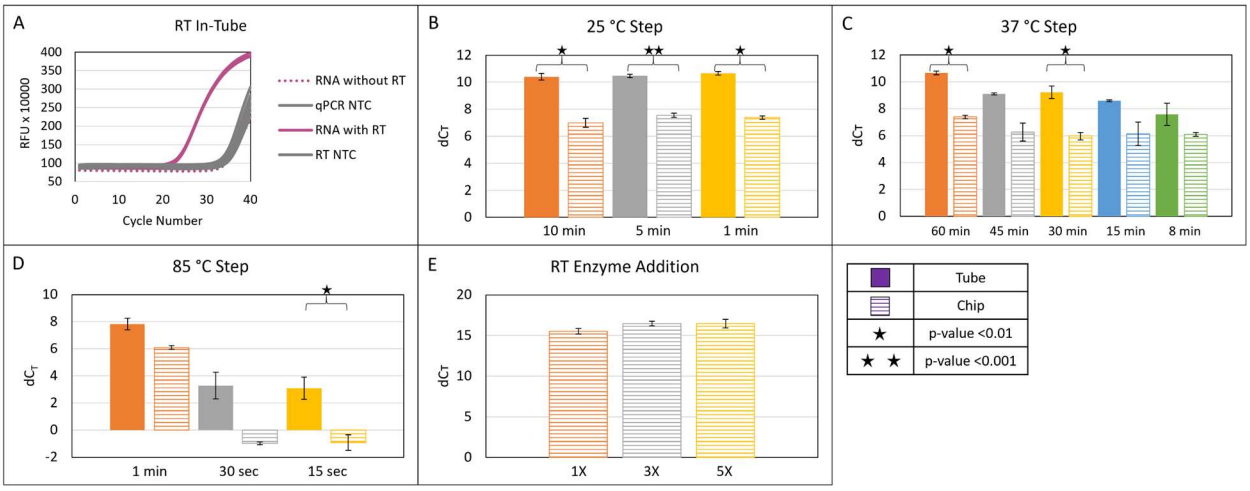

Figure 15: Optimization of each RT step for sufficient cDNA production using a neat venous blood or saliva Total RNA sample. (A) RT performed in-tube (solid) using previously optimized protocol. (B-D) Decreasing time of each step in the RT protocol to compare tube (solid) vs chip (striped) cDNA production. (E) Additional enzyme was added to optimized protocol. The dC_T was calculated the negative control minus sample for in-tube and on-disc.

slightly increase cDNA production, however, there was no significant difference. Additionally, if more RT enzyme were added to the reaction, the price per reaction would increase by $2 – 4 (USD). To be time-reducing, the final RT protocol was optimized at ~11 minutes with 1X RT enzyme, which saves roughly 110 min from the RT protocol.

This RT protocol was used to amplify known single source body fluids obtained from ESR. The fluids were lysed and purified for RNA by the scientists at ESR and sent to the Landers lab at UVA. Donors from all five body fluids were reverse transcribed using the optimized protocol (**Fig. 16**). All of the samples amplified at or before cycle 25 using the 18S rRNA targets and were determined to be statistically different from the NTC (p-value <0.01: Tube Buccal D2, Tube V Fluid D1, Disc Buccal D2, Disc M Blood D1; p-value <0.001: remaining samples). Comparing the in-tube vs on-disc RT reactions, there was ~ 2-5 cycle difference with more cDNA being produced in the

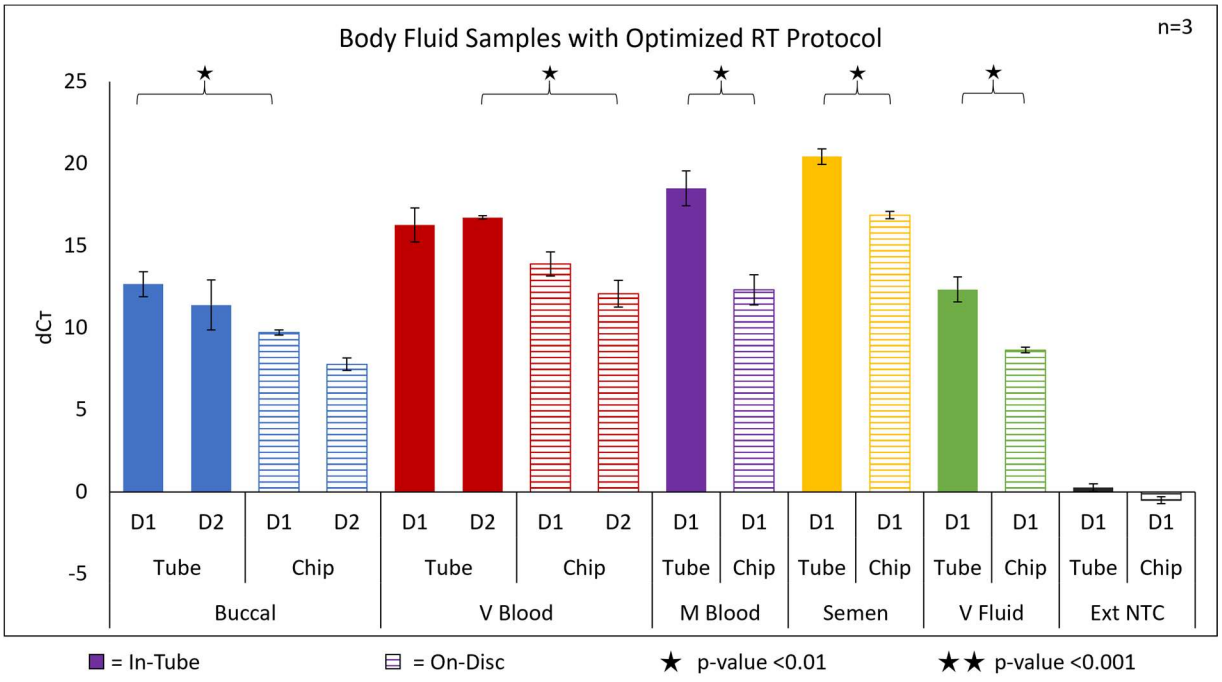

Figure 16: Bar graph showing optimized RT protocol with various body fluids. The 18S rRNA gene was quantified to determine cDNA productions via Total RNA concentration in triplicate of two donors.

in-tube reactions, but no statistical difference between the in-tube and on-disc RT reactions. The on-disc reactions produced sufficient cDNA that can be amplified in downstream PCR reactions and electrophoresed for body fluid profiling. Overall, this data sets up the next phase of this project: optimization of the ESR's PCR protocol on-disc.

4.4 Summary

This research showed proof-of-concept microfluidic electrophoresis with on-disc fluorescence detection and on-disc reverse transcription of a transcriptome-based method for forensic body fluid identification. Given that forensic laboratories are overburdened, it was important to achieve rapid time and amenability to high throughput with these techniques. To address this, the μEDisc was designed to accommodate three parallel domains to enable analysis of three samples with a single disc and in 15 mins. Importantly, all mRNA markers for single-source samples of five body fluids, as well as mixed samples, were detected using three primer panels. The μAmpDisc was designed for 6 samples/disc for rapid RT and PCR protocols. This disc reverse-transcribed multiple single source body fluids 10X faster (120 min → 11 min) than the in-tube reactions.

These results demonstrate progress towards a fully integrated *sample-in-answer-out* system for simultaneous forensic body fluid identification of six body fluids. Through incorporation of on-disc RNA extraction with the optimized RT, PCR, separation, and detection reported here, a μTAS device will be developed. Such a device would have important implications in expediting the forensic body fluid identification process with high sensitivity and specificity of mRNA targets. To realize this, the next steps will be to optimize the PCR amplification method

previously used with these panels onto the microdevice. (1) The existing discs' architecture will be augmented to accommodate RNA extraction using the PCL fabrication method. Subsequent optimization of amplification parameters (i.e., temperatures, clamping pressure) will be conducted to maximize RT-PCR efficiency and yield, then applied to both single-source and mixture samples. The resulting micro total analysis system (μTAS) (52) will permit complete, automated, direct-from-sample RNA-based body fluid identification amenable for use by nontechnical personnel. This instrument will then be compared to ubiquitous standard instruments used in the forensic field. Overall, this research shows promise for a new body fluid detection method that can rapidly and consistently identify any of the five forensically relevant body fluids on the three panels.

4.5 References

1. Albani PP, Fleming R. Developmental validation of an enhanced mRNA-based multiplex system for body fluid and cell type identification. Science & Justice. 2019 2019/05/01/;59(3):217-27.

2. Harbison S, Fleming R. Forensic body fluid identification: state of the art. Research and Reports in Forensic Medical Science. [Review]. 2016;6:11.

3. Kamanna S, Henry J, Voelcker NH, Linacre A, Kirkbride KP. Direct identification of forensic body fluids using matrix-assisted laser desorption/ionization time-of-flight mass spectrometry. International Journal of Mass Spectrometry. 2016 2016/03/15/;397-398:18-26.

4. Quinn AA, Elkins KM. The Differentiation of Menstrual from Venous Blood and Other Body Fluids on Various Substrates Using ATR FT-IR Spectroscopy. Journal of Forensic Sciences. 2017 2017/01/01;62(1):197-204.

5. Liu W, Butler E, Yang H, Fenyö D, Siegel D. Informatics Approaches to Forensic Body Fluid Identification by Proteomic Mass Spectrometry. Applications in Forensic Proteomics: Protein Identification and Profiling: American Chemical Society; 2019;81-90.

6. Muro CK, Doty KC, de Souza Fernandes L, Lednev IK. Forensic body fluid identification and differentiation by Raman spectroscopy. Forensic Chemistry. 2016 8//;1:31-8.

7. Takamura A, Watanabe K, Akutsu T, Ozawa T. Soft and Robust Identification of Body Fluid Using Fourier Transform Infrared Spectroscopy and Chemometric Strategies for Forensic Analysis. Scientific Reports. 2018 2018/05/31;8(1):8459.

8. Hanssen EN, Avershina E, Rudi K, Gill P, Snipen L. Body fluid prediction from microbial patterns for forensic application. Forensic Science International: Genetics. 2017;30:10-7.

9. Park J-L, Kwon O-H, Kim JH, Yoo H-S, Lee H-C, Woo K-M, et al. Identification of body fluid-specific DNA methylation markers for use in forensic science. Forensic Science International: Genetics. 2014;13:147-53.

10. Antunes J, Balamurugan K, Duncan G, McCord B. Tissue-Specific DNA Methylation Patterns in Forensic Samples Detected by Pyrosequencing®. In: Lehmann U, Tost J, editors. Pyrosequencing: Methods and Protocols. New York, NY: Springer New York; 2015;397-409.

11. Kitamura E, Igarashi J, Morohashi A, Hida N, Oinuma T, Nemoto N, et al. Analysis of tissue-specific differentially methylated regions (TDMs) in humans. Genomics. 2007 2007/03/01/;89(3):326-37.

12. Silva DSBS, Antunes J, Balamurugan K, Duncan G, Alho CS, McCord B. Developmental validation studies of epigenetic DNA methylation markers for the detection of blood, semen and saliva samples. Forensic Science International: Genetics. 2016;23:55-63.

13. Forat S, Huettel B, Reinhardt R, Fimmers R, Haidl G, Denschlag D, et al. Methylation Markers for the Identification of Body Fluids and Tissues from Forensic Trace Evidence. PLOS ONE. 2016;11(2):e0147973.

14. Haas C, Hanson E, Anjos MJ, Ballantyne KN, Banemann R, Bhoelai B, et al. RNA/DNA co-analysis from human menstrual blood and vaginal secretion stains: results of a fourth and fifth collaborative EDNAP exercise. Forensic science internationalGenetics. 2014;8(1):203-12.

15. Roeder AD, Haas C. Body Fluid Identification Using mRNA Profiling. In: Goodwin W, editor. Forensic DNA Typing Protocols. New York, NY: Springer New York; 2016;13-31.

16. O'Leary KRaG, Claire L. Investigating the Isolation and Amplification of microRNAs for Forensic Body Fluid Identification. MicroRNA. 2018;7(3):187-94.

17. Mayes C, Seashols-Williams S, Hughes-Stamm S. A capillary electrophoresis method for identifying forensically relevant body fluids using miRNAs. Legal Medicine. 2018 2018/01/01/;30:1-4.

18. Song F, Luo H, Xie M, Zhu H, Hou Y. Microarray expression profile of circular RNAs in human body fluids. Forensic Science International: Genetics Supplement Series. 2017 2017/12/01/;6:e55-e6.

19. Liu B, Song F, Yang Q, Zhou Y, Shao C, Shen Y, et al. Characterization of tissue-specific biomarkers with the expression of circRNAs in forensically relevant body fluids. International Journal of Legal Medicine. 2019 2019/09/01;133(5):1321-31.

20. Albani PP, Fleming R. Novel messenger RNAs for body fluid identification. Science & Justice. 2018 2018/03/01/;58(2):145-52.

21. Richard ML, Harper KF, Craig RF, Onorato AF, Robertson JF, Donfack J. Evaluation of mRNA marker specificity for the identification of five human body fluids by capillary electrophoresis. Forensic Science International: Genetics. 2012 20120522 DCOM- 20120925;6(4):452-60.

22. Roeder AD, Haas C. mRNA profiling using a minimum of five mRNA markers per body fluid and a novel scoring method for body fluid identification. International Journal of Legal Medicine. 2013 2013/07/01;127(4):707-21.

23. Li Z, Bai P, Peng D, Long B, Zhang L, Liang W. Influences of different RT-qPCR methods on forensic body fluid identification by microRNA. Forensic Science International: Genetics Supplement Series. 2015;5:e295-e7.

24. Sauer E, Reinke A-K, Courts C. Differentiation of five body fluids from forensic samples by expression analysis of four microRNAs using quantitative PCR. Forensic Science International: Genetics. 2016;22:89-99.

25. Wang Z, Zhao X, Hou Y. Exploring of microRNA markers for semen stains using massively parallel sequencing. Forensic Science International: Genetics Supplement Series. 2017 2017/12/01/;6:e107-e9.

26. Hanson E, Ingold S, Haas C, Ballantyne J. Messenger RNA biomarker signatures for forensic body fluid identification revealed by targeted RNA sequencing. Forensic Science International: Genetics. 2018 2018/05/01/;34:206-21.

27. Satoh T, Kouroki S, Ogawa K, Tanaka Y, Matsumura K, Iwase S. Development of mRNA-based body fluid identification using reverse transcription loop-mediated isothermal amplification. Analytical and Bioanalytical Chemistry. [journal article]. 2018 July 01;410(18):4371-8.

28. Jackson KR, Layne T, Dent DA, Tsuei A, Li J, Haverstick DM, et al. A novel loop-mediated isothermal amplification method for identification of four body fluids with smartphone detection. Forensic Science International: Genetics. 2020 2020/03/01/;45:102195.

29. Wang Z, Zhou D, Cao Y, Hu Z, Zhang S, Bian Y, et al. Characterization of microRNA expression profiles in blood and saliva using the Ion Personal Genome Machine System (Ion PGM System). Forensic Science International: Genetics. 2016;20:140-6.

30. Dørum G, Ingold S, Hanson E, Ballantyne J, Russo G, Aluri S, et al. Predicting the origin of stains from whole miRNome massively parallel sequencing data. Forensic Science International: Genetics. 2019;40:131-9.

31. Whitesides GM. The origins and the future of microfluidics. Nature. 2006 2006/07/01;442(7101):368-73.

32. Thompson BL, Ouyang Y, Duarte GRM, Carrilho E, Krauss ST, Landers JP. Inexpensive, rapid prototyping of microfluidic devices using overhead transparencies and a laser print, cut and laminate fabrication method. Nature Protocols. 2015 2015/06/01;10(6):875-86.

33. Qin P, Park M, Alfson KJ, Tamhankar M, Carrion R, Patterson JL, et al. Rapid and Fully Microfluidic Ebola Virus Detection with CRISPR-Cas13a. ACS Sensors. 2019 2019/04/26;4(4):1048-54.

34. Fan J-B, Luo J, Luo Z, Song Y, Wang Z, Meng J, et al. Bioinspired Microfluidic Device by Integrating a Porous Membrane and Heterostructured Nanoporous Particles for Biomolecule Cleaning. ACS Nano. 2019 2019/07/23;13(7):8374-81.

35. DuVall JA, Le Roux D, Thompson BL, Birch C, Nelson DA, Li J, et al. Rapid multiplex DNA amplification on an inexpensive microdevice for human identification via short tandem repeat analysis. Analytica Chimica Acta. 2017 2017/08/08/;980:41-9.

36. Clark CP, Xu K, Scott O, Hickey J, Tsuei A-C, Jackson K, et al. Acoustic trapping of sperm cells from mock sexual assault samples. Forensic Science International: Genetics. 2019 2019/07/01/;41:42-9.

37. Mou L, Jiang X. Materials for Microfluidic Immunoassays: A Review. Advanced Healthcare Materials. [https://doi.org/10.1002/adhm.201601403]. 2017 2017/08/01;6(15):1601403.

38. Jackson KR, Borba JC, Meija M, Mills DL, Haverstick DM, Olson KE, et al. DNA purification using dynamic solid-phase extraction on a rotationally-driven polyethylene-terephthalate microdevice. Analytica Chimica Acta. 2016 2016/09/21/;937:1-10.

39. Krauss ST, Remcho TP, Lipes SM, Aranda R, Maynard HP, Shukla N, et al. Objective Method for Presumptive Field-Testing of Illicit Drug Possession Using Centrifugal Microdevices and Smartphone Analysis. Analytical Chemistry. 2016 2016/09/06;88(17):8689-97.

40. Lin M-H, Albani PP, Fleming R. Degraded RNA transcript stable regions (StaRs) as targets for enhanced forensic RNA body fluid identification. Forensic Science International: Genetics. 2016;20:61-70.

41. Haas C, Hanson E, Ballantyne J. Capillary Electrophoresis of a Multiplex Reverse Transcription-Polymerase Chain Reaction to Target Messenger RNA Markers for Body Fluid Identification. In: Alonso A, editor. DNA Electrophoresis Protocols for Forensic Genetics. Totowa, NJ: Humana Press; 2012;169-83.

42. Thompson BL, Birch C, Nelson DA, Li J, DuVall JA, Le Roux D, et al. A centrifugal microfluidic device with integrated gold leaf electrodes for the electrophoretic separation of DNA. Lab on a Chip. [10.1039/C6LC00953K]. 2016;16(23):4569-80.

43. Birch C, DuVall JA, Le Roux D, Thompson BL, Tsuei A-C, Li J, et al. Rapid Fabrication of Electrophoretic Microfluidic Devices from Polyester, Adhesives and Gold Leaf. Micromachines. 2017;8(1):17.

44. Le Roux D, Root BE, Hickey JA, Scott ON, Tsuei A, Li J, et al. An integrated sample-in-answer-out microfluidic chip for rapid human identification by STR analysis. Lab on a Chip. [10.1039/C4LC00685B]. 2014;14(22):4415-25.

45. Woolf MS, Dignan LM, Lewis HM, Tomley CJ, Nauman AQ, Landers JP. Optically-controlled closable microvalves for polymeric centrifugal microfluidic devices. Lab on a Chip. [10.1039/C9LC01187K]. 2020;20(8):1426-40.

46. Cao XH, Stojkovic I, Obradovic Z. A robust data scaling algorithm to improve classification accuracies in biomedical data. BMC Bioinformatics. 2016 2016/09/09;17(1):359.

47. Butler JM. Chapter 9 - Fundamentals of DNA Separation and Detection. Fundamentals of Forensic DNA Typing. San Diego: Academic Press; 2010;175-203.

48. Burch AM, Durose MR, Walsh KA, Tiry E. Publicly Funded Forensic Crime Laboratories: Resources And Services, 2014. Bureau of Justice Statistics: US Department of Justice; 2016 Contract No.: Document Number|.

49. Woolf MS, Dignan LM, Scott AT, Landers JP. Digital postprocessing and image segmentation for objective analysis of colorimetric reactions. Nature Protocols. 2020 2020/12/09.

50. Farrar JS, Wittwer CT. Extreme PCR: Efficient and Specific DNA Amplification in 15–60 Seconds. Clinical Chemistry. 2015 2015-01-01;61(1):145-53.

51. Wittwer C. Rapid Cycle Real-Time PCR: Methods and Applications. In: Meuer S, Wittwer C, Nakagawara K-I, editors. Rapid Cycle Real-Time PCR: Methods and Applications. Berlin, Heidelberg: Springer Berlin Heidelberg; 2001;1-8.

52. Kopp MU, Mello AJd, Manz A. Chemical Amplification: Continuous-Flow PCR on a Chip. Science. 1998;280(5366):1046.

Chapter 5: Microfluidic RT-PCR methods for liver immune response and SARS-CoV-2 targets

5.1 Introduction

Microfluidic alternatives for detection and analysis are attractive for clinical applications for several notable reasons. Critically, the microscale regime minimizes manual intervention, decreases reagent and sample volume requirements, and reduces the time necessary to perform chemical reactions. (1) Another major benefit of using microfluidic technology is the ease with which such devices can be adapted for a wide array of applications with an integrated system. In particular, rotationally driven microfluidic platforms enable fluid flow without the need for bulky external hardware. This permits all fluidic handling steps to be automated within a fully enclosed system, significantly minimizing analyst exposure and potential sample contamination. (2) The preliminary experiments for two clinical applications geared towards reducing the overall assay time, while maintaining the sensitive detection of mRNA targets, are described here.

The first clinical application investigated was the rapid detection of the novel beta Coronavirus Severe Acute Respiratory Syndrome Coronavirus-2 (SARS-CoV-2), the virus at the root of the world-wide pandemic of 2020. First identified in December 2019 in Wuhan, China, the virus spread quickly, causing a global pandemic. (3, 4) As of May 2021, the coronavirus disease 2019 (COVID-19) pandemic has affected over 164 million people and caused more than 3.39 million deaths. (5) Diagnostic testing for SARS-CoV-2 has primarily focused on symptomatic individuals. These tests are performed using samples collected from nasopharyngeal swabs , as

per the Centers for Disease Control and Prevention (CDC) recommendations. (6-9) After sample collection, virions must be lysed, and viral mRNA purified before performance of reverse transcriptase quantitative polymerase chain reaction (RT-qPCR). However, there are shortcomings with RT-qPCR (e.g., amplify one target per reaction, long assay times) that emerging technology can improve. Several alternative detection methods for detection have emerged in recent months to 1) address the increased demand for diagnostic laboratory testing, 2) include surveillance of asymptomatic persons, and 3) to accommodate specific clinical community needs. (10, 11) In addition to diversifying available testing methodologies, it is important that all novel approaches for coronavirus clinical testing remain inexpensive, expedient, and require minimal training to implement. Since the emergence of the pandemic in late December of 2019, only a handful of centrifugal microfluidic platforms have been developed for SARS-CoV-2 nucleic acid-based testing; of these, many either employ isothermal techniques with limited sensitivity (12) or use cost-prohibitive injection-molded discs for fluidic handling. (13)

The second clinical application involved amplification of immunoregulatory biomarkers to identify whether a transplanted organ, e.g., liver, was being 'tolerated' or rejected by the host. Organ transplants are an annual necessity in hospitals worldwide. (14) Specifically, liver transplants are the second most commonly transplanted organ in the US, with nearly 6,000 such surgeries performed annually. (14) In the months immediately following the transplant, weekly patient testing is required to monitor the organ's functionality. Pending satisfactory results, the testing frequency is then reduced to once per month. While these tests are necessary to monitor and prevent organ rejection, the required time commitment and cost of testing are burdensome

to the transplant patient. Currently, the 5-year survival rate of liver transplantation is 68%, and the patients must follow an immunosuppressive drug regimen for the remainder of their lives. (15) While these medications vitally prevent graft rejection by weakening the immune response, their side effects include increased susceptibility to infections, sepsis, cancer, and renal failure. (16) Research efforts from the University of Toronto have compiled a panel of immunoregulatory genes whose relative expression levels indicate allograft tolerance or rejection. (17) Following this finding, the Liver Immune Tolerance Marker Utilization Study (LITMUS) was established, in which patients are weaned off of their antirejection regimen based on his previously studied patterns of immunoregulatory biomarker expression in peripheral blood mononuclear cells (PBMCs). Successful withdrawal from immunosuppressive medications alleviates the side effects commonly experienced by patients. The LITMUS research currently shows promising results in clinical trials. (18)

In the following sections, a rotationally driven polymeric microdevice, and corresponding integrated device, is described for rapid nucleic acid amplification of mRNA targets that were adapted for two separate clinical applications. In both applications, the device was constructed using inexpensive polymeric materials according to the print-cut-laminate (PCL) method (19). On-disc RT-PCR was enabled with a corresponding mechatronic system for rapid, accurate thermal cycling. (20) This method for rapid amplification is characterized with the intention of integration with other microfluidic detection methods (e.g., fluorescence, colorimetric, size separation).

5.2 Methods & Materials

5.2.1 Sample collection for SARS-CoV-2 detection

Standard of care testing was performed according to the manufacturer's protocol with one of the three available methods with emergency use authorization (EUA) from the FDA. These methods are the Abbott Alinity-m SARS-CoV-2 assay, the Abbott M2000 Real-Time SARS-CoV-2 Assay, and the Xpert Xpress SARS-CoV-2 Assay. Previously tested and refrigerated clinical samples in viral transport medium (VTM) were de-identified according to the IRB-approved protocol and assigned a study sample number. Each sample was vortexed for 10 sec, and a 1 mL aliquot was removed and placed in a labeled 2 mL microcentrifuge tube. Aliquoted patient samples were inactivated by heat treatment for 30 mins at 65 °C and stored at -20 °C until further analysis.

5.2.2 Cell lysis and RNA purification

Patient samples were previously analysed for diagnostic purposes by real-time RT-PCR in the clinical laboratory at the University of Virginia Health System. Any sample received with an assigned C_T value was considered clinically positive. Clinical C_T values were also used to infer comparative viral titres.

Sample extractions included a pre-concentration step in which 25 µL of Nanotrap Magnetic Virus Particles (CERES Nanosciences, Inc. Manassas, VA, USA) were mixed with 250 µL of the heat-inactivated patient sample to capture viral particles. Following a brief incubation, the nanoparticles were magnetically separated, and the supernatant removed. Nanotrap particles were resuspended in an RNAGEM (MicroGEM Int., Charlottesville, VA, USA) cocktail comprised

of 44 µL water, 5 µL BLUE buffer, and 1 µL RNAGEM enzyme solution to lyse the viral coat and release the viral RNA. Following incubation for 10 min at 75 °C then 5 min at 95 °C in a thermal cycler, the nanoparticles were again separated magnetically, and the supernatant was collected and retained. The RNA extracts were stored at -80 °C until analysis.

5.2.3 Primer and probe information

The CDC developed an assay for SARS-CoV-2 detection under an EUA in February 2020. (21) The N1 gene was targeted for RT-PCR in-tube and on-chip analysis (**Table 1**).

Table 1: Primer and Probe sequences for the CDC's SARS-CoV-2 mRNA assay. FAM = Fluorescein and BHQ1 = Black Hole Quencher®-1 dye oligonucleotide modification.

mRNA Target: N1 gene	Sequence
Forward Primer	5'-GACCCCAAAATCAGCGAAAT-3'
Reverse Primer	5'-TCTGGTTACTGCCAGTTGAATCTG-3'
Probe	5'- FAM-ACCCCGCATTACGTTTGGTGGACC-BHQ1-3'

Beckman Coulter commercialized the GenomeLab™ GeXP Human Reference*Plex* kit, (22, 23) which was used for optimizing the LITMUS RT-PCR protocol (Sykesville, MD, USA). The kit contains 25 mRNA targets between 150 – 350 bp in length tagged with fluorescent D4. The Kanamycin resistance (Kan^R) target was used as the normalizing target.

5.2.4 RT-PCR method

The CDC 2019-nCoV Real-Time RT-PCR Diagnostic Panel was used for amplification. C_T values obtained via real-time RT-PCR were used for relative quantification of SARS-CoV-2 mRNA. (24) Each 20 µL reaction was composed of 5 µL TaqPath™ 1-Step RT-qPCR Master Mix (Thermo

Fisher Scientific, Waltham, MA, USA), 1.5 µL SARS-CoV-2 (2019-nCoV) CDC RUO N1 primer-probe mix (Integrated DNA Technologies, Coralville, IA, USA), 8.5 µL PCR-grade water (Molecular Biologicals International, Inc.), and 5 µL of extracted viral RNA. The 2019-nCoV_N_Positive Control plasmid (Integrated DNA Technologies) was used for positive controls. Samples were run in duplicate on either a MyGo Pro real-time PCR instrument (IT-IS Life Science Ltd., Dublin, Ireland) or a 7500 Fast Real-Time PCR system (Applied Biosystems, Foster City, California, USA) with detection in the FAM channel. The most rapid assay conditions were: 1) reverse transcription at 50 °C for 60 sec, 95 °C step for 180 sec followed by 2) amplification of cDNA for 40 cycles of denaturation and annealing (95 °C for 3 sec and 60 °C for 30 sec). The ramp rates were +5 °C/sec and -4 °C/sec, respectively for both the MyGo Pro and 7500 Fast instruments. Successful detection was defined as any sample which met the fluorescence cut-off threshold prior to a $C_T = 40$, as described for the CDC RUO kit.

The Human Reference*Plex* RT-PCR kit is a 20 µL reaction for RT and PCR individually. For RT, the reaction contained 4 µL RT Buffer 5X, 2 µL RT Reverse Primer Plex, 1 µL Reverse Transcriptase, 5 µL pre-diluted Kan^R RNA (1:50 dilution with 10 mM Tris-HCl, pH 8), 3 µL of DNase/RNase free water, and 5 µL Sample RNA at 5-20 ng/µL. The positive control was a Control RNA Template at 100 ng/µL from the Human Reference*Plex* kit. The RT reaction was performed on a Veriti thermal cycler at 48 °C for 1 min, 42 °C for 60 min, 95 °C for 5 min, and held at 4 °C until amplification. For PCR, the reaction contained 4 µL PCR Buffer 5X, 4 µL of 25 mM $MgCl_2$, 2 µL PCR Forward Primer Plex, 0.7 µL of Thermo-Start DNA Polymerase, and 9.3 µL of cDNA samples. The PCR reaction was performed on a Veriti thermal cycler at 95 °C for 15 min, 35 cycles

of 94 °C for 30 sec, 55 °C for 30 sec, 70 °C for 1 min, and held at 4 °C until electrophoretic separation.

5.2.5 Capillary electrophoresis

The Human Reference*Plex* was size separated on a GenomeLab GeXP system with Fragment Analysis and GeXP Data Tool software (Beckman Coulter). The reactions consisted of 1 µL of the amplified sample, 0.5 µL DNA Size Standard-400, and 38.5 µL Sample Loading Solution in a 96-well plate. One drop of mineral oil was added to the top of each well.

5.2.6 Microchip fabrication

Centrifugally driven microfluidic devices for real-time RT-PCR were fabricated according to the print-cut-laminate (PCL) method. (19) The architecture was designed using AutoCAD 2019 software (Autodesk, Inc., Mill Valley, CA, USA), then ablated into five polyethylene terephthalate (PeT) layers (Film Source, Inc. Maryland Heights, MO, USA) using a CO_2 laser (VLS3.50, Universal® Laser Systems, Scottsdale, AZ, USA). The fluidic layers (2 and 4) were coated on both sides with a heat-sensitive adhesive (EL-7970-39, Adhesives Research, Inc. Glen Rock, PA, USA). (25) An intervening layer of black PeT (Lumirror* X30, Toray Industries, Inc., Chhuo-ku Tokyo, Japan) prevented flow between discrete fluidic layers before laser valving. (26) All five layers were washed in two 10-min cycles of deionized water and dried in a chemical hood overnight. The layers were bonded together using an office laminator (UltraLAM 250B, Akiles Products, Inc. Mira Loma, CA, USA). A laser-ablated polymethyl methacrylate (PMMA) component was adhered to the device surface using pressure-sensitive adhesive (ARcare 7876, Adhesives Research, Inc.). A 20 µL RT-PCR reaction was pipetted into a loading chamber, which flowed into the PCR chamber.

The associated instrumentation for fluidic and temperature control has been described in detail in Chapter 4 (**Fig. 1**). The integrated system has two Peltier clamps for heating and a red laser for valve control. The Peltier heaters were found to have a ramp rate of ~8-9 °C/sec, whereas most conventional thermal cyclers have ramp rates of ~5 °C/sec or less. Off-disc electrophoretic detection was achieved using a DNA microchip in the Bioanalyzer 2100 (Agilent Technologies, Santa Clara, CA, USA).

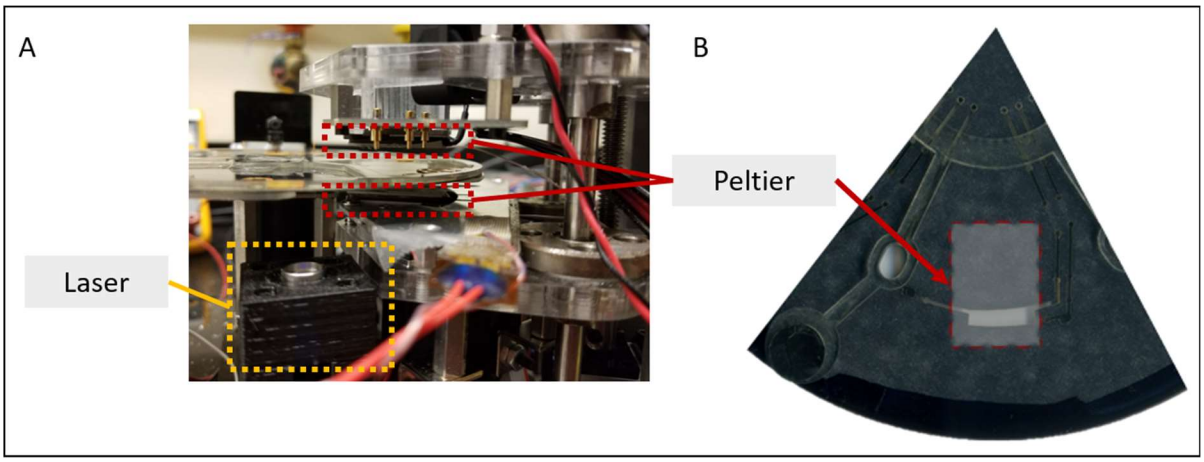

Figure 1: Hardware diagram for PCR on a microfluidic disc. (A) System with laser and dual Peltier heaters. (B) Placement of PCR chamber sandwiched between Peltier heaters.

5.3 Results & Discussion

Microfluidic technology has many advantages for advancing current biochemical assays and has shown reduced cost, footprint, overall assay time, and portability. The results below detail initial experimental findings for two clinical assays on a microfluidic disc for one-step RT-PCR heat cycling. For the SARS-CoV-2 project, amplification of a plasmid and clinical samples were detected after reducing the overall assay time. For the LITMUS project, the inclusion of closable valves on the disc and reduction of steps in the protocol show good prospects for a portable device to assess gene expression of mRNA targets.

5.3.1 Optimization of Peltier heating for the integrated system

The protocol for the CDC SARS-CoV-2 assay was adapted to a microfluidic platform to decrease the overall assay time while maintaining the specificity and sensitivity of the in-tube reaction (**Fig. 2**). All of these conditions were tested using the RNA plasmid control in a microfluidic disc. First, PCR reactions were prepared in-tube and pipetted into the PCR chamber. The microfluidic disc was then spun to align the red laser underneath the laser valve on the disc. After the laser valve was opened, the reaction mix moves from the top fluidic layer to the bottom fluidic layer via centrifugation, filling the PCR chamber. Finally, the Peltier heaters on the integrated system moved vertically to sandwich the chamber in the disc.

Due to the micro scale of the chamber (~450 µm depth), it was initially thought that one Peltier heater (either above or below) would suffice to produce the correct in-chamber

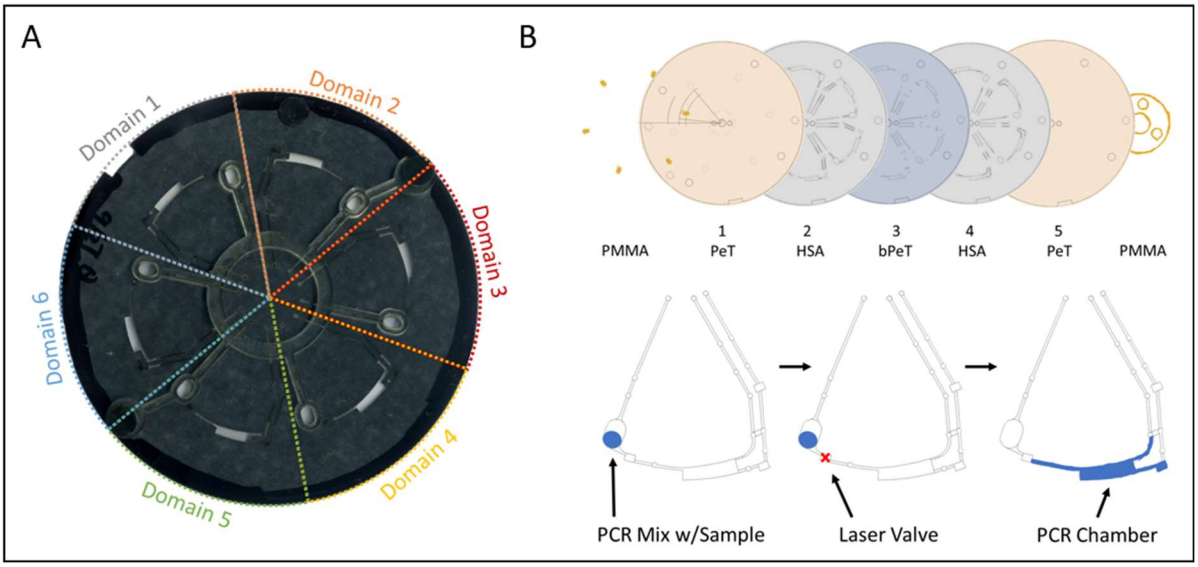

Figure 2: Microfluidic disc and architecture. The microfluidic disc contained 6 domains / disc and was fabricated using 5 alternating layers of plastics and adhesives via the Print-Cut-Laminate method. To the top of the disc, PMMA with PSA pieces are adhered for pipetting in the PCR reaction. To the bottom of the disc, PMMA with PSA is adhered to the center of the disc as an adapter for the integrated system.

temperature. This presumption was evaluated by inserting thermocouples both within the chamber and outside the disc (**Fig. 3A**). The thermocouples were taped either to the top or bottom Peltier heater as well as to the inner and outer surfaces of the PCR chamber. The temperature was recorded every 5 sec over the course of 1 min. According to the temperature profiles, a much higher temperature gradient through the depth of the PCR chamber was observed when using a single Peltier heater. The temperature gradient would change depending on ambient temperature changes and create variable results during amplification due to the

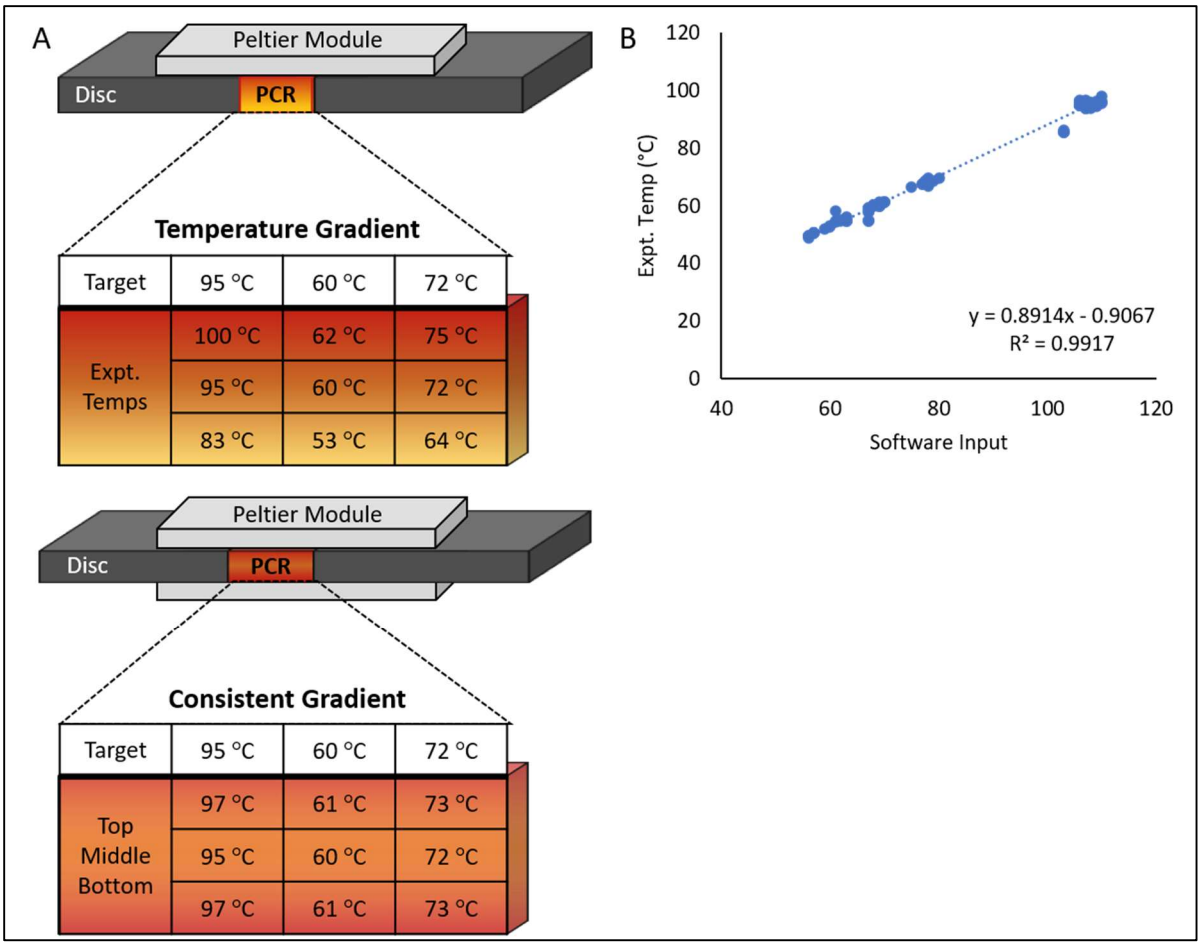

Figure 3: Microfluidic temperature optimization. (A) The in-chamber temperature was assessed with 1 and 2 Peltier heaters. Using a Peltier heater above and below the PCR chamber, there was a minimal temperature gradient. (B) A linear relationship was demonstrated between the software inputs and in-chamber temperatures.

temperature gradient. As such, the initial assertion that a single Peltier heater would suffice was disproven, and two Peltier heaters were evaluated next to determine whether they would provide a consistent temperature throughout the PCR chamber.

As shown in **Fig. 3A**, the temperature gradient when employing two Peltier heaters was within 1 - 2 degrees Celsius of the intended temperature, as compared to a 2 – 8 degrees Celsius range observed using a single Peltier heater. This finding confirms that the chambers of a microdevice should be heated bilaterally for optimal results. The precise software input temperature needed to achieve the temperatures in-chamber was also determined via this process (**Fig. 3B**). A linear correlation between the increase in software input and in-chamber temperature was observed ($R^2 = 0.9917$). This high degree of correlation is significant as it ensures that any future temperature assessments can be accurately extrapolated and tested with the integrated system and microfluidic disc.

In addition to temperature accuracy, the timing of each step in the PCR protocols was reduced to determine how rapidly the integrated system could change temperature while achieving the correct temperature. The Peltier heaters were able to maintain the correct temperatures for a minimum of three seconds per step. Any further decrease in step time was shown to disrupt this stability. The initial enzyme activation step was decreased from 3 min to 1 min, thereby reducing the total time by 2 mins. The denature step in the cycles were kept at 3 sec (**Fig. 4A**). This step facilitated the achievement of the target temperature with a shorter hold time but was less sustainable over 40 cycles. Although the denaturation cycling step could be decreased to 1 sec, the reactions were tested at 3 sec to allow for sufficient denaturing of the

amplicons. The annealing step was varied the most to achieve the fastest PCR while consistently amplifying the target; this was decreased from 30 sec to 3 sec, thereby reducing the fastest total amplification time from 34 mins to approximately 11 mins (**Fig. 4B**).

The denature and annealing steps were also tested at 1 sec for accurate temperatures. However, the integrated system was unable to accommodate the speed of the temperature change required for cycling. The later cycles did not reach the required temperature when this speed was employed, and consequently, 3 sec was the minimum time used for any step in PCR cycling.

A

System	Initial		40 cycles				Total Time
7500 Fast	95 °C	180 s	95 °C	3 s	60 °C	30 s	~75 mins
MyGo Pro	95 °C	180 s	95 °C	3 s	60 °C	30 s	~60 mins
On-Chip	95 °C	180 s	95 °C	3 s	60 °C	30 s	~34 mins
On-Chip	95 °C	180 s	95 °C	3 s	60 °C	**15 s**	~24 mins
On-Chip	95 °C	**60 s**	95 °C	3 s	60 °C	30 s	~32 mins
On-Chip	95 °C	60 s	95 °C	3 s	60 °C	**15 s**	~19 mins
On-Chip	95 °C	60 s	95 °C	3 s	60 °C	**7 s**	~14 mins
On-Chip (Fastest time)	95 °C	60 s	95 °C	3 s	60 °C	**3 s**	~11 mins

B

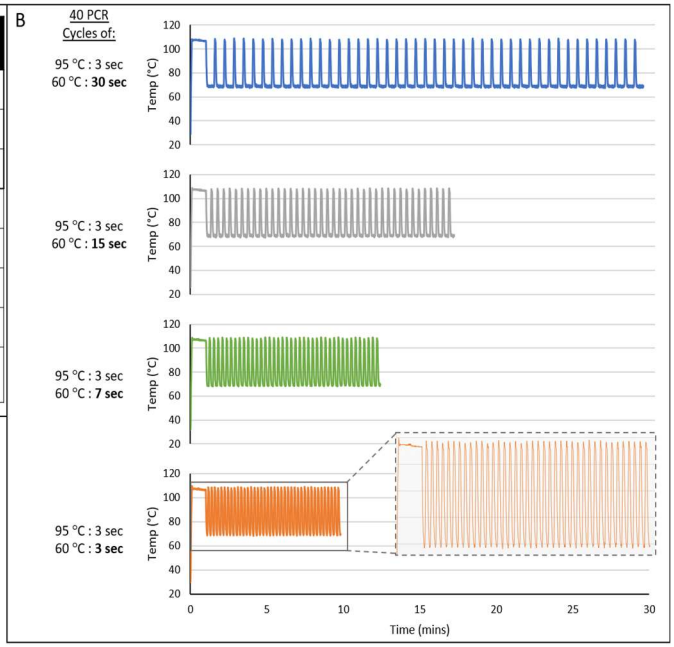

Figure 4: Microfluidic time optimization. (A) Total time comparison between amplification instruments. (B) The integrated system was tested with decreasing times to determine the fastest time for each step in a cycle.

5.3.2 On-disc detection of SARS-CoV-2

5.3.2.1 Comparison to conventional methods

Conventional methods were used as a baseline comparison for the overall time of the assay while optimizing the integrated system for rapid PCR. Samples were amplified using the fastest times with fluorescence monitoring at every cycle using the ABI 7500 Fast Real-Time PCR system by using the maximum ramp rate and smallest times at each step. (**Fig. 5A**). The total amplification time was ~40-45 min using 3 and 30 sec cycles for denaturing and annealing, respectively. The instrument has a fixed minimum time of 30 sec for any step where fluorescent data is collected. The annealing step could be held for a minimum of 5 sec if an end-point assay were used, that is, there was no stepwise data collection. The use of an end-point essay, which is how the microfluidic disc was tested, reduced the total runtime to ~25-28 min.

A MyGo Pro Real-Time PCR system was also used to evaluate overall amplification time (**Fig. 5B**). The amplification was completed by the MyGo Pro in ~37-42 min using the same protocol. However, this included detection at every cycle's annealing step. This instrument has a fixed minimum time of 20 sec for any step where fluorescence data is collected. This restriction could be circumvented by conducting an end-point assay, whereby the minimum time required was reduced to 5 sec and an overall PCR assay time of ~20–25 min was achieved.

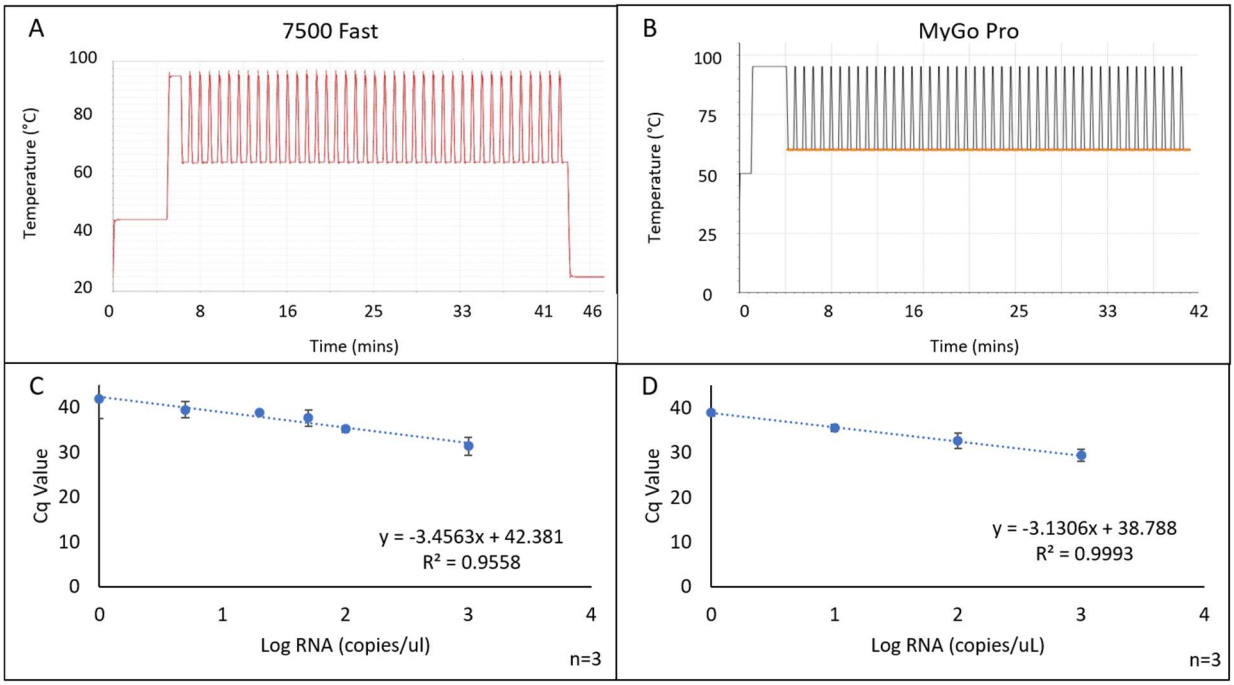

Figure 5: Assessment of conventional methods. (A) Total time to run 40 cycles on the ABI 7500 Fast system was ~40-45 minutes with detection at every cycle. (B) Total time to run 40 cycles on the MyGo Pro system was ~37-42 minutes with detection at every cycles. (C-D) Standard curve using dilutions of the plasmid on both the 7500 and MyGo Pro systems.

The two conventional systems were further tested with an RNA plasmid dilution to evaluate the amplification performance (**Fig. 5C & 5D**). The data obtained from these systems were used to deduce the overall runtime to be targeted or improved upon when adapting the amplification protocol for on-chip amplification. The data also indicated the minimum plasmid concentration that could be detected with rapid amplification. When compared to conventional methods, the microfluidic device held promise for reducing the overall PCR assay time due to the faster ramp rate of the Peltier heater and ability to reduce steps in PCR cycling to <5 sec. Ultimately, if the assay proved sufficiently sensitive, the adaptation to the microfluidic platform would provide 'sample-to-answer' results in a greatly reduced timeframe for point-of-need applications.

5.3.2.2 Time optimization of on-disc PCR protocol

One of the main goals for this project was to reduce the overall PCR assay time by reducing the time for each step in the protocol. The CDC's plasmid provided in the SARS-CoV-2 kit was used as a positive control for optimizing the PCR protocol on-disc. Optimization was completed by sequentially reducing each step within the protocol, followed by electrophoretic analysis via the Agilent 2100 Bioanalyzer. The electropherograms generated by the Bioanalyzer can be displayed as a software-generated "gel-like" image. The optimization data are shown according to both depictions.

The initial 95 °C step was compared at 180 and 60 sec (**Fig. 6**). In this step, the reverse transcriptase is inactivated while the DNA polymerase is activated (27). Antibodies inhibit the enzyme activity of the DNA polymerase until the first 95 °C step, preventing non-specific

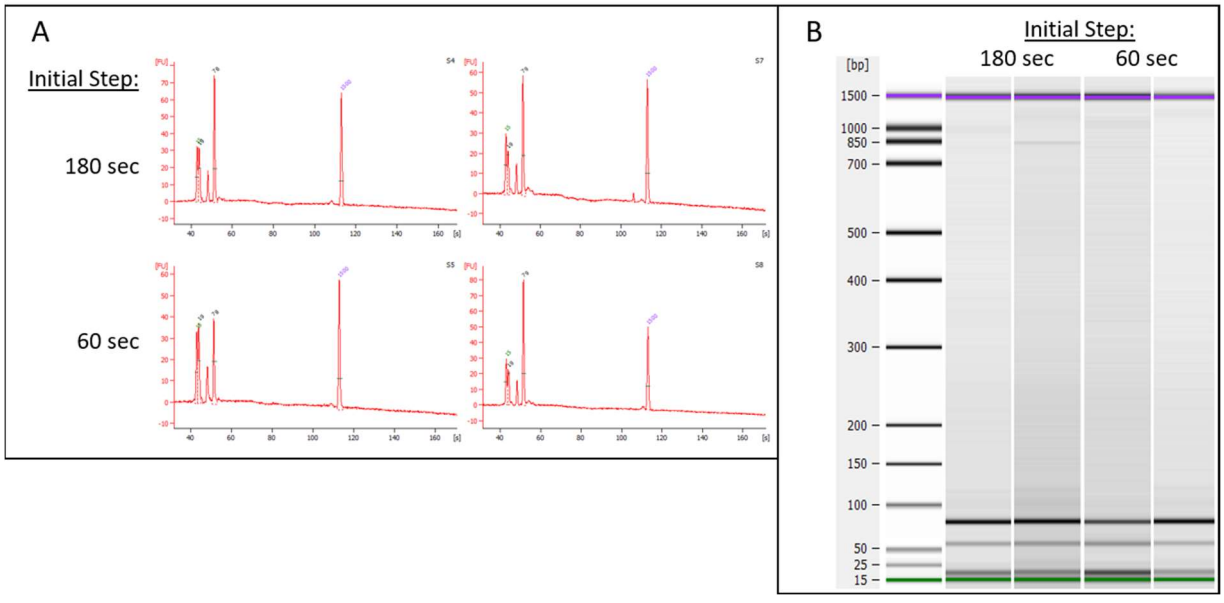

Figure 6: Decreasing initial time in the PCR protocol. The denature and anneal steps were kept constant at 3 sec and 30 sec, respectively. (A) Using a plasmid at 10,000 copies/µL, the initial time was decreased from 180 to 60 sec and size separated on the Bioanalyzer. The fastest time was ~32 mins on-disc. (B) The Bioanalyzer transforms the electropherograms into gel-like images. The peak of interest is ~79 base pairs in length.

amplification and primer degradation. Theoretically, the reduction in time of the initial 95 °C step should provide less activated polymerase to amplify the mRNA target. However, it was found that both 180 and 60 sec hold times had peak heights of similar magnitude from the amplicons for the mRNA target. The initial step was thus set at 60 sec for future experiments.

This PCR protocol is a 2-step cycling method for: (1) denaturing the DNA strands which allows for (2) annealing of the primers with their complementary sequences. This is followed by elongation of the target amplicon by the DNA polymerase. The initial denaturation step was kept at 95 °C for 3 sec, primarily due to the limitations of the integrated system. However, the annealing step was assessed at 60 °C with various hold times between 30 and 3 sec (**Fig. 7**). As expected, the peak heights for the mRNA target decreased as the hold time decreased, which means the number of amplicons produced decreased as the hold time decreased. However, all of the time reductions enabled detection of the amplicons for the mRNA target. The fastest annealing hold time gave an overall amplification time of ~11 mins, 4X faster than the conventional methods. While the 3 sec hold temperature produced results with 10,000 copies/µL

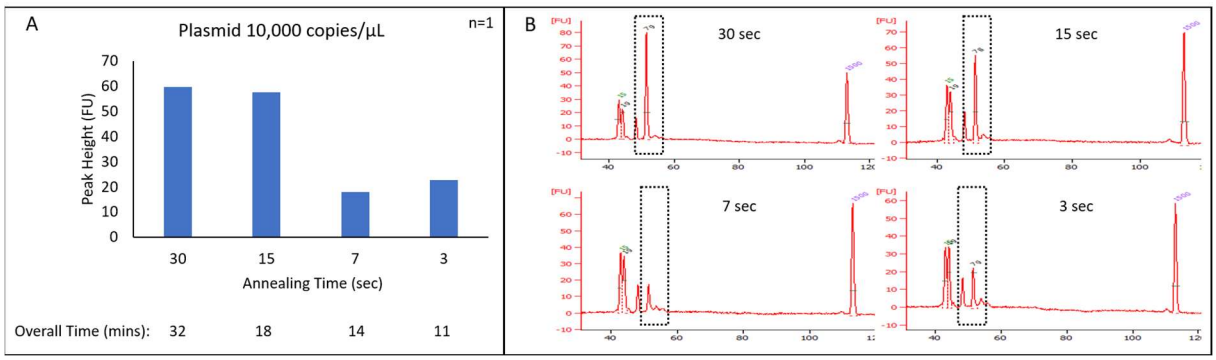

Figure 7: Decreasing annealing time in the PCR protocol. The initial and denature steps were kept constant at 60 sec and 3 sec, respectively. (A) Using a plasmid, the annealing time was varied from 30 to 3 sec and size separated on the Bioanalyzer. The fastest time was ~11 mins on-disc. (B) Electropherogram results from decreasing the annealing time with 40 cycles via the Bioanalyzer.

of the input plasmid, future experiments were conducted with a 15 sec anneal hold time. This was due to the significant decrease in peak height of the mRNA target with an annealing step less than 15 sec, and the purpose of this project was to have a protocol that is as sensitive as conventional methods while reducing the overall time. The 15 sec anneal hold time is faster than the fixed minimum time on the conventional methods, thus the overall PCR assay time was reduced from ~45 min to ~18 min using the microfluidic platform.

In order to investigate if the shortened initial or annealing steps provided adequate time for the denaturation and annealing processes, the CDC plasmid was serially diluted (from 10,000-10 copies/µL) and amplified on-disc. The protocols employing 30 and 15 sec annealing steps were used for these experiments and resulted in overall assay times of 32 and 18 min, respectively. The peak heights for the mRNA target amplicon and the gel-like image after amplification are shown in **Fig. 8**. 1,000 and 100 copies/µL of plasmid were detected at both time points by the Bioanalyzer. However, the sample comprising 10 copies/µL of plasmid was only detected with the 15 sec annealing step. The absence of the mRNA

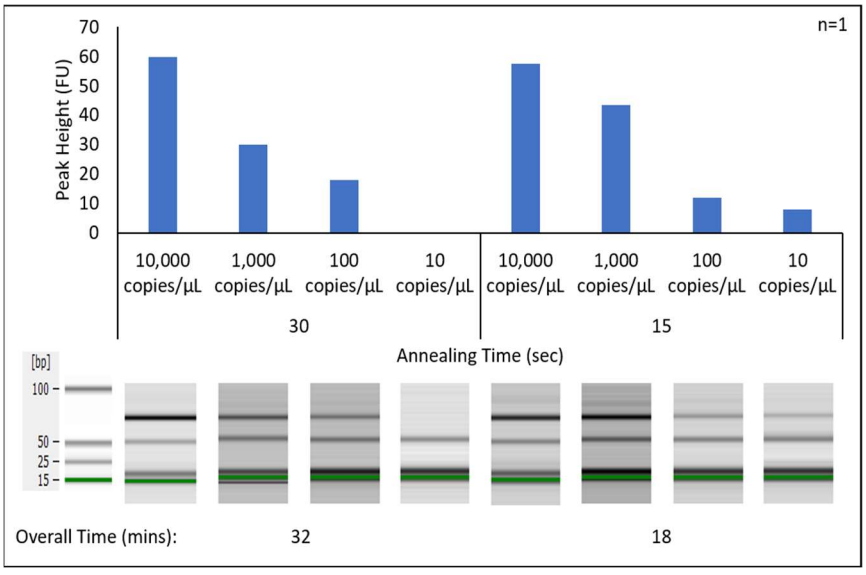

Figure 8: Decreasing plasmid concentration with fast PCR protocols. The PCR protocol used was an initial step of 60 sec, with cycles of denaturing for 3 sec and annealing for 30 or 15 sec. The size of the amplified fragment was detected via Bioanalyzer, shown in the gel-like images.

target with the 30 sec annealing time was likely due to user error (e.g., pipetting error), rather than poor assay performance. In contrast to traditional methods, the attempted amplification of <100 copies/µL on-disc were unsuccessful. Still, this method could potentially enable the acquisition of results on a much faster time scale and with cost-efficient materials.

5.3.2.3 Evaluation of clinical samples

Finally, rapid amplification in authentic SARS-CoV-2 nasopharyngeal samples on the microfluidic device system were performed to determine diagnostic sensitivity and specificity. The results of time studies were used to infer that a reduced number of cycles could feasibly be utilized. Excluding the ramp rate of the Peltier heaters, each cycle was a total of 18 sec. Each 5-cycle reduction of the protocol resulted in an overall PCR time reduction of ~2 min.

For this set of experiments, a clinical sample previously determined to have a high quantity of the mRNA target, according to conventional qPCR, was amplified. The sample was amplified with an increasing number of cycles to determine the point at which detection occurred via microchip electrophoresis on the Bioanalyzer. To mimic a less concentrated sample, a neat nasopharyngeal sample was diluted 1:2 in nuclease-free water, and the annealing time was decreased. Results from both tests are shown in **Fig. 9**, where amplification of the mRNA target was minimally present after 25 cycles and increased in peak height up to 35 cycles. The absence of the amplified mRNA target after 40 cycles was thought to be due to user error and not poor assay performance. The diluted sample yielded low peak height only after 40 cycles. The overall time of the amplification method using the microfluidic device was 12–18 min, depending on the number of cycles. This data showed that decreasing the annealing step was not advantageous for

the on-disc protocol, and the assay may not be as sensitive as conventional methods. Theoretically, the reduction in time of the annealing step did not provide enough time for the primers to find and anneal to the complementary sequences to produce amplicons of the mRNA target.

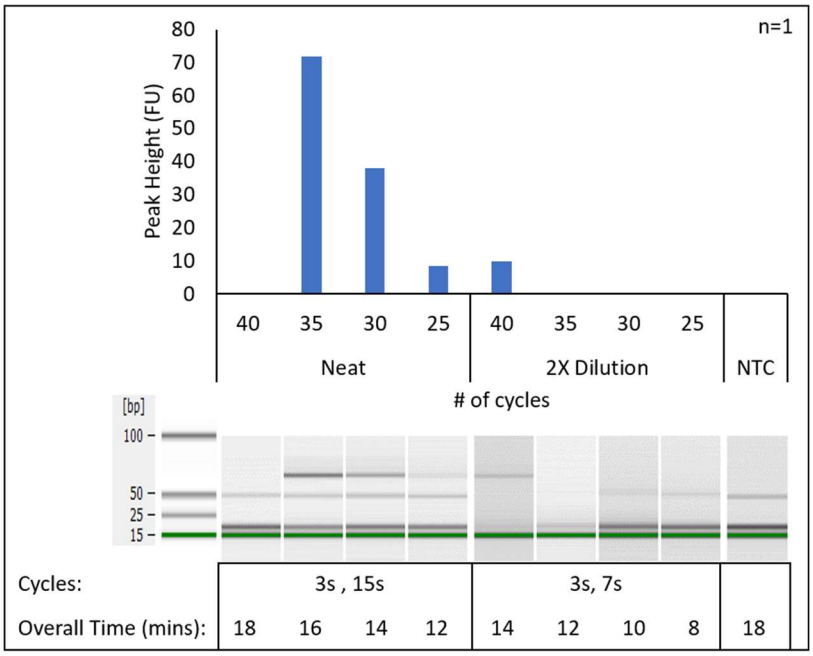

Figure 9: Clinical sample amplified on-disc with varying cycles. The PCR protocol used was an initial step of 30 sec, with cycles of denaturing for 3 sec and annealing for 15 or 7 sec. The size of the amplified fragment was detected via Bioanalyzer, shown in the gel-like images.

Three clinical samples were amplified (in triplicate) either on-disc or in-tube for a direct comparison of assay performance between the microfluidic system relative and conventional methods. Patient samples were classified as having either high, moderate, or low quantities of the mRNA target by previously performed qPCR at the UVA hospital. Plasmid at 1,000 copies/µL diluted in nuclease-free water served as the positive control. A fourth patient sample, which did not contain the SARS-CoV-2 mRNA target, and nuclease-free water, both served as negative controls. As expected, **Fig. 10** shows a decrease in peak height in correlation to the quantity of the mRNA target within the patient samples. This data also indicates that a sample considered to have low quantities of the mRNA target was detected after 40 cycles of amplification on-disc. This is significant because the nasopharyngeal samples received for testing using conventional methods

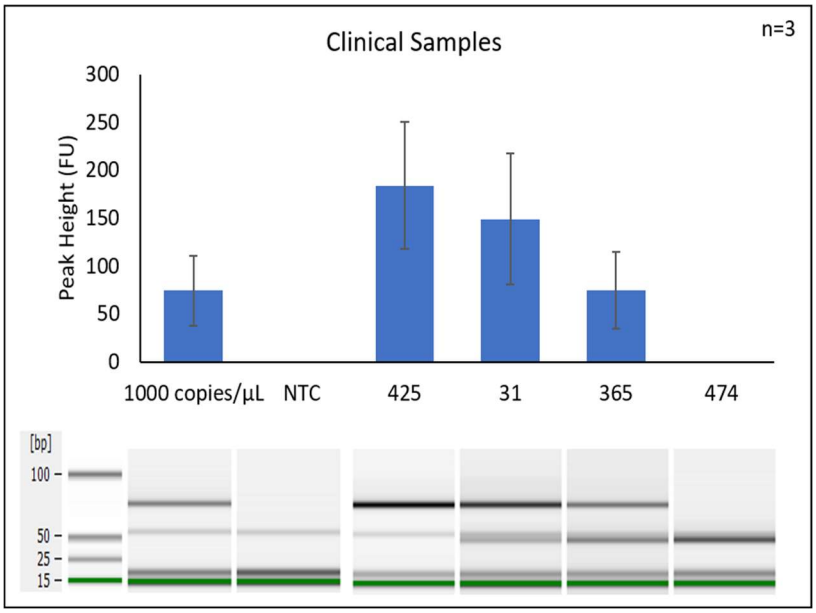

Figure 10: Clinical samples amplified by PCR on-disc. Each sample was amplified in triplicate and the controls in quadruplet. The size of the amplified fragment was detected via Bioanalyzer, shown in the gel-like images.

(qPCR) were undetected with lower quantities of the mRNA target, thus the microfluidic approach is comparable to the data from the conventional approach in less time. None of the negative control samples were observed to have amplified on-disc. This further demonstrates the comparative viability of the microfluidic disc vs. conventional methods in regard to specific amplification of the mRNA target for SARS-CoV-2.

Although the clinical and diagnostic sensitivity of the assay on-disc was found to be twofold less than conventional methods, the total assay time was reduced two to threefold and analytical and diagnostic specificity remained above 95%. Overall, this data shows promise for continuing optimization of the on-disc method to improve sensitivity with the reduced time.

5.3.3 On-disc amplification of LITMUS targets

5.3.3.1 Initial testing of disc architecture modifications

A second clinical application for RT-PCR on-disc is based on clinical trials from the University of Toronto assessing organ tolerance titled Liver Immune Tolerance Marker Utilization

Study (LITMUS). Their research entails developing a panel of mRNA targets that indicate if a patient is accepting or rejecting a transplanted liver by evaluating gene expression relative to a 'housekeeping gene'. A housekeeping gene is a gene that is found abundantly and consistently within a particular sample (e.g., 18S rRNA, β-2-microglobulin, β-actin). (28) To assess gene expression, their protocol was to use conventional instruments for in-tube RT-PCR and capillary electrophoresis. RNA is extracted from a venous blood draw and tested for the gene expression of 22 specific mRNA targets, 5 housekeeping genes, and 1 internal control. (29)

As preliminary testing for these particular targets, Sciex developed the Human Reference*Plex* containing 24 mRNA reference targets with Kan^R as the internal control, a panel similar to that resulting from University of Toronto's research (**Fig. 11A**). Since this is a two-step

A

Number	Target Gene	Size (bp)
1	Ezrin	150
2	QRSHs glutaminyl-tRNA synthetase	160
3	Histone deacetylase HD1	165
4	Transferrin Receptor	172
5	Nuclear factor NF45	186
6	MLN51	197
7	glycerol kinase	201
8	Proteasome subunit Y	211
9	Ribosomal protein L37a	214
10	18s-rRNA	220
11	E2 Ubiquitin conjugating enzyme UbcH5B	225
12	Elongation factor EF-1-alpha	233
13	cyclophilin A	237
14	Lysosomal hyaluronidase	253
15	Transcription Factor IID	258
16	beta-actin	267
17	GAPDH	277
18	ATP synthase	281
19	18kDa Alu RNA binding protein (SRP14)	291
20	Hypoxanthine ribosyl transferase	305
21	Beta 2 microglobulin	314
22	Ca2-activated neutral protease large subunit	317
23	Kanamycin resistance**	325
24	Acidic Ribosomal Protein (RPLP0)	330
25	beta-glucuronidase	338

B

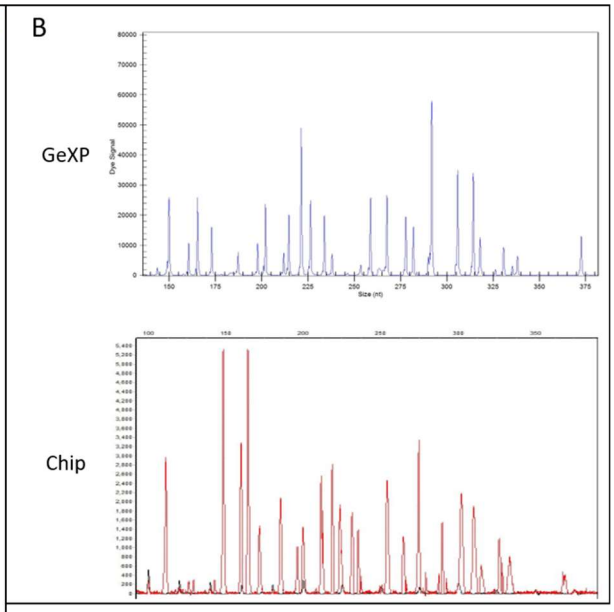

Figure 11: Human ReferencePlex successfully separated on a conventional instrument (GeXP) and micro-disc. (A) The Human ReferencePlex was separated and amplified for adaptation to microfluidic devices. (B) All 25 mRNA targets were identified via micro-disc electrophoresis.

process (RT-PCR then capillary electrophoresis), one of the main goals was to adapt both biochemical assays to microfluidic platforms and integrate the architecture to provide a disc that performs both assays in succession. Previous research conducted in our Lab detailed the size-separation of this panel using a microfluidic device with the same architecture and an integrated system mentioned in Chapter 4. Compared to separations on a gold standard capillary electrophoresis instrument (GenomeLab GeXP Genetic Analysis System), all 25 genes in this panel were detected with similar peak height ratios using the microfluidic device (**Fig. 11B**). The next phase in this project was the optimization of the RT-PCR protocol for on-disc amplification.

The in-tube RT-PCR reaction is ~2.5 hours on a conventional thermal cycler, with an initial 15 min 95 ^{o}C enzyme activation step. The high heat removes the thermolabile monoclonal antibodies that render the DNA polymerase inactive, which 'activates' the polymerase to elongate the target sequence. (30) This step is critical in the PCR reaction because it prevents the amplification of non-specific products and allows for room temperature reaction setup. However, holding at this high temperature for extended periods was problematic for the microfluidic disc integrity. The HSA which used to bind the disc layers together, softens at this temperature. Therefore, as the air between the various layers expands, slow delamination of the disc occurs and liquid from within the HSA layer or the PCR chamber begins to permeate beyond the chamber borders. In order to rectify this issue, two solutions were tested in combination: 1) a shorter initial 95 ^{o}C step was tested and 2) the PCR chamber on the microfluidic disc was sealed.

Woolf *et al.* showed that channels leading to chambers could be 'closed' on a microfluidic disc by adjusting the height of the red laser used to open valves. (31) Since the middle layer of the discs are black, increasing the distance between the red laser and the disc results in melting (as opposed to ablating) of the material next to a channel, essentially closing the channel and blocking liquid or air from passing. The disc used for this application took advantage of 'closing valves' by incorporating two into the architecture (**Fig. 12A**). The reaction was spun into a PCR chamber flanked by 'closable valves' which were then irradiated. The new architecture was used to amplify the panel between 120-40 sec for the activation step and then electrophoresed on the GeXP system. Post amplification, most of the PCR chambers (75%) were found to contain little (~5 µL of the 20 µL) to no amplified sample for electrophoresis theoretically from the long amplification time. Although the production of amplification fragments was observed (**Fig. 12B**) in cases where liquid was successfully retained after heating, low peak heights were obtained

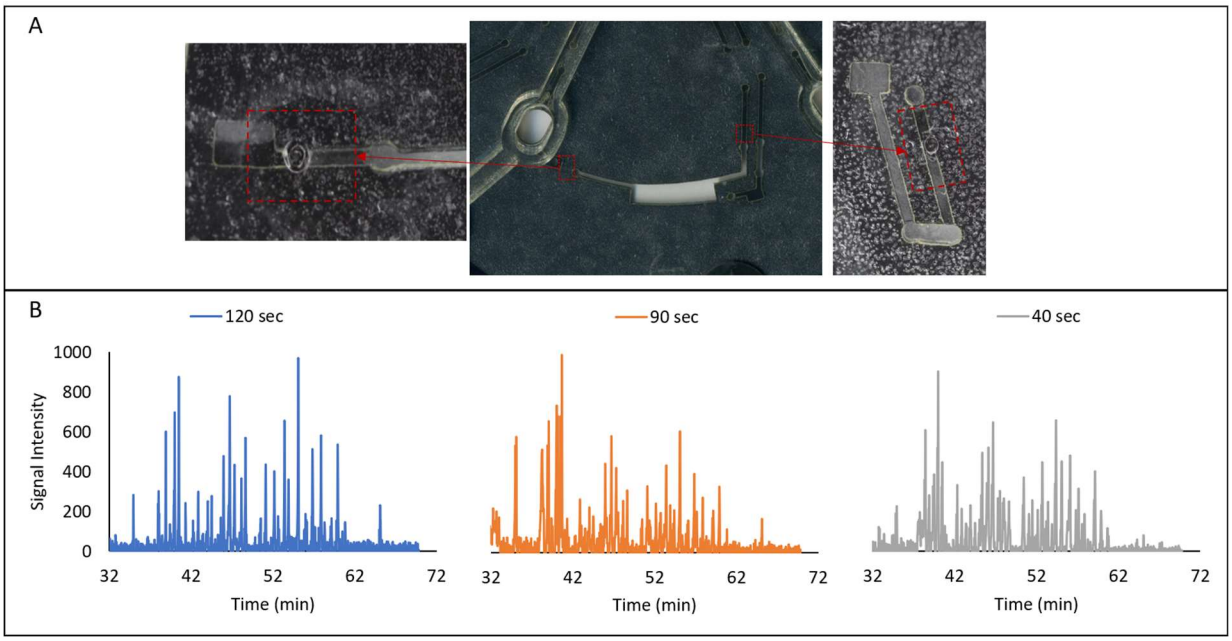

Figure 12: Initial closed chamber testing on microfluidic disc. (A) Two air vent channels were closed by laser irradiation. (B) The initial 95 °C step was varied to show the minimum time needed for amplification.

from all of the reactions. There was a slight decrease in signal intensity as the time of the activation step was decreased. Thus, the results indicate that reducing the initial step from 15 mins to 2 mins activates some of the polymerase to perform PCR, but loss of reaction liquid is still a problem.

5.3.3.2 Optimization of PCR protocol

In order to address the fluid loss observed during initial testing of on-disc PCR activation, a series of time-reduction studies were performed using a new architecture which employed two closeable valves and a simple dye solution to visualize fluid movement post-incubation. These studies were designed to determine the maximum period that liquid could be retained on-disc when exposed to high (95 °C) applied heat before evaporation of the reaction liquid. It was found that when retention times were increased while the channels were closed, the fluid moved between the layers of the disc or breached the closable valve and evaporated. As previously mentioned, the high heat makes the HSA layers of the disc malleable, and thus liquid can be forced into these layers. It was theorized that since the HSA has a melt temperature close to 100 °C and becomes malleable at 95 °C, the air in this layer displaced liquid from the chamber. As presumed, it was found that large air bubbles developed in the PCR chamber after heating for 5 min, and much of the liquid was expelled from the PCR chamber (**Fig. 13**). This was determined by capturing images at various times during the heating and using ImageJ to count pixels attributed to the dye color. The increase in time (2 min to 5 min) was shown to inversely correlated with the number of pixels attributed to the inside of the chamber. Next, the activation step was conducted for a 4 min period. Although numerous tiny air bubbles were observed after

4 min of heating, most of the liquid was retained inside the PCR chamber. Consequently, a maximum holding time of 4 min at 95 °C was deemed optimal for the initial step of the PCR reactions due to minimal liquid loss and all targets detected via capillary electrophoresis.

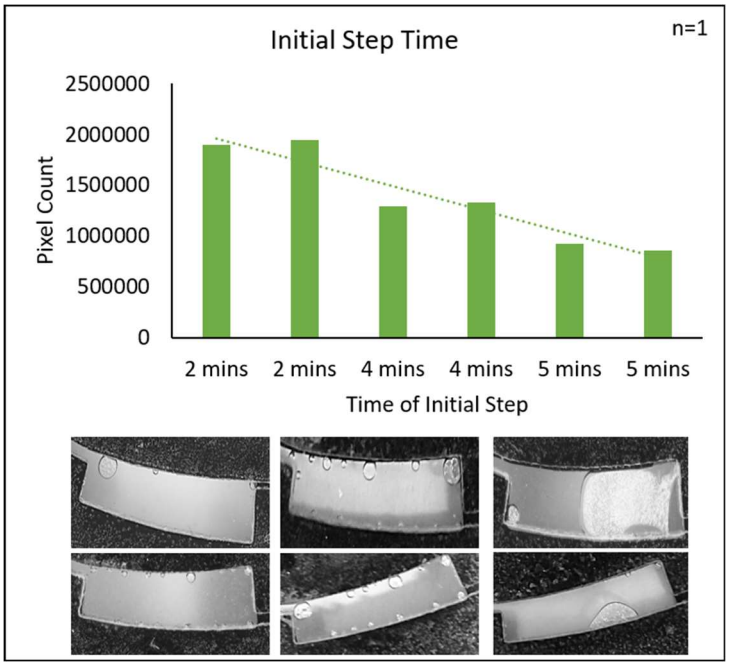

Figure 13: Assessment of evaporation after cycling. Using colored dye, the initial step was varied, and the cycle times were kept constant for 40 cycles. Images were captured after cycling and, using Image J, the number of pixels were calculated. As the initial time increased, less colored dye was in the PCR chamber.

Following the establishment of optimal holding time for the initial step of on-disc amplification, the focus shifted to optimization of additional parameters. Again, optimization was first explored using in-tube amplifications. The 4-min initial step was used to amplify the positive control with an increasing number of cycles to determine the minimum cycle requirement. Given that each cycle is approximately 90 seconds, and if ramping times of the Peltier heaters are not considered, reducing the number of cycles by 5 decreases the overall time by approximately 7.5 min. The peak height for fluorescence at the detector corresponds to the number of amplicons produced at a given amplicon size. While the peak height of the targets in the panel were higher in-tube than the previous on-disc results, the conventional GeXP instrument did not detect targets in the panel until 35 heating cycles had elapsed (**Fig. 14**). As expected, the signal intensity

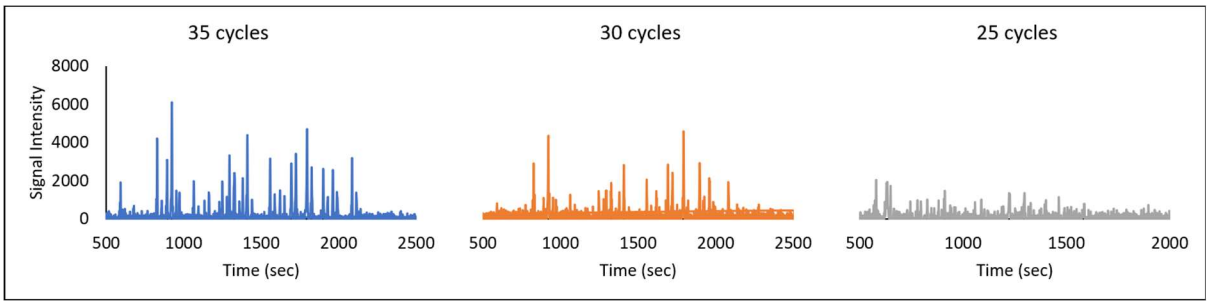

Figure 14: Decreasing cycle number in closed channel amplification. The initial step was 4 mins with cycles of 20 sec for each step (denature, anneal, extend). As expected, with more cycles the signal intensity was greater.

for the targets increased as the number of cycles increased due to exponential amplification of the target sequences. This indicated that reduction in the number of cycles might not be possible, but this could be revisited following optimization of other parameters (e.g., step times in cycles, polymerase concentration, primer concentration).

Lastly, reduction of the total reaction volume was assessed as a means of reducing the cost per test. Additionally, reducing the total reaction volume results in an increased sample concentration, which could improve sensitivity. If the sample is more concentrated, the PCR reaction may produce more target amplicons and higher peak heights. Moreover, a lower total reaction volume allows for a reduction of the PCR chamber size. This could allow multiple PCR chambers to be placed under the Peltier heaters (as opposed to a single chamber currently) which could vastly improve assay throughput.

The total reaction volume was reduced from 20 µL to either 10 or 5 µL then amplified in-tube and electrophoresed on the GeXP system. **Fig. 15** shows the peak heights for all 25 targets in the Human Reference*Plex* panel. All 25 targets were detected in all three reaction volumes evaluated. Roughly half of the targets yielded a lower peak height in the 10 and 5 µL reactions,

specifically, the shorter fragments (~150-200 bp) were lower in the 5 µL reaction than the 20 µL reaction. Regardless, the data indicated that, with further optimization to the PCR protocol, reducing total volume could produce enough amplicons to assess the gene expression compared to the internal control (Kan^R).

Despite significant advancements in assay optimization, this RT-PCR protocol requires substantially more fine-tuning to be fully optimized for on-disc reactions. Future experiments could evaluate the effects of an increase in polymerase and primer concentrations, a shortened step time in enzyme activation or cycling, a higher number of cycles, or using a different polymerase in the reaction that does not require a long activation time. An increased polymerase concentration would increase the quantity of amplified targets within the same 4 min time period

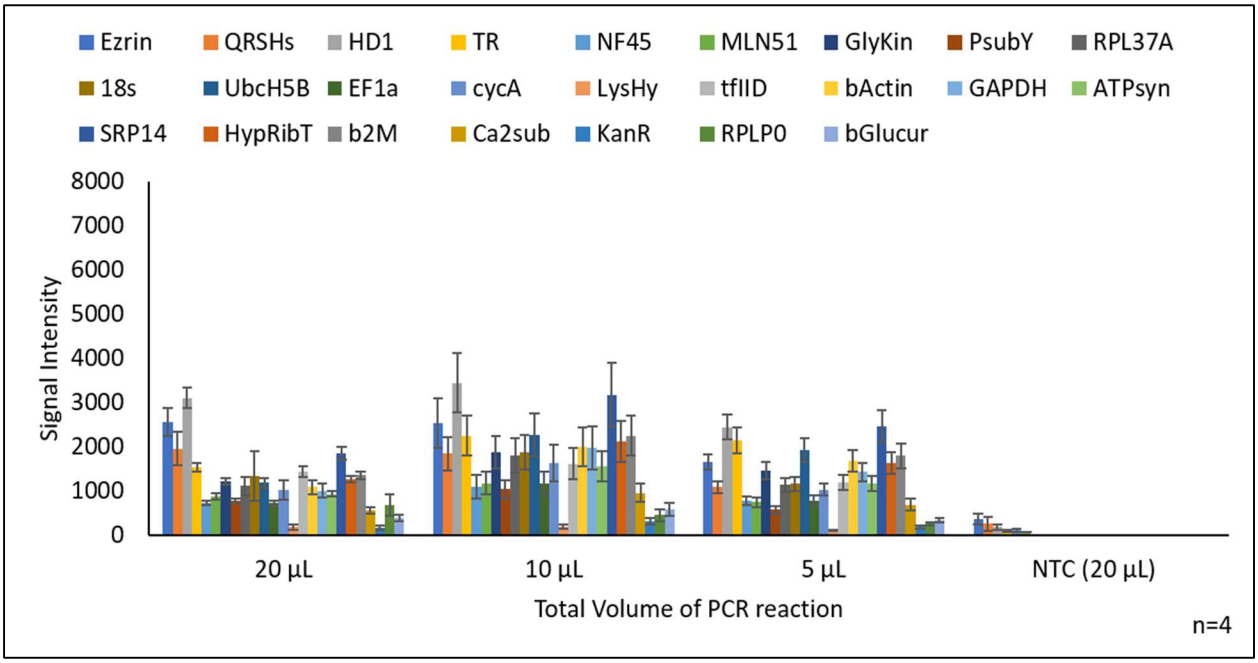

Figure 15: Total volume reduction with in-tube PCR reactions. All 25 mRNA genes in the Human Reference Panel were detected via capillary electrophoresis after reducing the total volume. By decreasing the total volume, the sample concentration will be increased. Additionally, the smaller total volume means smaller chamber size, which means more PCR chambers can be fit under the Peltier heaters.

but could be limited by the number of primers available. Therefore, an increase in the primer concentration would also require exploration. Regarding the reduction of step time, although counterintuitive, a time reduction may result in the accommodation of additional cycles with a minimal impact on overall assay time. The additional cycles could potentially enable the production of more amplicons in a given period.

If it is determined that the protocol is not adaptable to a microfluidic platform due to the need to reach and maintain 95 °C, similar results could be obtained by changing the components in the reaction. Many PCR reactions occur with polymerases that do not need a hot-start step or are designed for rapid amplification in-tube, which is advantageous for this application. The data shown in this chapter for the LITMUS project result from the initial optimization experiments for RT-PCR on-disc. Thus, justification is provided for continuing protocol optimization efforts, with the goal of a significantly reduced overall time and reagent cost without hindering the analysis method.

5.4 Summary

In a point-of-need setting, an ideal device and accompanying biochemical test would typically be user-friendly, time and cost-efficient, and produce easy-to-understand results. The experiments in this chapter focused on decreasing the overall assay time while maintaining sensitivity of the assay for two clinical applications. The architecture on the microfluidic disc allowed for six samples to be amplified per disc and was fabricated with off-the-shelf, cost-effective materials. It was determined that two Peltier heaters were needed for accurate heating during amplification in both applications. The use of a single Peltier resulted in a non-ideal

temperature gradient within the PCR chamber. Using two Peltier heaters flanking the PCR chamber, the overall PCR time was assessed for two clinical applications.

For the SARS-CoV-2 project, the overall assay time was reduced from ~45 min using a conventional qPCR system to a minimum of ~11 min on-disc. While the initial enzyme activation step could be decreased by 2 min, reducing the annealing step of each cycle was shown to have a more significant effect on the overall assay time. Comparatively, the time taken for the annealing step could be reduced to ≤5 sec on-disc, a feat that was not possible using the conventional methods. Despite reducing the time, low quantities of the mRNA target were detected after amplification on-disc as seen on the conventional methods.

For the LITMUS project, the move to microfluidic technology was made more challenging due to a long enzyme activation step requiring high heat. Even with the incorporation of closable valves in the architecture of the disc, evaporation or displacement of the reaction liquid from the PCR chamber persisted. However, a maximum of just 4 min was feasible for the enzyme activation step with small air bubble accumulation. This is significantly shorter than the 15-min step demonstrated in the original protocol. Low peak heights post-amplification indicate that a smaller quantity of DNA polymerase becomes activated with a shorter heat enzyme activation step. Preliminary studies revealed that a minimum of 25 cycles is needed for detection using a conventional capillary electrophoresis instrument, which can serve as a minimum number of cycles when optimizing this protocol on-disc. Additionally, the total reaction volume could be reduced to 5 µL while producing signal intensity similar to the original 25 µL reaction. Reducing the total reaction volume allows for a smaller chamber on the microfluidic disc, and possibly

multiple reactions to occur simultaneously under a single Peltier heater to increase sample throughput.

5.5 References

1. Beebe DJ, Mensing GA, Walker GM. Physics and Applications of Microfluidics in Biology. Annual Review of Biomedical Engineering. 2002 2002/08/01;4(1):261-86.

2. Gorkin R, Park J, Siegrist J, Amasia M, Lee BS, Park J-M, et al. Centrifugal microfluidics for biomedical applications. Lab on a Chip. 2010 2010-01-01;10(14):1758.

3. Zhu N, Zhang D, Wang W, Li X, Yang B, Song J, et al. A Novel Coronavirus from Patients with Pneumonia in China, 2019. New England Journal of Medicine. 2020 2020-02-20;382(8):727-33.

4. Guan W-J, Ni Z-Y, Hu Y, Liang W-H, Ou C-Q, He J-X, et al. Clinical Characteristics of Coronavirus Disease 2019 in China. New England Journal of Medicine. 2020 2020-04-30;382(18):1708-20.

5. Allen J, Almukhtar S, Aufrichtig A, Barnard A, Bloch M, Cahalan S, et al. Coronavirus in the U.S.: Latest Map and Case Count. [Web Page] The New York Times; 2021 [updated 2021 May 19, 2021; cited]; Available from: https://www.nytimes.com/interactive/2021/us/covid-cases.html.

6. Ravi N, Cortade DL, Ng E, Wang SX. Diagnostics for SARS-CoV-2 detection: A comprehensive review of the FDA-EUA COVID-19 testing landscape. Biosensors and Bioelectronics. 2020 2020-10-01;165:112454.

7. World Health O. Laboratory testing for coronavirus disease 2019 (COVID-19) in suspected human cases: interim guidance, 2 March 2020. Geneva: World Health Organization; 2020 2020 Contract No.: Document Number|.

8. Loeffelholz MJ, Tang Y-W. Laboratory diagnosis of emerging human coronavirus infections – the state of the art. Emerging Microbes & Infections. 2020 2020-01-01;9(1):747-56.

9. Kogoj R, Kmetič P, Valenčak AO, Komloš KF, Seme K, Sagadin M, et al. Real-life head-to-head comparison of performance of two high-throughput automated assays for detection of SARS-CoV-2 RNA in nasopharyngeal swabs: the Alinity m SARS-CoV-2 and cobas 6800 SARS-CoV-2 assays. The Journal of Molecular Diagnostics. 2021 2021-05-01.

10. Arena F, Pollini S, Rossolini GM, Margaglione M. Summary of the Available Molecular Methods for Detection of SARS-CoV-2 during the Ongoing Pandemic. International Journal of Molecular Sciences. 2021 2021-01-28;22(3):1298.

11. Esbin M, Whitney O, Chong S, Maurer A, Darzacq X, Tjian R. Overcoming the bottleneck to widespread testing: A rapid review of nucleic acid testing approaches for COVID-19 detection. RNA. 2020 05/01;26:rna.076232.120.

12. Xiong H, Ye X, Li Y, Wang L, Zhang J, Fang X, et al. Rapid Differential Diagnosis of Seven Human Respiratory Coronaviruses Based on Centrifugal Microfluidic Nucleic Acid Assay. Analytical Chemistry. 2020 2020-11-03;92(21):14297-302.

13. Ji M, Xia Y, Loo JF-C, Li L, Ho H-P, He J, et al. Automated multiplex nucleic acid tests for rapid detection of SARS-CoV-2, influenza A and B infection with direct reverse-transcription quantitative PCR

(dirRT-qPCR) assay in a centrifugal microfluidic platform. RSC Advances. [10.1039/D0RA04507A]. 2020;10(56):34088-98.

14. Fayek SA, Quintini C, Chavin KD, Marsh CL. The Current State of Liver Transplantation in the United States. American Journal of Transplantation. 2016;16(11).

15. Watt KDS, Pedersen RA, Kremers WK, Heimbach JK, Charlton MR. Evolution of Causes and Risk Factors for Mortality Post-Liver Transplant: Results of the NIDDK Long-Term Follow-Up Study. American Journal of Transplantation. 2010;10(6).

16. Moini M, Schilsky ML, Tichy EM. Review on immunosuppression in liver transplantation. World journal of hepatology. 2015;7(10):1355-68.

17. Xie L, Ichimaru N, Morita M, Chen J, Zhu P, Wang J, et al. Identification of a novel biomarker gene set with sensitivity and specificity for distinguishing between allograft rejection and tolerance. Liver Transplantation. 2011;18(4).

18. Levy G. Liver Immune Tolerance Marker Utilization Study (LITMUS). ClinicalTrials.gov: U.S. National Library of Medicine; 2015.

19. Thompson BL, Ouyang Y, Duarte GRM, Carrilho E, Krauss ST, Landers JP. Inexpensive, rapid prototyping of microfluidic devices using overhead transparencies and a laser print, cut and laminate fabrication method. Nature Protocols. 2015 2015/06/01;10(6):875-86.

20. DuVall JA, Le Roux D, Thompson BL, Birch C, Nelson DA, Li J, et al. Rapid multiplex DNA amplification on an inexpensive microdevice for human identification via short tandem repeat analysis. Analytica Chimica Acta. 2017 2017/08/08/;980:41-9.

21. Hadaya J, Schumm M, Livingston EH. Testing Individuals for Coronavirus Disease 2019 (COVID-19). JAMA. 2020 2020-05-19;323(19):1981.

22. Inc. BC. GenomeLab™ GeXP

Human ReferencePlex Kit. A21780AK ed; 2015.

23. Lee C, Lee L-J, Chong P-P, Chang K-M, Abdullah M. Selection of reference genes for quantitative studies in acute myeloid leukaemia. The Malaysian journal of pathology. 2019;41(3):313-26.

24. Dignan L, Turiello R, Layne TR, O-Connell KC, Hickey J, Chapman J, et al. An Ultrafast SARS-CoV-2 Virus Enrichment and Extraction Method Compatible with Multiple Modalities for RNA Detection Analytica Chimica Acta. [Full Length]. 2021.

25. Birch C, DuVall JA, Le Roux D, Thompson BL, Tsuei A-C, Li J, et al. Rapid Fabrication of Electrophoretic Microfluidic Devices from Polyester, Adhesives and Gold Leaf. Micromachines. 2017;8(1):17.

26. Garcia-Cordero JL, Kurzbuch D, Benito-Lopez F, Diamond D, Lee LP, Ricco AJ. Optically addressable single-use microfluidic valves by laser printer lithography. Lab on a Chip. 2010 2010-01-01;10(20):2680.

27. Chen Y, Xu W, Sun Q. A novel and simple method for high-level production of reverse transcriptase from Moloney murine leukemia virus (MMLV-RT) in Escherichia coli. Biotechnology Letters. 2009 2009-07-01;31(7):1051-7.

28. Ali H, Du Z, Li X, Yang Q, Zhang YC, Wu M, et al. Identification of suitable reference genes for gene expression studies using quantitative polymerase chain reaction in lung cancer in vitro. Molecular medicine reports. 2015.

29. Xie L, Ichimaru N, Morita M, Chen J, Zhu P, Wang J, et al. Identification of a novel biomarker gene set with sensitivity and specificity for distinguishing between allograft rejection and tolerance. Liver Transplantation. [https://doi.org/10.1002/lt.22480]. 2012 2012/04/01;18(4):444-54.

30. Dahiya R, Deng G, Chen K, Haughney PC, Cunha GR, Narayan P. Terms and techniques: New approach to hot-start polymerase chain reaction using Taq DNA polymerase antibody. Urologic Oncology: Seminars and Original Investigations. 1995 1995/01/01/;1(1):42-6.

31. Woolf MS, Dignan LM, Lewis HM, Tomley CJ, Nauman AQ, Landers JP. Optically-controlled closable microvalves for polymeric centrifugal microfluidic devices. Lab on a Chip. [10.1039/C9LC01187K]. 2020;20(8):1426-40.

Chapter 6: Final Remarks

6.1 Conclusions

This dissertation has described advances made in rapid nucleic acid amplification methods using in-tube and microfluidic technology for forensic science and clinical applications. Specifically in forensic science, body fluid identification (bfID) has been researched to develop new methods to update the conventional assays. While there are promising techniques published in literature, no technologies have been introduced in forensic laboratories to address the current analytical weaknesses. The current bfID methods are destructive towards DNA material needed for downstream profiling, readily available for only three body fluids, and detect biological material that is not specific to humans or a single body fluid. Two methods described in this dissertation were developed for this application: (1) using a novel isothermal amplification method with fluid-specific mRNA targets and objective colorimetric image analysis detection as a laboratory technique and (2) an automated microfluidic platform to convert RNA to cDNA, amplify mRNA targets, and fluorescently size separate the amplicons as an on-scene technique. Along with the forensic application, novel technology for two clinical applications were developed as point-of-care or on-scene analysis methods, which highly advantageous and can easily be accomplished by a microfluidic approach. Microfluidics offer advantages for these applications with the ability to achieve specificity and sensitivity similar or better than conventional methods. The research presented here demonstrates the rapid technology that

addresses some of the core issues pertaining to the conventional methods utilized in the clinical and forensic communities.

The work in **Chapter 2** aimed to develop a colorimetric isothermal amplification method that specifically identifies mRNA targets for forensic bfID. This workflow was chosen due to the minimal steps required to complete the assay, simple technology for heating, and its simple incorporation into the forensic workflow. Using the LAMP method, five mRNA targets were optimized for single fluid specificity with comparable sensitivity levels to conventional methods. The temperature, primer concentration, and mRNA target were varied to determine the best conditions for producing rapid results. There was a significant increase in specificity for all five mRNA targets after a DNase treatment was implemented in the lysis and purification method. After optimization, the LAMP method was able to show a consistent color change for picogram levels of total RNA for blood, semen, vaginal fluid, and menstrual blood mRNA targets, and nanogram levels of total RNA for the saliva mRNA target. To circumvent the subjective visual detection of color change, image capture and hue color analysis was implemented. An imaging box with static lighting and a smartphone was used for image capture, and Image J software was utilized to assess the hue (or shade of the color) of each reaction for a positive or negative result. The results in this chapter provide a first step towards developing a novel approach for forensic bfID.

Building on this optimization, **Chapter 3** details a 3D-printed system (cLAMP system) for combined heating of the LAMP reactions and automated image analysis as an objective detection method. The cLAMP system is user-friendly, compatible with multiple colorimetric dyes that can

increase or decrease in hue via color change, and provides consistent, steady isothermal heating. Similar to in-tube analysis, the cLAMP software calculates a threshold based on the average of all reactions' initial hues and deems a reaction positive once the hue passes the threshold. This system was built to be a one-step analysis method for LAMP reactions. Compared to the conventional thermal cycler, this system showed similar temperature and ramp times across the 96 well plate. The initial testing with the five mRNA targets with single-source body fluids was successful, providing a color change in < 30 minutes. To assess the performance of the cLAMP system with forensic type samples, a mock study with various mixtures of 2 or 3 fluids, aged samples, post-coital samples, and substrates known to inhibit PCR were tested using the LAMP method. From the single-blind mock study, the saliva and vaginal fluid targets worked effectively (>80%), the venous blood target performed moderately (>70%), and the semen and menstrual blood targets performed the worst (>50%). Further analysis determined the Se target is not as sensitive as a lateral flow assay (conventional method), and the Mb target is not fluid specific due to amplification in V Fluid. While the cLAMP system did not perform as well as a conventional thermal cycler with these mRNA targets, the hardware and software do provide a rapid objective method for heating and analyzing LAMP reactions that can be used in various laboratory applications.

Alternatively, **Chapter 4** details a novel on-scene method for forensic bfID using microfluidic technology and a panel of mRNA targets for the identification of six body fluids. Scientists at the Institute of Environmental Science and Technology (ESR) in New Zealand developed a panel of three plex's with one or two mRNA targets that specifically determines venous blood from menstrual blood (Quadruplex), buccal fluid (Duplex), and vaginal fluid from

semen or seminal fluid (Pentaplex). Each of the targets are tagged with either FAM or HEX fluorophores and are less than 200 bp in length. The current workflow for this panel, which starts with DNA/RNA co-elution and RNA purification, then RT and PCR of the RNA, followed by size separation on a capillary electrophoresis instrument, was adapted to a microfluidic platform. Starting with fluorescent size separation, a microElectrophoresis Disc (μEDisc) was fabricated to allow 3 samples/disc with separations in <15 minutes. Single source and mixture samples were detected on the μEDisc using the three plex's at a 1:2 dilution of 5 µL of semen, 1:16 dilution of a vaginal fluid swab, 1:8 dilution of a buccal swab, and 1:32 dilution of liquid venous blood or a menstrual blood swab. Next, the RT reaction was optimized on a 'micro-amplification' disc (μAmpDisc) using Peltier heaters to amplify the mRNA targets with the final goal of integration on one device. The μAmpDisc was designed for rapid RT and PCR of 6 samples/disc. After adapting the RT protocol to the μAmpDisc, the reaction was completed 10X faster (120 min → 11 min) than the in-tube protocol with minimal loss in cDNA production in single-source body fluid samples. The results in Chapter 4 demonstrate advancement towards a fully integrated *sample-in-answer-out* system for simultaneous forensic bfID of six body fluids. Through integration of on-disc RNA extraction and purification with the optimized RT, PCR, separation, and detection, a µTAS device can be developed. Such a device would have important implications in expediting the forensic bfID process with high sensitivity and specificity of mRNA targets.

The experiments in **Chapter 5** focused on decreasing the overall assay time while maintaining its sensitivity for two clinical applications. It was found that heating with Peltiers above and below the PCR chamber allowed for a much smaller temperature gradient than only using one Peltier heater. For the SARS-CoV-2 application, the overall PCR assay time was reduced

from ~45 minutes using a conventional qPCR system to a minimum of ~11 minutes on-disc. Reducing the annealing step time in the PCR cycles had the most significant effect on reducing the overall time. The positive control plasmid was detected at 10 copies/µL on the microfluidic disc within 18 minutes. While detection at this concentration level is good, compared with the conventional methods, the PCR on-disc is not as sensitive. The conventional methods were able to consistently detect < 10 copies/µL of the plasmid. However, the microfluidic disc was able to detect known clinical samples classified as having either high, moderate, or low quantities of the mRNA target by conventional qPCR. The data in this chapter supports ongoing efforts to optimize the PCR protocol by reducing the overall assay time while maintaining the sensitivity found using conventional methods.

The move to microfluidic technology for the LITMUS application was more challenging, primarily due to a long enzymatic activation step at high heat. The panel for detection in **Chapter 5** contained 25 mRNA targets ranging from 150 to 338 bp in length. The microfluidic disc for this application included closable valves in an effort to minimize reagent evaporation or flow out of the PCR chamber. Long heating steps produced large air bubbles in the PCR chamber. Using the microfluidic disc with closable valves, the enzyme activation step was reduced from 15 to 4 minutes, resulting in the formation of smaller air bubbles. All targets within the panel were detected with a minimum of 30 cycles with the 4-minute enzyme activation step, and the total volume was able to be reduced from 20 µL to 5 µL. Despite significant advancements in assay optimization, this RT-PCR protocol requires substantially more fine-tuning to be fully optimized for on-disc reactions.

6.2 Future Work

The LAMP method developed for forensic bfID showed promise for a specific and sensitive method but could be improved upon. While the vaginal fluid and saliva targets amplified well in the mock study in terms of correctly identifying the fluid, the venous blood, semen, and menstrual blood targets did not amplify well producing less than 80% correct fluid identification. For the venous blood mRNA target, the issue was false positive color changes, presumably due to primer dimers. A future endeavor to circumvent this issue would be to redesign the primers for the same location on the human β-hemoglobin gene (HBB) and amplify no-template controls to determine whether primer dimers would be an issue. Data from Chapter 2 showed high sensitivity (total RNA picogram level) for the detection of HBB, and high specificity towards venous or menstrual blood. Ideally, a different set of primers for the same locus would produce similar results. Furthermore, if none of the new primer sets were suitable, a completely new mRNA target could be assessed for venous blood.

The issue with the semen target (SEMG1) was assay sensitivity due to low concentrations of the target in known and mock semen samples, hindering amplification during the LAMP reaction. There are a few different approaches to fixing this issue. One approach would be to add in a mRNA concentration step before the LAMP reaction. In theory, this could increase assay sensitivity to the Se mRNA target by providing a better chance at amplifying the low target concentrations. Another strategy could be to increase the volume of sample in the LAMP reaction. Not only could this expedite the color change to produce faster results, but there would be more sample in the reaction to facilitate amplification. The more complex approach would be

essentially starting over by finding another mRNA gene that is highly concentrated in semen and design primers for LAMP to provide suitable specificity and sensitivity.

Finding a mRNA target for menstrual blood identification was the most challenging with this project. The mRNA targets that were assessed did not provide the specificity required to distinguish menstrual blood from the other body fluids, most notably from venous blood, due to the presence of this target in both fluids. Specifically, the only mRNA target (MMP10) that did not amplify in venous blood showed expression in vaginal fluid samples, thus this target was not specific to menstrual blood. The next steps for this fluid would be to research the literature to compile a list of mRNA targets highly expressed in menstrual blood, design LAMP primer sets for the targets, and optimize the reaction to obtain single fluid specificity and high sensitivity. Alternatively, if a single mRNA target cannot be found to differentiate menstrual blood from the other fluids, the use of two mRNA targets might. However, this approach would require two LAMP reactions due to the single-target character of colorimetric LAMP or optimization for a multiplexed target and color change LAMP reaction.

The 3D-printed system developed for automated, one-step LAMP heating, and image analysis performed very well in the mock study. Nonetheless, improvements could be made to confer the system a smaller footprint, faster preheat time, more controlled heating, and better portability for on-scene analysis. One improvement would be to replace the Raspberry Pi camera with a flatbed scanner (**Fig. 1**). The fixed focus lens on the Raspberry Pi lacks a software-based auto focus function; thus, each camera module must be individually focused by hand through trial and error. This has produced a lack of consistency in image quality between the four cLAMP

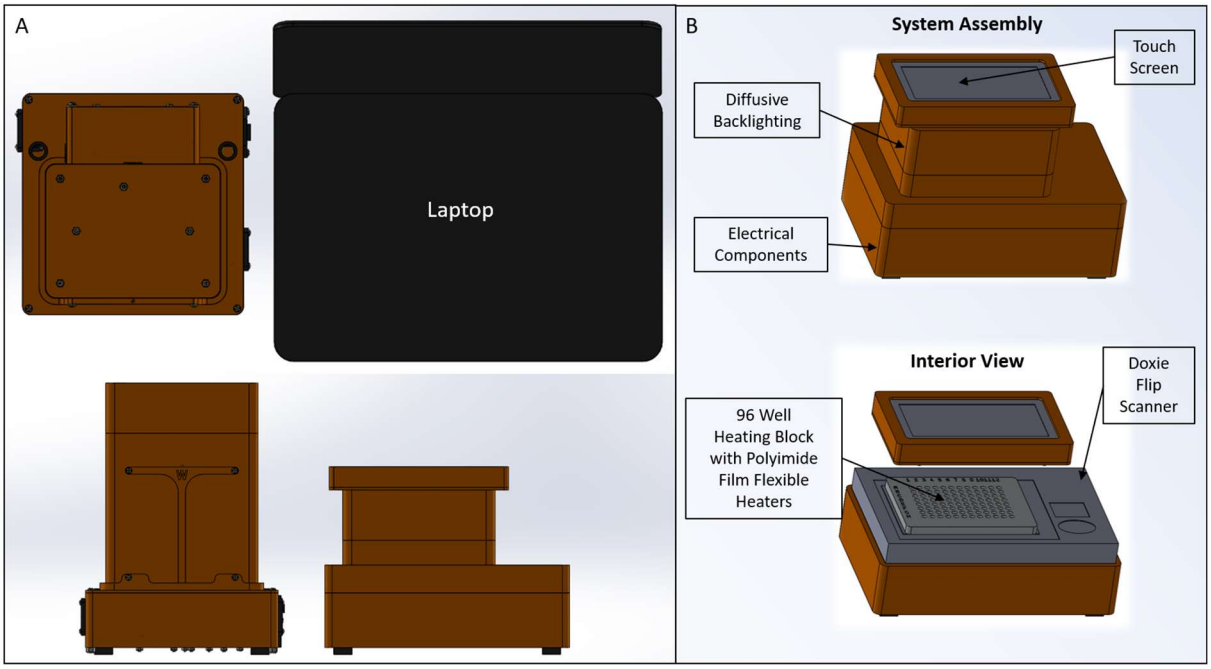

Figure 1: Current and future versions for cLAMP system comparison. (A) Current version with Raspberry Pi camera and laptop. (B) Design for version cLAMP v4.0 with laptop, scanner camera, and touch screen computer.

systems described in Chapter 3. A flatbed scanner would gain better consistency in image quality due to the auto focus function. Moreover, the z-axis form factor of the system can be reduced by as much as 32%, as the distance set for the camera to capture the entire 96-well plate is removed. Additionally, with the reduced height of the system there is less air to be preheated, thus decreasing the preheat time from the current 45 min. Another improvement would be to replace the laptop with a touch screen computer that fits on top of the system. Along with the switch in camera, this addition would decrease the overall footprint and allow for portability for on-scene use to identify body fluids. Finally, an improvement would be to replace the convective heating with other heating units (e.g., Peltier heating, flexible heaters, adhesive heaters). Another type of heating could produce faster ramp times and less temperature deviation between wells. However, the trade off with switching the heating unit would be the cost of

materials. Overall, the combined system that was built for LAMP heating and image analysis worked well when tested, but improvements could produce better results when identifying mRNA targets for forensic bfID.

For the microfluidic approach to forensic bfID described in Chapter 4, the next steps would be to optimize the PCR protocol on-disc and develop an DNA/RNA co-extraction method amenable to a microfluidic platform. The main advantage of transferring the in-tube PCR protocol to a microfluidic platform would be to reduce the overall assay time from ~3+ hours to <30 min (**Table 1**). This could be achieved with the fast ramp rate of the Peltier heaters and by decreasing the time for each step in the PCR cycling. Currently, there are 35 cycles at 4.5 min/cycle (95 °C 30 sec, 60 °C 3 min, 72 °C 1 min). Furthermore, the in-tube protocol optimized by ESR recommends a 15 min enzyme activation step and 10 min extension step after cycling to allow the polymerase to finish adding nucleotides to complete the amplicons.

Table 1: Optimization of PCR protocol to microfluidic platform.

PCR Steps													Total Time
Platform	Reagents	Initial		Cycling							Extension		
		Time	Temp	Cycles	Time	Temp	Time	Temp	Time	Temp	Time	Temp	
Tube	Normal	15 min	95 C	35	30 sec	95 C	3 min	60 C	1 min	72 C	10 min	72 C	**182.5 min**
Disc	+Polymerase +Primers +dNTPS	1 min	95 C	35	3 sec	95 C	3 sec	60 C	3 sec	72 C	1 min	72 C	**7.25 min**

The results in Chapter 5 showed a maximum of 4 minutes for the holding at 95 °C for the enzyme activation step, thus, the protocol will be decreased by at least 11 min initially. Each step in the cycling could be reduced to a minimum of 3 sec, shaving 4 min from each cycle for a total of 140 min saved. While the final extension step is very important for quality amplification, reducing the time of this step would also save up to 9 min on the protocol. To determine if the time reductions had a major impact on the amplicons produced, the results could be size

separated on a conventional capillary electrophoresis instrument and assessed for peak height imbalance and fluorescent signal of each target. In addition to time reduction, the concentration of reagents could be assessed with the faster protocol in an attempt to increase fluorescent signal. The main reagents which concentrations could be increased are the polymerase to allow for more enzyme to be activated and produce more amplicons, and the primers to allow for more annealing during cycling.

The second future endeavor with this project (Chapter 4) would be to assess efficient co-extraction methods easily amenable to a microfluidic platform and integrating each section of the workflow together (**Fig. 2**). Currently, most forensic co-extraction methods are silica column-

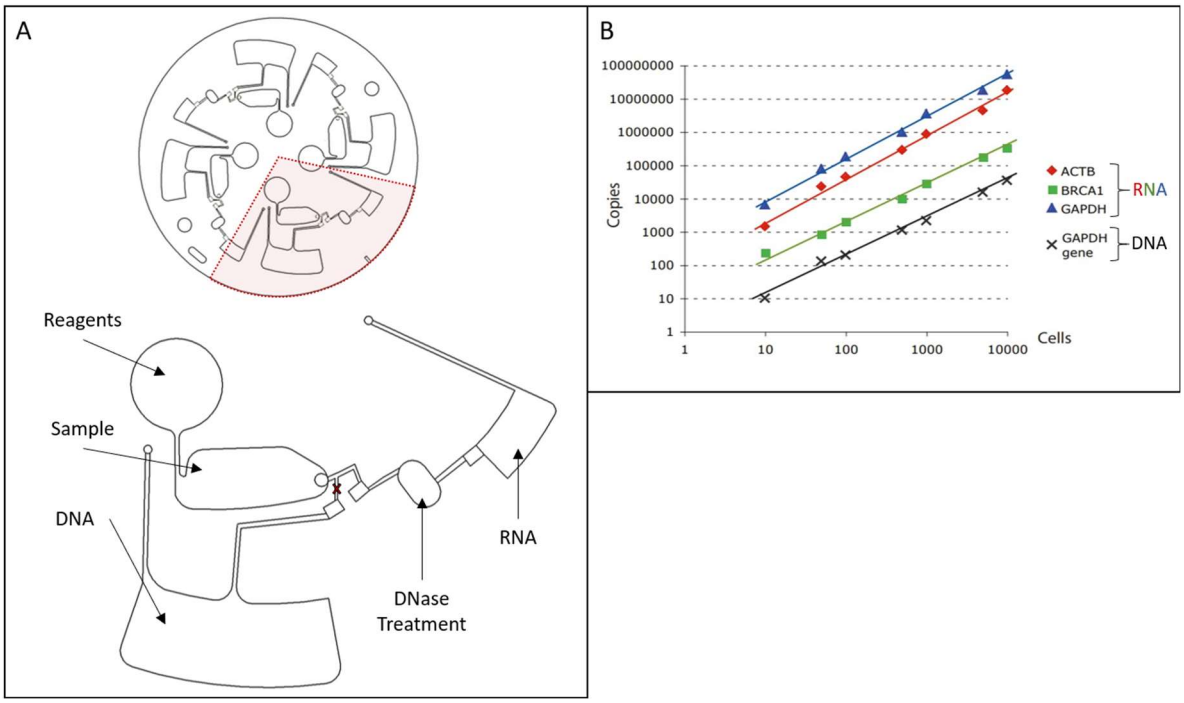

<u>Figure 2</u>: Initial design for on-disc RNA extraction method. (A) The disc would allow for simultaneous extraction of four samples where DNA is kept in one chamber, while the RNA portion undergoes a DNase treatment and is kept in a second chamber. 'X' denotes channel closure to separate DNA and RNA fractions. (B) In-tube enzymatic liberation of PCR-ready DNA and RNA is a 10 min assay that is temperature controlled. Copies of the human GAPDH gene (DNA) detected by qPCR plotted alongside copies of mRNA detected by RT-qPCR for three separate targets. (Miles & Saul, 2019, MicroGEM with permission)

based, with downstream DNase treatments for RNA purification. While adapting the silica column to a microfluidic platform is possible, an alternative method would be to use an enzymatic lysis to separate the DNA from the RNA material. To perform an enzymatic method, typically the hardware required is a heating platform which could be performed by the Peltier heaters on the integrated system. The separation of DNA from RNA would be more complex but could be separated via magnetic beads or using lithium chloride to precipitate the RNA from solution. Once the method for co-extraction is optimized, the architecture from the co-extraction disc, the RT-PCR disc, and the microelectrophoresis disc can be integrated onto a single device. Ideally, the integrated disc would allow for 3-4 samples to be processed from sample to body fluid profile on a single disc in < 1 hour. This integrated disc and system would allow for specific and sensitive mRNA target detection that easily fits into the current forensic workflow, has minimal hands-on steps, and is portable for in-lab or on-scene utilization.

Additionally, the integrated disc and system can be adapted for rapid amplification and detection of mRNA targets for two clinical applications, detailed in Chapter 5. Since the SARS-CoV-2 project only detected one mRNA target, the integrated disc could contain only the co-extraction and RT-PCR architecture. The amplicons could be detected via end-point fluorescent detection via the optical detector on the integrated system. Alternatively, the mRNA panel for the organ tolerance project would require microelectrophoresis of all 25 genes. Currently, this project is undergoing optimization of the one-step RT-PCR protocol on-disc, which will be integrated with the microelectrophoresis architecture. While both of these projects have much optimization to be performed, the results in this dissertation show the essential first steps for achieving a rapid, simple mRNA detection method for point-of-care assessment.

6.3 Summary

Developing novel methods that offer solutions to complex problems in both the forensic and clinical communities help to drive science forward and create technology that will improve current conventional methods. Forensic clues that piece together the real narrative of a crime is instrumental in casework and the identification of the perpetrator, thus the technology and assays used to find said clues should be cutting-edge and reliable. Similarly, better screening methods and technology geared towards clinical applications help identify biothreats faster such as SARS-CoV-2 which caused the 2020 pandemic. Alternatively, improved screening methods and technology can monitor the tolerance of a transplanted organ and may allow for a less stringent lifestyle for the patient. Every day new threats are emerging, and with it, scientific methodology and technology should grow to improve limitations and fill in gaps created by current technology. The methods described in this thesis offer solutions to each of these problems and are driven by strong forensic and clinical needs for competitive technology to existing techniques.